NTNU

Norwegian University of
Science and Technology

Large-Scale Granulation of CaO-Based Pellets for High-Temperature Carbon Dioxide Capture

Maria Olsvik

Chemical Engineering and Biotechnology
Submission date: June 2018
Supervisor: Edd Anders Blekkan, IKP
Co-supervisor: Kumar Rout, IKP
De Chen, IKP
Li He, IKP

Norwegian University of Science and Technology
Department of Chemical Engineering

Science is organized knowledge. Wisdom is organized life.

Immanuel Kant

Abstract

Pelletized CaO-based sorbents are made for the use in Moving Bed Carbonate Looping (MBCL) technology capturing CO_2 at a low partial pressure of CO_2 and high temperature, producing approximately 100% pure CO_2. Developing this technology will be an important step in reducing CO_2 emissions and prevent temperature increase on the globe. The main goal of this thesis was to develop a procedure for making these pellets in large scale. Material properties such as good CO_2-capture capacity and stability, and good mechanical strength are important. A "rotary drum" granulation machine was used to produce granules made of 100g calcined dolomite/cement ADDA, calcium aluminate cement, extra magnesium and zirconium with water as a liquid binder. The preparation method lasted for two days due to the exothermic reaction between dolomite/ADDA and water, and water was slowly added to avoid early strength gain and increased hydration kinetics at higher temperatures. Six pellets based on calcined dolomite were made; NO-1 (pure dolomite), NO-3 (1.9% Zr from nitrates), NO-6 (1.6% Zr from $ZrCl_4$ and 5.8%Al from cement), NO-8 (2.9%Mg from magnesium nitrate and 5.5%Al (from cement)), NO-10 (6.1%Al from cement) and NO-12 (1.6% Zr from nitrates and 5.8%Al from cement). In addition, four pellets were made of cement ADDA.

Results from nitrogen adsorption/desorption showed largest surface area for unpromoted pellets and smallest pores for the doped samples. Scanning electron microscope pictures, and mechanical tests seem to demonstrate good performance of pellets NO-3, NO-8 and NO-10. They have a similar pellet surface and sphericity, low cumulative attrition loss and weight loss in each drop in the falling test. The x-ray diffraction identified phases of mayenite ($Ca_{12}Al_{14}O_{33}$), which might be the reasons for the excellent mechanical strength of NO-8 and NO-10.

Results from sorption/desorption cycling in a thermogravimetric analyzer with 8% steam demonstrated promising CO_2-carrying capacity and stability over 34 cycles for all pellets. Even though sample NO-1 has the worst stability, the stability was surprisingly high compared to other studies on powdered dolomite which have shown poor cyclic stability. The reason might be the preparation method and the raw material (calcined dolomite (3h 800°C) <106μm) used, but further investigation and calibration of the TGA are necessary. Sample NO-12 showed that the up-scaling procedure is comparable to small-scale granulation. The best cyclic stability is found for sample NO-8 and NO-12 believed to be due to doping by magnesium/aluminum, and zirconium/aluminum. Al, Mg, and Zr inhibit sintering due to higher melting points of the mixed oxides (mayenite and $CaZrO_3$).

The kinetic study demonstrated the fastest reaction rate for 650°C at a high CO_2 concentration in the reaction controlled regime. At low partial pressures of CO_2, 620°C gave faster reaction kinetics than 650°C, due to higher driving force. A pellet size of 250μm-1.2mm indicated minimal diffusion limitations, and smooth s-curves during sorption at 650°C, reaching 80% of their capacity in 5 minutes.

Sammendrag

Granulerte CaO-baserte sorbenter er laget for bruk i "Moving Bed Carbonate Looping (MBCL)" teknologi for å fange CO_2 ved lavt partialtrykk av CO_2 og produsere omtrent 100% ren CO_2. Utviklingen av denne teknologien vil være et viktig steg for å redusere utslipp av CO_2, og forhindre temperatur økning på kloden. Hovedmålet med denne masteroppgaven var å utvikle en prosedyre for å lage disse granulatene i stor skala. Materialegenskaper som god CO_2-fangst kapasitet og god mekanisk styrke er viktig. Granulater ble laget med en granulerings maskin bestående av en roterende beholder basert på 100g kalsinert dolomitt/sement ADDA, kalsium aluminium sement, ekstra magnesium og zirkonium med vann som bindemiddel. Fremstillingsmetoden varte over to dager på grunn av eksoterm reaksjon mellom dolomitt/ADDA og vann, og vann ble langsomt tilsatt for å unngå tidlig styrke økning og økt hydratiseringskinetikk ved høyere temperaturer. Seks pellets basert på kalsinert dolomitt ble laget: NO-1 (ren dolomitt), NO-3 (1.9% Zr fra nitrater), NO-6 (1.6% Zr fra $ZrCl_4$ og 5.8%Al fra sement), NO-8 (2.9%Mg fra magnesium nitrat og 5.5%Al (fra sement)), NO-10 (6.1%Al fra sement) and NO-12 (1.6% Zr fra nitrater og 5.8%Al fra sement). I tillegg ble fire pellets basert på ADDA sement laget.

Resultater fra nitrogen adsorpsjon/desorpsjon viste størst overflate areal for upromoterte prøver og de minste porevolumene for dopede prøver. Bilder fra mikroskop, og mekaniske tester demonstrerte gode egenskaper for pellets NO-3, NO-8 og NO-10. De har en lignende pellet overflate og kuleform, lavt kumulativt tap av masse grunnet slitasje og lavt vekttap per fall målt i en falle test. Røntgendiffraksjonen identifiserte faser av mayenitt ($Ca_{12}Al_{14}O_{33}$), som kan være årsaken til den gode mekaniske styrken til NO-8 og NO-10.

Resultatene fra sorpsjon/desorpsjons sykluser i en termogravimetrisk måler med 8% damp demonstrerte lovende CO_2 kapasitet og stabilitet over 34 sykluser for alle pelletene. Selv om prøve NO-1 har den verste stabiliteten, var stabiliteten overraskende høy sammenlignet med andre studier på pulverisert dolomitt, som har vist dårlig syklisk stabilitet. Årsaken kan være granulerings prosedyre og råmaterialet (kalsinert dolomitt (3h 800°C) <106 μm) brukt, men ytterligere undersøkelse og kalibrering av TGA er nødvendig. Prøve NO-12 viste at oppskaleringsprosedyren er sammenlignbar med småskala granulering. Den beste sykliske stabiliteten er funnet for prøve NO-8 og NO-12 som antas å skyldes doping med magnesium/aluminium og zirkonium/aluminium. Al, Mg og Zr hemmer sintring på grunn av høyere smeltepunkt i blandede oksider (mayenitt og $CaZrO_3$).

Analyse av reaksjonskinetikk viste at reaksjonshastigheten er raskest for 650°C ved høy CO_2 konsentrasjon i det reaksjonskontrollerte regimet. Ved lavt partialtrykk av CO_2, ga 620°C raskere reaksjonskinetikk enn 650°C på grunn av større drivende kraft. Pellet størrelse på 250μm-1.2 mm indikerte minimale diffusjonsbegrensninger og pene s-kurver under sorpsjon ved 650°C, og de oppnådde 80 % av deres kapasitet etter bare 5 minutter.

Preface

This thesis is written as part of a "CO_2-capture project" in cooperation with SINTEF and NTNU with Fjell Technology AS as partner. Thus, a lot of parameters and test conditions are already set by the project. The work provided is performed during summer job 2017, Specialization Project (TKP4580) fall 2017 and Master Thesis spring 2018 at the Catalysis Group (KinCat) within Department of Chemical Engineering, NTNU. Therefore, part of the thesis contains the same theory and methods (introduction, characterization theory and methodology for nitrogen adsorption/desorption, x-ray diffraction, scanning electron microscope and mechanical tests) as for the Specialization Project [1].

I would like to thank the Catalysis Group and Prof. De Chen for the opportunity to work for them during the summer 2017, and to work with the "CO_2-capture project"-group throughout the whole 5^{th} year of my master's degree.

I would also like to thank Prof. Edd A. Blekkan for supervising be through the Specialization project and Master thesis, and Dr. Kumar Ranjan Rout and Dr. Li He for their guidance the whole year. In addition, I would like to thank Karin Wiggen Dragsten, Harry Bruun and Lars Erik Mollan Parnas (SINTEF) for technical support.

I would like to thank my family and friends for their support during my years at NTNU. NTNU has given me good academic knowledge, I have learned so much and got friends for life.

Table of Contents

Abstract i

Sammendrag ii

Preface iii

Table of Contents viii

List of Tables ix

List of Figures xiv

List of Abbreviations xv

List of Symbols xviii

1 Introduction 1
- 1.1 Adsorption Using Solids . . . 2
  - 1.1.1 Dolomite ($CaMg(CO_3)_2$) as Sorbent Material . . . 2
  - 1.1.2 CaO-Based Pellets with Cement Binder . . . 8
- 1.2 Main Goal . . . 10

2 Literature Review 11
- 2.1 Research on Improved Stability of CaO-Based Sorbents . . . 11
  - 2.1.1 Improved Stability of CaO-Based Sorbents by Doping . . . 11
  - 2.1.2 Improved Stability of CaO-Based Sorbents by Different Preparation Methods . . . 12
  - 2.1.3 Investigation of Stability of CaO-Based Sorbents by Different Testing Conditions . . . 13
- 2.2 Research on CaO-Based Pellets with Cement Binders . . . 13

3 Theory **15**
3.1 Pelletization Techniques . . . 15
3.2 Formation and Growth of Granules . . . 15
3.3 Characterization Methods . . . 17
3.3.1 Nitrogen Adsorption/Desorption . . . 17
3.3.2 Mercury Intrusion Porosimetry (MIP) . . . 19
3.3.3 CO_2 Capture Performance Test with a Thermogravimetric Analyzer (TGA) . . . 20
3.3.4 X-Ray Diffraction (XRD) . . . 20
3.3.5 Scanning Electron Microscope (SEM) . . . 22
3.4 Mechanical Properties . . . 22

4 Methods and Materials **25**
4.1 Material Preparation . . . 25
4.1.1 Calcination . . . 27
4.1.2 Granulation . . . 28
4.1.3 Extrusion-Spherionization . . . 29
4.2 Characterization . . . 30
4.2.1 CO_2-sorption Capacity and Kinetic Study . . . 30
4.2.2 Surface Area and Pore Size Measurements . . . 32
4.2.3 X-Ray Diffraction Phases and Crystalline Size . . . 33
4.2.4 Morphology and Surface Structure in SEM . . . 33
4.3 Mechanical Properties Test . . . 35
4.3.1 Attrition Test . . . 35
4.3.2 Falling Test . . . 36

5 Results **37**
5.1 Large-Scale Procedure for Production of Pellet . . . 37
5.1.1 Granulation Procedure - Rotary Drum . . . 37
5.1.2 Granulation procedure - Extrusion/Spherionization . . . 39
5.2 Characterization . . . 40
5.2.1 Surface Area and Pore Size Distribution . . . 40
5.2.2 Phase Identification and Crystalline Size of Dolomite and Cement Based Pellets . . . 42
5.2.3 CO_2-Sorption/Desorption Cycles in TGA without Steam . . . 44
5.2.4 CO_2-Sorption/Desorption Cycles in TGA With Steam . . . 45
5.2.5 Up-Scaling of NO-12 - Comparing 20g vs. 100g for 68 Cycles in Steam . . . 47
5.2.6 Investigation of Pellets NO-6 . . . 48
5.2.7 Kinetic Study of Sample NO-12 . . . 49
5.2.8 Morphology and Surface of Pellets . . . 54
5.3 Mechanical Properties of Pellets . . . 56
5.3.1 Attrition Test . . . 56
5.3.2 Falling Test . . . 59

6 Discussion **61**

6.1 Large-Scale Procedure for Production of Pellet 61
6.2 Characterization 62
6.2.1 Surface Area and Pore Size Distribution 62
6.2.2 Phase Identification and Crystalline Size 64
6.2.3 High Temperature Sorption Capacity without Steam 65
6.2.4 Investigation of pellets NO-6 66
6.2.5 High Temperature Sorption Capacity with Steam 66
6.2.6 Kinetics of NO-12 68
6.2.7 Morphology and Surface of Pellets 69
6.3 Mechanical Properties of Pellets 71
6.3.1 Attrition test 71
6.3.2 Falling test 72
6.4 Future Work 73
6.4.1 Granulation and Extrusion 73
6.4.2 Surface Area, Pore Size Distribution, X-ray Diffraction and Morphology 73
6.4.3 Mechanical Properties 74
6.4.4 High-temperature CO_2 Cyclic Stability 74
6.4.5 Kinetic Study 74

7 Conclusion **77**

Bibliography **77**

Appendix **i**
A7.1 Calcination in Tube Oven i
A7.2 Rotary drum granulation procedure ii
A7.2.1 Rotary Drum Granulation Scale-Up (500g) iii
A7.2.2 Rotary Drum Granulation With 100g Calcined Dolomite and Dopants v
A7.2.3 Rotary Drum Granulation With 100g Calcined ADDA, 100g Uncalcined ADDA and Dopants ix
A7.3 Extrusion/Spherionization for Dolomite-Based Pellets xi
A7.4 More Results - Rotary Drum - calcined dolomite and ADDA xiii
A7.4.1 Surface Area and Pore Size distribution xiii
A7.4.2 Phase Identification xix
A7.4.3 NO-6 xxi
A7.4.4 Morphology and Surface of Pellets xxx
A7.4.5 BET SA vs. CO2-capacity xxxviii
A7.4.6 TGA (dry) - NO-1 vs. Raw Material of Calcined Dolomite (500-850um) xxxix
A7.4.7 Mechanical strength test xl
A7.5 Investigation of NO-6 xli
A7.6 Results- Kinetic study of sample NO-12 xliv
A7.7 Granulation with GMX-LAB Micro GRANUMEIST® Granulator xlvii
A7.7.1 Method - GMX-LAB Micro GRANUMEIST® Granulator xlix

A7.7.2 Result from Characterization using GMX-LAB Micro GRANUMEIST® Granulator l
A7.8 Raw data files - BET lix
A7.9 PDF Overview of Granulation Experiments cxliv
A7.10 Raw data - Mercury Intrusion Porosimetry clviii
A7.11 Raw data TGA clxix
A7.11.1 Raw data from TGA-dry clxix
A7.11.2 Raw data from TGA w/Steam cxcv
A7.12 Temperature scanning program cciv
A7.13 Product Spezification for Cement Fondu ccvii
A7.14 Risk assessment ccx
A7.15 Theory - Mercury Porosimetry ccxxi

List of Tables

1.1 Chemical properties of a calcium aluminate cement (Cement Fondu) . . . 9

4.1 Samples prepared based on calcined dolomite (CaO . MgO) as raw material 26
4.2 Samples prepared on basis of calcined ADDA and uncalcined ADDA . . 26
4.3 Calculated theoretical max CO_2-capture capacity for the dolomite-based sorbents . . . 27
4.4 Specifications for Ankarsum rotary drum. . . . 28
4.5 Specifications for extruder. . . . 30
4.6 CO_2 concentrations for the 10 cycles in the kinetic study of sample NO-12. 31
4.7 Conditions for kinetic study . . . 32

5.1 Yield (%) . . . 39
5.2 BET surface area, BJH average pore diameter and BJH pore volume . . . 40
5.3 Pore diameter for the dolomite-based samples . . . 42
5.4 Crystalline size . . . 43
5.5 Summary from dry CO_2-sorption capacity measurement . . . 44
5.6 Summary of the CO_2-sorption capacity for 34 cycles in presence of steam 46
5.7 Shericity measurement . . . 56

A7.1 Calcination check . . . ii
A7.2 Granulation in Specialization project 2017 . . . xlvii
A7.3 Granulation in Specialization project 2017 . . . li
A7.4 Granulation in Specialization project 2017 . . . li
A7.5 Granulation in Specialization project 2017 . . . lii
A7.6 Granulation in Specialization project 2017 . . . lii
A7.7 Granulation in Specialization project 2017 . . . lii
A7.8 Granulation in Specialization project 2017 . . . lvii
A7.9 Parameters for the 10 cycles in the kinetic study of sample NO-12. . . . ccxxiii

List of Figures

1.1 MBCL technology 4
1.2 Equilibrium curve for carbonation/calcination 5
1.3 Schematic of the gas-solid reaction model 6
1.4 Schematic of the different stages in sorbent conversion 7
1.5 Sintering phenomena of the CaO-sorbent in sorption/desorption cycles . . 7

3.1 Formation and growth mechanism of pellet 16
3.2 Schematic of agglomeration and granulation 16
3.3 Isotherms and hysteresis 19
3.4 X-ray diffraction and Braggs law 21
3.5 Operational mode for SEM 22
3.6 Pellet crush strength versus particle porosity 23

4.1 Calcination procedure in air 28
4.2 Rotary drum kitchen machine used as Granulator/Mixer 29
4.3 Extrusion 30
4.4 SEM specimen holder. 34
4.5 Sphericity measurement with Fiji Image Analysis 34
4.6 Ball miller (Cat) roller (RM10W-30V Cat) machine. 35
4.7 A 1.5m long glass tube used to simulate the fall of pellets in MBCL . . . 36

5.1 Granulation procedure 38
5.2 Result of large-scale granulation 38
5.3 Adsorption isotherms 41
5.4 BJH pore size distribution 41
5.5 MIP pore size distribution 42
5.6 XRD phases 43
5.7 Dry sorption/desorption cycles for the dolomite-based samples 44
5.8 Dry sorption/desorption cycles for the cement ADDA-based samples . . . 45
5.9 34 sorption/desorption cycles in presence of steam 46

5.10 Small-scale vs. large-scale granulation 47
5.11 Calcination check of pellet NO-6 48
5.12 CO_2-sorption curve for 5mg and 30mg sample load 49
5.13 CO_2-sorption curve for three different temperatures 50
5.14 Time derivative for the slope of the CO_2-sorption curve for 620°C and 650°C in the 10 cycles 51
5.15 CO_2-sorption at 650°C for different granule size 52
5.16 Percentage of max sorption capacity for different granule size 53
5.17 Time derivative for the slope of the CO_2-sorption curve at different partial pressure of CO_2 for different granule size 53
5.18 Time derivative for the slope of the CO_2-sorption curve at 2% CO_2 concentration for different cycles 54
5.19 SEM pictures of fresh pellets 54
5.20 SEM pictures of spent pellets 55
5.21 SEM pictures of dolomite-based pellets 55
5.22 SEM pictures of dolomite-based pellets 55
5.23 Binding mechanism for the granulation process 57
5.24 Attrition test 58
5.25 Attrition residue 58
5.26 Falling test on large granules (residue between 500-250μm) 59
5.27 Falling test on large granules with residue between 250-0μm 59
5.28 Falling test on smallest granules 60
5.29 Falling test residue 60

A7.1 SEM pictures of granulation batch at 500g iv
A7.2 BET isotherms for dolomite-based samples xiii
A7.3 BET isotherms for dolomite-based samples xiv
A7.4 BET isotherms for cement ADDA-based samples xv
A7.5 BJH pore size distribution plot for dolomite-based samples. xvi
A7.6 BJH pore size distribution plot for dolomite-based samples. xvii
A7.7 BJH pore size distribution plot for cement ADDA-based samples. xviii
A7.8 Isotherms test 3 xix
A7.9 XRD phases of NO-1 xx
A7.10 XRD phases of NO-3 xx
A7.11 XRD phases of NO-3 xxi
A7.12 XRD phases of NO-6 xxi
A7.13 XRD phases of NO-6 xxii
A7.14 XRD phases of NO-8 xxii
A7.15 XRD phases of NO-8 xxiii
A7.16 XRD phases of NO-10 xxiii
A7.17 XRD phases of NO-10 xxiv
A7.18 XRD phases of NO-10 xxiv
A7.19 XRD phases of NO-10 xxv
A7.20 XRD phases of NO-12 xxv
A7.21 XRD phases of NO-12 xxvi
A7.22 XRD phases of NO-12 xxvi

A7.23 XRD phases of NO-12 . . . xxvii
A7.24 XRD phases of NO-20 . . . xxvii
A7.25 XRD phases of NO-20 . . . xxviii
A7.26 XRD phases of NO-20 . . . xxviii
A7.27 XRD phases of NO-21 . . . xxix
A7.28 XRD phases of NO-22 . . . xxix
A7.29 XRD phases of NO-22 . . . xxx
A7.30 XRD phases of NO-23 . . . xxx
A7.31 Calcined cement ADDA pellets. Resolution x50. . . . xxxi
A7.32 Calcined cement ADDA pellets. Resolution x50. . . . xxxi
A7.33 Calcined cement ADDA pellets. Resolution x150. . . . xxxii
A7.34 Uncalcined cement ADDA pellets. Resolution x150. . . . xxxiii
A7.35 Calcined cement ADDA pellets. Resolution x300. . . . xxxiv
A7.36 Uncalcined cement ADDA pellets. Resolution x300. . . . xxxv
A7.37 SEM pictures NO-20 . . . xxxvi
A7.38 SEM pictures NO-21 . . . xxxvi
A7.39 SEM pictures NO-22 . . . xxxvi
A7.40 SEM pictures NO-23 . . . xxxvii
A7.41 SEM pictures NO-1 . . . xxxvii
A7.42 SEM pictures NO-3 . . . xxxvii
A7.43 SEM pictures NO-6 . . . xxxviii
A7.44 SEM pictures NO-8 . . . xxxviii
A7.45 SEM pictures NO-10 . . . xxxviii
A7.46 SEM pictures NO-12 . . . xxxix
A7.47 BET surface area vs. CO2 sorption capacity in cycle 1. . . . xxxix
A7.48 Crystalline size of CaO vs. CO2 sorption capacity in cycle 1. . . . xl
A7.49 TGA: NO-1 vs. grains of raw calcined dolomite with size 500-850um . . xl
A7.50 Attrition residue . . . xli
A7.51 Attrition residue . . . xli
A7.52 Attrition residue . . . xli
A7.53 Attrition residue . . . xlii
A7.54 TGA: 11 cycles of NO-6 pellets vs. milled pellets (5 min) . . . xlii
A7.55 Calcination Check of pellet NO-6 using TGA with MS . . . xliii
A7.56 Calcination Check of pellet NO-6 using TGA with MS . . . xliv
A7.57 BET isotherms and BJH pore size distribution for NO-6 . . . xliv
A7.58 Kinetic study . . . xlv
A7.59 Kinetic study . . . xlv
A7.60 Kinetic study . . . xlv
A7.61 Kinetic study . . . xlvi
A7.62 Kinetic study . . . xlvi
A7.63 Kinetic study . . . xlvii
A7.64 GMX-LAB Micro GRANUMEIST® Granulator/Mixer . . . xlviii
A7.65 Granulation in Specialization project 2017 . . . xlix
A7.66 Granulation in Specialization project 2017 . . . xlix
A7.67 Granulation in Specialization project 2017 . . . l

A7.68 Granulation in Specialization project 2017 li
A7.69 Granulation in Specialization project 2017 liii
A7.70 Granulation in Specialization project 2017 liii
A7.71 Granulation in Specialization project 2017 liv
A7.72 Granulation in Specialization project 2017 liv
A7.73 Granulation in Specialization project 2017 lv
A7.74 Granulation in Specialization project 2017 lvi
A7.76 Granulation in Specialization project 2017 lviii
A7.75 Granulation in Specialization project 2017 cxcv
A7.77 TGA - Raw data NO-1 17 cycles cxcvi
A7.78 TGA -Raw data NO-1 17+17 cycles cxcvii
A7.79 TGA -TGA steam, NO-3 17 cycles. cxcviii
A7.80 TGA steam, NO-8 17 cycles. cxcviii
A7.81 TGA steam, NO-8 17+17 cycles. cxcix
A7.82 TGA steam, NO-10 17 cycles. cxcix
A7.83 TGA steam, NO-10 17+17 cycles. cc
A7.84 TGA steam, NO-12 17 cycles cc
A7.85 TGA steam, NO-12 17+17 cycles cci
A7.86 TGA steam, NO-12 17+17+17 cycles ccii
A7.87 TGA steam, NO-12 17+17+17+17 cycles cciii
A7.88 Baseline correction cciv

List of Abbreviations

A	Al_2O_3
BET	Brunneuer-Emmet-Teller
BJH	Barret-Joyner-Halenda
C	CaO
CAC	Calcium aluminate cement
CaL	Carbonate looping
CCL	Combustion Carbonate looping
CCS	Carbon Capture and Storage/Sequestration
$CFCB$	Circulated fluidized bed combustion
FBC	Fluidized bed combustion
GC	Gas chromatography
H	H_2O
IR	Infrared spectrometer
$IUPAC$	International union of pure and applied chemistry
$MBCL$	Moving bed carbonate looping
MBR	Moving bed reactor
MS	Mass spectrometer

OPC Ordinary Portland cement

$PCCC$ Post-combustion CO_2 capture

S SiO_2

SEM Scanning electron microscopy

SER Sorbent enhanced reforming

$SEWGS$ Sorbent-enhaced water gas shift

TGA Termogravimetric analysis

XRD X-ray diffraction

List of Symbols

Symbols	Description
A	Area over which pressure is applied
C	Constant in the BET-equation
C_{CO2}	CO_2 concentration
$C_{CO2,e}$	Equilibrium CO_2 concentration
d_{hkl}	Distance between two h,k,l lattice planes in XRD measurement
d_p	Average pore diameter
f_R	Resisting force
f_{ext}	Externally pressure
gs	Granule size
D	Diamater in pore
ΔH°_{298K}	Standard enthalpy of formation at 298K
k	Constant in Schrerrer equation
k_r	Kinetic rate expression constant
L	Crystalline size
m	Order of the rate expression
n	Order of reflection or Order of the rate expression
P	Partial pressure or pressure applied in mercury intrusion method
P_0	Saturation pressure at experimental temperature
q_1	Heat of adsorption in first monolayer
q_L	Heat of condensation of the adsorbate
r	Radius of pore
R	Gas constant
S_{BET}	BET surface area
t	Time
T	Absolute temperature
V	Adsorbed volume by BET method or molar volume of liquid nitrogen
V_m	Volume adsorbed at monolayer coverage

V_p	Pore volume
X_{CaO}	Practical CaO conversion
X_D	Molar conversion of CO_2 in diffusion controlled regime
X_k	Molar conversion of CO_2 in reaction controlled regime
X_N	Molar conversion of CO_2
X_t	Weight of sorbent at given time
X_0	Weight of completely calcined material
X_u	Maximum carbonation conversion
Y_{weight}	Weight on Y-axis
β	Breadth of half-peak height of an XRD line
Θ	Angle between incoming X-rays and the normal to the reflecting lattice plane or contact angle in BET method or surface tension for mercury intrusion method
λ	X-ray wavelength or photon wavelength
σ	Surface tension of liquid nitrogen
γ	Surface tension of mercury

Chapter 1

Introduction

The Paris Agreement aims to reduce greenhouse gas emission to keep the temperature rise below 2°C. Carbon dioxide gas is claimed to be the main contributor of the temperature increase, and power production from fossil fuels accounts for one-third of the CO_2 emissions [2]. To reach the goal set in the Paris Agreement, new technology and financial aspects are important. Also, to reduce the CO_2 emissions, energy consumption can be reduced by using more energy efficient systems, or using alternative energy sources, or reduce emission by carbon capture and sequestration (CCS) [3]. Three types of CO_2 capture technologies are already in use; post-, pre-, and oxy- combustion. Post-combustion CO_2 capture (PCCC) is separation of CO_2 from the gas stream (for example flue gas and other off-gases), and can be achieved by cryogenic distillation, membrane purification, absorption with liquids, and adsorption using solids. There are several drawbacks with the capture technologies already in use. Cryogenic distillation is costly due to the energy required, and membrane purification need improvement regarding CO_2 permeability, selectivity and cost [4]. Amine scrubbing has in the latest years been used as the preferred solution for post-combustion to separate carbon dioxide from natural gas and hydrogen. Amines are an aqueous solution in which contains alkanoamines. The alkanoamines act as the absorbent reacting with acidic CO_2 forming dissolved carbamates and bicarbamates. The major drawback with the amine technology is that it is costly, operated under low temperature (40-150°C) [5], and energy intensive in regeneration of the solvent [6]. In post-combustion, the separated and captured CO_2 must be stored, thus the technology is called Carbon Capture and Storage. To store the carbon dioxide, it must be compressed, and injected deep underground in secure geologic formations, and ensure that it remains stored there indefinitely.

1.1 Adsorption Using Solids

Solids can also be used to capture CO_2, either as adsorbents or sorbents. The adsorption can either be a physisorption process, or it via strong chemisorption interactions [2]. For CO_2 separation, the solid operates in cycles where CO_2 is adsorbed on the solid before it is subsequently desorbed. To be able to handle several cycles, the adsorbent quality is substantial. An ideal adsorbent should; have infinite regenerability, excellent stability, be able to handle a wide range of operating condition, fast desorption and adsorption kinetics, and a large adsorption capacity. Different physisorbents can be zeolites and activated carbons, known for their microporous and mesoporous structure. Zeolites have favorable properties such as having the fastest CO_2 adsorption kinetics and relatively high adsorption capacities. Zeolites have their major weakness in handling the flue gas. Flue gas contains a lot of H_2O which compete with CO_2 for adsorbing on the active cites of the zeolite, and this effect can have both positive and negative outcomes depending on the CO_2 concentration.

Activated carbon has its benefits in low cost wide availability of carbon sources, thus it is cheap in large scale. Production of activated carbon can either be by coal, industrial byproducts, wood or other biomass resources. Pore size distribution, pore structure and active surface can vary a lot depending on raw material used, thus adsorption properties are highly variable. Over all, the adsorption capacity at ambient conditions of activated carbon is lower than that of zeolites. While zeolites are sensitive towards water in the flue gas, activated carbons are less affected. Another advantageous property with activated carbon as CO_2 capture material is the easy regeneration. Both activated carbon and zeolites have limitation in temperature, and cannot capture CO_2 above 300°C, thus they will be useless in processes where CO_2 must be separated from the hot flue gas (500°C), unless more money in spent on cooling and additional cost [7].

1.1.1 Dolomite ($CaMg(CO_3)_2$) as Sorbent Material

Alkaline earth metal oxides such as CaO and MgO is two types of chemisorbents [2]. When reacting with CO_2, they form forms mono- and multidentate species. Monodentate means that one atom in the ligand binds to the metal, whereas several atoms in the ligand binds to the metal oxide for multidentate species. Some metal oxides have basic sites and the acidic nature of CO_2 will therefore adsorb on these sites. This thesis will not cover the adsorption of CO_2 by CaO-based sorbents, but the sorption process to capture CO_2. CaO is a metal oxide with strong basic sites, and can capture CO_2 via sorption on the active sites forming $CaCO_3$ as given in equation 1.1.

$$\mathrm{CaO} + \mathrm{CO_2} \rightleftharpoons \mathrm{CaCO_3} \qquad \Delta H^{\circ}_{298\mathrm{K}} = -179 kJ/mol \tag{1.1}$$

Dolomite ($CaMg(CO_3)_2$) and limestone ($CaCO_3$) are minerals containing calcium. The advantages with dolomite and limestone are their low cost, high availability and good sorption capacities. Dolomite can be used in different processes to capture CO_2 at high temperature. Post combustion carbonate looping (CCL), sorbent enhanced reactions such

as sorbent-enhanced water gas shift (SEWGS) or sorbent-enhanced reforming (SER) for production of high purity H_2 is some of the processes were dolomite can be applied [8]. A technology called Moving Bed Carbonate Looping (MBCL) is a post combustion technology where CO_2 is captured via sorption. To use calcium oxide as CO_2-capture sorbent, certain criteria are desired:

- High sorption capacity (for CaO the theoretical is 0.785 g CO_2/g sorbent and for MgO theoretical is 1.092 g CO_2/g sorbent) at high temperature [9]
- Cycle stability
- High availability
- Low cost
- Easily regenerated (4.042 kJ/g of CO_2 for CaO and 2.681 kJ/g of CO_2 for MgO)
- Stable in the presence of steam
- Fast kinetics

MBCL Process Description

The MBCL technology uses carbonation and calcination cycles where CO_2 is captured and released. A figure of the moving bed carbonate looping is given in figure 1.1 where the reactor to the left is a moving bed reactor (MBR). The flue gas enters in the CO_2 capture reactor (carbonator), where the CO_2 in the flue gas reacts with CaO-based sorbent at temperatures between 570-600°C according to equation 1.1. The residence time should be a few minutes. Afterwards, the $CaCO_3$ is regenerated in a calciner before the sorbent is blown around by gas. The pure CO_2 is removed in the calciner, and subsequently stored.

Heat integration is also beneficial for a more thermally efficient process as temperatures up to 950°C is necessary for regeneration of the sorbent. The efficiency penalty is relatively low (7-8%), where it is the oxygen requirement for heat production in the calciner, that accounts for 2-3% of this penalty [10][11]. However, despite the many advantages, dolomite has much slower sorption kinetics than physisorbents. The thermodynamics of the equilibrium is another limitation. [12].

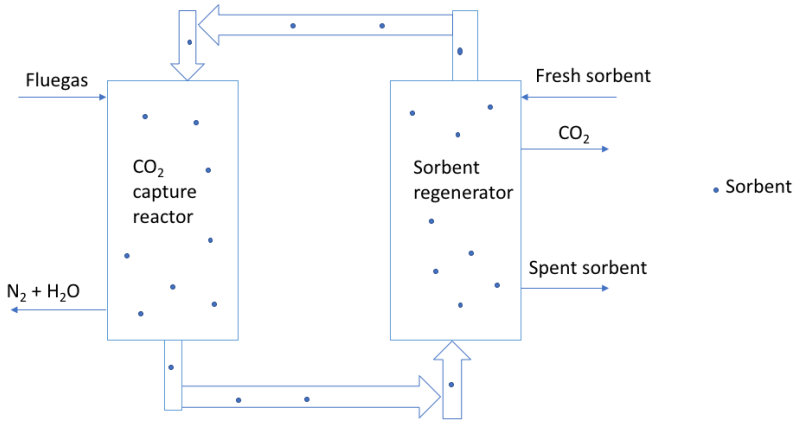

Figure 1.1: A simplified schematic of sorbent circulation in the moving bed carbonate looping (MBCL) technology.

Thermodynamics of Cao-Based Sorbent

The reaction in equation 1.1 is an equilibrium reaction depending on pressure and temperature as shown in the equilibrium curve in figure 1.2 [13]. It can proceed both ways, and the forward reaction is exothermic and is called carbonation or sorption [8]. This means that calcium carbonates must be heated at high temperature (approximately 900-950°C) to proceed backwards. This reaction where carbon dioxide is released is called calcination. During calcination, the $CaCO_3$ and $MgCO_3$ form $CaO \cdot MgO$. The CaO is an active component to capture CO_2 up to 757 °C, whereas MgO (and $Mg(OH)_2$) only have moderate sorption capacities and will only capture CO_2 up to 400 °C [14]. MgO is therefore an intermediate temperature sorbent, and CaO is a high temperature CO_2 sorbent.

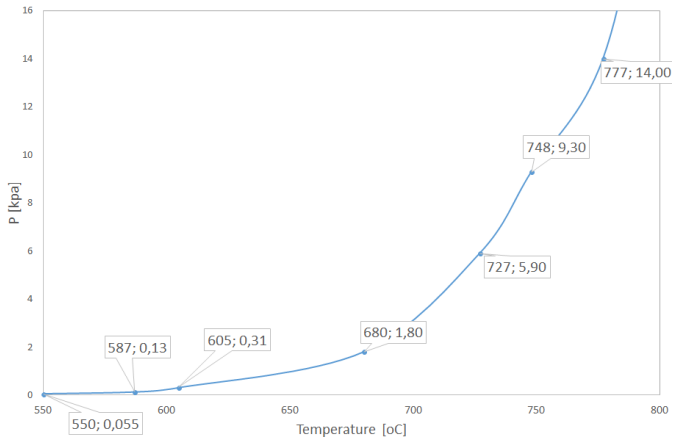

Figure 1.2: Equilibrium curve for reaction 1.1 [13].

The calcination of dolomite is given in equation 1.2, and if the reaction occurs at lower temperatures, as described above, the product is called half-calcined dolomite [15]. This calcination stage is also more rapid, and the fact that MgO has lower molar volume than $MgCO_3$ will lead to higher porosity of the half-calcined dolomite.

$$MgCO_3 \cdot CaCO_3 \rightarrow MgO \cdot CaCO_3 + CO_2 \tag{1.2}$$

Further calcination will result in $MgO \cdot CaO$ and carbon dioxide, equation 1.3. When the dolomite is fully calcined, the porosity and surface area will be at its highest.

$$MgO \cdot CaCO_3 \rightarrow MgO \cdot CaO + CO_2 \tag{1.3}$$

Chemisorption of CO_2 on CaO happens both on oxide surface and in the lattis, whereas sorption of CO_2 by MgO only occur on the oxide surface [2]. Due to low reactivity between CO_2 and MgO, the magnesium oxide has an inert function acting as the catalyst support. This support function of MgO serve to keep the calcium oxide particles at fixed distance. The $CaCO_3$ sinter at 527°C, whereas MgO sinter at 1289°C (higher melting point) [12][16]. Thus, MgO functions as a physical barrier for $CaCO_3$, which is the reason for the better sintering resistance of dolomite than that of limestone. After calcination, the aggregate consisting of CaO and MgO contain small pores. This pore porosity makes the CO_2 able to enter the interior of the aggregate.

Dolomite (1:1 $MgO \cdot CaO$) will have lower initial sorption capacity of CO_2 than that of limestone because $MgO \cdot CaO$ have lower amount of the active component CaO, or the fact that MgO block some of the active sites on CaO [17]. But, after several cycles, the dolomite shows better stability than limestone due to the MgO content. Different weight percent of MgO can also increase the CO_2-cyclic stability.

For high CO_2-capture efficiency in the calcination and carbonation cycles, the partial pressure of CO_2 is very important [12]. For high CO_2-uptake, a high CO_2 partial pressure if favored in the carbonation surroundings [18]. The CO_2 partial pressure and CO_2 equilibrium pressure differences act as the driving force for the sorption and desorption.

Kinetics of CaO-based sorbent

The rate of the carbonation reaction is fast when growing the carbonate layer (illustrated in figure 1.4 as stage 1) [16], and this stage is called the reaction controlled regime (fast). This stage is affected by the surface area of the particles, and the growth of product layer of $CaCO_3$ inhibits fast kinetics [12]. Both temperature and partial pressure of CO_2 also influence the fast reaction rate (first stage), and the carbonation reaction rate increases as the temperature increases. Then the reaction is followed by a slow step (stage 2) called product layer diffusion limited regime (slow), that in the end reaches a conversion plateau (stage 3) [2]. Gas-solid reaction models can be used to describe the carbonation reaction, and figure 1.3 is such a model [19].

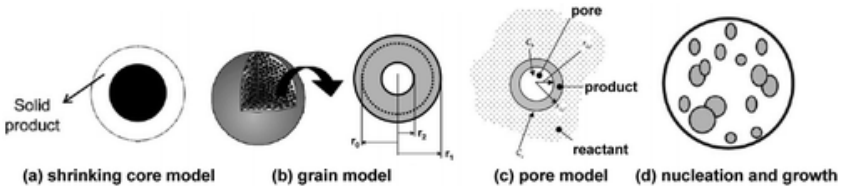

Figure 1.3: Schematic of the gas-solid reaction model [19]. (a) is a shrinking core model assumed as a nonporous sphere and a layer of solid product is outside of the solid reactant [20]. (b) Is a grain model [21][22]. (c) The pore model [23]. (d) Nucleation and growth model [24].

This model has rate expression as given in equation 1.4 [25] [26].

$$\frac{\mathrm{dX_{CaO}}}{\mathrm{dt}} = \mathrm{k_r}(1-(\mathrm{X_{CaO}}/\mathrm{X_u}))^{\mathrm{m}}(\mathrm{C_{CO2}}-\mathrm{C_{CO2,e}})^{\mathrm{n}} \tag{1.4}$$

Where X_u is the maximum carbonation conversion, X_{CaO} is the practical CaO conversion, k_r the kinetic rate expression constant, and C_{CO2}-$C_{CO2,e}$ is the average CO_2 concentration. And m and n are just the order of the equation. The nucleation and growth model are describing the kinetic of some gas-solid reaction that is showing a S-curve (sigmoid curve) when solid conversion is plotted versus time, as when $CaCO_3$ conversion is plotted with respect to time (minutes) [19].

For decarbonation reaction, the formation of $CaCO_3$ is a substantial step. Because when CO_2 and CaO is starting to form a product layer of $CaCO_3$, it gets more difficult for the carbon dioxide gas to get in contact with the CaO and CO_2 must diffuse through the product layer [19]. Further production of surface layer, $CaCO_3$, will tighten the pores, and the space for CO_2 to enter will be limited (pore blockage). This affects the surface reaction, pore diffusion and product layer diffusion. The rate of the carbonation reaction

slowly decreases due to pore filling and this stage is hardly affected by CO_2 pressure. The mean critical product layer thickness is found to be in the range from 38-70nm [27][28] [29]. This critical product layer is used to describe maximum conversion level.

After several cycles the pore will get so small and the particles tend to come so close that they might merge into one solid piece. The phenomena are called sintering and leads to changes in the particle morphology. The sintering process increases with increasing partial pressure of steam and CO_2, and with impurities [30]. An illustration of this sintering process is given in figure 1.5. Sintering and pore blocking will lead to capacity reduction during the carbonation/calcination cycles, and the CO_2 capture capacity of the CaO-based sorbent will decrease. Sintering occurs due to calcination above Tamman temperature for $CaCO_3$ (533 °C) [31]. Despite the capacity loss during the first cycles, adsorption capacities of CaO stabilizes after a while.

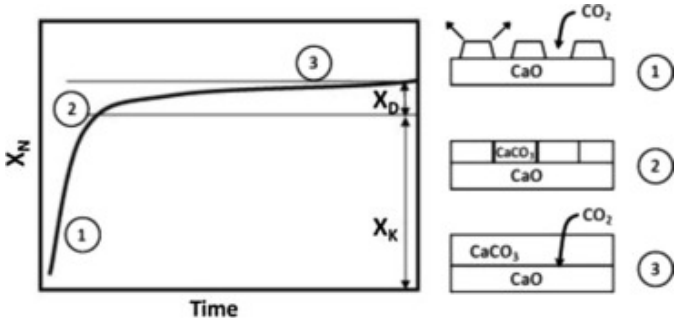

Figure 1.4: Schematic of the different stages in sorbent conversion. Stage 1 is the fast reaction controlled stage, stage 2 is a slower diffusion limited stage and complete conversion is at stage 3. X_N is molar conversion of CO_2 in each cycle, X_k is conversion of CO_2 in the reaction controlled stage, and X_D is conversion of CO_2 in the diffusion controlled regime [16].

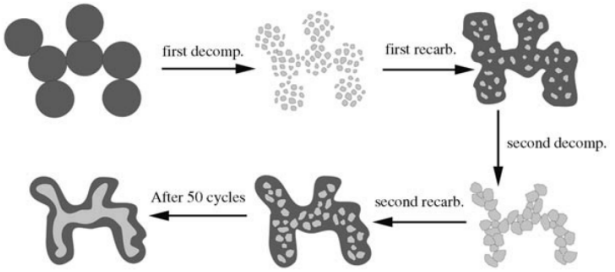

Figure 1.5: Sintering phenomena of the CaO-sorbent in sorption/desorption cycles. The dark gray illustrates the $CaCO_3$ while the light gray illustrates the CaO. The fist decomposition of calcium carbonate results in dispersed active calcium oxide, but the recarbonation in the next step is not complete. Further sintering is prevented after several cycles with incomplete recarbonation [2].

Thus, the degree and rate of CO_2 uptake of the CaO-based sorbent are affected by tem-

perature, pressure, residence time and initial CO_2 concentrations [32]. Reaction rate and capacity loss during adsorption/desorption cycles are parameters that limits the regenerability of calcium oxide and the sorbent material must be replaced after a while. This will in turn result in more down time at the plant. Thus, it is desired to improve the regenerability of the sorbent.

In addition to sintering, attrition/fragmentation between particles and between particles and the reactor wall is producing fines, which is reducing the reactivity of the sorbents. Particle size, reactor bed temperature, gas velocity, heating rate, configuration and size of the plant are all factors that have an impact on the attrition [16]. Physical characteristics such as particle size, porosity, surface area, etc. can be modified to increase the regenerability [2]. A stable pore structure and increased surface area are desired, and these material properties can be modified by; techniques using rigid supports, use of dopants (Al_2O_3, MgO, La_2O_3, TiO_2 and SiO_2 etc.), preparation of nanoparticles, use of different synthetic precursors and thermal pre-treatment. When using dopants, the precursor of both the sorbent and sorbent support, and mixing techniques of the sorbent and support affects the CO_2 capacity and cyclic stability [12].

1.1.2 CaO-Based Pellets with Cement Binder

The CaO-based sorbents can also be re-used by milling and shaping by making pellets [33]. The spent sorbent can be reused by hydration, if water is added according to equation 1.5. Calcium aluminate cements (CAC) can be used as binder for palletization of powdered dolomite. Properties like low cost, good setting performance and possibilities for use at extremely high temperatures are some of the advantages of using CAC as binder [34]. Thus, the refractory material can be used in corrosive environments. The calcium aluminate cement mainly consists of calcium- and alumina-containing compounds, as for example Al_2O_3. The alumina in the cement serves to give the dolomite-based pellets improved CO_2 sorption several sorption/desorption cycles.

$$\mathrm{CaO} + \mathrm{H_2O} = \mathrm{Ca(OH)_2} \qquad \Delta \mathrm{H}^{\circ}_{298\mathrm{K}} = -65\mathrm{kJ/mol} \tag{1.5}$$

Two types of alumina containing cements is typical, the calcium aluminate cement (CAC) and the ordinary Portland cement (OPC). They differ from each other due to chemical make-up and that CAC contains more alumina and less silica [35]. Cement Fondu is on type of calcium aluminate cement and have a alumina content at approximately 40%. The chemical composition of Cement Fondu is given in table 1.1 and more specifications are given in Appendix A7.13.

Characteristics of the CAC are its high early strength gain, heat of hydration and it has a compression strength of 4629 MPa (after 4 hours in 20°C). With increasing temperature, the strength gain will also increase. Further, the water/cement ratio (w/c) also affect the mechanical strength of the cement where lower w/c ratio serves to give lower strength of the material. The water/cement ratio also has an effect hydration and on early-age properties as setting time, semi-adiabatic temperature and autogeneous shrinkage [36].

Poisoning in the cement or dolomite also affects the hydration, where calcium from the aggregate can contribute to more stability in the hydrate.

Not every cement material behaves the same way. Their reaction rate can be different, and they have a tendency of forming different solid phases during hydration [37]. The hydration is complex, and throughout hydration, all minerals dissolve into the same pore solution. The reactions of CAC are depending on the amount of sulfate ions present in the pore solution. According to reaction 1.6, the $(CaO)_3$ is very soluble and will during hydration with water (H), form calcium aluminate hydrates (C_3AH_6). Cement chemistry notation is used in reaction 1.6, where C=CaO, S=SiO_2, A=Al_2O_3 and H=H_2O. The first reaction is fast, and the second reaction is slow.

$$2\,C_3A + 21\,H \rightarrow C_4AH_{19} + C_2AH_8 \rightarrow 2\,C_3AH_6 + 9\,H \tag{1.6}$$

Table 1.1: Chemical properties of a calcium aluminate cement (Cement Fondu). More specification is given in Appendix A7.13.

Component	**Usual range** (%)	**Specification limit** (%)
Al_2O_3	37.5-41.0	> 37.0
CaO	35.5-39.0	<41.9
SiO_2	3.5-5.5	<6.0
Fe_2O_3	13.0-17.5	<18.5
MgO	-	< 1.5
SiO_2	-	< 4.0

Hydration kinetics of cement material are depending on mixing conditions such as addition sequence of the components and the curing temperature [38, 39]. The kinetics for hydration is also determined by formation of finer particles acting as nuclei for the precipitation of the hydrates. The hydration kinetics of cement and mixing energy are linked by the fact that hydration kinetics increase by increased temperature, and the increase in temperature occurs when there is friction between particles. Thus, the hydration kinetics and mixing energy can be controlled by mixing time or by controlling the viscosity. The viscosity is controlled by the intensity of the mixing.

For a mix of CaO/MgO and aluminate cement, the Al_2O_3 in cement will react with CaO according to equation 1.7 and form mayenite ($Ca_{12}Al_{14}O_{33}$). Mayenite has high Tamman temperature and will inhibit sintering of CaO, thus improving the cyclic stability of the CaO-based pellets [12].

$$12CaO + 7Al_2O_3 \rightarrow Ca_{12}O_{14}O_{33} \tag{1.7}$$

1.2 Main Goal

The main goal of this thesis is to develop a procedure for making large-scale pellets for high temperature CO_2-capture for the use in MBCL technology. Calcium aluminate cement (CAC) and water should be added as liquid binder, in addition to other additives to obtain pellets with good CO_2-capture capacity and stability at high temperature, and good mechanical properties.

Chapter 2

Literature Review

2.1 Research on Improved Stability of CaO-Based Sorbents

2.1.1 Improved Stability of CaO-Based Sorbents by Doping

Doping by titanium-, zirconium- and aluminum nanoparticles have been investigated to see if an increased CO_2 capture/regeneration cycle stability at high temperature was achieved [40]. The cyclic stability was tested for 30 cycles with sorption in 10% dry CO_2 at 600 °C and desorption at 850°C in N_2 flow. Results showed a lowered capacity compared to pure calcined dolomite, but the cyclic stability of the doped dolomite seemed to be improved. In another study, the same authors further investigated the Zr-doped dolomite [8]. They studied the deactivation trend for the cyclic CO_2 sorption/desorption. Result demonstrated improved cyclic stability at rapid sorption-desorption cycling. A high Zr-content (5wt%) lowered the surface area due to pore blocking by Zr but using 1wt% Zr the sorbent showed more stable cyclic properties in a fixed bed reactor using short sorption time.

The use of supports with a higher Tamman temperature than that of the temperature of carbonation/calcination has also been shown to improve the cyclic stability of the CaO-based sorbent [31]. High-performance CaO-based CO_2 sorbents were developed on Al_2O_3 and MgO support. The two CaO-based sorbents were prepared by Pechini and RF carbon-gel templating methods respectively. The morphology of the two developed sorbents were of nano- and micro structure. When using MgO as support, the RF carbon-gel method was better than the Pechini method regarding cyclic stability. Result showed 300 % more CO_2 uptake for 10 cycles of carbonation/calcination for the synthetic sorbent than that of limestone.

2.1.2 Improved Stability of CaO-Based Sorbents by Different Preparation Methods

Researchers have also found that the calcination procedure affects the CO_2-uptake capacity of dolomite [15]. A new calcination atmosphere was tested where 100% N_2 and 50/50% CO_2-N_2 were used, in addition to a novel pre-treatment method the sorbent was half-calcined in CO_2 with additional calcination in pure nitrogen as atmosphere. The best results were found for the novel pre-treatment method in addition to short calcination under severe conditions and moderate carbonation times (30 min). The CO_2-capture capacity was improved by 24 % for 150 sorption/desorption cycles, claimed to be due to the structural changes in the lattice of the dolomite. The one-step pre-treatment was less stable in the TGA than the porosity of sorbent pre-treated by the new method.

CaO-based sorbents can be made in various ways. Different preparation techniques as wet mixing, co-precipitation and sol-gel auto-combustion synthesis have been tested [41]. Various mixing of additives was also tested to make calcium-based sorbents with additional Al_2O_3. The preparation method strongly influences the characteristic of the sorbents, such as CO_2 capture capacity and stability, due to morphology and porosity changes. The sorbents prepared by sol-gel method showed very good sorption capacities while the sorbents from co-precipitation method did not. Also, the Al_2O_3 gave a positive effect in addition to good stability for sorbents originating from wet-mixing. The aluminum was present as Al_2O_3, $Ca_{12}Al_{14}O_{33}$ or $Ca_3Al_2O_6$.

Calcium oxide-based sorbents have also been made with a screw extruder mixing calcium hydroxide and cement (37wt% CaO and 39.8wt% Al_2O_3) [42]. The production method is also easy to scale-up, thus a potential method for CaL. The cement act as binder for extrusion, and as a support. Samples exhibited relatively good mechanical strength during attrition resistance testing. Their CO_2-carrying capacity were tested in a TGA (18 cycles) were good results were obtained with a higher CO_2 capacity than that of pure CaO, claimed to be due to $Ca_{12}Al_{14}O_{33}$.

Synthetic CaO-based sorbents have been studied with doping by aluminum, zirconium, lanthanum and magnesium [43]. They were made by sol-gel auto-combustion synthesis and tested in the TGA for 50 to 100 cycles. The sorption took place in 15% CO_2 in N_2 for 30 minutes at 650 °C and desorbed at 100 %N2 for 5 minutes at 850 °C. Results revealed high initial CO_2-sorption capacity and only 30% loss in capacity after 100 cycles (except the La-doped sorbent). It was not found any parallel between initial sorption capacity and surface area, but the good capacity and stability were probably due to formation of thermally resistant compounds such as $Ca_3Al_2O_6$ and $CaZrO_3$ respectively.

Hydration can either be used as pre-treatment of dolomite or it can reactivate spent sorbent. During hydration, cracks in the CaO particle is formed. This enables CO_2 to enter the interior of the particle and higher CO_2-capture capacity is achieved [44]. Others have also reported formation of larger pores after hydration, and consequently, pore blockage is easier to prevent [45]. Steam is believed to be best for reactivation of spent sorbent due to formation of small pores [46]. The improved reactivity is not only improved in the first cycle, but also over several cycles. It has been shown that steam hydration increases the

carbonation in the diffusion controlled regime [47].

2.1.3 Investigation of Stability of CaO-Based Sorbents by Different Testing Conditions

Testing conditions for the CaO sorbents have been studied in detail by researchers [48]. Realistic testing conditions for a coal fired plant is 650°C and CO_2 concentration at 15% for CO_2 sorption, and 900-950°C and 80-100 vol% CO_2 for regeneration of sorbent. Thus, CO_2 concentration and the heating rate were varied, while realistic carbonation and calcination conditions were applied. Results demonstrated that transition from sorption at low temperature to calcination at a high temperature affects the cyclic stability of the sorbent. Also, higher heating rate promote a higher cyclic stability because $CaCO_3$, which is exposed to high temperatures, is exposed to higher temperatures for shorter period. High heating rate have been reported to be consistent with a realistic pilot plant for CO_2-capture by carbonate looping (CaL) with a residence time at 3-5 minutes (between carbonator and calciner) [49] [50]. This equals a heating rate above 50°C/min. Thus, laboratory testing might give unrealistic results if tested at low heating rates.

Steam activation has shown improved sorbent reactivity [51]. The CO_2 partial pressure is reduced when introducing steam in the calcination, thus intensify the rate of calcination of $CaCO_3$. In addition, the adsorption of H_2O of active CaO lowers the binding force between CO_2 and CaO, and the heat-transfer between steam and $CaCO_3$ is increased. Furthermore, the presence of steam in the carbonator more than doubled the activity of the sorbent due to formation of OH^-. Thus, the presence of steam during sorption seem to improve sintering and therefore increase sorbent reactivity.

2.2 Research on CaO-Based Pellets with Cement Binders

A screening of binders for pelletization of CaO-based have been studied, where Na-and Ca-bentonite and calcium aluminate cements (CA-14, CA-25, Secar 51 and Secar 80) were used as binders [34]. The capture capacity properties of binders mixed with powdered dolomite were tested for 30-35 cycles in a TGA. The bentonite binder demonstrated poor stability due to formation of calcium-silica compounds with low melting points, whereas calcium aluminate cement showed promising results. The good results were attributed the $Ca(OH)_2$ as binder. Calcium aluminate cements also have desirable qualities like fast setting and good refractory properties, low cost and high availability. The calcium alumina cement content in the sorbent were 5%, 10%, 20% and 40% and with the best result for 10% cement. Test conditions were set to 850°C for sorption in 100% CO_2 in 10 minutes, and desorption in 100% N_2 for 10 minutes. Also, results from XRD revealed phases of mayenite where Al_2O_3 (calcium aluminate cement as binder) was added as binder.

Due to the promising results with calcium aluminate cement as binder for pellets, they were further tested [52]. The binders were mixed with limestone and hydrated limes, and

their CO_2-capture capacity and stability were tested for 30 cycles in TGA. Due to promising results for the addition of 10% cement, the ratio of dolomite and cement used in the study was 9:1 resulting in 10% Al_2O_3 in the calcined pellets. The CAC doped powdered limestone achieved more than 50% conversion after 30 cycles. Mayenite ($Ca_{12}Al_{14}O_{33}$) was formed during the CO_2 cycles. The favorable performance of mayenite is the fact that aluminum nanoparticles creates a porous surface structure of the pellet, thus increase the cyclic stability of the CaO-based pellets. Another advantage of these pellets is good mechanical strength desirable for use in fluidized bed combustion (FBC) .

Comparison of powdered and pelletized MgO sorbents have been studied to investigate their mechanical properties [53]. The pelletized MgO-sorbent showed extremely good strength during a compression and an attrition test. The compression test was performed by applying pressure on the pellets until it was crushed, and the friability test were performed in a cylindrical drum at 25 rpm. These tests are gives a good prediction of the mechanical strength of the pellets before they are used in circulating fluidized bed combustion (CFCB). Results showed a crushing strength above 3N, being more than 1N, which is desired to be applied at industrial scale [54].

Other studies have investigated pellets made with 10 wt.% alumina cement and 5 – 10 wt.% starch as pore forming agent [55]. Results showed enhanced mechanical property adding the alumina cement (Al_2O_3) due to less attrition in the alumina containing pellets. They also found correlation between degree of attrition and parameters such as particle size, reaction temperature, exposure time and fluidization number. With increased temperature the thermal stress was enhanced, more CO_2 released and consequently a strong internal pressure of the granules caused changes in particle size and increased attrition rate. Also, high attrition between particles were obtained with increased fluidization number due to higher gas velocity and more frequent particle collision and particle-reactor wall collision. Smaller particles were found to experience greater attrition resistance than that of the larger particles. The addition of starch improved CO_2-uptake due to higher BET surface area and BJH pore volume. The improved CO_2 uptake was attributed the starch ability to form micropores during decomposition at about 400°C.

Re-pelletisation is also a technique with benefits such as increased porosity, enhanced capture/reactivity (unreacted CaO in the inner core of the particle can be exposed to CO_2), low cost (used sorbent and water), easily implemented and it is hydrated and pelletized at the same time without the same attrition problem as for only hydration [16]. Reactivation by steam or water and remaking (reshaping) of the pellets have been investigated [56]. The pellets were made of limestone and calcium aluminate cements (CA-14 (71% Al_2O_3 and 28% CaO)) as binder. CO_2-capture capacity was tested in a thermogravimetric analyzer (TGA) for 300 cycles (isothermal at 850°C, 100% CO_2 during calcination and 100% N2 for carbonation). New pellets were made of grounded, spent pellets and water and compared to the fresh-made pellets. Their activity was recovered and after 70 cycles, the conversion of pellets increased by 23% (33% in cycle 210). X-ray diffraction (XRD) identified mayenite ($Ca_{12}Al_{142}O_{33}$) as the major alumina compound in the re-shaped pellet, which is important for the CO_2-cycling. The morphology was restored, and pore surface area were also like the fresh-made pellet, and thus re-making of the calcium aluminate pellet is efficient.

Chapter 3

Theory

This section contains theory about granulation, characterization methods and the importance of mechanical properties of catalysts.

3.1 Pelletization Techniques

To obtain particles with desired size and shape a huge number of process options are available [57]. The processes can be spherionization, granulation, pelletization, and agglomeration. Factors like raw material, formulation, final product specification and flexibility of plant must be considered when selecting the suitable process.

3.2 Formation and Growth of Granules

Growth of pellets follow phenomena such as nucleation (A), coalescence (B), layering (C), abrasion (D) and size reduction (attrition, breakage and shatter) [58]. A schematic of the pellet formation is given in figure 3.1. The nucleation process involves formation of larger aggregates from primary particles due to mechanical forces to bring the primary particles close to each other, and different types of bonding forces [59]. These bonding forces are attractive forces (between solid-solid), interfacial forces, capillary pressure (related to mobile liquid surfaces), adhesive and cohesive force (respectively in immobile and mobile bonding bridges). The mechanical strength is not depending on forces working over a short distance (valence-, van der Waals- and electrostatic forces). For wet pellets, the interfacial and capillary pressure forces affect mechanical strength, and for dried pellets, the solid bridges dominate.

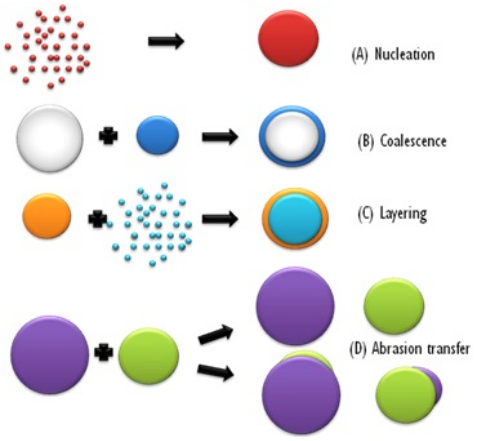

Figure 3.1: Formation and growth mechanism of pellet; (A) nucleation, (B) coalescence, (C) layering and (D) abrasion transfer [60].

Agglomeration can be used to produce coarser particles. The process is based on binding small particles/powder by a liquid to from coarser particle structures (figure 3.2 left). The wet agglomerates can then be spherionized by a granulator with high stirring rate. A figure of the granulation process is given in figure 3.2 (right). The advantageous characteristics of pellets made by granulation are the possibility to incorporate support material to stabilize the pellet structure, pore formation, and an upgraded pore structure by incorporating pore-forming materials [16]. Other benefits such as scale-up and the ability to combine oxygen carriers and catalysts, are beneficial.

The granulator is most often a batch type of equipment provided with a mixer to move material around in the bowl, a (liquid) spray on top of the bowl to introduce the liquid binder and a chopper to avoid local over wetting and lump formations. The machine can have a top- or bottom driven impeller. This makes the process more applicable in larger scale, and it is easier to clean afterwards.

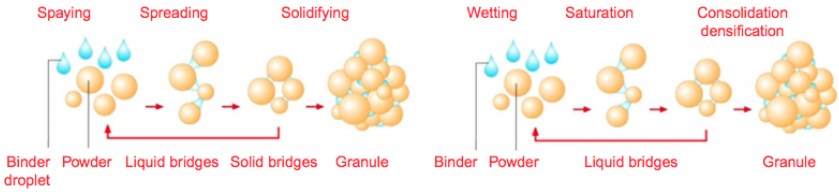

Figure 3.2: Schematic of agglomeration (left) and high-shear (wet) granulator (right) [57].

Production of pellets by extrusion-spherionization technique is used a lot. The procedure follows 4 steps; granulation, extrusion, spherionization and drying [58]. Some of the parameters affecting the pellets are moisture content, granulating liquid, mixer, extruder, extrusion speed and temperature, spherionization time and speed. The main disadvan-

tage with extrusion-spherionization is that it is a multi-step batch process. While some of the advantages are high sphericity, dust free, smooth surface and narrow particle size distribution. A low water content will result in a lot of dust, and high water content will agglomerate the pellets. The sphere density is affected by both water content and spherionizer speed [61]. Also, surface morphology of granule and torque of extrusion is affected by the water content [62].

First, a liquid is added to moisture the powder into wet mass in a mixer or granulator. Then, the material undergoes extrusion where the wet material is pressed through an orifice to produce the extrudates. The spherionization process breaks down extrudates (cylindrical shaped pellets) to spherical shaped pellets by a fast-rotating frictional base plate [59]. The frictional base plate is an important part as it is shaping the spheres. The spherionization time determine the shape of the pellet. And finally, the drying of pellets can be in room temperature, or a fluid bed dryer or in an oven.

3.3 Characterization Methods

3.3.1 Nitrogen Adsorption/Desorption

The internal surface area of catalyst can be measured by nitrogen adsorption/desorption in Brunauer Emmett Teller (BET) machine. This method is valid for material with surface areas greater than 1-2 m^2/g [63]. The BET machine measures the number of nitrogen molecules adsorbed when a monolayer is covering the surface, and the number of N_2 molecules at the surface is used to find the internal surface area of the catalyst [63]. If the material have surface area below 2m^2/g, krypton adsorption at 77K should be applied. In addition, the BET method should not be applied on micro porous catalysts such as molecular sieve zeolite due to the fact that the pores are of molecular dimensions, and will therefore not have monolayer/multilayer adsorption. In equation 3.1, the relationship between N_2 volume adsorbed (V_m at standard pressure and temperature) at monolayer coverage and at a given partial pressure (P) of N_2. The term P_0 is given as saturation pressure at the experimental temperature, V (standard pressure and temperature) is the adsorbed volume at P. The constant C is a defined in equation 3.2. Heat of adsorption in the first monolayer is defined by q_1, and q_L is the heat of condensation of the adsorbate.

$$\frac{P}{V(P_0 - P)} = \frac{1}{V_m C} + \frac{(C-1)P}{V_m C P_0} \tag{3.1}$$

$$\mathrm{C} = e^{\frac{q_1 - q_L}{RT}} \tag{3.2}$$

The equation $\frac{P/P_0}{V(1-P/P0)}$ can be plotted versus P/P_0 to get a linear plot with slope $\frac{C-1}{V_m C}$, and intercept $\frac{1}{V_m C}$. Assuming that C » 1, simplifies the slope to $\frac{1}{V_m}$. Assumptions for applying the N_2 adsorption/desorption method are:

1. Constant heat of adsorption

2. Heat of adsorption for the subsequent layer is different for that of the first one

3. Multilayer physical adsorption

A relative pressure (P/P_0) between 0.05-0.3 will give the most predictable result. The micropore and mesopore volume (V_p) can be gathered by the t-plot method where the volume adsorbed in either the inclining or declining curve, as shown in figure 3.3 (left), where the relative pressure is close to 1. Figure 3.3 (left) show the most commonly isotherms which are entitled in agreement with the IUPAC classification of physisorption isotherms [64]. Point B on the isotherm indicates where monolayer coverage is complete and multilayer adsorption begins. Type I isotherms are assigned microporous catalysts. Type II is common for nonporous or macroporous adsorbent, often calculated from equation 3.1 (when C exceeds 2), and isotherm IV are normal for mesoporous adsorbents with condensation at high pressure. The four most typical hysteresis loops are presented in figure 3.3 (right). Type H1 is classified by uniform mesopores with particles crossed by approximately cylindrical channels or made by aggregates of spherical particles in which pores have uniform size and shape [64]. H2 hysteresis is common for complex pores with network effects. Hysteresis H3 and H4 do not maintain well-defined mesopore structures.

The pore size distribution of the catalyst can be found by applying the Barrett, Joyner, and Halenda (BJH) model to the adsorption- or desorption curve of the isotherms at high relative pressure. The Kelvin equation, equation 3.3, is related to the capillary condensation that arise in the pores.

$$\ln(\frac{P}{P_0}) = -\frac{2\sigma V cos\Theta}{rRT} \tag{3.3}$$

The notation can be explained by:

- σ = surface tension of liquid nitrogen
- Θ = contact angle
- V = molar volume of liquid nitrogen
- r = radius of the pore
- R = gas constant
- T = absolute temperature
- P = measured pressure
- P_0 = saturation pressure

The BJH method is one of the most used to calculate the pore size distribution. The desorption isotherm is described as it requires a lower pressure compared to the adsorption. Often, the BJH model is applied on mesoporous materials measured at 77K, but several other assumptions are made in this method [63]. The assumptions are:

- The Kelvin equation is applicable over the mesopore range

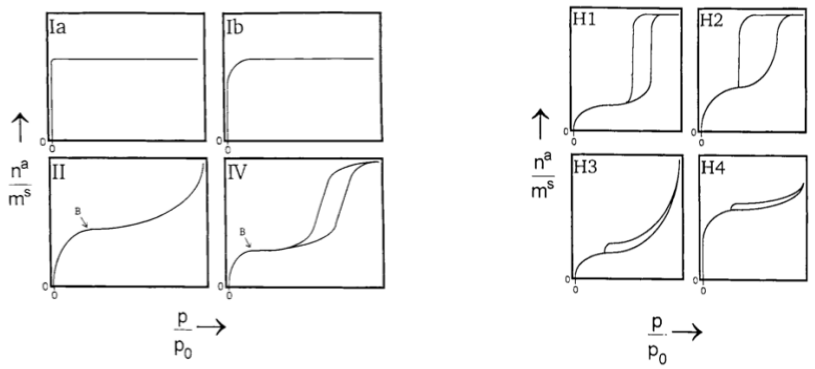

Figure 3.3: The left figure shows isotherms of adsorption/desorption. The isotherms Ia, Ib, II and IV is related to microporous, nonporous/macroporous and mesopores respectively. The figure to the right show four types of hysteresis. Hysteresis H1 and H2 are representing pores with uniform size and shape and network pores respectively, and H3 and H4 does not have any well-defined mesoporous structures [63].

- Meniscus curvature are dealt with by pore size and shape
- Pores are rigid and uniform in shape
- The distribution is limited to the mesopore area
- Pore-blocking is not present
- Adsorption on the wall of the pore is consistent with standard isotherm

3.3.2 Mercury Intrusion Porosimetry (MIP)

Mercury porosimetry is used to measure both large macropores and small pores, where information such as pore size, volume, distribution and density can be gathered [65](Appendix A7.15). The method is based on the principle that mercury has high surface tension and does not wet most substances without any force. The force applied to penetrate mercury into pores and capillaries is much higher for small pores than that of larger pores. At different pressures it is possible to find the pore volume for all the pores at this size range. A sensitive mercury penetrometer measures the volume of mercury entering the pore. The resisting force, f_R, is given in equation3.4, where D is diameter, γ is the surface tension and Θ is the contact angle.

$$f_R = \pi D \gamma cos\Theta \tag{3.4}$$

The externally pressure applied to force mercury into the pore opening is given as f_{Ext}, equation 3.5, where P is pressure, A is area over which the pressure is applied. It is assumed that pores are cylindrical, and that the outer surface of the material is entirely and equally accessible to mercury [66].

$$f_{Ext} = PA = \frac{P\pi D^2}{4} \tag{3.5}$$

Thus, the diameter of the pore is always calculated as described by the Washburn equation,3.6, at any pressure where mercury has intruded.

$$D = \frac{-4\gamma cos\Theta}{P} \tag{3.6}$$

3.3.3 CO_2 Capture Performance Test with a Thermogravimetric Analyzer (TGA)

A thermogravimetric analyzer (TGA) is used to analyze a substance during heating/cooling and to monitor the microscopic weight increase or decrease [67]. It can give information about phenomena such as fusion, vaporization, sublimation, absorption, adsorption, desorption etc. [68]. The TGA might detect the weight loss of carbon dioxide from calcium carbonates during calcination to calcium oxide as given in 1.1, and for example for testing of the CO_2 capture carrying capacities for X carbonation/calcination cycles. The graph will then indicate the weight loss/increase of the sample at a defined temperature over a certain time.

The device consists of a sample pan, where the sample can be loaded, a precision balance and a furnace that is programmed for a linear rise of temperature with time [68]. The device is very sensitive towards any weight change. Inside the furnace a sample purge gas, an inert or reactive gas, act as protection and control the sample surroundings.

A TGA can also be equipped with a mass spectrometer (MS), infrared spectrometry (IR) or gas chromatograph (GS/MS) to detect the released gas from the solid sample [67]. If the TGA is equipped with a MS, the off-gases from the sample can be measured as a function of temperature.

3.3.4 X-Ray Diffraction (XRD)

X-Ray Diffraction is used to investigate the crystalline phases of a catalyst and to estimate the crystallite size. The method is based the fact that all crystals as have a unique diffraction pattern, which will give a certain angle of diffraction by irrading the sample with x-rays. Parameters such as position, intensity, shape and width on the diffraction pattern will provide data of the sample [63]. Angles are measured by information provided by the diffracted x-ray beam (wavelength Λ). An illustration of how this works is shown in figure 3.4, in addition to Bragg law (also given in equation 3.7). Bragg law gives the connection between the space, d_{hkl}, between the two planes, hkl, and the diffraction angle 2Θ and the order of the reflection space (n). Bragg's law must be fulfilled to get constructive interference. The different planes in the crystal is named by miller indices, and a family of lattice planes is set by the integers h,k,l [69].

$$n\lambda = 2d_{hkl}sin\theta_{hkl} \tag{3.7}$$

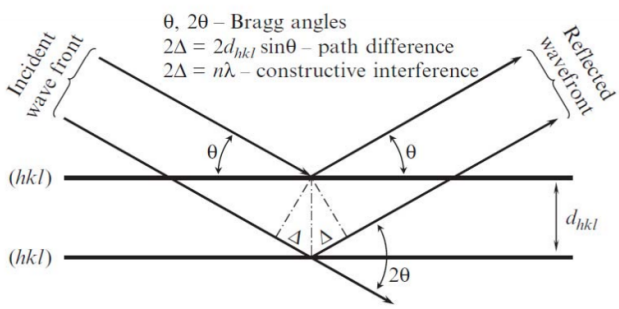

Figure 3.4: An illustration of how the x-ray diffraction works in addition to Braggs law. The path difference between diffracted x-rays is used to probe interlayer spacing [70].

To calculate the crystalline size, L (nm), Scherrer equation, equation 3.8, is used [70]. The letter k is a constant, often close to 1, but for spherical particles k=0.9. The shape of the peak gathered from the XRD pattern gives a prediction of the size of the crystal. With increasing crystallite size, the line breadth, β, decreases.

$$\text{Crystallite size (nm)} = L = \frac{k\lambda}{\beta cos\theta} \tag{3.8}$$

The different symbols in equation 3.8 are:

L = Crystalline size (nm)

k = Constant

λ = X-ray wavelength (1.5406 Å)

β = Breadth of half-peak height of an XRD line (radians)

θ = Diffraction angle

To get good results from x-ray diffraction measurements, several tricks can be used. If the crystal consists of particles with low symmetry, it can be hard to find the values of the h, k, l indices for each reflection line, but iterations on computer can be applied. It is important that the powdered sample have a smooth flat surface to obtain good results. If the powder loaded on the sample holder is not smooth and flat, x-ray adsorption can reduce the intensity of low-angle peaks. Also, if the grains are larger than 10 microns, it will difficult to get over ten thousand of grains irradiated by the x-ray beam, which is desired. In addition, amorphous particles cannot be detected. The sample must be 'infinite' thick, as a constant volume is assumed.

3.3.5 Scanning Electron Microscope (SEM)

Scanning Electron microscopes can be used to determine the morphology of a material and to disclose information on the composition and internal structure of the particles [71]. SEM is a simple technique operated under high vacuum. SEM can be applied on catalysts with a magnification in range from 3 to 10nm, but if a lower magnification is desired, then the transmission electron microscope is more helpful. Characterization of particle sizes in the range from 10^{-7}m to 10^{-4}m is appropriate, and oxide phases, zeolite crystals, carbon grains, unsupported metals are in favor. Morphology and surface of pellets can also be studied.

A set-up of the SEM is presented in figure 3.5. A thin sample is subjected to a narrow beam of electrons with high energy and high intensity [71]. By recording secondary electrons or back scattered electrons emitted from the area irradiated by the electron creates an image of the surface. The secondary or the back-scattered electrons are detected by the detector and is compared to the position of the beam before hitting the sample. The difference between secondary electrons and back-scattered electrons are detection of catalyst due to low energies (5 to 50 eV) and information about sample composition respectively. Contrast appears brighter when part of the surface is pointed towards the detector and other parts of the surface, where the surface normal pointing away from the detector, appears darker. The contrast detected is also depending on the atomic number of the elements in the catalyst [63], thus heavier element will appear brighter because they are more efficient scattered.

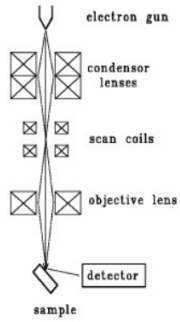

Figure 3.5: Schematic of the operational mode of the scanning electron microscopy (SEM) [71] .

3.4 Mechanical Properties

Catalyst are fragile materials manufactured to possess high porosity and good pore distribution. In addition to good catalytic activity and selectivity, they need to possess good physical properties such as mechanical strength. Activity is increased by increasing porosity due to more access to reactants, but catalyst will collapse if the porosity increases above 0.5Θ as shown in figure 3.6 [72]. Catalyst geometry is important because form, shape and

size affects the reactor design. Granules may deactivate due to thermal, chemical and mechanical stress in the reactor or during transport/storage. Fragments and fines can occur when the pellet experiences mechanical failure and result in loss of active surface material, uneven distribution of fluid flow, blockage, high pressure drop across the reactor, heat flux variations and fouling downstream [72]. Thus, it is important to optimize the pellets according to mechanical-, chemiophysical- and catalytic properties.

Also, for reliable and efficient performance of the reactor the mechanical strength of solid catalyst is important. For the cyclic MBCL, the pellets are expected to possess god mechanical properties because failure of catalyst pellets is more often the cause of process shutdown and catalyst replacements than their loss of activity. Simple mechanical testing as attrition resistance, compression test and falling test can be applied.

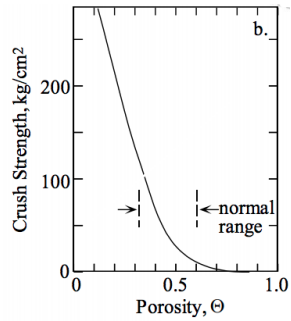

Figure 3.6: Typical pellet crush strength versus particle porosity [73].

Chapter 4

Methods and Materials

The following chapters includes pre-treatment procedure for dolomite and cement. The experimental procedures for characterization are given in following section given. The main goal is to develop a procedure for making pellets with dolomite and calcium aluminate cement with properties has high mechanical strength and good CO_2 capture capacity and high regenerability. Thus, the granulation procedure is given as a result.

4.1 Material Preparation

Dolomite from Franzefoss Miljøkalk and cement ADDA were used as raw material. ADDA is a type of cement mainly consisting of MgO and CaO after calcination. To get desired particle size, the dolomite was crushed in a Herzog crusher before it was sieved to get particle size less than 106 μm. A Herzog crusher is a big device with high power used to crush large particles.

The calcined dolomite was mixed with liquids, both water and low concentrated solutions as shown in table 4.1. Also, dry cement Fondu were added as aluminum source for some of the samples, where cement Fondu is a calcium aluminate-based hydraulic binder. Other promoters such as ZrN_2O_7 and $ZrCl_4$ were added as zirconium source, and $Mg(NO_3)_2 \cdot 6H_2O$ was added as additional magnesium source. The desired percentage of the components were 2% Zr, 3%Mg and 6%Al but after weighing, the actual wt% were back-calculated giving the nominal wt%. In addition, both calcined and uncalcined cement ADDA were granulated with dry cement Fondu, and liquid solutions of ZrN_2O_7 and $ZrCl_4$ as given in table 4.2. All samples prepared are listed in table 4.1 and 4.2 where nominal weight percentage for each component is given.

Table 4.1: Samples prepared based on calcined dolomite (CaO . MgO) as raw material. Nominal wt% for additives given.

Sample	Primary additive	Secondary additive	Additive Source
NO-1	-	-	-
NO-3	-	1.9 wt% Zr	Zr (ZrN_2O_7))
NO-6	5.8 wt%Al	1.6 wt% Zr	Al (cement) Zr ($ZrCl_4$)
NO-8	5.5 wt%Al	2.9 wt%Mg	Al (cement) $Mg(Mg(NO_3)_2 \cdot 6H_2O)$
NO-10	6.1 wt%Al	-	Al (cement)
NO-12	5.8 wt%Al	1.6% Zr	Al (cement) Zr (ZrN_2O_7))

Table 4.2: Samples prepared on basis of calcined ADDA and uncalcined ADDA. Samples NO-20 and NO-21 are made of calcined ADDA, and sample NO-22 and NO-23 are made of uncalcined ADDA. Nominal wt% for additives given.

Sample	Primary additive	Secondary additive	Additive Source
NO-20 (Cal. ADDA)	5.6 wt%Al	1.6 wt% Zr	Al (cement) Zr (ZrN_2O_7)
NO-21 (Cal. ADDA)	5.6 wt%Al	1.6 wt% Zr	Al (cement) Zr ($ZrCl_4$)
NO-22 (Uncal. ADDA)	5.6 wt%Al	1.8 wt% Zr	Al (cement) Zr (ZrN_2O_7)
NO-23 (Uncal. ADDA)	5.6 wt%Al	1.6 wt% Zr	Al (cement) Zr ($ZrCl_4$)

The liquid solution made of water and zirconium nitrate (ZrN_2O_7) were made by weighing desired amount of liquid ZrN_2O_7 and adding approximately 20g water to get a clear solution. The zirconium chloride ($ZrCl_4$) solutions were prepared by weighing the salt and adding approximately 20g water. To dissolve the salt, an ultrasonic bath at 60°C were used. The same method was used for the magnesium nitrate ($Mg(NO_3)_2 \cdot 6H_2O$) solution as well. The salt was mixed with 15g water and dissolved by using the ultrasonic bath at 60°C. All the solutions were added to the dry mix through a spray for homogeneous dispersion. The exact preparation methods are given appendix A7.2, and the proposed method of making pellets is presented in the result section.

Theoretical maximum CO_2-capture capacity for the dolomite-based sorbents are presented in table 4.3.

Table 4.3: Calculated theoretical max CO_2-capture capacity for the dolomite-based sorbents.

Sample	Theoretical max capacity %
NO-1	45.6
NO-3	43.5
NO-6	33.5
NO-8	34.3
NO-10	34.8
NO-12	33.4

4.1.1 Calcination

After crushing, the dolomite (<106 μm) and cement ADDA were calcined at 800 °C for 6 hours in air in a tube oven to get fully calcined dolomite (MgO·CaO) and cement ADDA (MgO·CaO). A calcination check was carried out to investigate the degree of calcination in the tube oven. An example of the calcination check is given in appendix A7.1.

Pellets ranging from 250μm to 1.2mm were calcined after granulation. The samples containing nitrates (NO-3, NO-8, NO-12, NO-20 and NO-22), were calcined in the tube oven for 3h at 800°C with ramp at 5°C/min and N_2 flow at 0.5 mL/min, to avoid explosion. All samples (also NO-3, NO-8, NO-12, NO-20 and NO-22) were finally calcined in air according to the following program:

1. Temperature ramp from 30 to 200°C at 5°C/min (35 min)
2. Isotherm at 200°C for 3 hours
3. Ramp from 200°C to 500°C at 1°C/min (5 hours)
4. Isotherm at 500°C for 2 hours
5. Ramp from 500°C to 950°C at 5°C/min (1.5 hour)
6. Isotherm at 900°C for 3 hours
7. Cooling

The calcination procedure is given in figure 4.1.

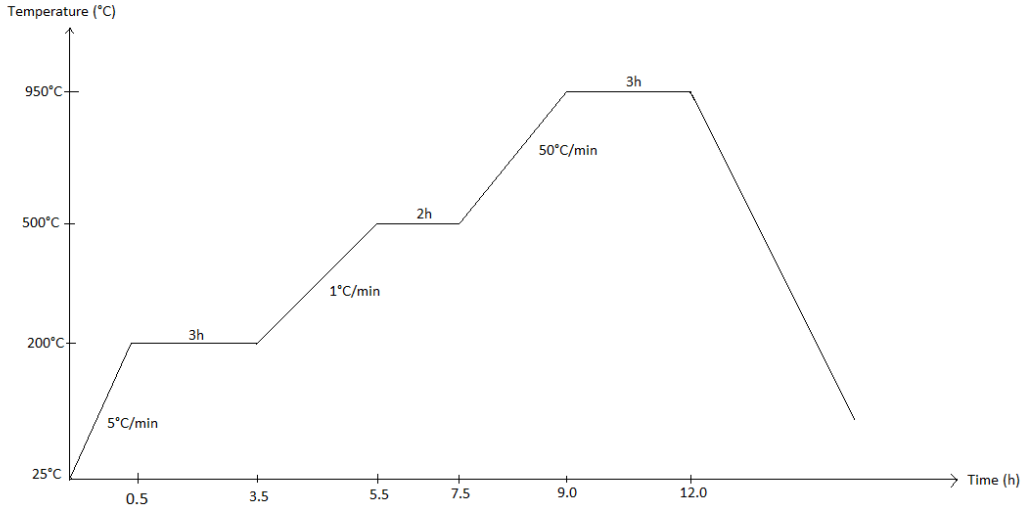

Figure 4.1: An illustration of the calcination procedure in air. All pellets were calcined according to this program.

4.1.2 Granulation

An Ankarsum Original Black Diamond AKM 6230BD kitchen machine was used to make pellets with solid cement powder, calcined dolomite, additives and water in ambient temperature in the fume hood. The Ankarsum Granulator/Mixer is equipped with a scraper to remove solids from the wall and a roller to break down larger particles into small pellets with desired shape. Water/dopant-solution was added through a spray into the bowl in the granulator and mixed with fine solid powder. To maintain moisture in the bowl, a humidifier was supplying water vapor to the bowl (some of the water evaporated from the open bowl).

The rotary drum machine is equipped with a motor rated at 1.5 kW which supplies high shear stirring to ensure mixing of water and solid. The mixing speed varies from 1-8, where level 1 is approximately 15 rpm and level 8 is approximately 45 rpm, depending on the viscosity of the material. A frequency counter was used to measure the rotational speed in rpm. Specifications for the rotary drum is given in table 4.4.

Table 4.4: Specifications for Ankarsum rotary drum.

Specification	Value of specification
Power	1500 watt
Bowl material	Steel
Size (D x B x H)	460.0 x 325.0 x 435.0 mm
Mixer Bowl Capacity	7L

Agitation by the rotary drum and the scraper can lead to a temperature increase in the bowl. In addition, the reaction between the cement/dolomite and water is an exothermic reaction and will give a temperature increase in the bowl (reaction between water and active calcium oxide is given in equation 1.5). Therefore, water was added slowly to minimize the effects of heat release due to the exothermic hydration process.

The granulation procedures are given as a part of the result because the main task was to develop a procedure for making the CaO-based pellets with cement binder or other additives in a large scale.

Figure 4.2: Rotary drum kitchen machine used as Granulator/Mixer. Equipped with humidifier to maintain near constant humidity in the bowl.

4.1.3 Extrusion-Spherionization

A powerful Kenwood Pro 2000 Excel Electric Mincer MG700 were used as extrusion machine, as the other alternative to granulation. Specification for the mincer machine is given in table 4.5. The extrusion machine is equipped with three mincer screens with holes at 3mm, 8mm and 10mm. In addition, it was made a mincer screen with 1mm holes. A trial on both the 3mm and the 1mm mincer screen were carried out, but the dye with 1mm holes could not be used do to power limitations of the machine. Thus, the 3mm mincer plate were used during extrusion. A picture of the extrusion machine is given in figure 4.3.

The dry materials used for testing of the extrusion equipment were uncalcined cement ADDA due to low cost and availability, calcined dolomite (<106μm) and cement Fondu. For making sample NO-12 with the extrusion method, the dry material was moistened with the liquid, ZrN_2O_7 solution. The wetting process were carried out in the granulator by adding liquids through a large pipette. The moisture content necessary for extrusion

were investigated. After extrusion, the material was put back in the granulation bowl (rotary drum) for the spherionization process.

The extrusion/spherionization process is given in the result section with additional description in appendix A7.3.

Table 4.5: Specifications for extruder.

Specification	Value of specification
Power	2.0 kW
Material	Aluminum
Mixer Capacity (meat)	3kg/min

Figure 4.3: (left) Extrusion with calcined dolomite and cement Fondu through a dye with 3mm holes, (right) Kenwood Pro 2000 Excel Electric Mincer MG700.

4.2 Characterization

The samples were characterized in TGA (with and without steam), BET, MIP, XRD and SEM. The mechanical strength of the pellets was investigated in an attrition test and in a simple falling test. A kinetic study was performed in the TGA to simulate a fixed bed.

4.2.1 CO_2-sorption Capacity and Kinetic Study

The CO_2-capture capacity was measured in a thermogravimetric analyzer. The CO_2 sorption capacity can be defined as in equation 4.1:

$$\text{CO}_2 \text{ captured (wt}\%) = \frac{W_t - W_0}{W_0} \tag{4.1}$$

where W_t is the weight of sorbent at a given time, t is time (min), and W_0 is weight of completely calcined material, only the metal oxide (MgO·CaO). The subtraction W_t - W_0 equals the mass of CO_2 captured.

The CO_2-sorption capacity was first tested for 11 cycles in a TGA at dry conditions (no steam present). The calcined pellets had a size ranging from 500 to 850 μm. The sample load was approximately 15mg loaded onto the sample pan. The conditions for carbonation were 10% CO_2-partial pressure for 6 minutes at 625°C. The calcination program used was 100% N_2 at 950 °C. For more information on the temperature scanning program, see Appendix A7.12

The promising sorbents tested in the dry TGA were further tested for 34 (67 cycles for NO-12) cycles in a TGA (Linseis TGA) with steam present. The size of the granules was 500-699μm. The reason for this size range was that a small size distribution was desired when the fresh and spent sorbents were analyzed in SEM afterwards. Sorption capacity were tested at temperature scanning program using 10% CO_2 and approximately 8% steam, the rest being inert gas, at sorption temperature from 550°C to 800°C and 100% CO_2 from 800°C to 950 °C for desorption. A deep sample pan with sample load at approximately 17mg was used.

A kinetic study was performed on sample NO-12 in the TGA simulating a fixed bed reactor. First, different sample load of pellet with size 250-400μm were tested. Both 5mg and 30mg were loaded onto the sample pan. The sorption temperature was 620 °C. 10 cycles with different CO_2 partial pressures were applied (2%, 3.3%, 11.3 and 15.6%) as presented in table 4.6. Gas flow properties are given in table in appendix A7.9.

Table 4.6: CO_2 concentrations for the 10 cycles in the kinetic study of sample NO-12.

Cycle number	**CO_2 concentration** (%)
1	2
2	11.3
3	15.6
4	3.3
5	2
6	2
7	11.3
8	15.6
9	3.3
10	2

After studying the kinetic variations with maximum and minimum sample load, 15mg of size 250-400μm pellets were tested at sorption temperature 550°C, 620°C and 650°C. In addition, 15mg of granules with size 1.2mm were also tested at 620°C and 650°C for

comparison. To investigate diffusion limitations further, extrudes (made with dye holes at 3mm) of 2mm, 3mm and 4mm were tested at carbonation temperature 650°C. For 3mm and 4mm only one pellet could be loaded onto the sample pan, but for 2mm samples, 2 granules were loaded onto the sample pan. A full view of the different kinetic test in the fixed bed reactor can be viewed in table 4.7.

Table 4.7: Conditions (sample load, T, size) for kinetic study of sample NO-12, both granulated samples and extruded samples.

Sample mass (mg)	**Carbonation temp. (°C)**	**Particle size (μm)**	**Preparation method**
5	620	250-400	Granulation
30	620	250-400	Granulation
15	550	250-400	Granulation
15	620	250-400	Granulation
15	650	250-400	Granulation
15	620	1200	Granulation
15	650	1200	Granulation
23	650	2000	Extrusion
11	650	3000	Extrusion
28	650	4000	Extrusion

The differential mass with respect to time is given in equation 4.2 where the differential represents the slope of the sorption curve, also called the reaction rate.

$$\lim_{\Delta t \to 0} = \frac{-\Delta Y_{weight}}{\Delta t} \tag{4.2}$$

The rate expression in equation 1.4, is like the rate expression, equation 4.2, gathered from TGA measurement. Where Y_{weight} is the weight on the Y-axis ant t is time. These reactions can be used for studying reaction kinetics of the dolomite-based sorbents doped with zirconium and aluminum.

4.2.2 Surface Area and Pore Size Measurements

Surface area and pore size were determined by a BET machine using nitrogen adsorption/desorption. To prepare the pellet for analysis, both mass of empty class tube and glass tube plus sample were weighed. Amount of sample was approximately 70-80mg. The samples were degassed overnight in a VacPrep 061. During the first hour, the samples were evacuated in the cooling station before they were heated at 300°C under vacuum. The samples were ready for BET analysis when the pressure in the degas unit reached 100 mTorr or less. The weight of the glass tube and sample after degassing was measured. After weighing, the samples were installed in the BET machine. The mass of sample tube

without sample and the mass of sample tube plus sample after degassing were used in creating a new file.

The surface area, pore size and pore size distribution were calculated from multipoint adsorption data. "Full report set" was selected when creating the report. After analysis, the sample plus sample tube were weighed and the weight after the BET measurement were used in creating the final file.

The mercury intrusion porosimetry measurement was performed by Lars Erik Mollan Parnas in SINTEF AS Industry. Only sample NO-12 and pure calcined dolomite (powder) were investigated due to high cost of the measurement. The standard of investigating the pore structure is first drying to remove water, before samples are weighed and placed in a chamber [74]. To remove air, the chamber with the material is evacuated. Then, mercury is filled up in the chamber, and to wet the cement material pressure is applied, and the mercury intrudes into the pores of the sorbent. The volume of the intruded mercury at corresponding pressure gives the data for calculating the pore diameter according to equation 3.6. The result from MIP is mainly used to investigate the pore size distribution.

4.2.3 X-Ray Diffraction Phases and Crystalline Size

Calcined pellets were ground in a mortar for 5 minutes. Powdered samples were placed on the XRD sample holder, trying to obtain a smooth surface. Analysis were performed using Bruker D8 Advance DaVinci X-ray Diffractometer (”DaVinci 1”). The DaVinci X-ray Diffractometer is equipped with CuKα radiation 2.6° primary and secondary Soller slits with LynxEyeTM SuperSpeed Detector and it is operating in the Θ-Θ mode. The data collection is typically from 5 to 105 2Θ whereas the calcined dolomite pellets were scanned at 2Θ ranging from 5-75° at step size 0.013°. The samples were scanned for 30 (one sample was investigated for both 30 and 60 minutes for comparison) minutes using variable divergence slit V6. Divergence slit is the slit between the X-ray source and the sample, and V6 slit means that the divergence slit opens automatically such that the illuminated length on the sample always remains 6mm. A Bruker EVA software with standard PDF-4+2016 RDB database were used to identify all phases of the diffractograms. The Bruker EVA software was also used to determine average crystallite sizes of calcium oxide and magnesium oxide according to Scherrer equation 3.8. The crystalline size was an average of the peaks (5 peaks for CaO and 2 peaks for MgO) measured for each sample.

4.2.4 Morphology and Surface Structure in SEM

A scanning electron microscope (Table Top) TM3000 from Hitachi was used to look at the pellet surface, shape and morphology of the pellet. The table top microscope is operating under the principle of low-vacuum observation and this means that more gas molecules are present inside the specimen chamber. This SEM provides a great focal depth and permits high magnification ranging 15 to 30000x and a digital zoom (2x, 4x). The SEM is equipped with a tilt/rotation stage, making it possible to maneuver the stage while the

sample is inside the vacuum chamber. The table top features three beam conditions depending on the information required, these are 5 kV, 15 kV and 'Analysis' where the 5 kV emphasizes surface detail, the 15 kV gives better resolution and can be used throughout the magnification range and the analysis mode is used for elemental analysis or low contrast specimens. To look at the surface of the dolomite pellet the 5 kV mode is sufficient, but during the spring 2018, the 5kV mode was broken, and the analysis mode was used instead.

The granules were placed on a thin carbon tape which was subsequently loaded into the sample stage of the microscope. A picture of the specimen is shown in figure 4.4. The granules were scanned at magnification x50, x120, x150 and x300. The magnification at x50 was used to get an overview of most of the granules on the specimen. Scanning magnification at x150 was used to look at one pellet to be able to measure the width and length. The magnification at x300 was applied to look closer into the surface of the pellet.

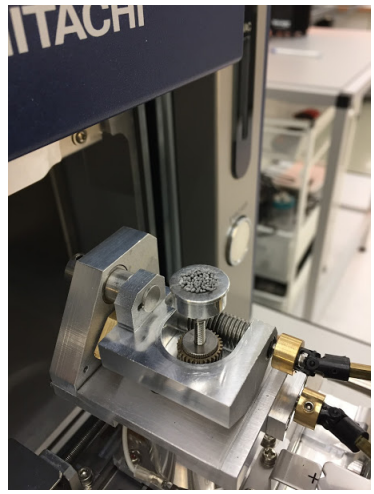

Figure 4.4: SEM specimen holder.

To investigate the morphology of the granules, the sphericity was calculated in Fiji ImageJ Analysis software. SEM pictures at magnification x50 were used. Approximately 100 pellets were investigated, and an average of the whole batch was calculated. An example is given in figure 4.5.

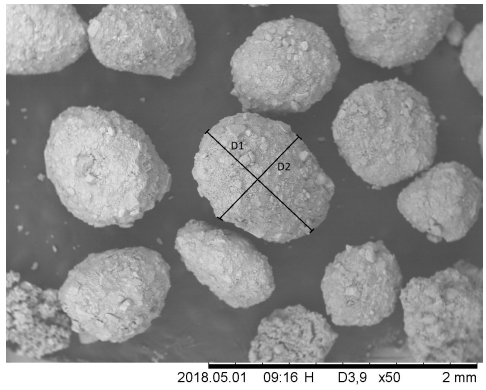

Figure 4.5: Width and length of granules analyzed in Fiji Image Analysis software. Sphericity of pellets calculated based on measure of D1/D2.

4.3 Mechanical Properties Test

For the cyclic MBCL, the pellets are expected to possess god mechanical properties. Thus, simple mechanical testing as attrition resistance and falling tests are applied.

4.3.1 Attrition Test

The main goal of the attrition tests was to determine the attrition resistance of the produced pellets. The attrition test was performed on a Ball milling "Cat" roller (RM10W-30V Cat) machine using revolving speed 25 rpm. A picture of the instrument is given in figure 4.6 The calcined pellets were sieved to a particle size ranging from 250-850 μm and put in small glass bottles ($\frac{1}{2}$-$\frac{2}{3}$ of the class bottle were filled). The glass bottle with granules were placed on the Ball Miller. After 0.5h, 1h, 1.5h, 2h, 4h and 6h the pellets were sieved for 20s and pellets/powder smaller than 250μm were weighed, and cumulative weight loss was calculated.

Figure 4.6: Ball miller (Cat) roller (RM10W-30V Cat) machine.

4.3.2 Falling Test

For the cyclic MBCL, the pellets are expected to possess god mechanical properties. In the MBCL reactor the pellet might crush when falling down the reactor. A 1.5m long glass tube were placed vertically in the lab to simulate a typical Moving Bed Circulating Looping reactor. A paper was placed under the glass tube to collect the pellets after the fall. For all samples 1g of calcined pellets ranging between 250-500 μm and 500-850 μm was dropped, and subsequently they were sieved for 10s. The amount of pellets crushed to a size lower than 250μm where weighed, and the weight loss were calculated. The percentage loss of sorbent was calculated from the fines in each drop divided by initial weight of the sample (1g). Also, for the pellet ranging from 500-850 μm, the loss between 250-500 μm were weighed. The pellets still intact, were dropped three more times using the same procedure for calculating weight loss.

Figure 4.7: A 1.5m long glass tube used to simulate the fall of pellets in MBCL

Chapter 5

Results

The result section contains the developed granulation procedure and characterization of the different pellets.

5.1 Large-Scale Procedure for Production of Pellet

To produce pellets with desired chemical composition and mechanical strength, two methods are developed: granulation in a rotary drum and extrusion/spherionization.

5.1.1 Granulation Procedure - Rotary Drum

A granulation procedure was developed based on several attempts on making pellets. The first day, water or a solution containing water and additives are supposed to be added to the dry mix of calcined dolomite (<106 μm 800°C 3h). If cement Fondu is added as aluminum source, the Fondu is mixed with the dry material for 5 minutes in the bowl at low rpm to get a homogeneous mix. The liquid solution is made as described in section 4.

A graphical description of the granulation is given in figure 5.1. More detailed description is given in A7.2. The first day, 25g of solution is slowly added at low rotation speed (level 1 = 15rpm) for 15 minutes. The last 5 minutes, the rotation speed is turned up to level 6 (approximately 30rpm) before the material is stored on a closed container overnight. The second day, 10g water is added the first 5 minutes at revolving level 1. The speed is turned up to level 8 (approx. 45rpm) after 6 minutes. After 15 minutes, 30g water is added. At this point, the humidifier (low level) is applied to keep moisture in the open bowl. After 25 minutes, the water addition is stopped with approximately 40g water added. Also, the roller is removed at this point. The granulation is stopped after 45 minutes where a few sprays of water is added the last 15 minutes if the grain size is too small. The granules are

dried in room temperature before they are sieved to desired particle size. The measured yield for all samples are given in table 5.1. The yield does not add up to 100(%) as the remaining material is left in the bowl or is larger than 1200μm. A result of the large-scale production of pellets is presented in figure 5.2.

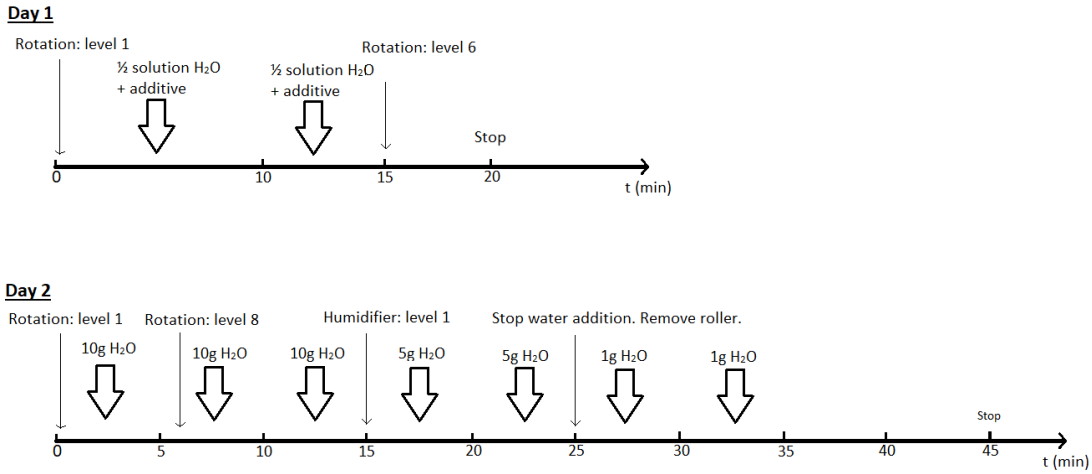

Figure 5.1: Schematic of granulation procedure using 100g calcined dolomite as raw material with cement as binder in addition to liquids and other promoters.

Figure 5.2: Picture showing the result of large-scale granulation.

Table 5.1: Yield (%) from granulation of dolomite-based and ADDA-based samples. The term "gs" mean granule size. The yield does not add up to 100(%) as the remaining material is left in the bowl or is larger than 1200μm.

Yield (%)	**250<gs<500** μ**m**	**500<gs<850** μ**m**	**850<gs<1200** μ**m**
NO-1	39	38	18
NO-3	3	19	19
NO-6	9	46	6
NO-8	5	23	57
NO-10	2	21	22
NO-12	14	34	11
NO-20	60	14	5
NO-21	68	16	3
NO-22	1	6	18
NO-23	55	18	5

5.1.2 Granulation procedure - Extrusion/Spherionization

The extrusion/spherionization process is carried out using 200g raw material (dolomite at size <106μm, calcined in 800°C for 3h). The process is divided in 4 steps:

1. Granulation (day 1 and day 2)
2. Extrusion
3. Spherionization
4. Drying

The first step, granulation, is similar to the process description described in section 5.1.1. The first day, a mix of 200g calcined dolomite and 40g cement Fondu (for 6% alumina content) is first mixed for 5 minutes at rotary level 1, to maintain a homogeneous mixture. Liquid solution and water is added in moderate portions for 30 minutes to control temperature in the bowl. The rotation speed is turned up to level 8 the last 10 minutes of granulation, before the material is stored on a bottle after 40 minutes granulation.

Day 2, approximately 50g water is added for 20 minutes. A humidifier set to max level is used to moisten the material. The mix is set to rest for 5 minutes before extrusion. Extrudates of 3mm is pressed through the screen. To evaporate some of the liquid binder to avoid too large pellets, the material is dried for 20 minutes. Spherionization in the third stage last for 10 minutes at rotation level 8, before the granules is dried in room temperature overnight. More details for the extrusion/spherionization process are given in appendix A7.3.

5.2 Characterization

The results of the catalyst characterizations are given in this section with additional raw data given in Appendix. The characterization results are from N_2 adsorption/desorption, XRD, TGA (dry and with steam) and SEM.

5.2.1 Surface Area and Pore Size Distribution

The surface area [m^2/g] measurements from the BET for all 10 pellets are given in table 5.2. BJH desorption average pore diameter and BJH desorption cumulative volume of pores are also given. The full report set is given in Appendix A7.4.1. The BET values are based on two measurements and given as the average in table 5.2. BET surface area, BJH average pore size and BJH cumulative pore volume for calcined cement pellets (850-250 μm) are presented.

Table 5.2: The values are based on two measurements and given as the average. BET surface area, BJH average pore size and BJH pore volume for both calcined dolomite- and cement(ADDA)-based pellets (850-500 μm).

Sample	**S_{BET} (m^2/g)**	**V_p (cm^3/g)**	**d_p (nm)**
NO-1	13.7±0.5	0.035±0.005	11.2±0.9
NO-3	8.0±0.05	0.013±0.003	8.0±0.6
NO-6	2.7±0.10	0.006±0.000	26.3±8.1
NO-6 (powder)	1.3±0.10	0.004±0.001	29.4±11.1
NO-8	6.2 ±0.10	0.017±0.001	10.9 ±1.1
NO-10	13.6±0.05	0.050±0.011	15.6±2.5
NO-12	8.9±0.30	0.025±0.002	19.4±3.2
NO-20	1.34 ±0.50	0.003 ±0.001	26.1±14.2
NO-21	0.47 ±0.41	0.002 ±0.001	35.7±1.6
NO-22	1.72 ±0.19	0.003 ±0.001	24.4 ±12.1
NO-23	0.35 ±0.11	0.003 ±0.001	23.9±9.9

The isotherms for pellet NO-1, NO-6, NO-8 and NO-12 are given in figure 5.3. The isotherms for the other pellets are given in Appendix A7.4.1.

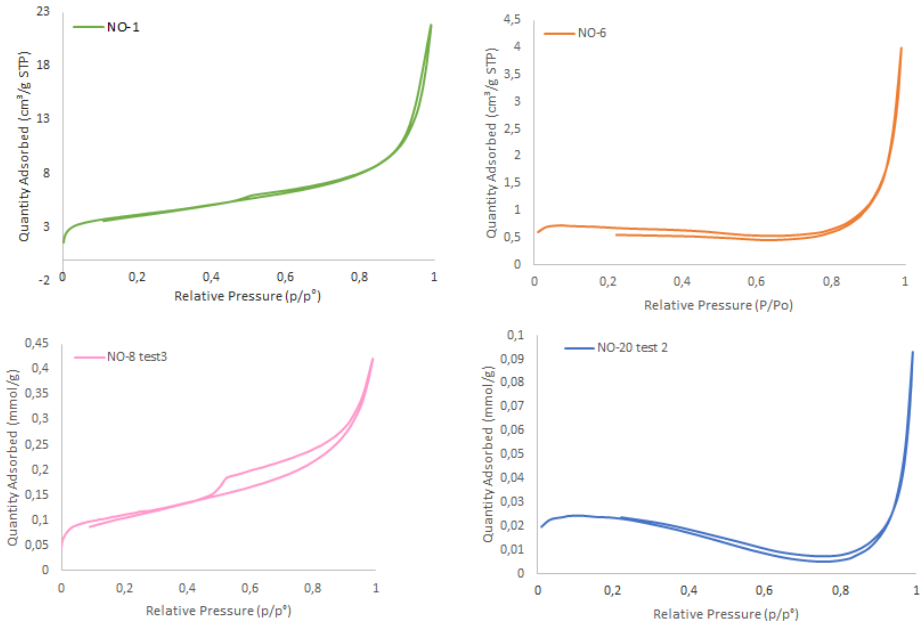

Figure 5.3: Adsorption isotherms for calcined samples NO-1, NO-6, NO-8 and NO-20. All samples of size 500-850μm

BJH pore size distribution for sample NO-10 and sample NO-23 is presented in 5.4. More BJH plots in Appendix A7.4.1. A summary of the typical pore diameter for dolomite-based samples are presented in table 5.3.

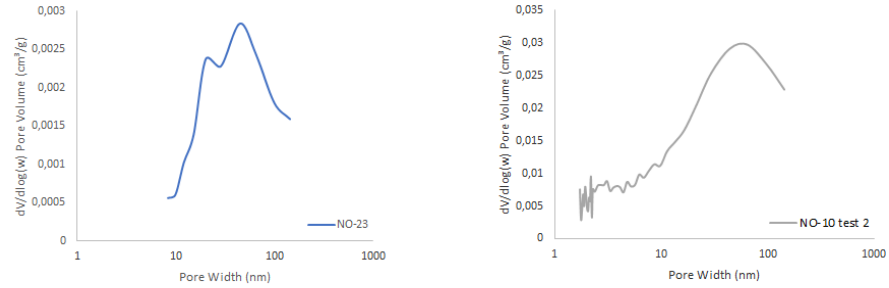

Figure 5.4: BJH plot of samples NO-23 and NO-10. Some noise is shown at low pore volume for NO-10.

Figure 5.5 is presenting the pore size distribution for pellets NO-12 (500-850μm) and raw material, calcined dolomite (<106μm) gathered from MIP measurements. More results from the MIP is given in Appendix A7.10. The peak for sample NO-12 at 30nm and

60nm, while the peak for pure dolomite is at 60nm.

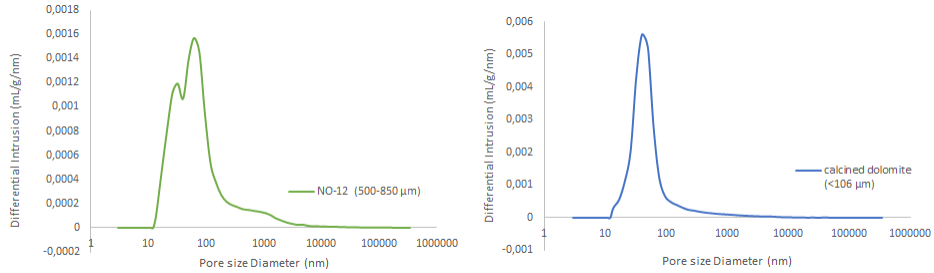

Figure 5.5: (left) Pore size distribution for pellets NO-12 (500-850 μm) measured by MIP. (right) Pore size distribution for powdered calcined dolomite (<106μm) measured by MIP

Table 5.3: Typical pore diameter for the dolomite-based samples. Three measurements conducted with BJH method and one sample for NO-12 with MIP method. The "-" sign means that there are no measurements, and the "*" means that the measurements are invalid.

Pore size (nm)	Test 1 (BJH)	Test 2 (BJH)	Test 3 (BJH)	MIP method
NO-1	65	*	45	-
NO-3	30	*	*	-
NO-6	125	75	75	-
NO-8	65	65	*	-
NO-10	100	65	-	-
NO-12	120	120		30 and 60

5.2.2 Phase Identification and Crystalline Size of Dolomite and Cement Based Pellets

Figure A7.69 show the results from phase identification of XRD results in EVA software. Sample NO-12 based on dolomite and sample NO-20 based on cement ADDA (calcined at 950 °C, 3h) are shown. Orange phase is NO-12 and blue phase is NO-20. Black star, red hat, blue sign, green smiley and purple dot can be identified as CaO, MgO, SiO_2, $Ca_{12}Al_{14}O_{33}$ and $CaZrO_3$ respectively. The black star, and red hat are only given for NO-20 in the figure, but they also count for NO-12. Other results from XRD measurements and he identification trial of the different components is given in Appendix A7.4.2.

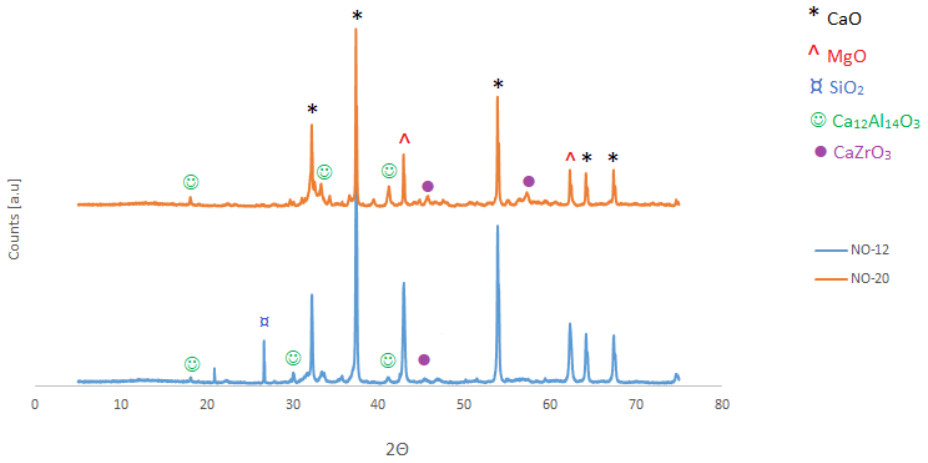

Figure 5.6: XRD phases of calcined samples NO-12 and NO-20. Orange phase is NO-12 and blue phase is NO-20. Black star, red hat, blue sign, green smiley and purple dot can be identified as CaO, MgO, SiO_2, $Ca_{12}Al_{14}O_{33}$ and $CaZrO_3$ respectively.

The crystalline size of CaO and of all the samples were found from EVA software where Scherrer equation is used. Calculated values are shown in table 5.4.

Table 5.4: Crystalline size of MgO and CaO calculated using Scherrer equation in EVA software.

Sample	CaO (nm)	MgO (nm)
NO-1	78.4±4.6	45.9±1.9
NO-3	82.2±6.4	50.7±1.7
NO-6	109.4±6.5	91.8±1.9
NO-8	79.6±8.8	49.2±1.7
NO-10	67.2±8.4	42.5±1.4
NO-12	73.7±38.2	48.9 ±1.1
NO-20	103.8±39.4	102.7±0.7
NO-21	114.5±25.7	106.4±9.0
NO-22	115.7±23.4	104.2±0.6
NO-23	106.9±26.5	108.3±0.8

5.2.3 CO_2-Sorption/Desorption Cycles in TGA without Steam

Results from 11 cycles of sorption/desorption in dry conditions for dolomite-based samples are given in figure 5.7. A summary of the CO_2-capture capacity for these samples are presented in table 5.5.

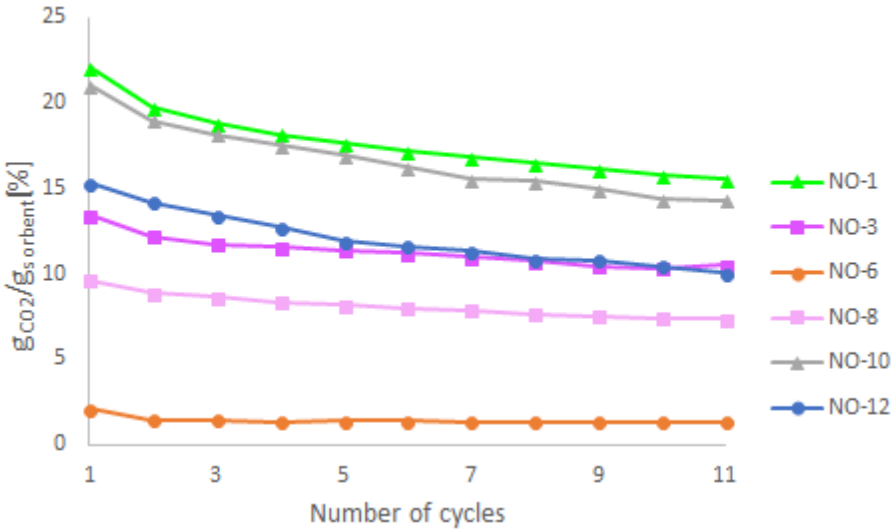

Figure 5.7: 11 sorption/desorption cycles measured in dry conditions for the dolomite-based samples.

Table 5.5: Summary of the CO_2-sorption capacity measured in TGA for 11 cycles. The loss (%) in capacity from cycle 1 to cycle 11 is also given.

Sample	**CO_2 capacity initial (g_{CO2}/g_{oxide})**	**CO_2 capacity cycle 11 (g_{CO2}/g_{oxide})**	**Loss in capacity from cycle 1-11 %**
NO-1	22	15	30
NO-3	13	11	22
NO-6	2	1	36
NO-8	10	7	24
NO-10	21	14	32
NO-12	15	10	34

Results from 11 cycles of sorption/desorption in dry conditions for cement ADDA based samples are given in figure 5.8.

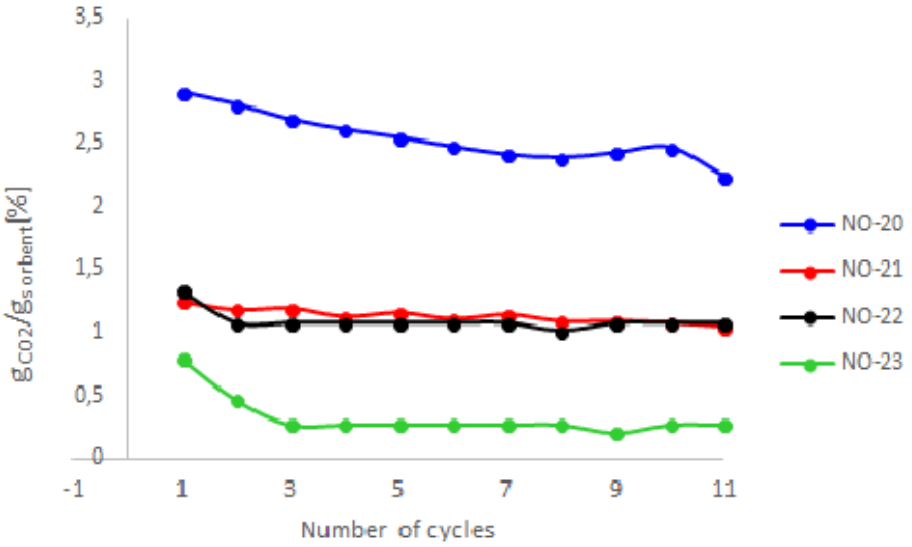

Figure 5.8: 11 sorption/desorption cycles measured in dry conditions for the cement ADDA-based samples.

5.2.4 CO_2-Sorption/Desorption Cycles in TGA With Steam

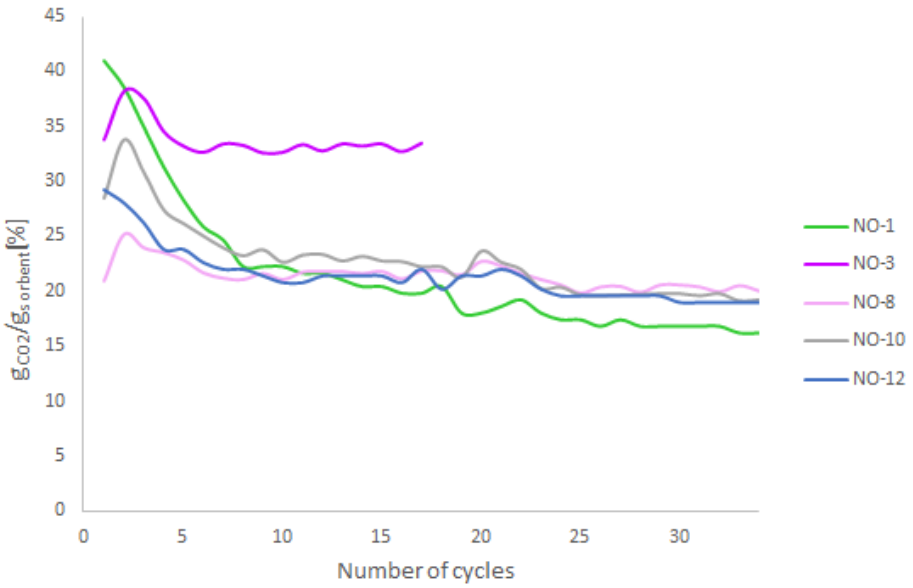

Figure 5.9: Result of 34 sorption/desorption cycles in presence of steam for samples NO-1, NO-8, NO-10 and NO-12. Only 17 cycles were tested for NO-3.

Table 5.6: Summary of the CO_2-sorption capacity (g_{CO2}/g_{oxide}) measured in TGA for 34 cycles in presence of steam. The loss (%) in capacity from cycle 1 to cycle 34 is also given

Sample	**CO_2 cap. cycle 2**	**CO_2 cap. cycle 15**	**CO_2 cap. cycle 34**	**Loss in cap. cycle 1-34 %**	**Loss in cap. cycle 15-34 %**
NO-1	38.6	20.5	16.3	57.8	20.6
NO-3	38.2	21.8	-	-	-
NO-8	25.2	21.8	20.0	20.6	8.2
NO-10	33.9	22.8	19.3	43.0	15.4
NO-12	28.0	21.4	19.0	31.9	11.1

5.2.5 Up-Scaling of NO-12 - Comparing 20g vs. 100g for 68 Cycles in Steam

Raw data for sample NO-12 (one-pot 20g calcined dolomite) is gathered from work provided by another author [75]. Thus, the scale-up of sample containing 5.8% Al from cement Fondu and 1.6%Zr from ZrN_2O_7 (NO-12) can be compared to the same sample made by hand in smaller scale (20g calcined dolomite). The up-scaled sample NO-12, has a capacity loss of 45% from cycle 1 to 68, and a capacity loss of 28% from cycle 15 to 68.

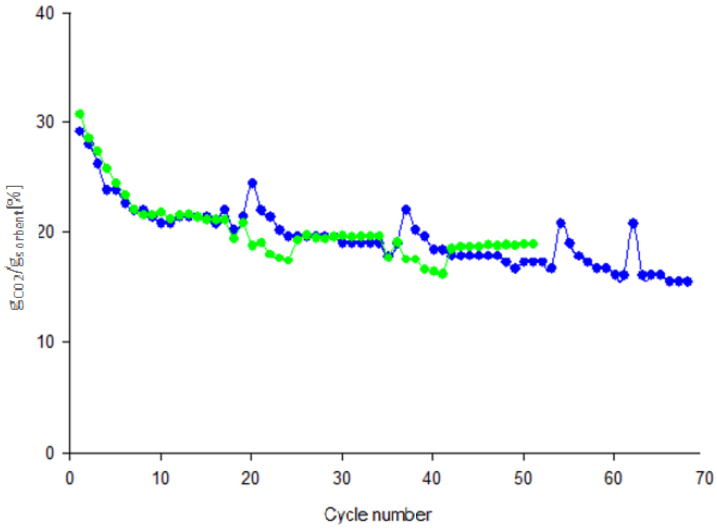

Figure 5.10: CO_2-sorption measurement comparing granules made by hand with 20g calcined dolomite (green) as raw material, and sample NO-12, a scaled-up batch consisting of 100g calcined dolomite (blue) made by the rotary drum. The handmade result is taken from work by an other author [75].

5.2.6 Investigation of Pellets NO-6

TGA-MS result calcination of NO-6 is presented in figure A7.56. The light blue curve is temperature (°C) and the dark blue curve is mass (%). The MS curve is given in Appendix A7.5

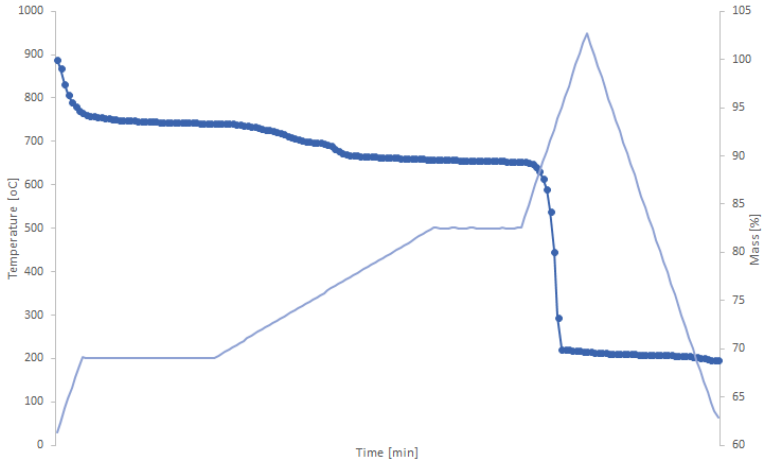

Figure 5.11: Calcination check of pellet NO-6 using TGA with MS to detect gases leaving the pellets during calcination.

5.2.7 Kinetic Study of Sample NO-12

Figure 5.12 show how sample load affects the sorption curve. The figure compares 5mg and 30mg of sample NO-12 with size 250μm at temperature 620°C for cycle number 5 (C5) and 10 (C10) (2 % CO_2 concentration). Data for time derivative of mass (mg/min) of the slope is given in Appendix A7.6.

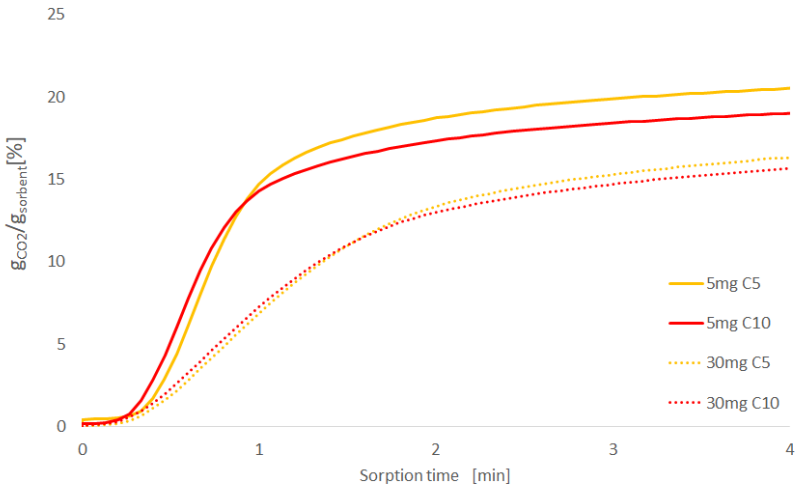

Figure 5.12: CO_2-sorption curve for 5mg and 30mg sample load. The curves selected are for cycle 5 (C5) and 10 (C10) where 2 % CO_2 concentration is applied.

Figure 5.13 show how sorption temperature affects the sorption curve and capacity. The figure compares 550°C, 620°C and 650°C of sample NO-12 (15mg) with size 250μm for cycle number 5 (C5) (2 % CO_2 concentration). Data for time derivative of mass (mg/min) of the slope is given in Appendix A7.6

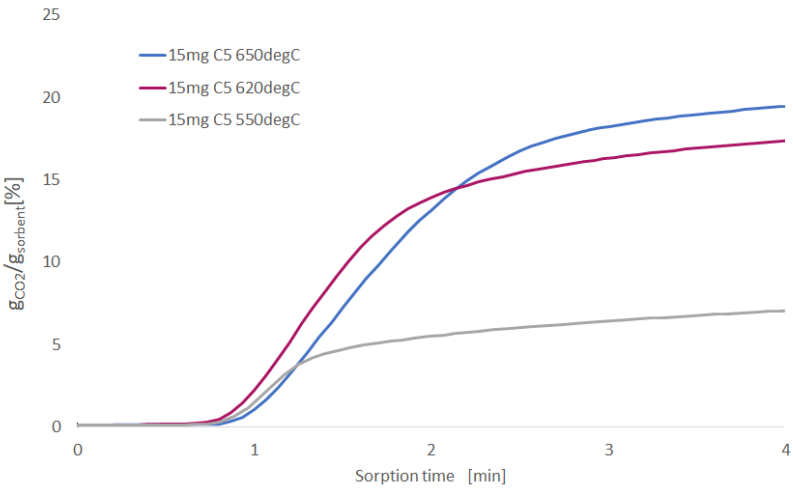

Figure 5.13: CO_2-sorption curve for three different temperatures; 550 °C, 620°C and 650°C. The curve selected is cycle 5 where 2 % CO_2 concentration is applied.

The plot in figure 5.14 gives the time derivative (mg/min) for slope of the CO_2-sorption curve for 620°C (blue) and 650°C (orange) in the 10 cycles. Cycle 5 where 2 % CO_2 concentration is the time derivatives for the blue and the purple curve in figure 5.13. Cycle from 1-10 have CO_2 concentration of 2%, 11.3%, 15.6%, 3.3%, 2%, 2%, 11.3%, 15.6%, 3.3% and 2% respectively.

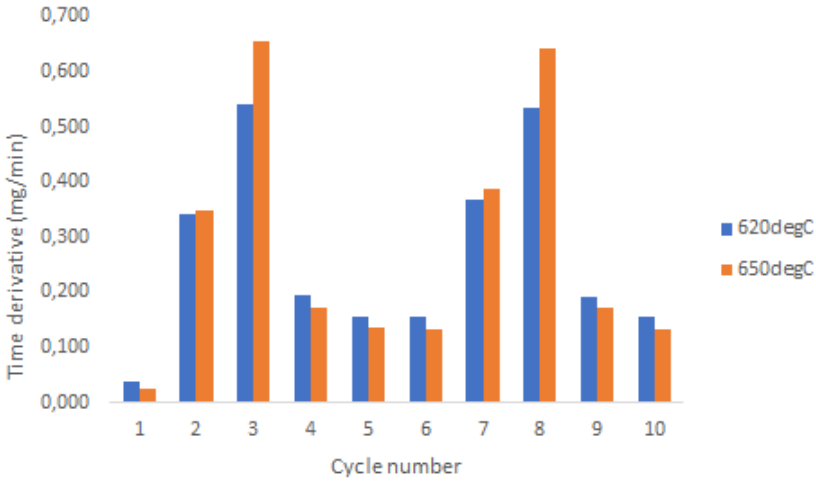

Figure 5.14: Time derivative (mg/min) for slope of the CO_2-sorption curve for 620°C (blue) and 650°C (orange) in the 10 cycles. Cycle 5 where 2 % CO_2 concentration is the time derivatives for the blue and the purple in figure 5.13. Cycle from 1 to 10 have CO_2 concentration of 2%, 11.3%, 15.6%, 3.3%, 2%, 2%, 11.3%, 15.6%, 3.3% and 2% respectively.

Graph in figure 5.15 show sorption curve for cycle 5 for different granule size of sample NO-12. Size between 250 μm and 1.2mm are made by granulation, while the granules NO-12 ranging from 2-4mm are made by extrusion. In cycle 5, a 2 % CO_2 concentration is applied. Sample loading for size 250μm and 1.2mm are 15mg, but for granules at 2mm, 3mm and 4mm, a loading of 23mg, 11mg and 28 mg were used respectively. This sorption curve gives an indication of reaction limitations during the CO_2-capture process. Figure 5.15 show the first 4 minutes of sorption, but the first 15 minutes of sorption and 60 minutes of sorption is given in appendix A7.6.

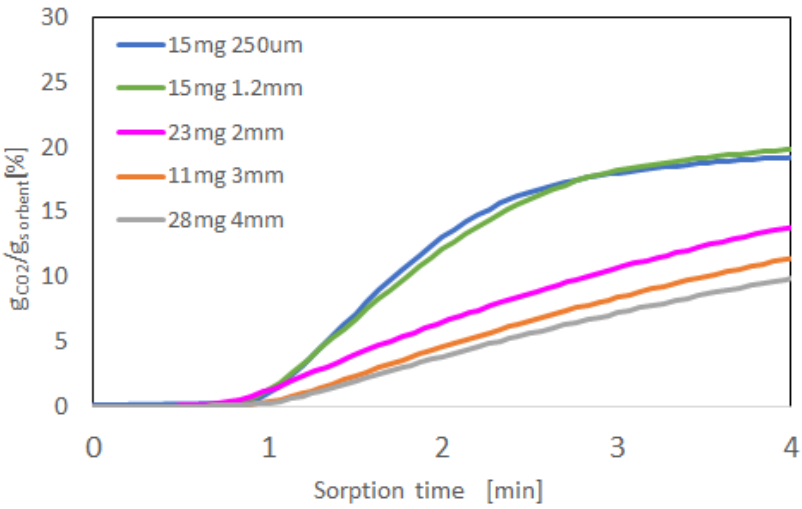

Figure 5.15: CO_2-sorption at 650°C for size 250μm, 1.2mm,2mm, 3mm and 4mm. Cycle 5 (C5) is applied using 2% CO_2 concentration.

Figure 5.16 show a representation of sorption time and corresponding percentage of max capacity. Sorption time is found for 20%, 30%, 40%, 50%, 60%, 70%, 80% and 90% of max capacity. At 5 minutes of sorption in the reactor, granules at 250μm and 1.2mm will have reached more than 80% capacity of maximum, while a size of 2mm will have reached 80% of maximum capacity, and 3mm and 4mm have reached a percentage of max capacity at 50-60 % after 5 minutes.

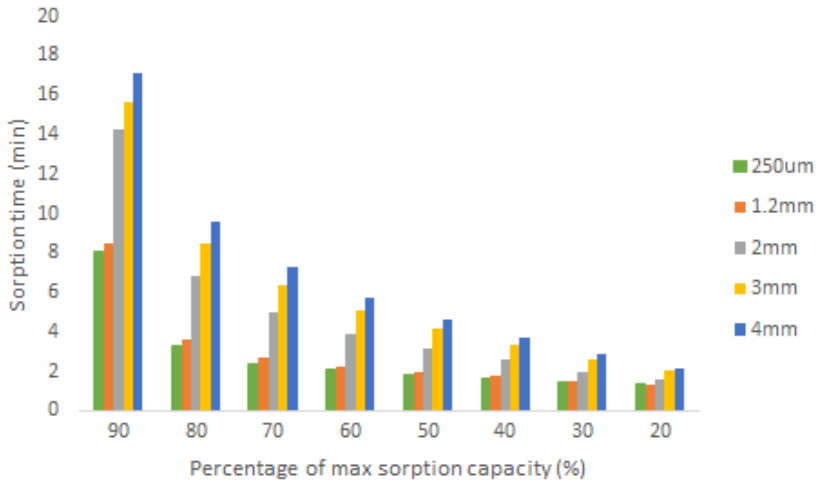

Figure 5.16: The bar plot present which sorption time 20%, 30%, 40%, 50%, 60%, 70%, 80% and 90% of max capacity are reached for pellets with size 250μm, 1.2mm,2mm, 3mm and 4mm.

Figure 5.17 show how the time derivative of mass (mg/min) of the slope (as in figure 5.15) for each pellet size vary with CO_2 concentration.

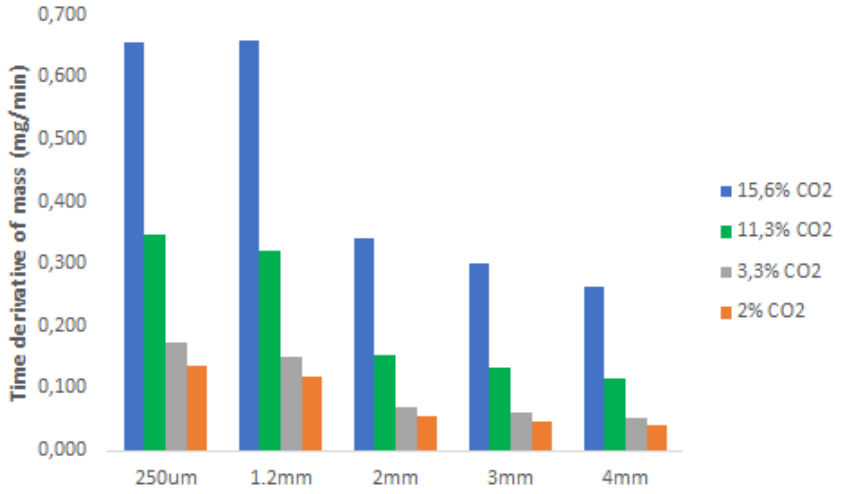

Figure 5.17: Time derivative (mg/min) for slope of the CO_2-sorption curve at different partial pressure of CO_2 for different granule size. The CO_2 concentrations are 15.6%, 11.3%, 3.3% and 2% for granules ranging from 250μm to 4mm

Figure 5.18 show how the time derivative of mass (mg/min) of the slope vary for each pellet at 2 % CO_2 concentration in different cycles.

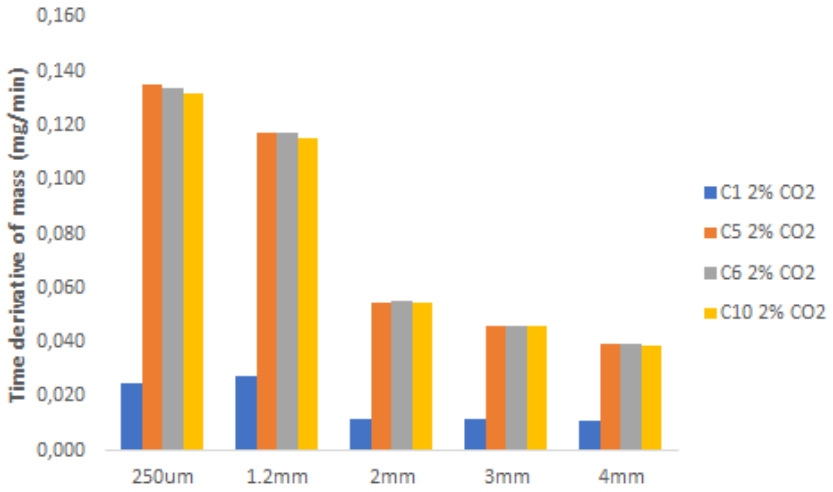

Figure 5.18: Time derivative (mg/min) for slope of the CO_2-sorption curve at 2% CO_2 concentration for different cycles and granule sizes. Cycle 1 (C1), 5 (C5), 6 (C6) and 10 (C10) are shown for pellets with size from 250μm to 4mm

5.2.8 Morphology and Surface of Pellets

This section present SEM pictures of the pellets.

Investigation of Surface for Fresh and Spent Pellets

SEM pictures of fresh and spent sorbent for sample NO-12 (500-699μm) are shown in figure 5.19 and 5.20 respectively.

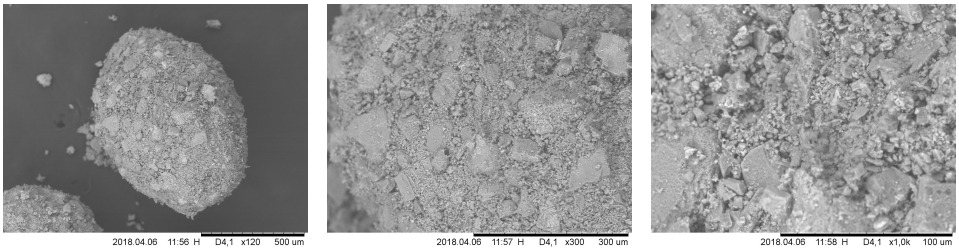

Figure 5.19: (left) NO-12 fresh x120 , (middle) NO-12 x300 fresh, (right) NO-12 x1000 fresh.

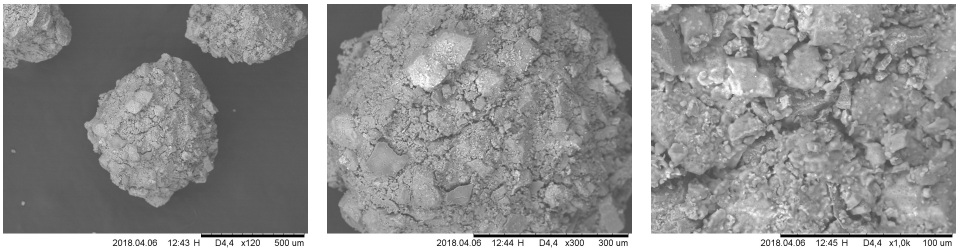

Figure 5.20: (left) NO-12 spent x120 , (middle) NO-12 x300 spent, (right) NO-12 x1000 spent.

Morphology of Dolomite-Based Pellets

SEM pictures of calcined pellets NO-1, NO-3 and NO-6 are given in figure 5.21. And SEM pictures of calcined pellets NO-8, NO-10 and NO-12 are given in figure 5.22. All of them are taken with resolution x150. Surface pictures of sample NO-20, NO-21, NO-22 and NO-23, and more pictures of sample NO-1 to NO-12 can be found in Appendix A7.4.4

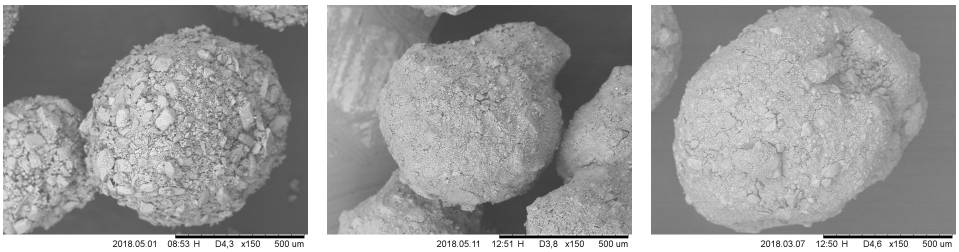

Figure 5.21: (left) NO-1, (middle) NO-3, (right) NO-6. All photos taken at resolution x150, and all samples are calcined (950°C, 3h).

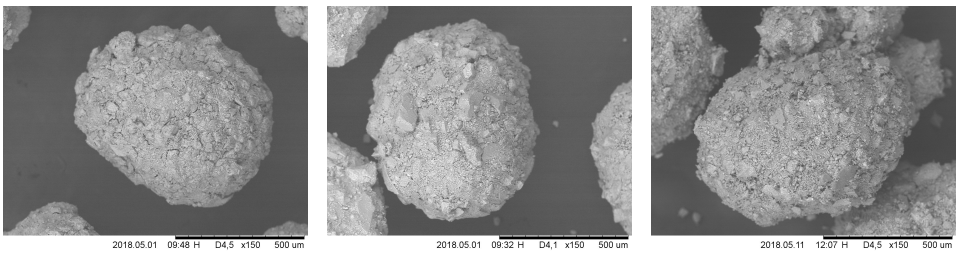

Figure 5.22: (left) NO-8, (middle) NO-10, (right) NO-12. All photos taken at resolution x150, and all samples are calcined (950°C, 3h).

Table 5.7 shows a prediction of the sphericity of calcined pellets with a size ranging from 500 to 850μm. Two diameters (D1 and D2) are measured from SEM pictures. Sample NO-1 is closest to 1, and NO-6 show the poorest morphology with a sphericity of 0.72.

Sample NO-8 and NO-10 is close to sample NO-1.

Table 5.7: Sphericity measured on sample NO-1 to NO-12, based on calcined pellets with size 500-850μm. Desired sphericity should be close to 1.

Sample	Sphericity
NO-1	0.88
NO-3	0.80
NO-6	0.72
NO-8	0.84
NO-10	0.84
NO-12	0.79

Investigation of binding mechanism on sample NO-10

The investigation on the binding mechanism for NO-10 is shown in figure 5.23. During granulation on NO-10, 7 samples were collected and analyzed in SEM. The first and the second sample were collected 10 and 5 minutes before the water addition was stopped respectively. And sample number 3 was gathered at the time were no more water was added. Sample 4, 5, 6 and 7 were collected after 5, 10, 15, and 20 minutes of granulation respectively (no more water added, only humidifier). Pictures of the final product is taken after sieving (no calcination) to desired size of 500-850μm. All pictures are taken with resolution x50.

5.3 Mechanical Properties of Pellets

This section contains results from testing of mechanical properties which includes the attrition resistance test and strength of the pellets obtained in a falling test.

5.3.1 Attrition Test

The attrition resistance is given in figure 5.24 and shows percentage cumulative weight loss (%) as a function of revolving cycles. The green, purple, orange, pink, gray and blue color represent sample NO-1, NO-3, NO-6, NO-8, NO-10 and NO-12 respectively. The attrition test was performed on samples ranging from 250-850μm.

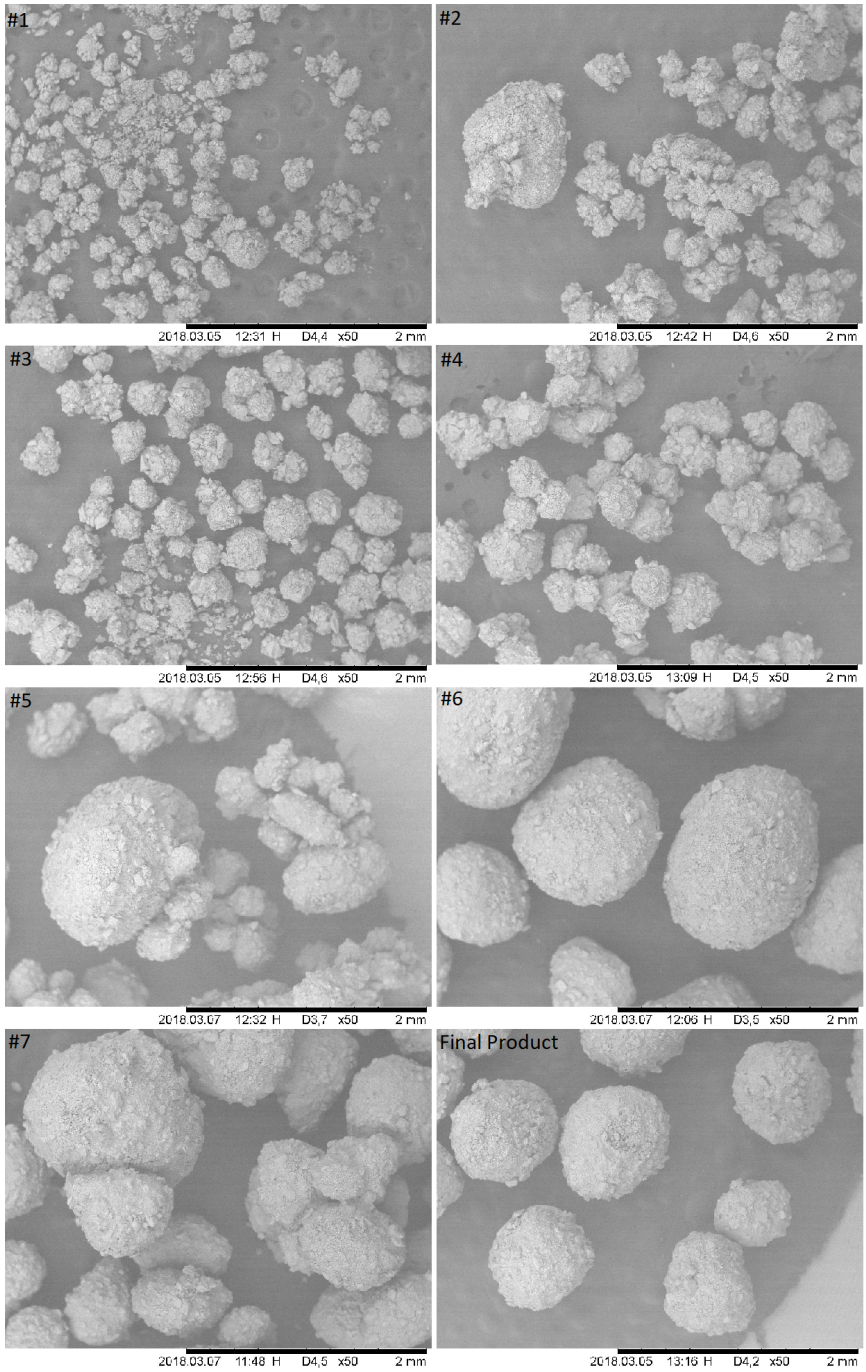

Figure 5.23: This picture show how the granules are being formed with respect to time, water amount and granulation time after water addition. The different samples from 1 to 7 is collected every 5 minute, and the final product is investigated after sieving to desired size of 500-850μm.

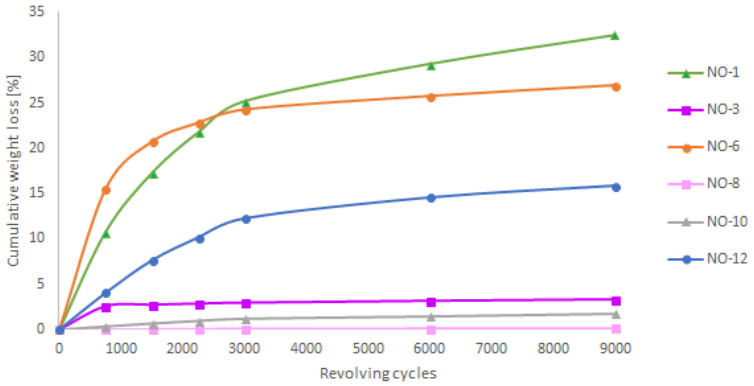

Figure 5.24: Cumulative weight loss (%) as a function of revolving cycles for granules between 250-850μm

Attrition residue - SEM

Residue (250-0μm) after the attrition test for sample NO-1 (850-250 μm), NO-3 (850-250 μm), NO-6 (850-250 μm), NO-8 (850-250 μm), NO-10 (850-250 μm) and NO-12 (850-250 μm) were investigated in SEM. Some of the pictures are shown in figure 5.25 and the rest are given in appendix A7.4.7.

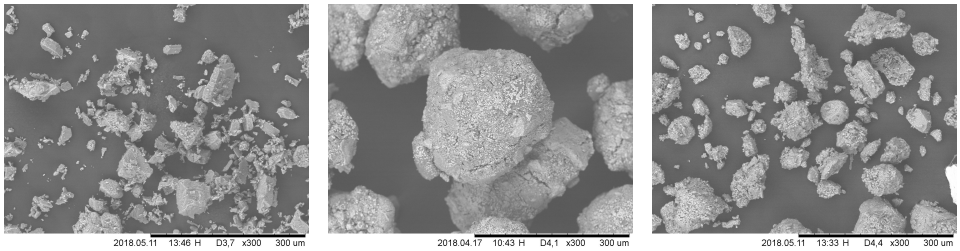

Figure 5.25: (left) NO-1 , (middle) NO-6, (right) NO-8. All SEM photos taken at resolution x300.

5.3.2 Falling Test

The results from the falling test on calcined pellets are given in this section. In figure 5.26, the plot of percentage weight loss (%) between 500-250μm for granules with size 850-500 μm is given. In figure 5.27, the plot of percentage weight loss (%) between 250-0μm for granules with size 850-500 μm is given. And in figure 5.28, the plot of percentage weight loss (%) between 250-0μm for granules with size 500-250 μm is given. The green, purple, orange, pink, gray and blue color represent sample NO-1, NO-3, NO-6, NO-8, NO-10 and NO-12 respectively.

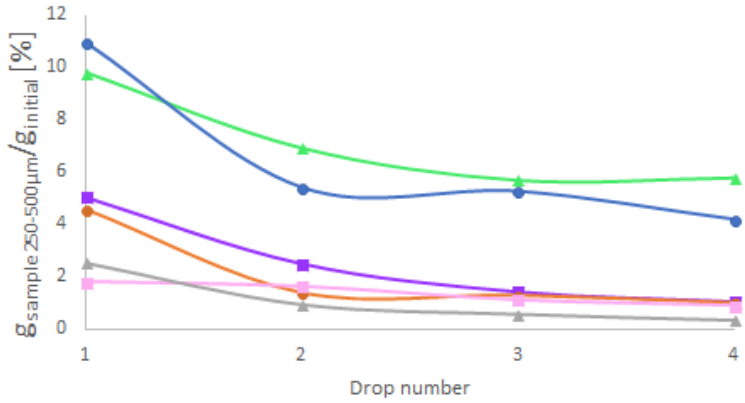

Figure 5.26: Percentage loss (loss between 500-250μm) of pellets with size 850-500 μm for 1,2, 3 and 4 throws. NO-1 (green), NO-3 (purple), NO-6 (orange), NO-8 (pink), NO-10 (gray) and NO-12 (blue).

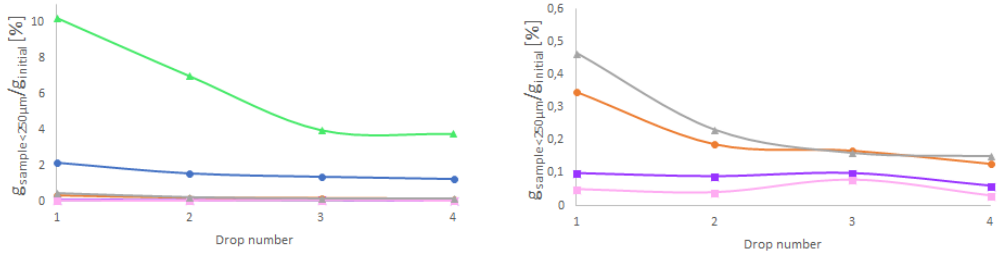

Figure 5.27: Percentage loss (loss between 250-0μm) of pellets with size 850-500 μm for 1,2, 3 and 4 throws. NO-1 (green), NO-3 (purple), NO-6 (orange), NO-8 (pink), NO-10 (gray) and NO-12 (blue). (left) All samples, (right) Only sample NO-3, NO-6, NO-8 and NO-10.

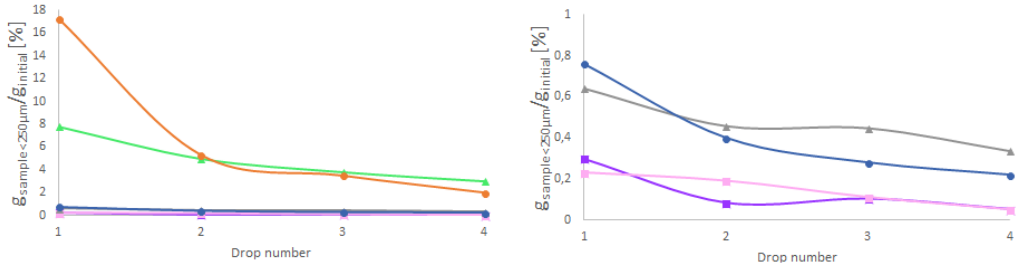

Figure 5.28: Percentage loss (loss between 250-0μm) of pellets with size 500-250μm for 1,2, 3 and 4 throws. NO-1 (green), NO-3 (purple), NO-6 (orange), NO-8 (pink), NO-10 (gray) and NO-12 (blue). (left) All samples, (right) Only sample NO-3, NO-8, NO-10 and NO-12.

Drop tested residue - SEM

Residue (500-250μm) after the falling test for sample NO-1 (850-500 μm), NO-8 (850-500 μm) and NO-10 (850-500 μm) were also investigated in SEM. SEM pictures in figure 5.29

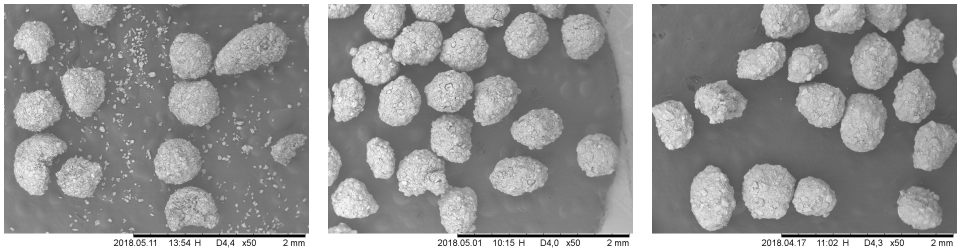

Figure 5.29: (left) NO-1 size 500-850um, (middle) NO-8 size 500-850um, (right) NO-10 size 500-850um. All SEM photos taken at resolution x50.

Chapter 6

Discussion

6.1 Large-Scale Procedure for Production of Pellet

Several experiments were conducted to develop a procedure for granulation of dolomite, cement, water and additives to produce pellets in a relatively large scale. Due to difficulties with granulator equipment during Specialization Project 2017 (TKP4580), a new machine was used to produce pellets. A kitchen machine (Ankarsum) were used to develop spherical pellets with good CO_2-capture capacity and stability, desired morphology and high mechanical strength.

Previous work [75], has revealed good CO_2-cyclic stability for pelletized sorbents made by 20g calcined dolomite, 2% zirconium from $ZrCl_4$ or ZrN_2O_7 and 6% aluminum from cement Fondu. Thus, the main goal for this thesis was to develop a procedure for the upscaling process of calcium oxide-based pellets. Sample NO-12 and NO-6 were made to see if a larger batch could compete with the sorption properties of a smaller scale. Also, another study by the project [76], have shown good stability of granules with additional 2.9% magnesium. Thus, sample NO-8 consisting of 2.9% magnesium from magnesium nitrate and 5.5% aluminum from cement Fondu was made to see if there was any upscaling effect.

Samples made by calcined dolomite require a lot of labor work and high cost due to crushing, sieving and calcination of the raw dolomite. Thus, four samples based on cement ADDA were made with the same additives as sample NO-12 and NO-6. These samples were easier to make, so they were made to see if there were any differences in characterization from dolomite-based pellets and cement ADDA based pellets.

The granulation is a typical batch type of process where both dry material and liquid binders is added in one pot. Each methodology has a limitation, and the rotary drum kitchen machine is equipped with a motor rated at 1.5kW, and it is suspected that this

granulation process has its limitations in rotation speed as the highest level (level 8) only rotates at 45 rpm. A machine with a motor rated at a higher power and thus giving a higher rotational speed of the bowl will be able to handle the high viscosity of the water, dolomite and cement mixture, and give stronger and more spherical pellets.

This production method is also limited by the fact that the bowl is not a closed container. Water evaporates during water addition and granulation. The humidifier is used to overcome the water evaporation problem, but it is still hard to keep a constant humidity in the bowl. This makes the granulation difficult because it is hard to extend the granulation time after water addition, thus mechanical strength and morphology are affected.

Also, the yield differs from batch to batch where it seems like high yield is decreasing with granulation time and water amount (table 5.1). The water:cement ratio is important for the yield and strength of the pellets, where a low water:cement ratio cause lower strength [35]. Lower strength implies more of the small granules, while more water and higher strength favor production of larger granules and lower yield (depending on desired particle size).

The granulation process is divided into two days due to the exothermic reaction (rx. 1.5) between dolomite/cement and water. Water is slowly added due to this temperature increase in the bowl and the fact that strength gain increases with temperature [35]. The granulation process is fast, and the second day of granulation it only takes about 40 minutes to make granules. This is due to the high early strength gain, high heat of hydration and a high compression strength after a short time in ambient temperature [35]. Thus, a short time after the water addition is stopped, the granules are getting hard, and prolonged granulation will only result in loose sand due to friction between the granules, the bowl and the scrape on the wall of the bowl.

To produce pellets with high mechanical strength and a small size distribution, the extrusion/spherionization process is an alternative to granulation. The process need further examination as the extrusion screen consist of either 1mm holes or 3mm holes. By using the extruder plate with 1mm holes the machine experienced power limitations, and 3mm holes produced too large granules.

6.2 Characterization

The different pellets were characterized using TGA, SEM, XRD, BET and MIP to know more about their chemical and mechanical properties.

6.2.1 Surface Area and Pore Size Distribution

Results from nitrogen adsorption/desorption measurement showed that pellets NO-1 and NO-10 have similar surface area around 13.5 m^2/g. Sample NO-12 showed the second highest surface area at approximately 8.9 m^2/g, and sample NO-6 show the same low surface area as cement ADDA-based pellets (NO-20 to NO-23). Pellets NO-8 have lower

surface area than NO-12, the only difference being more MgO present in NO-8 and zirconium in NO-12. Studies has shown that surface area is reduced with increased amount of MgO [77][78]. It seems like there is a trend where high BET surface area gives high initial capacity for CO_2 sorption. An illustration of this trend can be found in appendix, figure A7.47.

The average pore size of the dolomite-based granules (NO-1 to NO-12) range from 8-26 nm as shown in table 5.2. Sample NO-6 show the largest average pores with 26.3 nm, while sample NO-3 have pores at 8.0 nm. The pore volume of sample NO-6 is smallest, with 0.006 cm^3/g, while sample NO-10 have pores of 0.050 cm^3/g. Cement ADDA based samples also have large pore diameters (24-35nm) and small pore volume (0.002-0.003cm^3/g), like that of sample NO-6. The surface area and pore volume influence the CO_2-uptake capacity as the porosity is important for the gas-solid reaction [55].

As judged from the shape of the isotherm and the hysteresis pellets NO-1, NO-10 and NO-12 seem to have isotherms of type IV. The hysteresis is assumed to be of type H1 when compared to figure 3.3. If the pores are type H1, it means that the pellets consist of solids with particles crossed by cylindrical channels or that they are aggregates based on particles with spherical shape in which have pores with uniform size and shape [63]. Pellet NO-3 does not seem to have any typical hysteresis, thus it is suspected that they mainly consist of macropores, type II (in figure 3.3). Condensation occurs at relatively high pressure (P/P_0 = 0.9). This is consistent for large cavities and mesopores ranging from 3-50 nm [63]. This correlates with the measured average pore size of 8-35 nm. Sample NO-6 has an isotherm in almost negative direction, thus it is hard to say much about this sample. Pellet NO-8 has hysteresis like type H3 and H4 in figure 3.3, which means that its pores does not have any well-defined mesoporous structure.

In figure 5.5, the pore size distribution (measured by MIP method) for pellets NO-12 (500-850μm) and raw material, calcined dolomite (<106μm), is presented. Raw material of calcined dolomite has a peak at 40nm while pellets NO-12 seem to have two small peaks at 30nm and 60nm meaning that the pellets have a bimodal pore size distribution. Two peaks are usually found from the pore size distribution plot, which corresponds to the steepest slopes in the cumulative pore volume curve [79].

One may wonder if the small pores are from the material itself and that bigger pores appears when making granules. The MIP method often result in an overestimation of small pores and an underestimation of large pores, and the assumptions about cylindrical pores and that the pores are accessible to mercury, are not always correct [74]. Thus, the materials need to have pores directly accessible to mercury or that mercury can reach the smaller pores through larger pores [66]. The pores of cement material are such type, where there are chains of pores at varying size and shape. Thus, the largest pores will be measured as smaller pores because mercury will only intrude into the small chains when the pressure is adequate. In addition, the pore shape in hydrated cements differs from cylindrical pores assumed by equation 3.6. Still, the MIP method is the most used for cement materials.

The pore size distributions gathered from nitrogen adsorption/desorption are presented in figure 5.4 and in Appendix A7.4.1. BJH plot of pore size distribution for pellets NO-

1 have a broad peak at 60nm, which is not corresponding to the peak at 40nm as for powdered calcined dolomite, measured by MIP. Here, the appearance of bigger pores after granulation might be a reason. The width of peak seems to indicate a broad distribution of pores.

The pore diameter for dolomite-based samples are presented in table 5.3, and the results are difficult to analyze. The pore sizes seem to vary a lot, where samples NO-1, NO-3 and NO-8 seem to have smallest diameters. These samples have no/low content (1.5% Zr or 2.9% Mg) additives. Sample NO-6, NO-10 and NO-12 have the highest measured pore diameters which might be the addition of calcium aluminate cement. NO-8 also have addition of CAC, but the magnesium seems to make the pores narrower. These results seem to demonstrate that the BJH method is invalid for doped dolomite/cement materials because assumptions in the BJH method is not fulfilled. The addition of zirconium can block pores, thus assumption 5. is wrong. Assumption 3. about rigid and uniform shape of pores are also wrong because cement material is based on chains of pores at varying size and shape. Furthermore, if the pellets mainly consist of macropores, the Kelvin equation cannot be applied.

For cement ADDA-based samples it is not possible to read any from the pore size distribution plot. Sample NO-20, NO-21, NO-22 and NO-23 seem to have surface area, and pores with size and shape outside what's valid for the assumptions in the BET measurement. And with surface area below $2m^2/g$, krypton adsorption at 77K is preferred [63].

The amount and distribution of mesopores and macropores are important for the mechanical properties, and an increasing amount of mesopores and macropores gives less strength during attrition [55]. There should be a balance between large pore volume for decreased diffusion resistance of CO_2 to CaO, and smaller pore volume to increase attrition resistance.

6.2.2 Phase Identification and Crystalline Size

Figure A7.69 show phases and phase identification on pellets NO-12 and No-20 (both with 6%Al from cement Fondu and 2%Zr from nitrates). The dolomite-based pellets and the cement-based pellets seems very similar with high proportion of calcium oxide and magnesium oxide as the main phase. This means that the dolomite and cement ADDA mainly consist of CaO·MgO and that it is completely calcined. The sharp peak indicated that the samples have experienced sintering during calcination (950°C 3h). All samples show the same peaks for CaO and MgO (all phases with additional phase identifications are given in Appendix A7.4.2). The reflection set at 2Θ values of 32.2°, 37.4°, 53.9°, 64.2° and 67.5° might be assigned to CaO for all samples. The 2Θ values of 42.9°, 62.3° and 74.7° might be assigned to MgO phases for all samples.

Samples containing aluminum from cement Fondu seems to have small peaks at 2Θ values 18.1° 29.7° 33.3° 55.0° and 57.2° which might be Mayenite ($Ca_{12}Al_{14}O_{32}$) or other calcium aluminum oxide compounds in the CAC. The Al_2O_3 in the CAC is known for having high mechanical strength, have high tamman temperature and the ability to form mixed oxide as $Ca_9Al_6O_{18}$ and $Ca_{12}Al_{14}O_{33}$ during calcination [12].

Only dolomite-based samples indicate a peak at 26.7° and this phase is believed to be silicon oxide (SiO_2) being an impurity in dolomite and cement Fondu. Pellets NO-3, NO-6, NO-12, NO-20, NO-21, NO-22 and NO-23 contains zirconium. Small impurities of $CaZrO_3$ (or other zirconium oxide compounds) might be found by the reflection set at 2Θ values of 22.2°, 36.7°, 46.6° and 56.7°. As viewed in table 1.1, there is some iron (Fe) in the cement. Fe can form $Ca_2Fe_2O_5$ which is known to inhibit carbon capture and CaO conversion [12].

Crystalline size for CaO and MgO were also found from phases measured by x-ray diffraction. All samples have crystalline size ranging between 67-115nm, smallest size for NO-10 and larges size for cement ADDA based samples and NO-6. For MgO, the crystalline size varies from 42-108nm. Also, here it is the crystalline size of pellets NO-10 which is smallest, and cement ADDA-based pellets and NO-6 that has largest size. The active component for CO_2-capture is CaO, thus the crystalline size of CaO is important for CO_2-capacity of the sorbent. This will be discussed further. Also, here it seems like a trend, where high crystalline size gives a low initial sorption capacity (see figure in appendix A7.48), and vice versa. This can be supported by the fact that small particles have higher surface areas, thus better gas-solid reactions [80]. Also, the CO_2 diffusion is less in smaller particles.

6.2.3 High Temperature Sorption Capacity without Steam

The high temperature sorption capacity at dry conditions (no steam) of the pellets are shown in figure 5.7 and 5.8 for dolomite-based pellets and ADDA cement-based pellets respectively. Pellets NO-10 prepared with 6%Al from calcium aluminate cement show high initial capacity, like pure dolomite (NO-1). Also, sample NO-3 and NO-12 (the only difference is the Al content in NO-12) show good capacity and stability where NO-3 have a loss in capacity of 22% from cycle 1 to cycle 11, and sample NO-12 have a capacity loss of 34% in cycle 11 compared to cycle 1. Sample NO-8 with additional magnesium content and aluminum from cement show very promising cyclic stability as compared to the other, only with a CO_2-capacity loss of 24%. Aluminum doped sorbents have high melting point and been shown to have higher specific BET surface area and excellent CO_2-capture stability [81].

Previous work [75], has revealed promising CO_2-capture performance of sample NO-6 and NO-12, only at smaller scale (20g dolomite as raw material) [75]. This promising result is not obtained in this up-scaling study where initial sorption capacity of NO-6 is only 2%. As previously mentioned, the crystalline size of CaO (and MgO) in sample NO-6 is much higher than the crystalline size of CaO for the other dolomite-based samples. Other authors have ascribed high CO_2-capture performance to small crystalline size of CaO and high surface area [80]. In addition, the surface area of sample NO-6 was less than for the other samples, the pore volume was smaller, and the average diameter of the pores was higher than that of the other dolomite-based samples. So, due to this poor performance of NO-6, sample NO-1, NO-3, NO-8, NO-10 and NO-12 were further analyzed in another TGA with steam present. Samples made by cement ADDA were not further characterized due to low CO_2-capacity of the sorbents.

6.2.4 Investigation of pellets NO-6

Sample NO-6 has different behavior than that of the other dolomite-based samples. The pellets of NO-6 were crushed and measured in nitrogen adsorption/desorption to see if any of the properties changed. It was believed that if surface area increased, then pellets NO-6 have an outside shell blockage, and if the surface area did not change, then the whole pellet has the same problem. Analysis of the powder revealed a lower surface area which was not expected, and smaller pore volume and larger pore diameter than pellets. It can be suspected that the crushing of the pellets made the powder even more compact, thus lowering the pore volume etc (See Appendix A7.5). Going back to the low sorption capacity if granules NO-6, it seems like zirconium is blocking some of the active sites of CaO lowering its capacity, or the zirconium affects the pore diameter blocking the pores in the pellet. Studies have demonstrated that it is crucial to have a small amount of salt in the sorbent mixture to avoid pore blockage, thus a large amount of chloride can lower the sorbents capacity [12].

The low sorption capacity can also be due to; the ceramic bowl used for calcination, the pellet production procedure (large scale), physical parameters, melting point of $ZrCl_4$ or maybe the drying rate in the calcination oven (due to large quantities in the bowl). The $ZrCl_4$ is decomposed by water to form $ZrOCl_2$ ($ZrOCl_2 \cdot 8H_2O$) and HCl. So, it is also interesting to know how the chlorine dry in the pellet. The $ZrCl_4$ sublimes at 331°C and have melting point (triple point) at 437°C, while zirconyl chloride hydrate melts at 400°C. By looking at the calcination check of pellets NO-6 (250-500μm) in figure A7.56, it has a small decrease in mass from 20-200°C assigned to water evaporating from the pellets (as seen from MS in figure A7.55). It also has a large drop in mass at approximately 650°C due to release of CO_2 (also detected by the mass spectrometer in figure A7.55). The third weight loss, from 300-400°C, is not detected by MS and it is suspected that it can be several chlorine compounds as the temperature range is like to decomposition of $ZrCl_4$ with H_2O. Anyway, the use of chlorides as dopant can cause corrosion and chlorine products which is undesirable in large scale. So, maybe $ZrCl_4$ is not a good additive even though it is cheaper than ZrN_2O_7.

6.2.5 High Temperature Sorption Capacity with Steam

The sorption capacities were tested with steam, which influences the CO_2-capture. The same temperature scanning program were not tested on the dry TGA but, studies have shown a more than doubled CO_2-carrying capacity with steam/CO_2 during carbonation, compared to only using CO_2 [51]. Also, the study showed improved sintering resistance and enhanced recovery with steam present during sorption. This might explain the good results for sample NO-1 and NO-12, and extended cycles might show a prolonged good stability.

An excellent initial sorption performance as shown for sample NO-1 can be attributed its high porosity, high surface area and small crystalline size of CaO [41]. The carbonation reaction has been reported to be most affected by BET surface area at the rapid chemical

reaction regime [82]. Whereas, crystalline size has most effect on reaction rate when CO_2 start to react with the internal of the CaO particle (external reaction is complete) [83]. The decrease in sorption capacity for pellets with increasing cycles is due to sintering reactions that leads to the agglomeration of particles and the collapse of the porous structure. The sintering phenomena of CaO powdered sorbents seem to be worse than for CaO-based pellets, which seem to exhibit good capacity and cyclic stability with a loss at 57.8% over 34 cycles and only 20.6% loss from cycle 15 to 34. This relatively good cyclic stability has not been shown by others, but it can be suspected that the raw material (<106μm calcined at 800°C for 3h) used and the preparation method applied, might give improved performance of dolomite-based sorbent. This result is questionable, but as shown in the raw data file in Appendix A7.11, the base line drift seems okay, but a calibration of the Linseis TGA might be carried out before further testing.

To improve the cyclic stability, a support with good dispersion, a high specific BET surface area, and a high melting point was added [81]. The incorporation of support by a dopant can hinder sintering and reduce the formation of large CaO crystals [12]. For alumina doped sorbents, some authors have not found any trend in increasing initial capacity with increasing surface area [41], while other have found higher BET surface area and superior stability for Al-doped sorbents [81]. The difference can be in preparation method. Sample NO-8, NO-10 and NO-12 might attribute their good cyclic stability due to addition of alumina (Al_2O_3). Al_2O_3 have high mechanical strength, high Tamman temperature and can modify the microstructure by creation of mixed phases [12]. Such a mixed phase can be mayenite which can to enhance the diffusion of CO_2 into the pellet. Promoted sorbents also show more stable performance in the initial cycles due to inert material improving gas-solid diffusion and improve the carbonation reaction [34].

MgO functions as a physical barrier for $CaCO_3$, which is the reason for the good cyclic stability of NO-8 [84][12][16]. NO-8 have lower initial sorption capacity of CO_2 than that of NO-1 because more MgO gives lower amount of the active component CaO, or the fact that MgO block some of the active sites on CaO [17]. After several cycles, the magnesium doped dolomite show/should show better stability than unpromoted dolomite due to higher MgO content. Higher weight percent of MgO have shown low initial capacity but increased CO_2-cyclic stability [78].

Sample NO-3 was only tested for 17 cycles, and the reliability of the result is highly questionable. An electricity shut-down might have caused irregularities in the Linseis TGA's balance house. Sample NO-8, NO-10 and NO-3 were tested after the power break, and as viewed in figure 5.9, the curve has in increase from the first to the second cycle. A new CO_2-sorption capacity test is recommended, especially for sample NO-3. If the same good result is repeated, the excellent cyclic stability might be attributed formation of $CaZrO_3$ as the high melting point reduces growth of larger CaO particles and inhibits sintering [12].

The comparison of a batch of 20g and a batch of 100g calcined dolomite as raw material, in figure 5.10, seems to show comparable results for 50 cycles. It could be suspected that after 50 cycles, the handmade batch of 20g is slightly better than the rotary drum batch of 100, but the large-scale granulation method seems promising.

Testing CO_2-sorption capacity in TGA is suitable for screening purposes, but it also has some limitations [16]. Particle attrition is not considered, and reactions with sulphur and ash will have to be considered for industrial applications. There are also differences in using granules, and not powder, and most studies have only tested fine powder. When loading 17mg of granules into a deep crucible, there will be more diffusion limitations than if a thin layer of powder was applied. Thus, long sorption times are applied, which is not comparable to residence time used industrial.

6.2.6 Kinetics of NO-12

Flow pattern limitations were investigated (for sample NO-12 (250-400μm)) by loading the supposed minimum and maximum sample load onto the sample pan in the TGA. Part of the result is given in figure 5.12 where cycle 5 and 10 is presented (here the concentrations of CO_2 is 2%). With a partial pressure of CO_2 at 2% it can be wondered if the sample load of 5mg gets sufficient amount of CO_2, and if 30mg get sufficient amount of CO_2 at this pressure. The result clearly show that the less sample loaded in the TGA, the higher CO_2-capture capacity and faster reaction in the reaction controlled regime. A faster reaction in the reaction controlled regime is indicated by a more steep slope for the bold line (5mg sample). To do kinetics, an excess of flow reactant, here CO_2, is necessary. A sample load of approximately 15mg were used for further kinetic studies.

Further, three different sorption temperatures were investigated; 550°C, 620°C and 650°C. Different partial pressure of CO_2 were applied with a sample load of 15mg (250-400μm). Parts of the result is shown in figure 5.13 (only cycle 5 with CO_2 partial pressure of 2%). A sorption temperature at 550°C clearly show that this temperature is too low to reach the maximum CO_2-capacity of the CaO-based pellets, as the CaO can capture CO_2 up to 757 °C [14]. Also, studies have showed extra CO_2-uptake if the temperature is increased after the carbonation stage due to improved mass transfer in the diffusion controlled regime [48].

The blue graph (T=650°C) show a higher capture capacity than the purple graph (T=620°C), but the slope of the purple curve is steeper than the slope of the blue curve. Thus, it seems like the reaction rate in the reaction controlled regime is faster for sorption temperature at 620°C than that of 650°C (for low CO_2 concentration). This is also presented in the plot in 5.14, where the slope of the curve at 620°C, at CO_2 partial pressure of 2-3.3%, is higher than the slope of the curve for 650°C. For higher partial pressure of CO_2 (11.3 - 15.6), the slope of the curve for 650°C is higher than that of 620°C. This can be explained by the fact that not only reaction temperature affects the reaction kinetics, but also partial pressure of CO_2. The driving force for sorption/desorption reaction is the difference in partial pressure and equilibrium pressure. At 650°C, a low partial pressure of CO_2 will be close to the equilibrium pressure as shown in figure 1.2. Thus, the driving force will be small. Whereas for 620°C, the CO_2 partial pressure is further from the equilibrium pressure, resulting in a higher driving force and consequently a faster reaction rate.

A higher carbonation temperature has been shown to give unfavorable consequence on the long-term sorbent reactivity [85]. Higher temperatures and CO_2 partial pressures that

would be met in the industry will cause more sintering due to the change in the morphology of the sorbent. Also, extended carbonation time has a negative influence on sorbent reactivity accelerating its decay and must be considered with a fast reaction in the reaction controlled regime.

Diffusion limitations were also studied for larger particles as figure 5.15 show (cycle 5 with 2% CO_2 concentration). It must be taken into account that the largest particles (2-4mm) were made by extrusion, but the same aluminum and zirconium content were used. Also, the granules with size 250μm-1.2mm have several pellets loaded, while its only one or two pellets loaded for size 2-4mm. This also affect the diffusion of CO_2 to the interior of the pellet, where it is easier to get access the whole pellet where only one or two pellets are loaded on the sample pan. The pore structure also determines the diffusion of CO_2 into the pellet [55], and through large pores the diffusion is less limited and CO_2-capture capacity increases.

The green and the blue curve (250μm-1.2mm) have almost the same s-shape of the curve, where the reaction controlled regime last for approximately 2 minutes before the slow (50min) product layer diffusion limited regime kicks in. Granules at size 2mm has a slightly steeper slope than 3mm pellets, but at approximately 10 minutes of sorption, the orange curve (3mm) is crossing the pink curve (2mm). At this point, the sorption is no longer in the chemical reaction controlled regime but in the diffusion controlled regime. Thus, the crossing of curve for 2mm pellet and 3mm is not of importance for the reaction controlled regime, thus looking at the blue and the green curve is more interesting. The reason for the crossing of the curves might be that less sample (in mg) is used for 3mm compared to that of 2mm and 4mm.

As shown in figure 5.16, more than 80% of maximum sorption capacity is reached for pellets with size 250μm-1.2mm. Residence time for the moving bed reactor used in MBCL technology is limited, and it is expected that most of the CO_2 sorption takes place in the fast-chemical kinetic regime. Thus, pellet particle size will be important parameters when designing the MBCL reactors. A number of investigations have shown that MgO also enhances the CO_2-uptake kinetics of CaO, leading to more of the carbonation reaction occurring at the kinetic stage which is important for selecting a suitable sorbent [86][12]. By increasing the sorption time, the reaction in the diffusion controlled regime will be extended and as a consequence the particles will be more reactive in the following calcination [16]. This is favorable for the cyclic sorption process and should be considered when modelling the MBCL reactors.

6.2.7 Morphology and Surface of Pellets

Pictures from SEM of calcined pellets reveals information of the pellet surface and morphology. Figures 5.21 and 5.22 show pellets after calcination (950°C for 3h) for all dolomite-based samples, and differences in surface roughness and sphericity can be observed. Granules NO-3 and NO-6 seem to have smoother surface than the other four, but NO-8 also seem to have relatively smooth surface. Pellet NO-1 is very spherical, but the surface consists of small particles believed to result in undesired fragments and fines in

the reactor. Thus, it is believed that granulation time should be extended for this sample. Granules NO-10 and NO-12 seem to have similar surface roughness.

Even though the surface of sample NO-3 and NO-6 seem to be nice and smooth, the sphericity measurement of these two is poor with a sphericity of 0.80 and 0.72, where 1 is desired for a complete sphere. Also, NO-12 with sphericity of 0.80 has poor shape. Sample NO-1 has the most preferable shape which also can be seen in figure 5.21. Samples NO-8 and NO-10 both have a measured sphericity of 0.84, but the sphericity measurement must be combined with the mechanical tests to extract more information.

Results from the Specialization project fall 2017 (see Appendix A7.7), figure A7.71, revealed cracks in the pellet surface. These pellets were calcined at 1000°C for 3h with a heating rate at 10°/min. Therefore, the calcination procedure was changed and ramping-time prolonged. As viewed from picture 5.21 and 5.22, these cracks are avoided. When investigating the surface of fresh and spent pellets (figure 5.19 and 5.20), cracks are not observed for the fresh pellets, but they appear in the surface of the spent pellet. These cracks are believed to be due to fast heating rate during the cyclic test. The cracks in the surface might also be due to the presence of steam (disinfection) as expansion and break up of particles can occur during hydration and cycling at high temperatures [87]. Cracks in the pellet surface can reduce compression strength which is undesired for MBCL. It is found that particles with low porosity will experience more stress during hydration. Besides the cracks in the spent sorbent, the used sorbent seems like the fresh.

In figure 5.23, the binding mechanism of the granulation process for NO-10 is illustrated. For the first two samples, it is obvious that more water is needed, as seen from picture 1 and 2. Here, the particles are still very small, but the small grains have already started forming larger aggregates, a process called nucleation [58]. A higher water content will give larger particles with higher strength [35]. The mechanical forces from the machine brings the primary particles close to each other, while bonding forces bind them [59]. In picture number 3, the water addition is just stopped, while only humidifier provides moisture. Here, small granules are already formed by the primary particles, but for the use in the cyclic moving bed reactor, larger pellets are desired. Picture 4 also show the same granule size as picture 3, but here it can be observed that the small granules are starting to bond to form even larger aggregates, a process called coalescence. In these wet granules there are interfacial and capillary pressure forces that affect the mechanical strength. Granulation influences the morphology of the pellets, as shown for sample number 5. Picture 6 show pellets with smooth surface and desired morphology, while in sample 7 these nice particles are starting to merge into even larger granules. One can suspect that granulation should have been stopped at sample 6, but it is easy to be wise after the event. This means, after 20 minutes of granulation after the last water addition (only humidity added), the granulation can be stopped.

6.3 Mechanical Properties of Pellets

Mechanical strength of the pellets is a very important property of the CaO-based granules. The strength of a granule during production and after drying depend on the bonding forces involved. Pellets will be blown around in the MBCL technology and thus bump into other pellets, the wall of the reactor and the bottom of the reactor. Consequently, loss of active material will occur due to abrasion and breakage. Less material will be lost if the pellets have good strength, shape and smooth surface. Loss of material will require more of the fresh sorbent, thus increasing cost. The reactor is modelled to handle pellets larger than 250 μm, thus fines <250 μm will block pipes leading to an increased pressure drop in the reactor.

6.3.1 Attrition test

For CO_2-capture sorption/desorption cycles, high attrition rates are expected in the first cycle because of early particle fragmentation [88]. The loss of mass will decline afterwards due to thermochemical treatment that makes the particle structure harder.

Results from the mechanical attrition test is presented in figure 5.24. Here, the pellets can be classified in three categories according to mechanical strength; good, medium, bad. Sample NO-1 and NO-6 show poor performance in this test, and is classified as bad, where pellets NO-6 have sorbent loss stabilized at 25%. As shown in figure A7.52, the residuals from sample NO-6 are large particles. This can be called secondary fragmentation, which is caused by mechanical stresses from collisions between the particle and the reactor [88]. Sample NO-1 does not seem to reach a plateau as the weight loss continues to increase. This could also be suspected from the SEM picture in 5.21 where the surface contains more of the loose grains probably due to too short granulation time even though the sphericity is close to 1. This residue seems to be attrition by abrasion. This means that sorbent is lost due to mechanical contact which creates finer fragments than secondary fragmentation [88].

The medium strong pellet is NO-12, with a weight loss stabilized at 15%. Studies have shown that formation of mayenite is attributed the high mechanical strength of calcium aluminate based pellets [12]. Mayenite was found in dolomite-based pellets (NO-6, NO-10, NO-8 and NO-12) containing calcium aluminate cement (CAC). Granules NO-12 and NO-6 also contains calcium alumina cement and zirconium, but here it seems like the shape of the pellets are poor and that granulation time should have been extended to get higher mechanical strength. Granules NO-3, NO-8 and NO-10 are classified as good pellets. They have residual mass loss of 3%, 0.1% and 2% respectively which is better than studies based on MgO-based pellets, where weight loss is found to be 3.5-4.5% [53]. The high strength might be due to formation of mayenite, good sphericity and surface of the pellets.

In addition, during the CO_2-capture capacity cycling in steam, the pellets will get hydrated. A disadvantage with steam present in the reactor, is the fact that hydrated particles will experience a more intense attrition and as a result elutriation [44][89]. But a lot of

hydration problems are dealt with by pelletizing the sorbent. This must also be considered for the use of the pellets in MBCL.

6.3.2 Falling test

A falling test is a good prediction of the mechanical properties of pellets during circulation in MBCL [34]. The pellet will experience gravitational forces when falling down the reactor, thus a falling test was applied. The granules are also here classified according to mechanical strength; good, medium, bad.

Residue between 250-500μm of pellets with a size between 500 and 850μm are shown in figure 5.26. Pellets NO-12 and NO-1 lost most weight during 4 drops, and can it be said that they have poor mechanical strength. Granules NO-3 and NO-6 are said to be medium good as they have relatively high initial loss but stabilizes at 2% in the fourth throw. NO-8 and NO-10 have the best performance of the large granules, with a stable loss below 2% in each throw. As shown in figure 5.29 it is easy to see that NO-1 has crushed, while NO-8 and NO-10 are still intact. As previously mentioned, the lower limit for use in the cyclic moving bed reactor is grains less than 250μm, thus even though sample NO-12 and NO-6 has a high loss here, it does not mean the residues are useless for CO_2-capture.

The material left after throwing pellets between 500-850μm is residue less than 250μm, as shown in plot 5.27. Here, all pellets are classified as good except NO-1 (bad) and NO-12 (medium). The low strength of NO-1 was also presented in the attrition test, figure 5.24. The other dolomite-based pellets show extremely good mechanical strength where NO-8 has a weight loss at 0.05%, which was also demonstrated in the attrition test. This is believed to be due to high strength gain of CAC, and the fact that it has relatively low average pore diameter and a small pore volume meaning that the porosity is lower. This again, correlates with lower CO_2-uptake as shown in figure 5.7. A low porosity correlates with a high crush strength as demonstrated in figure 3.6. Also, sample NO-3 have a small average pore volume and pore diameter, thus low porosity, giving high crushing strength.

The smallest pellets (250-500μm) were also dropped down the tube, and the plot of the result is given in figure 5.28. Again, sample NO-1 have a poor crushing strength. In addition, sample NO-6 have high loss of pellets and can be classified as medium good. More water should have been added during granulation, because a low water:cement ratio causes lower strength [35]. The other samples with calcium aluminate cement (Fondu) and zirconium show very good crushing strength with a loss below 0.8%. Pellets NO-8 are also here very stable in each throw. Another reason for the good mechanical properties of samples containing CAC is that both the cement Fondu and the dolomite contain impurities which are affecting the hardening process due to "poisoning"[35]. Also, calcium from the aggregate might help the formation of more stable hydrates. These results are comparable to the pellets made during the specialization project as shown in Appendix A7.7.2

A decrease in percentage weight loss for each drop is desired because then the small grains on the surface of the pellets are removed, and the strong core of the granule remains. Over all, it looks like the good pellets according to mechanical strength, is NO-3, NO-8 and NO-

10. The medium good pellets are NO-12 and NO-6, while NO-1 show poor performance in the mechanical tests.

6.4 Future Work

The subsection will contain some thoughts for further research.

6.4.1 Granulation and Extrusion

The granulator equipment seems to function all right, but it has limitation in rotational speed. For these lab-scale experiments it seems like the machine has sufficient power as judged from the mechanical performance of some of the pellets. The granulator has already been tested with 500g raw material (A7.2), but for an even larger batch the machine might be too simple. Also, a closed rotary drum would have improved the granulation process. The granulation process needs improvements and further experimenting should be considered to improve the characteristics of the dolomite pellets.

The extrusion process is far from perfect and need more optimization. The screen used for extrusion contained 3mm holes, thus large pellets were produced. To produce pellets with a size suitable for MBCL, the wholes should be in a range of 1mm. A screen with 1mm holes was also tested, but due to power limitation of the extrusion machine, the cement material could not be pressed through. Thus, a machine rated at higher power is desired, or modification in the raw material, water amount, rest time or maybe the screen should be optimized for the process. Other binding material can also be an alternative. For example, wax can be used to shape the pellets, and subsequently burned of in calcination. Eventually, lubricants can be used as binder in the process.

6.4.2 Surface Area, Pore Size Distribution, X-ray Diffraction and Morphology

Results for surface area and pore size measurements gathered reveals limitations in using the BET and BJH method due to low surface areas and higher portion macropores. Thus, mercury intrusion porosimetry can be considered as a better alternative even though the assumption about cylindrical pores are not fulfilled using cement. Surface area and pore size can also be considered measured on spent pellets.

The crystalline size measurements and phase identification of the cyclic tested dolomite-based pellets have not been studied and will be important for investigation of the sintering phenomena. Studies have shown that crystalline size of CaO is larger after calcination at high CO_2 partial pressure and when the temperature is close to the equilibrium temperature and spent pellets will thus contain larger CaO crystals [48].

In this study, the surface morphology and shape of the pellets were studied on fresh and spent sorbent. Further investigation of the pellet interior should be carried out in a microscope at higher resolution (S(t)EM or SEM APREO etc.) to study the primary particles of fresh and used pellets. This might demonstrate that macro-porosity will increase while micro-porosity increases with increased sorption/desorption cycles [90].

6.4.3 Mechanical Properties

This report provides mechanical tests on the oxide, but not for carbonated pellets. Thus, further studies on mechanical strength on carbonated pellets after a cycle in the TGA can conducted. The cracks in the surface of spent sorbents are viewed on SEM pictures 5.20. If these sorbents were tested mechanically, their crush strength is believed to be weaker than for fresh pellets.

Attrition testing should also be performed at higher temperature as attrition rate is increasing with higher temperatures [16]. To get similar conditions as for MBCL, the attrition also should have been tested during cyclic stability in the TGA.

A compression test has been used by others to study the compression strength of dolomite/cement pellets [53]. This test will be able to investigate the force needed to crush the pellet, which gives a good prediction of the pellet strength before they are applied in industrial scale.

6.4.4 High-temperature CO_2 Cyclic Stability

Further testing of the CO_2-capture carrying capacity in presence of steam for pellets are desired. Due to limited availability on the Linseis TGA during the thesis, only 34 cycles of sorption/desorption were carried out for most of the granules. For an even more improved cyclic stability of the pellets, several compositions of calcium aluminate cements and other material with high Tamman temperature can be investigated. Sample tested in this thesis should also be re-tested for more reliable results.

Also, a pre-treatment method including half-calcination in CO_2 and calcination in N_2 atmosphere has revealed promising CO_2 sorption capacity and can also be considered tested [15].

6.4.5 Kinetic Study

In this study, only sample NO-12 were tested for kinetics, but it is known that the CaO content, and/or inert specie have an important effect on the average thickness of the product layer [91]. Thus, the CaO content and the inert compounds affect the transition between the reaction controlled regime and the slow product layer regime. For further study, several samples with different additives can also be investigated kinetically. Reaction kinetics should also be investigated in the TGA using steam to simulate more realistic conditions.

Also, from results in figure 5.15, it seems like further studies on pellets ranging from 1.2 mm in size to 2 mm in size will give a better understanding of a suitable pellet. Maybe, 1.5mm is the upper size limit pellets used to cycle around in the MBCL process. These properties are very important and will be used for reactor modeling when selecting an appropriate residence time.

Chapter 7

Conclusion

The main goal of this thesis was to develop a procedure for making pellets in large scale based on calcium oxide, capable to capture CO_2 at high temperatures. Desirable material properties as good CO_2-capture capacity and stability, and good mechanical strength are desirable for these pellets to be used in MBCL technology. A rotary drum granulation machine was used to produce granules made of calcined dolomite/cement ADDA, calcium aluminate cement, extra magnesium and zirconium with water as liquid binder. An extrusion/spherionization method were also applied to make bigger granules.

Scanning electron microscopy and mechanical tests demonstrate promising properties of pellets doped with aluminum from cement Fondu, zirconium and magnesium. They have a smooth pellet surface and sphericity, exceptional cumulative attrition loss with the lowest at 0.1% believed to be due to formation of mayenite ($Ca_{12}Al_{14}O_{33}$). Results from cycling tests in TGA in presence of steam showed promising CO_2-sorption capacity and stability for most of the dolomite-based pellets, and thus the up-scaling procedure is applicable. Also, the CO_2-capture stability seemed to be improved by adding aluminum, zirconium and magnesium as stabilizing agents to prevent sintering by the formation of mixed oxides. Investigation of the pellet kinetics demonstrated that diffusion limitations seem to be worst for larger granules, and pellets ranging from 250μm to 1.2mm show fast kinetics in the chemical reaction controlled regime.

Furthermore, the kinetic study should be extended to find the upper size limit which seems to be some place between 1.2mm to 2mm. The reaction rate in the chemically controlled regime should also be examined for the different pellet compositions. The granulation procedure can also be improved my making even stronger and more spherical pellets, in the granulator or the extruder. Characterization of spent material have a lot of potential, as cycling between oxides and carbonates will give different difficulties regarding mechanical strength.

Bibliography

[1] Maria Olsvik. Specialization project ntnu. 2017.

[2] Jeffrey H. Drese Sunho Choi and Christopher W. Jones. Adsorbent materials for carbon dioxide capture from large anthrophogenic point sources. *ChemSusChem*, 2009.

[3] Hongqun Yang, Zhenghe Xu, Maohong Fan, Rajender Gupta, Rachid B Slimane, Alan E Bland, and Ian Wright. Progress in carbon dioxide separation and capture: A review. *Journal of Environmental Sciences*, 20(1):14 – 27, 2008. ISSN 1001-0742. doi: https://doi.org/10.1016/S1001-0742(08)60002-9. URL http://www.sciencedirect.com/science/article/pii/S1001074208600029.

[4] Salam J.J. Titinchi, Marvin Piet, Hanna S. Abbo, Olav Bolland, and Wilhelm Schwieger. Chemically modified solid adsorbents for co2 capture. *Energy Procedia*, 63(Supplement C):8153 – 8160, 2014. ISSN 1876-6102. doi: https://doi.org/10.1016/j.egypro.2015.12.337. URL http://www.sciencedirect.com/science/article/pii/S1876610215030192.

[5] M. Kotyczka-Moranska, G. Tomaszewicz, and G. Labojko. Comparison of different methods for enhancing co 2 capture by cao-based sorbents. review. *Physicochemical Problems of Mineral Processing*, 48(1):77–90, 2012. URL https://www.scopus.com/inward/record.uri?eid=2-s2.0-84865422521&partnerID=40&md5=2f8da5be49aa3241f55a2a04af8a7130.

[6] José D. Figueroa, Timothy Fout, Sean Plasynski, Howard McIlvried, and Rameshwar D. Srivastava. Advances in co2 capture technology—the u.s. department of energy's carbon sequestration program. *International Journal of Greenhouse Gas Control*, 2(1):9 – 20, 2008. ISSN 1750-5836. doi: https://doi.org/10.1016/S1750-5836(07)00094-1. URL http://www.sciencedirect.com/science/article/pii/S1750583607000941.

[7] Zou Yong, Vera Mata, and Alırio E. Rodrigues. Adsorption of carbon dioxide at high temperature—a review. *Separation and Purification Technology*, 26(2):

195 – 205, 2002. ISSN 1383-5866. doi: https://doi.org/10.1016/S1383-5866(01)00165-4. URL http://www.sciencedirect.com/science/article/pii/S1383586601001654.

[8] BjÃžrnar Arstad, Anna Lind, Kari Anne Andreassen, Joanna Pierchala, Knut Thorshaug, and Richard Blom. In-situ xrd studies of dolomite based co2 sorbents. *Energy Procedia*, 63(Supplement C):2082 – 2091, 2014. ISSN 1876-6102. doi: https://doi.org/10.1016/j.egypro.2014.11.224. URL http://www.sciencedirect.com/science/article/pii/S1876610214020396.

[9] B. Feng, H. An, and E. Tan. Screening of co2 adsorbing materials for zero emission power generation systems. *Energy and Fuels*, 21(2):426–434, 2007. doi: 10.1021/ef0604036. URL https://www.scopus.com/inward/record.uri?eid=2-s2.0-34247175425&doi=10.1021%2fef0604036&partnerID=40&md5=5a1cf34f3105148a64694dd46680acf8.

[10] Dawid P. Hanak, Chechet Biliyok, Edward J. Anthony, and Vasilije Manovic. Modelling and comparison of calcium looping and chemical solvent scrubbing retrofits for co2 capture from coal-fired power plant. *International Journal of Greenhouse Gas Control*, 42:226 – 236, 2015. ISSN 1750-5836. doi: https://doi.org/10.1016/j.ijggc.2015.08.003. URL http://www.sciencedirect.com/science/article/pii/S1750583615300487.

[11] J.C. Abanades, E.J. Anthony, J. Wang, and J.E. Oakey. Fluidized bed combustion systems integrating co2 capture with cao. *Environmental Science and Technology*, 39(8):2861–2866, 2005. doi: 10.1021/es0496221. URL https://www.scopus.com/inward/record.uri?eid=2-s2.0-17644363749&doi=10.1021%2fes0496221&partnerID=40&md5=7e63f5b02e578eeeb14fa563b94b21c4.

[12] Shakirudeen A. Salaudeen, Bishnu Acharya, and Animesh Dutta. Cao-based co2 sorbents: A review on screening, enhancement, cyclic stability, regeneration and kinetics modelling. *Journal of CO2 Utilization*, 23:179 – 199, 2018. ISSN 2212-9820. doi: https://doi.org/10.1016/j.jcou.2017.11.012. URL http://www.sciencedirect.com/science/article/pii/S2212982017304560.

[13] David R. Lide (National Institute of Standards and Technology), editors. *CRC Handbook of Chemistry and Physics,*, volume 128. 86th edition, 2006. ISBN 0-8493-0486-5. doi: 10.1021/ja059868l. URL https://doi.org/10.1021/ja059868l.

[14] Yuhua Duan and Dan C. Sorescu. Co2 capture properties of alkaline earth metal oxides and hydroxides: A combined density functional theory and lattice phonon dynamics study. *The Journal of Chemical Physics*, 133(7):074508, 2010. doi: 10.1063/1.3473043. URL https://doi.org/10.1063/1.3473043.

[15] Carlos Herce, Stefano Stendardo, and Cristóbal Cortés. Increasing co2 carrying capacity of dolomite by means of thermal stabilization by triggered calcination. *Chemical Engineering Journal*, 262(Supplement C):18 – 28, 2015. ISSN

1385-8947. doi: https://doi.org/10.1016/j.cej.2014.09.076. URL http://www.sciencedirect.com/science/article/pii/S1385894714012728.

[16] María Erans, Vasilije Manovic, and Edward J. Anthony. Calcium looping sorbents for co2 capture. *Applied Energy*, 180:722 – 742, 2016. ISSN 0306-2619. doi: https://doi.org/10.1016/j.apenergy.2016.07.074. URL http://www.sciencedirect.com/science/article/pii/S0306261916310157.

[17] K.O. Albrecht, K.S. Wagenbach, J.A. Satrio, B.H. Shanks, and T.D. Wheelock. Development of a cao-based co2 sorbent with improved cyclic stability. *Industrial and Engineering Chemistry Research*, 47(20):7841–7848, 2008. doi: 10.1021/ie8007743. URL https://www.scopus.com/inward/record.uri?eid=2-s2.0-54949099256&doi=10.1021%2fie8007743&partnerID=40&md5=f6a2703c54e7f16737d95e1950124eba.

[18] Q. Xiao, Y. Liu, Y. Zhong, and W. Zhu. A citrate sol-gel method to synthesize li2zro3 nanocrystals with improved co2 capture properties. *Journal of Materials Chemistry*, 21(11):3838–3842, 2011. doi: 10.1039/c0jm03243c. URL https://www.scopus.com/inward/record.uri?eid=2-s2.0-79952268303&doi=10.1039%2fc0jm03243c&partnerID=40&md5=690bf307e2bae9d8d8560b247cad520e.

[19] Zhenshan Li, Hongming Sun, and Ningsheng Cai. Rate equation theory for the carbonation reaction of cao with co2. *Energy & Fuels*, 26(7):4607–4616, 2012. doi: 10.1021/ef300607z. URL https://doi.org/10.1021/ef300607z.

[20] Kim Johnsen, John R. Grace, Said S. E. H. Elnashaie, Leiv Kolbeinsen, and Dag Eriksen. Modeling of sorption-enhanced steam reforming in a dual fluidized bubbling bed reactor. *Industrial & Engineering Chemistry Research*, 45(12):4133–4144, 2006. doi: 10.1021/ie0511736. URL https://doi.org/10.1021/ie0511736.

[21] Stefano Stendardo and Pier Ugo Foscolo. Carbon dioxide capture with dolomite: A model for gas–solid reaction within the grains of a particulate sorbent. *Chemical Engineering Science*, 64(10):2343 – 2352, 2009. ISSN 0009-2509. doi: https://doi.org/10.1016/j.ces.2009.02.009. URL http://www.sciencedirect.com/science/article/pii/S0009250909001067.

[22] Behnam Khoshandam, Ramachandran Vasant Kumar, and Leila Allahgholi. Mathematical modeling of co2 removal using carbonation with cao: The grain model. *Korean Journal of Chemical Engineering*, 27(3):766–776, May 2010. ISSN 1975-7220. doi: 10.1007/s11814-010-0119-5. URL https://doi.org/10.1007/s11814-010-0119-5.

[23] Grasa Gemma, Murillo Ramón, Alonso Mónica, and Abanades J. Carlos. Application of the random pore model to the carbonation cyclic reaction. *AIChE Journal*, 55(5):1246–1255. doi: 10.1002/aic.11746. URL https://onlinelibrary.wiley.com/doi/abs/10.1002/aic.11746.

[24] C. N. R. Rao and J. Gopalakrishnan. *New Directions in Solid State Chemistry*. Cambridge University Press, 2 edition, 1997. doi: 10.1017/CBO9780511623141.

[25] Deuk Ki Lee. An apparent kinetic model for the carbonation of calcium oxide by carbon dioxide. *Chemical Engineering Journal*, 100(1):71 – 77, 2004. ISSN 1385-8947. doi: https://doi.org/10.1016/j.cej.2003.12.003. URL http://www.sciencedirect.com/science/article/pii/S1385894704000269.

[26] Zhen-shan Li and Ning-sheng Cai. Modeling of multiple cycles for sorption-enhanced steam methane reforming and sorbent regeneration in fixed bed reactor. *Energy & Fuels*, 21(5):2909–2918, 2007. doi: 10.1021/ef070112c. URL https://doi.org/10.1021/ef070112c.

[27] E. Bouquet, G. Leyssens, C. Schönnenbeck, and P. Gilot. The decrease of carbonation efficiency of cao along calcination-carbonation cycles: Experiments and modelling. *Chemical Engineering Science*, 64(9):2136–2146, 2009. doi: 10.1016/j.ces.2009.01.045. URL https://www.scopus.com/inward/record.uri?eid=2-s2.0-63249108474&doi=10.1016%2fj.ces.2009.01.045&partnerID=40&md5=36accaf4ebec763b0a6600ca859f597e.

[28] D. Alvarez and J. Carlos Abanades. Determination of the critical product layer thickness in the reaction of cao with co2. *Industrial and Engineering Chemistry Research*, 44(15):5608–5615, 2005. doi: 10.1021/ie050305s. URL https://www.scopus.com/inward/record.uri?eid=2-s2.0-22944490516&doi=10.1021%2fie050305s&partnerID=40&md5=c5df4b1053d306d0a3ab321a8f354ded.

[29] G. Grasa, I. Martínez, M.E. Diego, and J.C. Abanades. Determination of cao carbonation kinetics under recarbonation conditions. *Energy and Fuels*, 28(6):4033–4042, 2014. doi: 10.1021/ef500331t. URL https://www.scopus.com/inward/record.uri?eid=2-s2.0-84902844944&doi=10.1021%2fef500331t&partnerID=40&md5=fc04e4e4f34bbfbd20a1686520fb7bab.

[30] Robert H. Borgwardt. Calcium oxide sintering in atmospheres containing water and carbon dioxide. *Industrial & Engineering Chemistry Research*, 28(4):493–500, 1989. doi: 10.1021/ie00088a019. URL https://doi.org/10.1021/ie00088a019.

[31] Muhammad Awais Naeem, Andac Armutlulu, Agnieszka Kierzkowska, and Christoph R. Müller. Development of high-performance cao-based co2 sorbents stabilized with al2o3 or mgo. *Energy Procedia*, 114(Supplement C):158 – 166, 2017. ISSN 1876-6102. doi: https://doi.org/10.1016/j.egypro.2017.03.1158. URL http://www.sciencedirect.com/science/article/pii/S1876610217313310.

[32] Elliott T. Gall, Cem Sonat, William W. Nazaroff, and Cise Unluer. Investigating co2 removal by ca- and mg-based sorbents with application to indoor air treatment.

Building and Environment, 110:161 – 172, 2016. ISSN 0360-1323. doi: https://doi.org/10.1016/j.buildenv.2016.10.008. URL http://www.sciencedirect.com/science/article/pii/S0360132316303997.

[33] Vasilije Manovic and Edward J. Anthony. Screening of binders for pelletization of cao-based sorbents for co2 capture. *Energy & Fuels*, 23(10):4797–4804, 2009. doi: 10.1021/ef900266d. URL http://dx.doi.org/10.1021/ef900266d.

[34] Vasilje Manovic and Edward J. Anthony. Cao-based pellets supported by calsium aluminate cements for high-temperature co2 capture. *Environmental Science Technology*, 2009.

[35] Texas. *Calcium Aluminate Cement Concrete*. Texas Department of Transportation - Technical Advisory, August 2010. URL https://ftp.dot.state.tx.us/pub/txdot-info/cst/tips/calcium_concrete.pdf.

[36] John Winpigler Dale P. Bentz, Max A. Peltz. *Early-Age Properties of Cement-Based Materials. II. Influence of Water-to-Cement Ratio*, volume 21. 2009.

[37] Northwestern. Hydration and microstructure of portland cement paste, 2014. URL http://iti.northwestern.edu/cement/monograph/Monograph5_3.html.

[38] Maxime Liard, Luka Oblak, Mohammed Hachim, Martin Vachon, and Didier Lootens. Impact of viscosity on hydration kinetics and setting properties of cementitious materials. 3:20130096, 01 2015.

[39] Barbara Pacewska, Mariola Nowacka, Valentin Antonovič, and Marius Aleknevičius. Investigation of early hydration of high aluminate cement-based binder at different ambient temperatures. *Journal of Thermal Analysis and Calorimetry*, 109(2):717–726, Aug 2012. ISSN 1572-8943. doi: 10.1007/s10973-012-2233-6. URL https://doi.org/10.1007/s10973-012-2233-6.

[40] Bjørnar Arstad, Aud Spjelkavik, Kari Anne Andreassen, Anna Lind, Joanna Prostak, and Richard Blom. Studies of ca-based high temperature sorbents for co2 capture. *Energy Procedia*, 37:9 – 15, 2013. ISSN 1876-6102. doi: http://dx.doi.org/10.1016/j.egypro.2013.05.079. URL http://www.sciencedirect.com/science/article/pii/S1876610213000891.

[41] Nana Wang, Yuchuan Feng, Liang Liu, and Xin Guo. Effects of preparation methods on the structure and property of al-stabilized cao-based sorbents for co2 capture. *Fuel Processing Technology*, 173:276 – 284, 2018. ISSN 0378-3820. doi: https://doi.org/10.1016/j.fuproc.2018.02.005. URL http://www.sciencedirect.com/science/article/pii/S0378382017320659.

[42] C. Qin, J. Yin, H. An, W. Liu, and B. Feng. Performance of extruded particles from calcium hydroxide and cement for co 2 capture. *Energy and Fuels*, 26(1):154–161, 2012. doi: 10.1021/ef201141z. URL https://www.scopus.com/inward/record.uri?eid=2-s2.

0-84862907879&doi=10.1021%2fef201141z&partnerID=40&md5=2fcd24095b9ec3237b53c42278afd95b.

[43] Andy Antzara, Eleni Heracleous, and Angeliki A. Lemonidou. Development of cao-based mixed oxides as stable sorbents for post-combustion co2 capture via carbonate looping. *Energy Procedia*, 63:2160 – 2169, 2014. ISSN 1876-6102. doi: https://doi.org/10.1016/j.egypro.2014.11.235. URL http://www.sciencedirect.com/science/article/pii/S1876610214020505.

[44] Y. Wu, J. Blamey, E.J. Anthony, and P.S. Fennell. Morphological changes of limestone sorbent particles during carbonation/calcination looping cycles in a thermogravimetric analyzer (tga) and reactivation with steam. *Energy and Fuels*, 24(4):2768–2776, 2010. doi: 10.1021/ef9012449. URL https://www.scopus.com/inward/record.uri?eid=2-s2.0-77951137014&doi=10.1021%2fef9012449&partnerID=40&md5=59e17677f62d14f6df6fc8f05f17a78c.

[45] F.-C. Yu, N. Phalak, Z. Sun, and L.-S. Fan. Activation strategies for calcium-based sorbents for co 2 capture: A perspective. *Industrial and Engineering Chemistry Research*, 51(4):2133–2142, 2012. doi: 10.1021/ie200802y. URL https://www.scopus.com/inward/record.uri?eid=2-s2.0-84863393487&doi=10.1021%2fie200802y&partnerID=40&md5=d94bc82aeb3edc6be9dae340c1508a4b.

[46] B. Arias, G.S. Grasa, and J.C. Abanades. Effect of sorbent hydration on the average activity of cao in a ca-looping system. *Chemical Engineering Journal*, 163 (3):324 – 330, 2010. ISSN 1385-8947. doi: https://doi.org/10.1016/j.cej.2010.08.009. URL http://www.sciencedirect.com/science/article/pii/S1385894710006972.

[47] B.V. Materić, C. Sheppard, and S.I. Smedley. Effect of repeated steam hydration reactivation on cao-based sorbents for co2 capture. *Environmental Science and Technology*, 44(24):9496–9501, 2010. doi: 10.1021/es102623k. URL https://www.scopus.com/inward/record.uri?eid=2-s2.0-78650289218&doi=10.1021%2fes102623k&partnerID=40&md5=a132529e7bb1766a8fc38d76412abed9.

[48] Felix Donat and Christoph R. Müller. A critical assessment of the testing conditions of cao-based co2 sorbents. *Chemical Engineering Journal*, 336: 544 – 549, 2018. ISSN 1385-8947. doi: https://doi.org/10.1016/j.cej.2017.12.050. URL http://www.sciencedirect.com/science/article/pii/S138589471732171X.

[49] N. Rodríguez, M. Alonso, and J.C. Abanades. Experimental investigation of a circulating fluidized-bed reactor to capture co2 with cao. *AIChE Journal*, 57(5):1356–1366, 2011. doi: 10.1002/aic.12337. URL https://www.scopus.com/inward/record.uri?eid=2-s2.0-78751643324&doi=10.1002%2faic.12337&partnerID=40&md5=172b511254e7e6126df75439b86fd73e.

[50] J. Kremer, A. Galloy, J. Ströhle, and B. Epple. Continuous co2 capture in a 1-mwth carbonate looping pilot plant. *Chemical Engineering and Technology*, 36(9):1518–1524, 2013. doi: 10.1002/ceat.201300084. URL https://www.scopus.com/inward/record.uri?eid=2-s2.0-84882575991&doi=10.1002%2fceat.201300084&partnerID=40&md5=f52deff2feb4431d0386fbef551e77ba.

[51] Ze-Hua Li, Yin Wang, Kai Xu, Jing-Ze Yang, Shao-Bo Niu, and Hong Yao. Effect of steam on cao regeneration, carbonation and hydration reactions for co2 capture. *Fuel Processing Technology*, 151:101 – 106, 2016. ISSN 0378-3820. doi: https://doi.org/10.1016/j.fuproc.2016.05.019. URL http://www.sciencedirect.com/science/article/pii/S0378382016302168.

[52] Vasilije Manovic and Edward J. Anthony. Cao-based pellets supported by calcium aluminate cements for high-temperature co2 capture. *Environmental Science & Technology*, 43(18):7117–7122, 2009. doi: 10.1021/es901258w. URL http://dx.doi.org/10.1021/es901258w.

[53] Yingchao Hu, Xiaowei Liu, Zijian Zhou, Wenqiang Liu, and Minghou Xu. Pelletization of mgo-based sorbents for intermediate temperature co2 capture. *Fuel*, 187 (Supplement C):328 – 337, 2017. ISSN 0016-2361. doi: https://doi.org/10.1016/j.fuel.2016.09.066. URL http://www.sciencedirect.com/science/article/pii/S0016236116309292.

[54] Alexander Shulman, Erik Cleverstam, Tobias Mattisson, and Anders Lyngfelt. Chemical –looping with oxygen uncoupling using mn/mg-based oxygen carriers – oxygen release and reactivity with methane. *Fuel*, 90(3):941–950, 2011. doi: https://doi.org/10.1016/j.fuel.2010.11.044. URL http://www.sciencedirect.com/science/article/pii/S0016236110006599.

[55] Huichao Chen, Changsui Zhao, and Yanmei Yang. Enhancement of attrition resistance and cyclic co2 capture of calcium-based sorbent pellets. *Fuel Processing Technology*, 116:116 – 122, 2013. ISSN 0378-3820. doi: https://doi.org/10.1016/j.fuproc.2013.05.012. URL http://www.sciencedirect.com/science/article/pii/S0378382013002075.

[56] V. Manovic and E.J. Anthony. Reactivation and remaking of calcium aluminate pellets for co2 capture. *Fuel*, 90(1):233–239, 2011. doi: 10.1016/j.fuel.2010.07.054. URL https://www.scopus.com/inward/record.uri?eid=2-s2.0-78449268816&doi=10.1016%2fj.fuel.2010.07.054&partnerID=40&md5=e1d49842b15affa4b2c60b284a055c8e.

[57] Michael Jacob. Chapter 9 - spheronization, granulation, pelletization, and agglomeration processes. In Anilkumar G. Gaonkar, , Niraj Vasisht, , Atul Ramesh Khare, , and Robert Sobel, editors, *Microencapsulation in the Food Industry*, pages 85 – 98. Academic Press, San Diego, 2014. ISBN 978-0-12-404568-2. doi: https://doi.org/10.1016/B978-0-12-404568-2.00009-1. URL https://www.sciencedirect.com/science/article/pii/B9780124045682000091.

[58] Sagar Muley, Tanaji Nandgude, and Sushilkumar Poddar. Extrusion–spheronization a promising pelletization technique: In-depth review. *Asian Journal of Pharmaceutical Sciences*, 11(6):684 – 699, 2016. ISSN 1818-0876. doi: https://doi.org/10.1016/j.ajps.2016.08.001. URL http://www.sciencedirect.com/science/article/pii/S1818087616300721.

[59] Josephine Soh, Srimanta Sarkar, P W S Heng, and C V Liew. Pelletization techniques. pages 2515–24, 01 2013. URL https://www.researchgate.net/publication/285100361_Pelletization_Techniques.

[60] Kammili Lavanya, V Senthil, and Varun Rathi. Pelletization technology: A quick review. *INTERNATIONAL JOURNAL OF PHARMACEUTICAL SCIENCES AND RESEARCH*, 2(6):1337–1355, 11 2011. ISSN 0975-8232.

[61] Diva Sonaglio, Bernard Bataille, Claude Ortigosa, and Maurice Jacob. Factorial design in the feasibility of producing microcel mc 101 pellets by extrusion/spheronization. *International Journal of Pharmaceutics*, 115(1):53 – 60, 1995. ISSN 0378-5173. doi: https://doi.org/10.1016/0378-5173(94)00246-2. URL http://www.sciencedirect.com/science/article/pii/0378517394002462.

[62] M. Köster and M. Thommes. In-line dynamic torque measurement in twin-screw extrusion process. *Chemical Engineering Journal*, 164(2):371 – 375, 2010. ISSN 1385-8947. doi: https://doi.org/10.1016/j.cej.2010.03.076. URL http://www.sciencedirect.com/science/article/pii/S1385894710003128.

[63] Ferdi Schüth Jens Weitkamp Gerhard Ertl, Helmut Knözinger, editor. *Handbook of Heterogeneous Catalysis*. Wiley, 8 volume set, 2nd edition edition, 2008.

[64] Katsumi Kaneko, editor. *Determination of pore size and pore size distribution Determination of pore size and pore size distribution 1. Adsorbents and catalysts*. 1994.

[65] A.B. Abell, K.L. Willis, and D.A. Lange. Mercury intrusion porosimetry and image analysis of cement-based materials. *Journal of Colloid and Interface Science*, 211(1):39 – 44, 1999. ISSN 0021-9797. doi: https://doi.org/10.1006/jcis.1998.5986. URL http://www.sciencedirect.com/science/article/pii/S0021979798959860.

[66] Sidney Diamond. Mercury porosimetry: An inappropriate method for the measurement of pore size distributions in cement-based materials. *Cement and Concrete Research*, 30(10):1517 – 1525, 2000. ISSN 0008-8846. doi: https://doi.org/10.1016/S0008-8846(00)00370-7. URL http://www.sciencedirect.com/science/article/pii/S0008884600003707.

[67] *Thermogravimetric Analysis (TGA) - Beginners guide*. PerkinElmer, Inc, 940 Winter Street. URL https://www.perkinelmer.com/CMSResources/Images/44-74556GDE_TGABeginnersGuide.pdf.

[68] A. W. Coats and J. P. Redfern. Thermogravimetric analysis. a review. *Analyst*, 88: 906–924, 1963. doi: 10.1039/AN9638800906. URL http://dx.doi.org/10.1039/AN9638800906.

[69] Elaine McCash. *Surface Chemistry*. Oxford Univ. Press, 2001.

[70] Christopher Hammond. *The Basics of Crystallography and Diffraction*. Oxford Science Publications, second edition, 2001.

[71] J.W. Niemantsverdriet. *Spectroscopy in Catalysis*. VCH, Weinheim, 3 edition, 1993 (New version 2007).

[72] Dongfang Wu, Jiancheng Zhou, and Yongdan Li. Mechanical strength of solid catalysts: Recent developments and future prospects. *AIChE Journal*, 53(10):2618–2629, 2007. ISSN 1547-5905. doi: 10.1002/aic.11291. URL http://dx.doi.org/10.1002/aic.11291.

[73] Robert J. Farrauto Calvin H. Bartholomew. *Fundamentals of industrial catalytic processes*. Wiley Interscience, second edition, 2006.

[74] Jian Zhou, Guang Ye, and Klaas van Breugel. Characterization of pore structure in cement-based materials using pressurization–depressurization cycling mercury intrusion porosimetry (pdc-mip). *Cement and Concrete Research*, 40(7):1120 – 1128, 2010. ISSN 0008-8846. doi: https://doi.org/10.1016/j.cemconres.2010.02.011. URL http://www.sciencedirect.com/science/article/pii/S0008884610000487.

[75] De Chen, Li He, and Kumar Ranjan Rout. Co2-capture project. 2017.

[76] Ane Sofie Lilleng. Masters thesis ntnu. 2017-2018.

[77] Xinfang Yang, Lifeng Zhao, Shaojun Yang, and Yunhan Xiao. Investigation of natural cao–mgo sorbent for co2 capture. *Asia-Pacific Journal of Chemical Engineerin*, 8, 11 2013. doi: 10.1002/apj.1735. URL http://www.sciencedirect.com/science/article/pii/S0021979798959860.

[78] Yang S. Xiao Y. Yang X., Zhao L. Investigation of natural cao-mgo sorbent for co2 capture. *ASIA-PACIFIC J. Chem. Eng.*, 8:906–915, 2016. doi: 10.1021/ef500331t.

[79] Lu Cui and Jong Herman Cahyadi. Permeability and pore structure of opc paste. *Cement and Concrete Research*, 31(2):277 – 282, 2001. ISSN 0008-8846. doi: https://doi.org/10.1016/S0008-8846(00)00474-9. URL http://www.sciencedirect.com/science/article/pii/S0008884600004749.

[80] Jie ying Jing, Xue wei Zhang, Shi dong Wang, Ting yu Li, and Wen ying Li. Improving co2 sorption performance of cao/ca3al2o6 sorbents by thermally pretreated in co2 atmosphere. *Energy Procedia*, 142:3258 – 3263, 2017. ISSN 1876-6102. doi: https://doi.org/10.1016/j.egypro.2017.12.500. URL http://www.sciencedirect.com/science/article/pii/S1876610217362550.

[81] Yingchao Hu, Wenqiang Liu, Hongqiang Chen, Zijian Zhou, Wenyu Wang, Jian Sun, Xinwei Yang, Xian Li, and Minghou Xu. Screening of inert solid supports for cao-based sorbents for high temperature co2 capture. *Fuel*, 181:199 – 206, 2016. ISSN 0016-2361. doi: https://doi.org/10.1016/j.fuel.2016.04.138. URL http://www.sciencedirect.com/science/article/pii/S0016236116303039.

[82] A. Akgsornpeak, T. Witoon, T. Mungcharoen, and J. Limtrakul. Development of synthetic cao sorbents via ctab-assisted sol-gel method for co2 capture at high temperature. *Chemical Engineering Journal*, 237:189–198, 2014. doi: 10.1016/j.cej.2013.10.023. URL https://www.scopus.com/inward/record.uri?eid=2-s2.0-84886992991&doi=10.1016%2fj.cej.2013.10.023&partnerID=40&md5=f4be6a14a2b73b9cc5e86c4ad7488339.

[83] A. Antzara, E. Heracleous, and A.A. Lemonidou. Improving the stability of synthetic cao-based co2 sorbents by structural promoters. *Applied Energy*, 156:331–343, 2015. doi: 10.1016/j.apenergy.2015.07.026. URL https://www.scopus.com/inward/record.uri?eid=2-s2.0-84937956903&doi=10.1016%2fj.apenergy.2015.07.026&partnerID=40&md5=c9e3331fa9ae31d0c9041e9bb10f3e51.

[84] A. Silaban, M. Narcida, and D.P. Harrison. Characteristics of the reversible reaction between co2(g) and calcined dolomite. *Chemical Engineering Communications*, 146:149–162, 1996. doi: 10.1080/00986449608936487. URL https://www.scopus.com/inward/record.uri?eid=2-s2.0-0030364984&doi=10.1080%2f00986449608936487&partnerID=40&md5=031499a2404cc80d5f398d3f82b68b3e.

[85] Vasilije Manovic, Jean-Pierre Charland, John Blamey, Paul S. Fennell, Dennis Y. Lu, and Edward J. Anthony. Influence of calcination conditions on carrying capacity of cao-based sorbent in co2 looping cycles. *Fuel*, 88(10):1893 – 1900, 2009. ISSN 0016-2361. doi: https://doi.org/10.1016/j.fuel.2009.04.012. URL http://www.sciencedirect.com/science/article/pii/S0016236109001781.

[86] Farah Diana Mohd Daud, Kumaravel Vignesh, Srimala Sreekantan, and Abdul Rahman Mohamed. Improved co2 adsorption capacity and cyclic stability of cao sorbents incorporated with mgo. *New J. Chem.*, 40:231–237, 2016. doi: 10.1039/C5NJ02081F. URL http://dx.doi.org/10.1039/C5NJ02081F.

[87] J. Blamey, N.P.M. Paterson, D.R. Dugwell, and P.S. Fennell. Mechanism of particle breakage during reactivation of cao-based sorbents for co2 capture. *Energy and Fuels*, 24(8):4605–4616, 2010. doi: 10.1021/ef100476d. URL https://www.scopus.com/inward/record.uri?eid=2-s2.0-77955907858&doi=10.1021%2fef100476d&partnerID=40&md5=b594c510a60350ae3296d5186ec1758a.

[88] Antonio Coppola, Fabrizio Scala, Piero Salatino, and Fabio Montagnaro. Fluidized bed calcium looping cycles for co2 capture under oxy-firing calcination conditions: Part 1. assessment of six limestones. *Chemical Engineering Journal*, 231:

537 – 543, 2013. ISSN 1385-8947. doi: https://doi.org/10.1016/j.cej.2013.07.113. URL http://www.sciencedirect.com/science/article/pii/S1385894713010322.

[89] Vasilije Manovic, Dennis Lu, and Edward J. Anthony. Steam hydration of sorbents from a dual fluidized bed co2 looping cycle reactor. *Fuel*, 87(15):3344 – 3352, 2008. ISSN 0016-2361. doi: https://doi.org/10.1016/j.fuel.2008.04.035. URL http://www.sciencedirect.com/science/article/pii/S0016236108001713.

[90] D.Y. Lu, R.W. Hughes, and E.J. Anthony. Ca-based sorbent looping combustion for co2 capture in pilot-scale dual fluidized beds. *Fuel Processing Technology*, 89(12):1386–1395, 2008. doi: 10.1016/j.fuproc.2008.06.011. URL https://www.scopus.com/inward/record.uri?eid=2-s2.0-56249122246&doi=10.1016%2fj.fuproc.2008.06.011&partnerID=40&md5=677417a55547ba3ccf0456dae605791e.

[91] José Manuel López, Gemma Grasa, and Ramón Murillo. Evaluation of the effect of inert support on the carbonation reaction of synthetic cao-based {CO2} sorbents. *Chemical Engineering Journal*, pages –, 2018. ISSN 1385-8947. doi: https://doi.org/10.1016/j.cej.2018.05.014. URL https://www.sciencedirect.com/science/article/pii/S1385894718308015.

[92] P. J. Potts. *X-ray fluorescence analysis: principles and practice of wavelength dispersive spectrometry*. Springer Netherlands, Dordrecht, 1987. ISBN 978-94-015-3988-3. doi: 10.1007/978-94-015-3988-3_8. URL https://doi.org/10.1007/978-94-015-3988-3_8.

Appendix

A7.1 Calcination in Tube Oven

The Dolomite was calcined at 800 °C for 6 hours in air. A tube oven was used to in order to calcine a larger amount of dolomite. Five ceramic bowl were completely filled and weighed. They were placed from left to right in the tube oven. The tube oven had some heating problems in the right end of the oven, so the bowls were placed mostly on the left side of the oven. After calcination, the bowls and dolomite were weighed again to calculate the weight loss of the dolomite to make sure that it was completely calcined. One example of the calculated weight loss is given in table A7.1. Here, sample 1 indicates the sample to the left in the oven and sample 5 indicates the sample to the right in the oven. The weight loss of sample 1 and sample 5 clearly indicates that the tube oven had some heating problem on the right side. Assuming both $MgCO_3$ and $CaCO_3$ were calcined to MgO and CaO at 800°C, it was expected to achieve a 47.7% weight loss for these samples. This is given from calculation A7.2. Where M_i indicates mass of component i, Mw_i is molecular weight for the component i and n is mole (with a 1:1 relation between $MgCO_3$ and $CaCO_3$ in the dolomite).

$$\mathrm{m_{CaCO_3}} = \mathrm{Mw} \cdot \mathrm{n} = 100.09\mathrm{g/mole} \cdot 1\mathrm{mole} = 100.09\mathrm{g} \tag{A7.1}$$

$$\mathrm{m_{MgCO_3}} = 84.31\mathrm{g/mole} \cdot 1\mathrm{mole} = 84.31\mathrm{g} \tag{A7.2}$$

$$\mathrm{m_{CO2}} = 44.01\mathrm{g/mole} \cdot 1\mathrm{mole} = 44.01\mathrm{g} \tag{A7.3}$$

$$\text{Weight loss at 800} = \frac{44.01\mathrm{g} + 44.01\mathrm{g}}{100.09\,\mathrm{g} + 84.31\mathrm{g}} = 47.73\% \tag{A7.4}$$

$$\text{Weight loss at 650} = \frac{44.01\mathrm{g}}{100.09\,\mathrm{g} + 84.31\mathrm{g}} = 23.87\% \tag{A7.5}$$

Table A7.1: One example of the percentage weight loss after calcination of dolomite in the tube oven. Dolomite was calcined at 800°C for 6 hours in air.

Sample	Weight loss [%]
1	43.7 %
2	42.0 %
3	41.1 %
4	33.0 %
5	32.5 %

A7.2 Rotary drum granulation procedure

During the Specialization project 2017, the granulation procedure experienced some difficulties during granulation as explained in section A7.7. Thus, a trial on an other machine had to be tested. A kitchen machine with power rated at 1.5kW were used. The contents inside the rotating bowl were exposed to air, a so called open batch type of process for making the pellets. It was easier to control the stirring of powder and solution because you were able to observe the water addition.

The first 10 trials of granulation with the rotary drum Ankarsum machine were just to get to know the machine. A 100g of calcined dolomite with powder less than 106 μm was used in some of the first testings of the machine. Also, 100g cement (ADDA, mainly consisting of the same components as dolomite) were tested due to limited amount of calcined dolomite and the fact that ADDA cement have similar behavior as dolomite. The parameters that were tested was the added amount of water at given time, witch spray to use (small water droplets desired to get small pellets and not lump formation of liquid and solid), function of roller, rotating speed of the drum and time of shaping after water addition. During the testing it was observed that too slow water addition led to fast drying process and to production of sand (agglomeration stopped too early). In addition, fast drying occurred due to the open bowl and evaporation of liquid. Thus, it was important to avoid fast drying with good covery and steam. Steam were added to the bowl via a humidifier.

The procedure was divided into three stages: 1) slow addition of water at low rotating speed to control heat released and to hydrate ($Ca(OH)_2$) the calcined dolomite, and then store it in a closed container over night, 2) addition of water at high rpm with additional air moisturizer, 3) shaping of spheres at high rpm, moisturizer and a few spray to maintain the humidity in the bowl.

In the first stage a lot of heat was released for the first 20g water added. The first stage was stopped when when small aggregates were observed and the temperature in the bowl went back to normal. For the second stage it was important to find exactly water amount needed, when to remove the roller and when to add the humidifier. If the roller was removed too early, it had to be put back again to avoid large formation of material. A manual scraper was used to remove material from the wall of the bowl. In the third stage, the granulation time was important for the final product. If the granulation time was too short, the sphericity of granules were poor, and if the stirring time was extended too much, more

sand were produced. A view of all the procedures is given as PDF in chapter A7.9.

A7.2.1 Rotary Drum Granulation Scale-Up (500g)

An other objective of the granulation procedure was to investigate if the Ankarsum rotary drum was able to handle an even larger amount of dry material. Thus, a scale-up of the 100g dry mass to 500g dry material was performed. 500g cement ADDA, both calcined and uncalcined material, were used due to limited amount of calcined dolomite. In the first trial uncalcined cement ADDA were used to simulate upsclaing problems related phenomena. The use of uncalcined ADDA relates to the 2) and 3) stage of calcined ADDA/dolomite, whereas the first stage is included when the material is calcined and consist of oxides. Problems related to the up-scaling were:

- More material is stuck behind the scraper
- Mountain build-up in the middle of the bowl, thus manually stirring required
- More heat evolved, thus slower water addition
- Does not need 5 times more water than the 100g scale
- Rotating speed is lowered (rpm at level 1 with 100g dry material is different than rpm on level 1 with 500g dry material)

During the first water addition low rpm is required because at high rpm the powder is flying around. After adding approx. 50g water, small aggregates is formed thus medium rpm is used. Also, 50g water seemed to be enough to remove heat and hydrate the calcined ADDA. A sample named **NO-2** made of 500g calcined ADDA gave a yield of approximately 75 $\%$ (pellets ranging from 250μm to 1.2mm), which is very promising for the up-scaling. The procedure in the first stage was as follows:

- T=24 °C before start.
- 5g water T=35°C (1min) wait 2 min for cooling, speed level = 2
- +5g water T=36°C (4min) wait 3 min
- +5g water T=36°C (7min) wait 3 min
- +5g water T=38°C (10min) wait 5 min
- +5g water T=35°C (15min) wait 5 min
- +5g water T=34°C (20min) wait 5 min
- +5g water T=32°C (25min) wait 5min
- +5g water T= 30,5°C (30min) wait 5 min
- +5g water T =30,4°C (35min)
- +5g water T= 29.6°C (40min) speed level = 6
- Stopped after 45 min. tot time = 45min. tot water = 50g. Stored on closed bottle.

and the second stage (sencond day) as follows:

- 25g water T= 24C (5min), speed level = 2
- +10g water T= 43C (10min)
- +25g water (15min), humidifier = low level
- +15g water (20min), speed level =6
- +15g water (25min)
- +20g water (30min), removed roller, max speed level = 8
- +10g water (35min)
- +20g water (40min)
- +20g water (45min)
- +10g water (50min)
- +10g water (55min)
- +15g water (60min)

and finally, the third stage:

- One spray water(1g) to keep humidity (65min)
- +2g water to keep humidity (70min)
- Stopped water addition (80min)
- Stopped after 80 min. stirring time after water addition stopped was 20 min tot. tot. amount of water = 188g

SEM pictures of the uncalcined pellets NO-2 is given in figure A7.1.

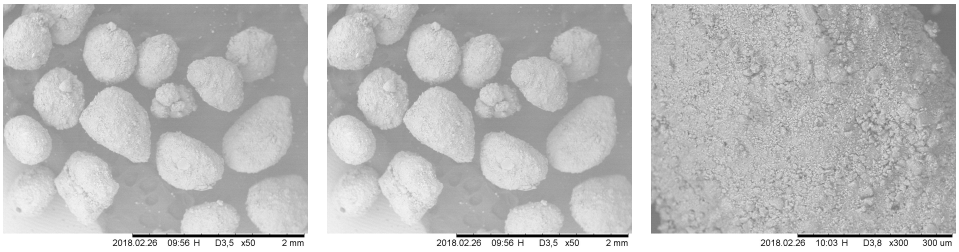

Figure A7.1: (left) NO-2 resolution x50 , (middle) NO-2 resolution x150 , (right) NO-2 resolution x300.

A7.2.2 Rotary Drum Granulation With 100g Calcined Dolomite and Dopants

After several experiments with both 100g and 500g, calcined dolomite and calcined ADDA, it was time to produce granules and test their characteristics in TGA, SEM, XRD, BET and mechanical tests.

Sample **NO-1** were made of pure calcined dolomite and water and it gave a yield of approximately 93% (which is a very high yield, so granulation time could have been extended to give stronger pellets)(pellets ranging from 250μm to 1.2mm). The temperature was also measured manually during granulation. The procedure is the first stage was as follows:

- T=24.6°C before start.
- +3g water T=32.8°C (1min), speed level = 1
- +4g water T=34.3°C (3min)
- +3g water T=33.8°C (5min)
- +5g water T=33.5°C (10min)
- +10g water T=26°C (15min), speed level = 8
- 5min stirring at level 8 after water addition (20min)
- tot. water added = 25g, tot.stirring = 20 min

and the second and third stage were as follows:

- add water at low rpm (6min)
- after adding 20g, turn up the speed to max rpm = level 8 (10min)
- removed roller (13min)
- +4g (15min) a few sprays every minute
- +1g (20min), add humidifier
- +2g (25min), stopped water addition.
- 10min mixing after water addition (35min), tot.water = 27,7g and tot. stirring = 35min

Sample **NO-3** were made of pure calcined dolomite and 2 wt.% Zr from ZrN_2O_7. This batch gave a yield at 42 %(pellets ranging from 250μm to 1.2mm). 14.47g of ZrN_2O_7 were mixed with 12g water and poured into the spray. The first stage was as follows:

- 10g water (6min), low rpm level = 1 almost whole solution (10min)
- +7g water (13min)
- water addition stopped (15min), max rpm level =8
- stopped (20min)

- tot. time = 20 min and tot amount of solution = 22.39g

and the second and third stage were as follows:

- 10g water (4min), low rpm
- +5g water (6min), high rpm level = 8, and add humidifier
- +5g water (20 min)
- +1g (10 min)
- +1g (12min), removed roller
- +0,5g (14 min)
- +4 spray to keep humidity (17min)
- +2gy (20min)
- turned of humidifier (23min)
- total stirring time= 25min and total water added g= 23.26

Sample **NO-12** were made of pure calcined dolomite, 6 wt.% Al from cement Fondu (maily consist of Al_2O_4) and 2 wt.% Zr from ZrN_2O_7. This batch gave a yield at 58 %(pellets ranging from 250μm to 1.2mm). 14,45g of ZrN_2O_7 were mixed with 15g water and poured into the spray. The dry powder of calcined dolomite(100g) were mixed 5 minutes with the dry cement Fondu powder (20.84g). The first stage was as follows:

- Half the solution added (H_2O+ZrN_2O_7) (5min), speed level = 1
- whole solution added (10min)
- +7g water (15min), speed level = 8
- stirring at level = 8 (20min)
- stored on closed bottle over night

followed by the second and third stage:

- 10g water (4min), speed level = 1
- +2g water (6min), speed level = 8
- +6g water (10min)
- +3g water (12min)
- +3g water (14min), add humidifyer
- removed roller (15min)
- +5g water (20min)
- +5g water (24min)
- +5g water (26min)

- +0,5g water (28min), stopped water addition
- stopped (31min)
- tot. stirring time= 31 and tot water= 41g

Sample **NO-6** were made of pure calcined dolomite, 6 wt.% Al from cement Fondu (maily consist of Al_2O_4) and 2 wt.% Zr from $ZrCl_4$. This batch gave a yield at 61 %(pellets ranging from 250μm to 1.2mm). 5.088g of $ZrCl_4$ were mixed with 24.7g water and to solve the salt in the water an ultrasonic bath of 60°C were used. The dry powder of calcined dolomite(100g) were mixed 5 minutes with the dry cement Fondu powder (20.95g). The first stage was as follows:

- added whole solution (H_2O+$ZrCl_4$) (15min) speed level = 1
- speed level = 8 (20min)
- stored on closed bottle over night

followed by the second and third stage:

- 10g water (4min), speed level = 1
- +2g water (6min), increased to speed level = 8
- +4g water (8min)
- +2 water (10min)
- +3g water (12min) humidifier level 1 added
- +0,5g water (18min), removed roller (tot water=26g), water addition stopped
- +2spray (26min)
- +2spray (30min)
- +2spray (34min)
- +2spray (36min)
- +2spray (38min)
- Sopped (40 min)
- tot. water added = 26g and tot.time = 40

Sample **NO-10** were made of pure calcined dolomite, 6 wt.% Al from cement Fondu (maily consist of Al_2O_4). This experiment were conducted to investigate the bonding mechanism during the granulation process, and to investigate at with time the granules are at their most spherical shape. This batch gave a yield at 42 % (pellets ranging from 250μm to 1.2mm). The dry powder of calcined dolomite(100g) were mixed 5 minutes with the dry cement Fondu powder (21.83g). The first stage was as follows:

- 15g water (8min), speed level = 1
- +12g (15min), speed level = 8

- stopped (20min)
- stored on closed bottle over night

followed by the second and third stage:

- 10g water (5min), level = 1
- level=8 (6min)
- +10g (10min)
- +5g (15min) add humidifier and remove roller (tot water=25g)
- +5g (took sample 1)(20min)
- +3g (took sample 2)(25min) stopped water addition
- sample 3(30min)
- +3spray sample 4 (35min)
- +3spray sample 5 (40min) humidifier at level 2 for some seconds
- sample 6 (45min) turned of humidifyer
- sample 7 (50min), stopped
- tot water = 33g + few sprays to keep humidity. tot time of stirring after water addition = 25min.

Sample **NO-8** were made of pure calcined dolomite, 6 wt.% Al from cement Fondu (maily consist of Al_2O_4) and 3 wt.% Mg from $Mg(NO_3)_2 \cdot 6H_2O$. This batch gave a yield at 51 %(pellets ranging from 250μm to 1.2mm). 35.95g of $Mg(NO_3)_2 \cdot 6H_2O$ were mixed with 20,0g water and to solve the salt in the water an ultrasonic bath of 60°C were used. The dry powder of calcined dolomite(100g) were mixed 5 minutes with the dry cement Fondu powder (19.74g). The first stage was as follows:

- Half the solution added (H_2O+$Mg(NO_3)_2 \cdot 6H_2O$) (10min), speed level = 1
- whole soultion added (15min)
- level 8 (20min)
- stored on closed bottle over night

followed by the second and third stage:

- 10g water (5min), speed level = 1
- level 8 (6min)
- +10g water(10min), add humidifyer level 1
- +5g water (15min), remove roller
- +5g (20min), stop water addition

- +4 spray (25min), humidifier level 2
- stopped (30min)
- tot water = 30g + few sprays to keep humidity. tot time of stirring after water addition = 10 min.

A7.2.3 Rotary Drum Granulation With 100g Calcined ADDA, 100g Uncalcined ADDA and Dopants

Four samples based on cement ADDA were made with the same additives as sample NO-12 and NO-6. These samples were made to see if there were any differences in characterization from dolomite based pellets and cement ADDA based pellets.

Sample **NO-20** were made of calcined ADDA, 6 wt.% Al from cement Fondu (maily consist of Al_2O_4) and 2 wt.% Zr from ZrN_2O_7. This batch gave a yield at 78 %(pellets ranging from 250μm to 1.2mm). 14.37g of ZrN_2O_7 were mixed with 20,24g water. The dry powder of calcined dolomite(100g) were mixed 5 minutes with the dry cement Fondu powder (20,42g). The first stage was as follows:

- Half the solution added (H_2O+ZrN_2O_7) (10min), speed level = 1
- whole solution added (15min), speed level = 6
- stopped (20min)
- stored on closed bottle over night

followed by the second and third stage:

- 10g (5min) speed level = 1
- speed level = 8 (6min)
- +10g (10min)
- +10g (15min), add humidifyer level 1
- +5g(20min), remove roller
- +5g (25min), stop water addition
- +1g = few sprays (30min)
- Stopped (45min)
- tot water = 42g and tot time of stirring after water addition = 15 min.

Sample **NO-21** were made of calcined ADDA, 6 wt.% Al from cement Fondu (maily consist of Al_2O_4) and 2 wt.% Zr from $ZrCl_4$. This batch gave a yield at 88 %(pellets ranging from 250μm to 1.2mm). 5.082g of $ZrCl_4$ were mixed with 25,24g water and to solve the salt in the water an ultrasonic bath of 60°C were used. The dry powder

of calcined dolomite(100g) were mixed 5 minutes with the dry cement Fondu powder (20,48g). The first stage was as follows:

- Half the solution added (H_2O+$ZrCl_4$) (10min), speed level = 1
- whole soution added (15min)
- speed level = 6 (20min)
- stored on closed bottle over night

followed by the second and third stage:

- 10g water (5min), speed level = 1
- level 8 (6min)
- +10g (10min)
- +10g (15min), add humidifier level 1
- +5g(20min)
- +5g (25min), removed roller, stopp water addition
- +1g to keep humidity (30min)
- +1g (35min)
- stopped (45min)
- tot. water = 42g , tot. time after water addition = 20 min

Sample **NO-22** were made of uncalcined ADDA, 6 wt.% Al from cement Fondu (mainly consisting of Al_2O_4) and 2 wt.% Zr from ZrN_2O_7. This batch gave a yield at 24 %(pellets ranging from 250μm to 1.2mm) (low yield due to too much water). 14g of ZrN_2O_7 were mixed with 10g water. The dry powder of calcined dolomite(100g) were mixed 5 minutes with the dry cement Fondu powder (21.18g). There is 3 stages in this procedure as well, but the all the liquids were added one day due to the chemistry of uncalcined adda. The stages are as follows: 1) addition of solution at low speed, 2) addition of water to form aggregates, 3) shaping of spheres.

- Half the solution added (H_2O+ZrN_2O_7) (10min), speed level = 1
- whole solution added (15min), speed level = 8
- +10g water (25min), add humidifier and remove roller
- +5g water (30min) +3spray, then water addition stopped
- stopped (35min)
- time after water addition stopped = 5min and tot water after solution = 15g

Sample **NO-23** were made of uncalcined ADDA, 6 wt.% Al from cement Fondu (mainly consisting of Al_2O_4) and 2 wt.% Zr from $ZrCl_4$. This batch gave a yield at 77 %(pellets ranging from 250μm to 1.2mm). 5.18g of $ZrCl_4$ were mixed with 20g water and to solve

the salt in the water an ultrasonic bath of 60°C were used. The dry powder of calcined dolomite(100g) were mixed 5 minutes with the dry cement Fondu powder (20.48g). The first stage was as follows:

- The whole the solution added (H_2O+$ZrCl_4$) (15min), speed level = 1
- speed level = 6 (20min)
- +10g water (25min) humidifier at level 1 and removed roller
- +4g water(30min) stopped water addition
- +1g water(35min) to keep humidity
- +1g (40min)
- +1g (45min), stopped
- tot. water = 17g and tot. time after water addition = 15min

A7.3 Extrusion/Spherionization for Dolomite-Based Pellets

To get to know the Kenwood Pro 2000 Excel Electric Mincer MG700, uncalcined cement ADDA was used. First 100g cement ADDA and 20g cement Fondu were mixed with water in a mortar. If too dry mixture, the more water needed. A batch based on 100g ADDA was too little and all the cement got stuck in the rotor of the extruder. Thus, a batch of 200g ADDA and 40g Fondu were used, and mixed in the rotary drum with the use of roller to improve the mixing. An amount of water of approximately 35-40g was too much, or a rest time is needed before spherionization. It was observed that the extruder struggle with the viscous cement and a lot of power and force is desired to press the cementitious material through the screen. The procedure of pellet production via extrusion follow 3 steps: 1) granulation, 2) extrusion and 3) spherionization. A proposed procedure for making cement ADDA-based pellets with the extruder is as follows:

- Mix 200g cement ADDA and 40g cement Fondu in granulator
- Granulation (stage 1): 30g water (5min), speed level = 1
- Granulation: +5g water (10min), speed level = 8, humidifier at level 3
- Granulation: +3g water (15 min), speed level = 8
- Resting: 5 min (20min)
- Extrusion (stage 2): extrude material through 3mm screen and let material rest for 5 minutes (25min)
- Spherionization (stage 3): speed level = 8, humidifier at level 3 (25min)
- Spherionization: stop humidifier (28min)

- Spherionization: stopped (45min)
- Drying in room temperature

Sample NO-12 was also made by extrusion with 200g raw material of calcined dolomite, 6 wt.% Al from cement Fondu (38g Fondu) and 2 wt.% Zr from ZrN_2O_7 (29,845g ZrN_2O_7). 40g water was added to the zirconium nitrate. Dry material of calcined dolomite and cement Fondu were mixed for 5 minutes before the zirconium solution was added. Heat was released for the first 20 minutes when adding solution. The granulation (stage 1) procedure the first day was as follows:

- Granulation (stage 1):
- Adding 1 pipette = 6.6g solution (H_2O and ZrN_2O_7) (4min),at speed level = 1
- 1 pipette of solution (8min)
- 1 pipette of solution (12min)
- 1 pipette of solution (16min)
- 1 pipette of solution (20min)
- 2 pipette of solution (24min), at speed level = 3
- 2 pipette solution (28min)
- adding the rest of solution plus additional 10g of H_2O (32min)
- speed level = 8 (36min)
- stopped (40min)
- stored on closed bottle over night

The second day, more liquid were added during granulation to obtain perfect moisture before extrusion and spherionization:

- Granulation (stage 1): 2 pipettes = 2*6g water(4min) speed level = 1
- speed level = 8 (5min), humidifier level 3
- +3*6g water(10min)
- +3*6g water (15)
- +6g water(20min) stopped. tot. water = 55g
- Resting: 5 minutes
- Extrusion (stage 2): extrude material through 3mm screen (25min) and let material rest 20 minutes (45min)
- Spherionization (stage 3): 10 minutes at speed level = 8 (55min)
- Drying in room temperature

A7.4 More Results - Rotary Drum - calcined dolomite and ADDA

A7.4.1 Surface Area and Pore Size distribution

Results for the 3 and 2 different measurements of the dolomite- and cement ADDA-based pellets respectively.

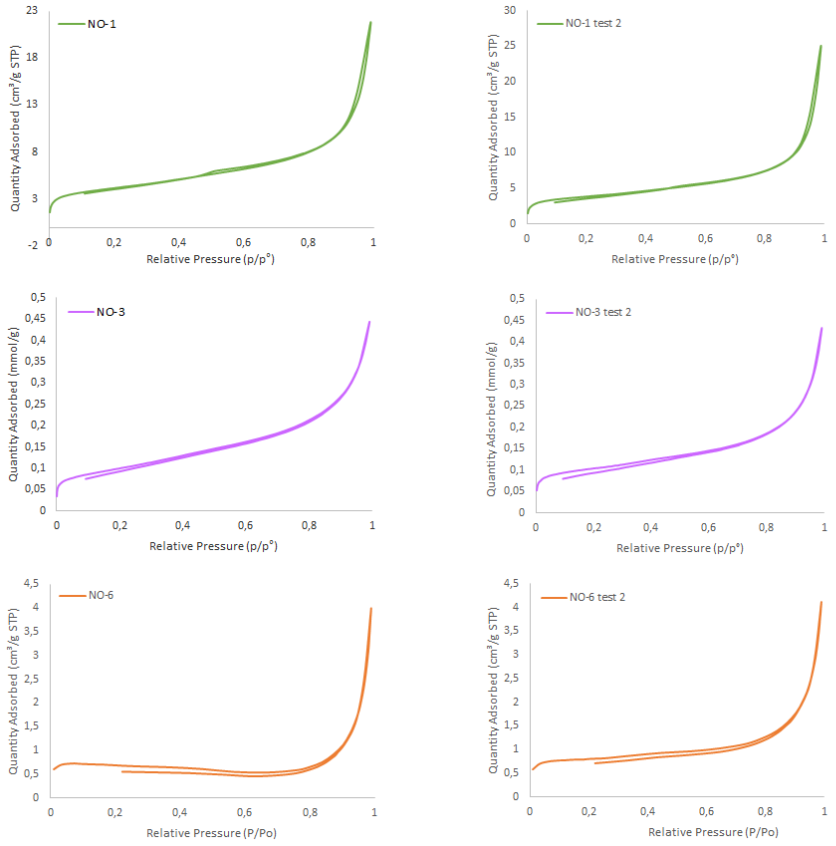

Figure A7.2: BET isotherms for dolomite-based samples

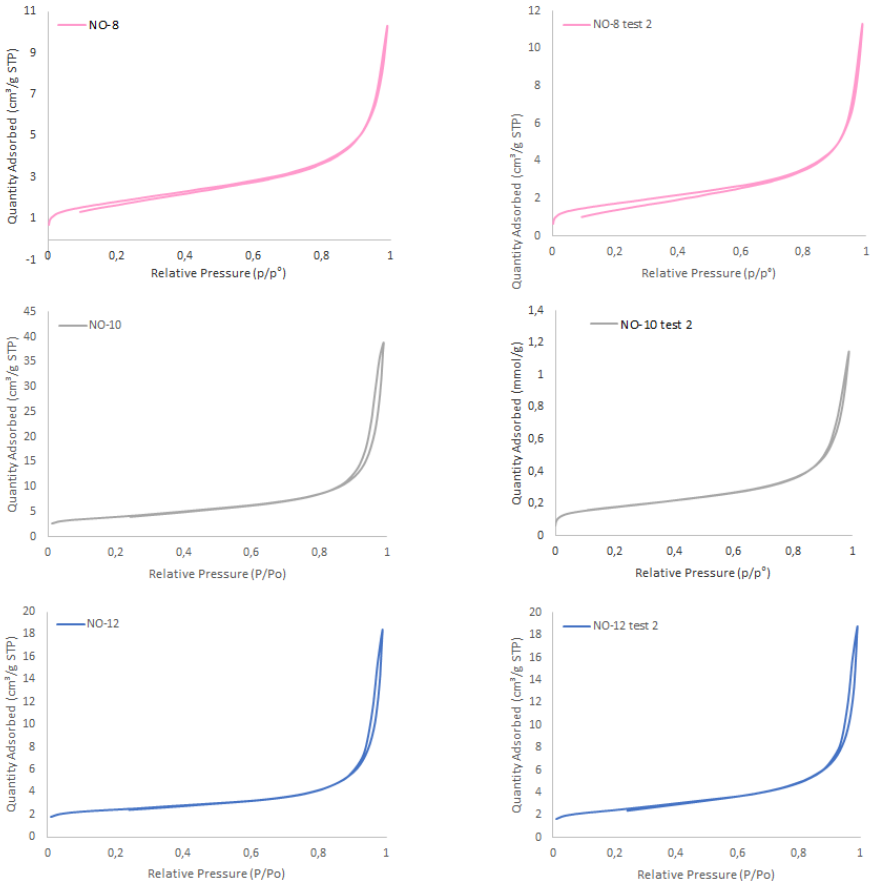

Figure A7.3: BET isotherms for dolomite-based samples

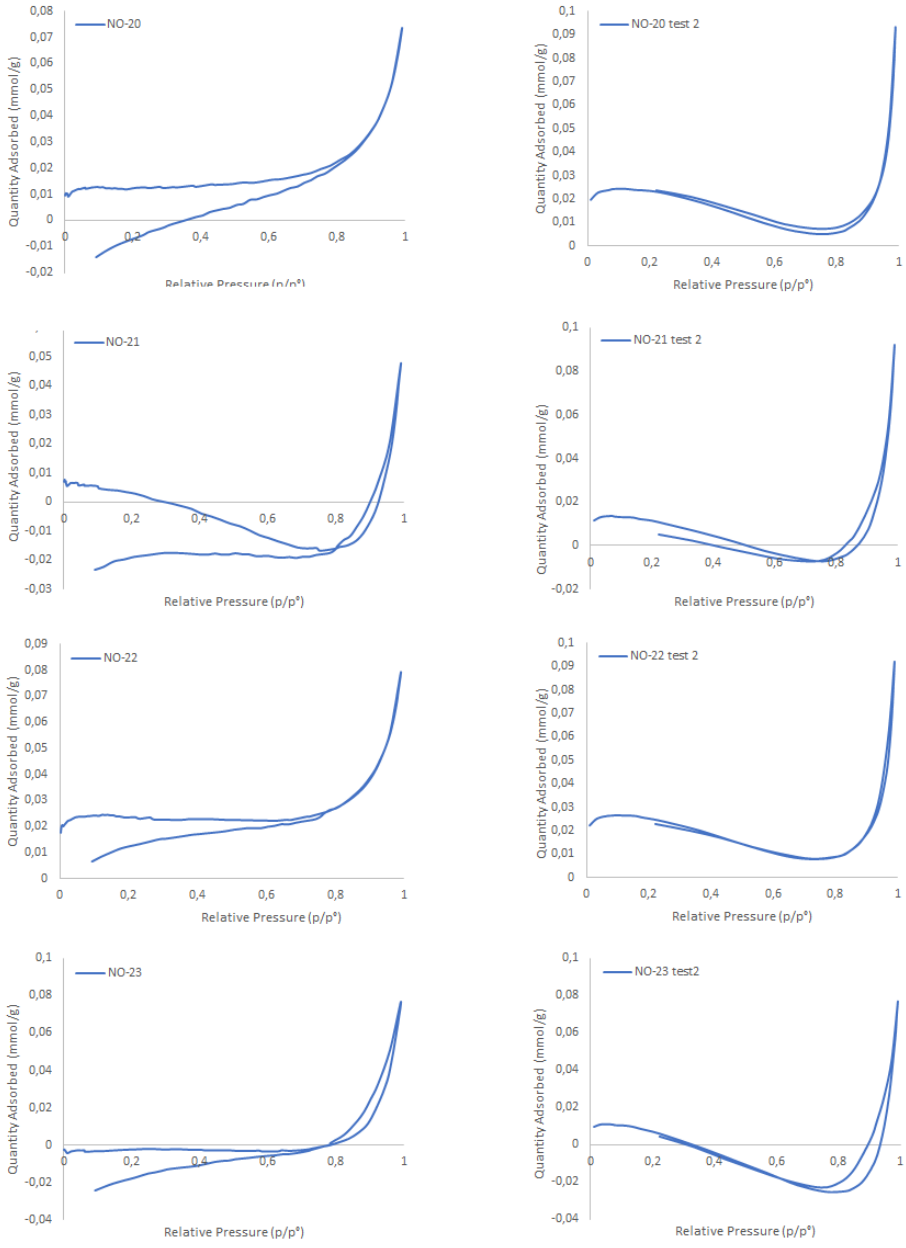

Figure A7.4: BET isotherms for cement ADDA-based samples

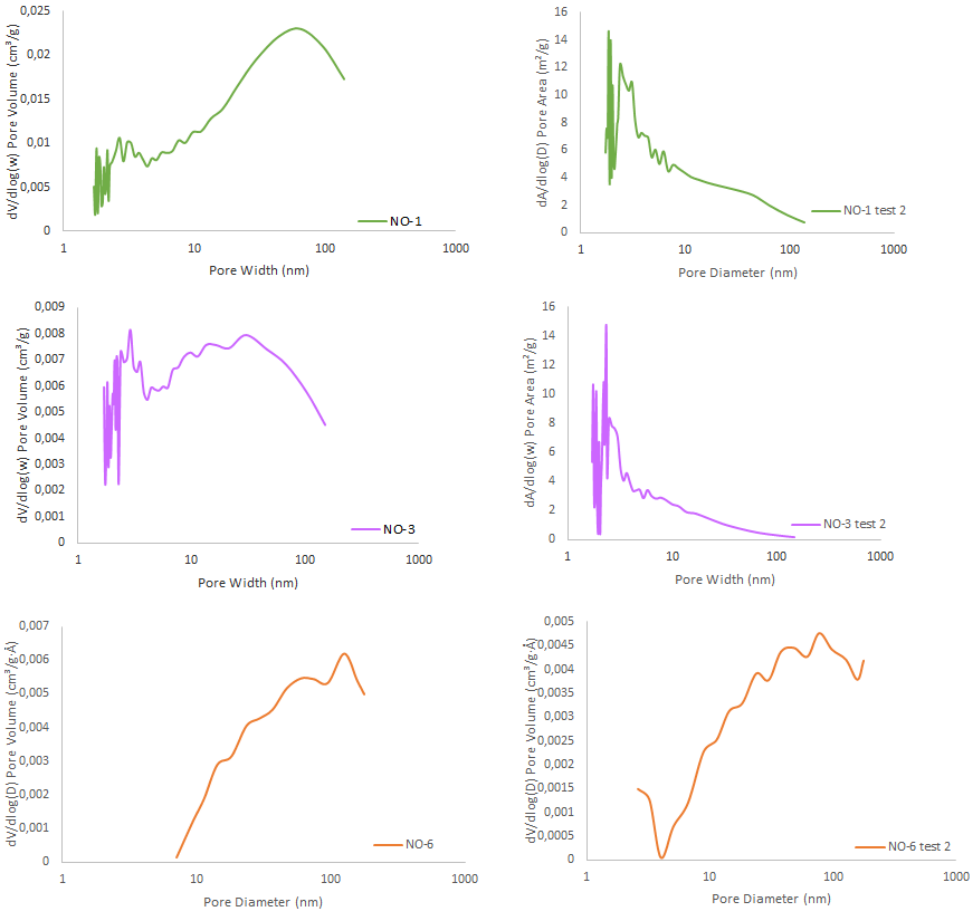

Figure A7.5: BJH pore size distribution plot for dolomite-based samples.

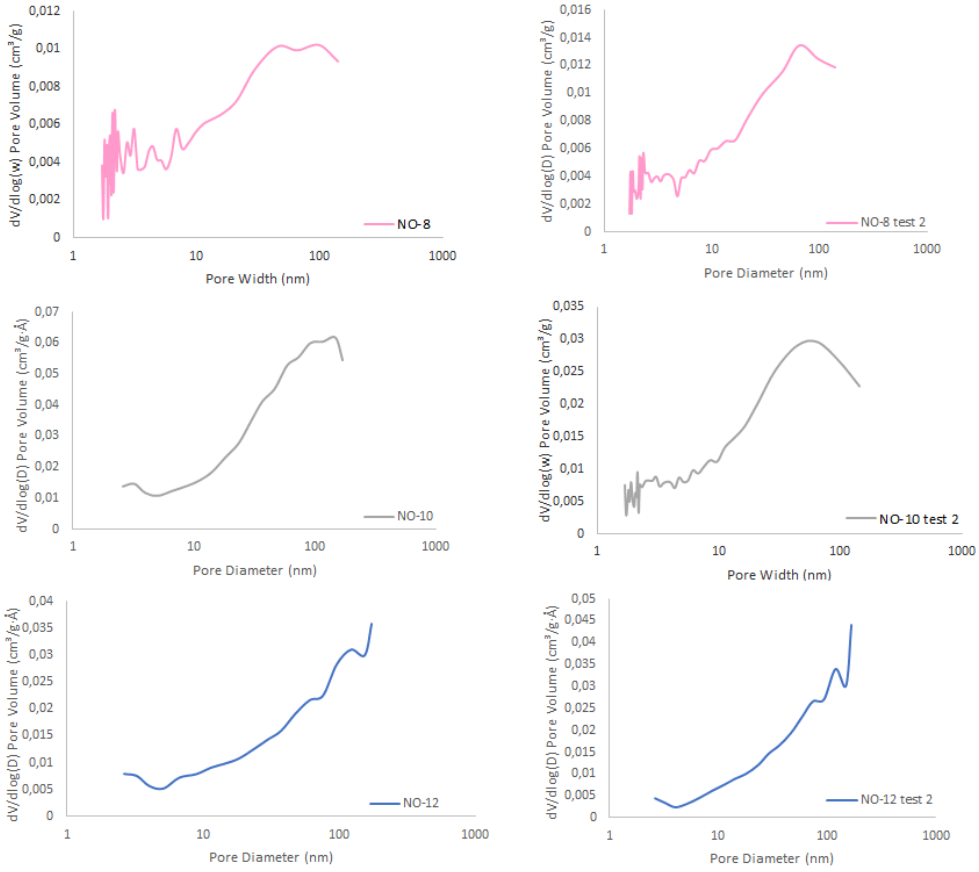

Figure A7.6: BJH pore size distribution plot for dolomite-based samples.

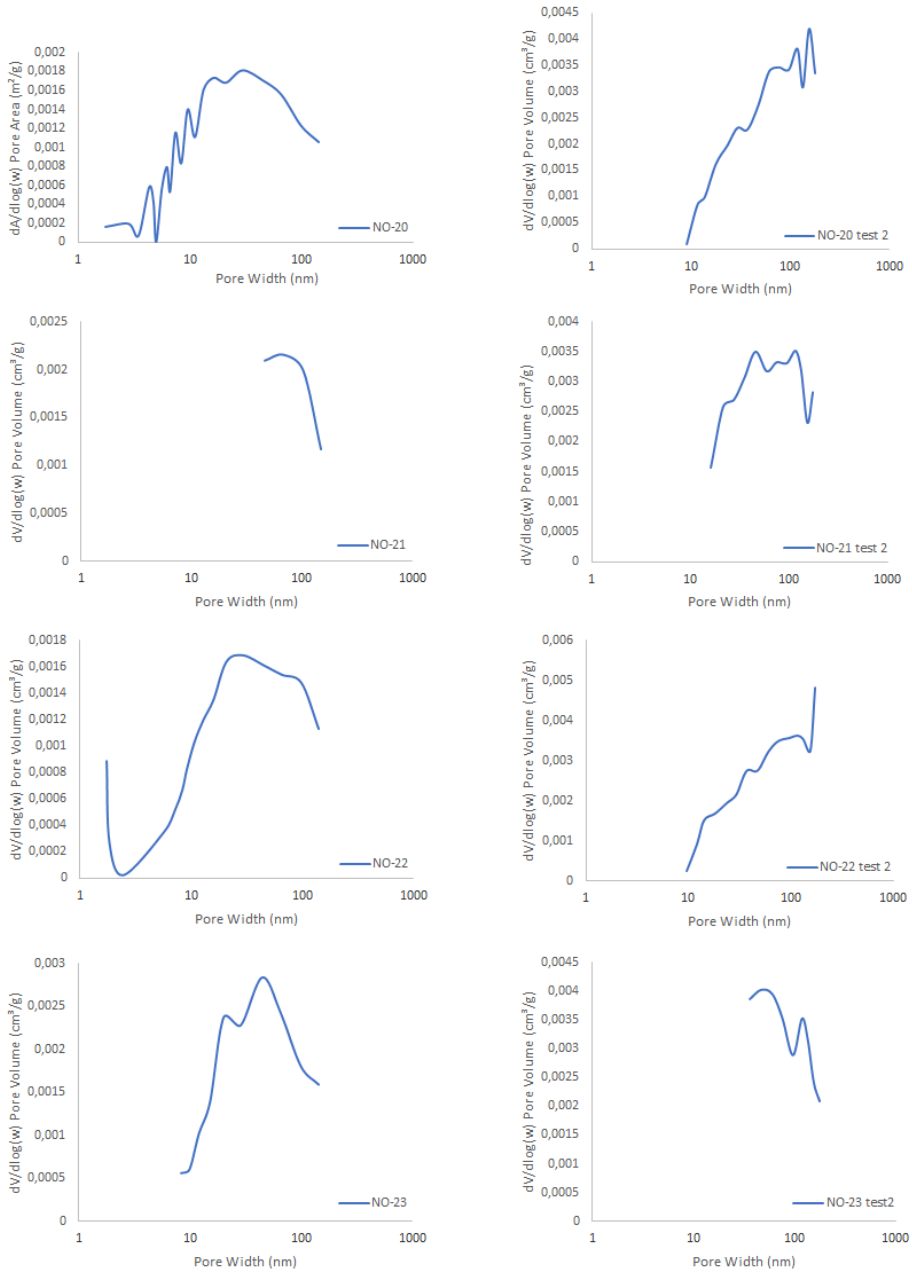

Figure A7.7: BJH pore size distribution plot for cement ADDA-based samples.

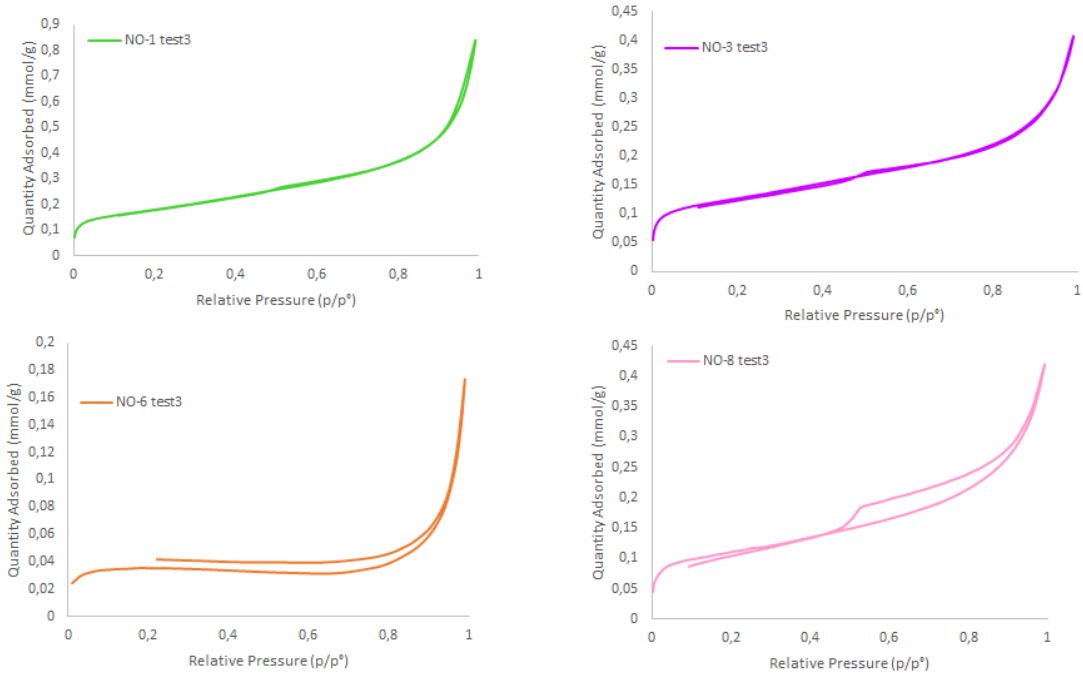

Figure A7.8: Isotherms test 3

A7.4.2 Phase Identification

NO-1

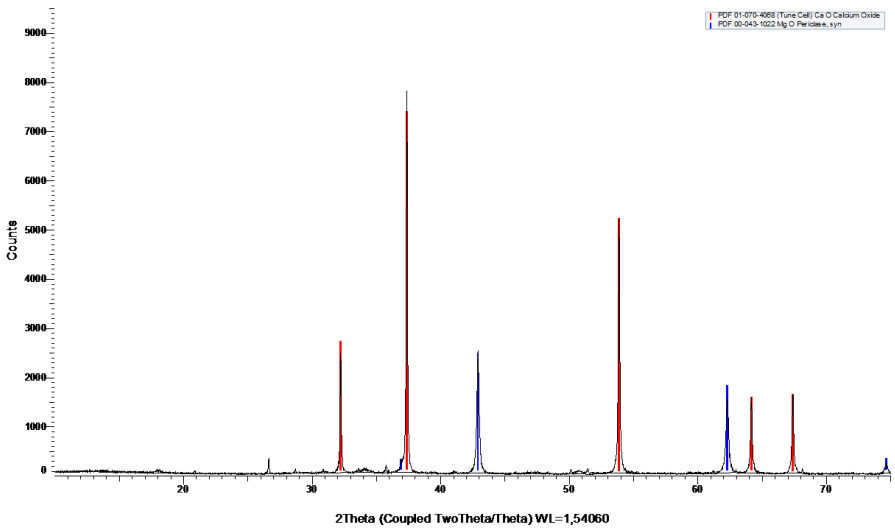

Figure A7.9: Phases measured by XRD of calcined sample NO-1. Red and blue peak indicates that the phase can be CaO and MgO respectively.

NO-3

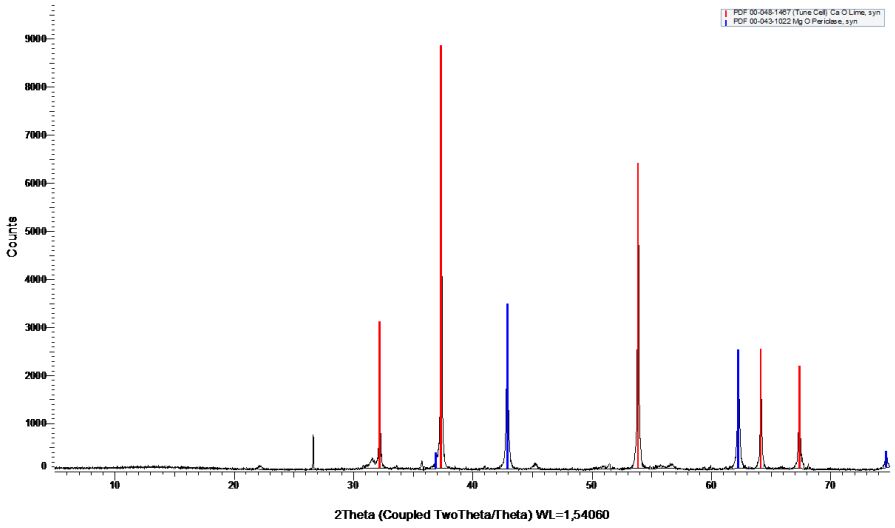

Figure A7.10: Phases measured by XRD of calcined sample NO-3. Red and blue peak indicates that the phase can be CaO and MgO respectively.

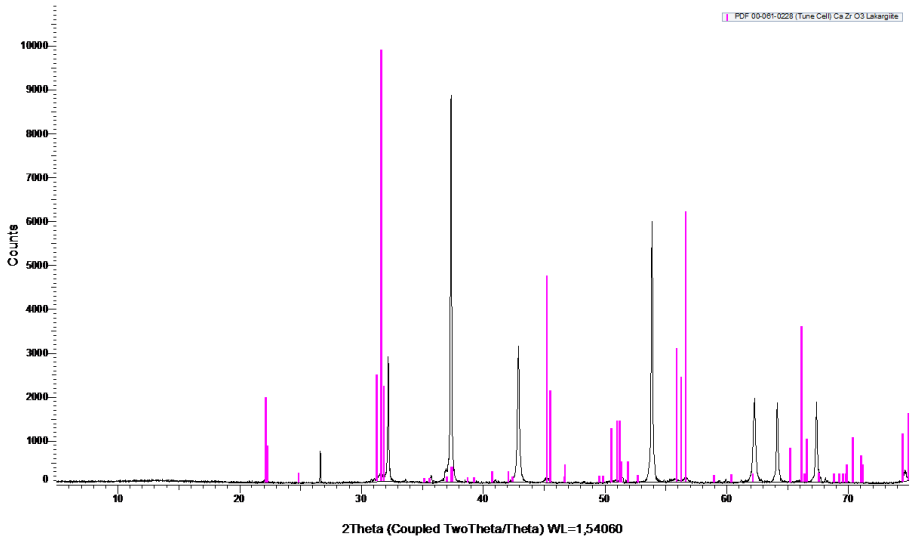

Figure A7.11: Phases measured by XRD of calcined sample NO-3. Pink peak indicates that the phase can be $CaZrO_3$.

A7.4.3 NO-6

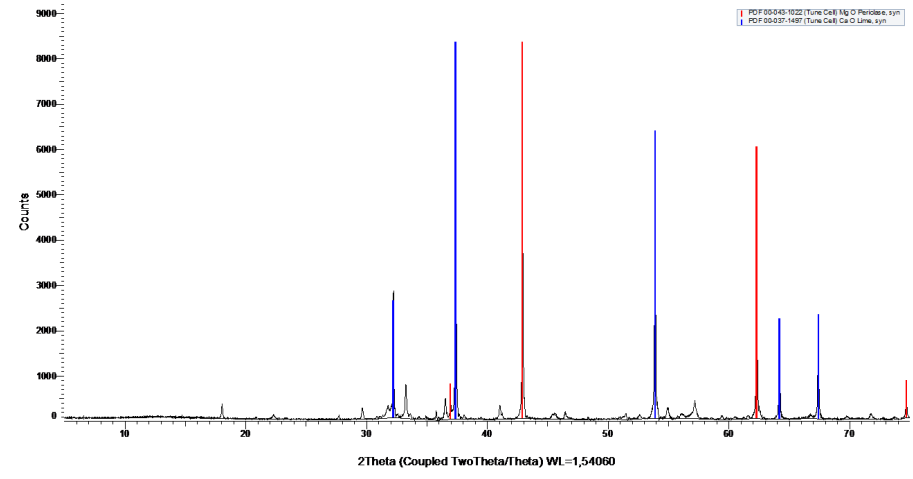

Figure A7.12: Phases measured by XRD of calcined sample NO-6. Red and blue peak indicates that the phase can be CaO and MgO respectively.

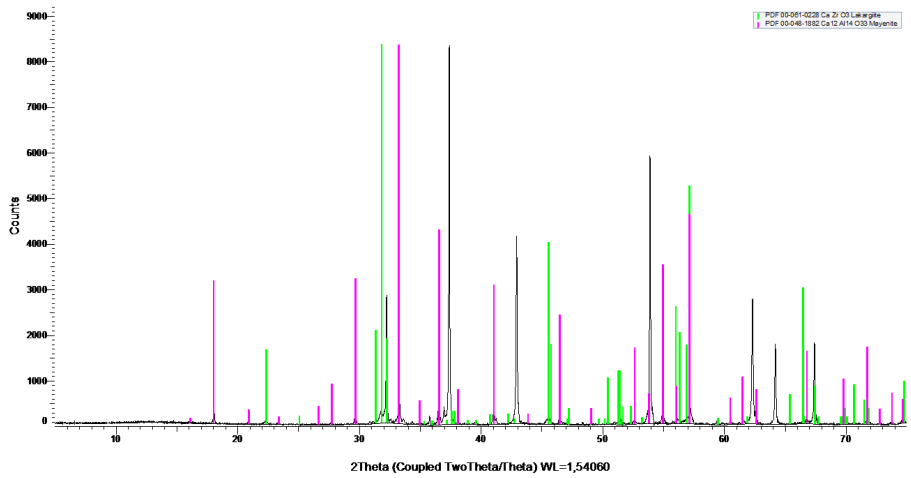

Figure A7.13: Phases measured by XRD of calcined sample NO-6. Limegreen peak indicates that the phase can be $CaZrO_3$, and pink peak might be mayenite ($Ca_{12}Al_{14}O_{33}$).

NO-8

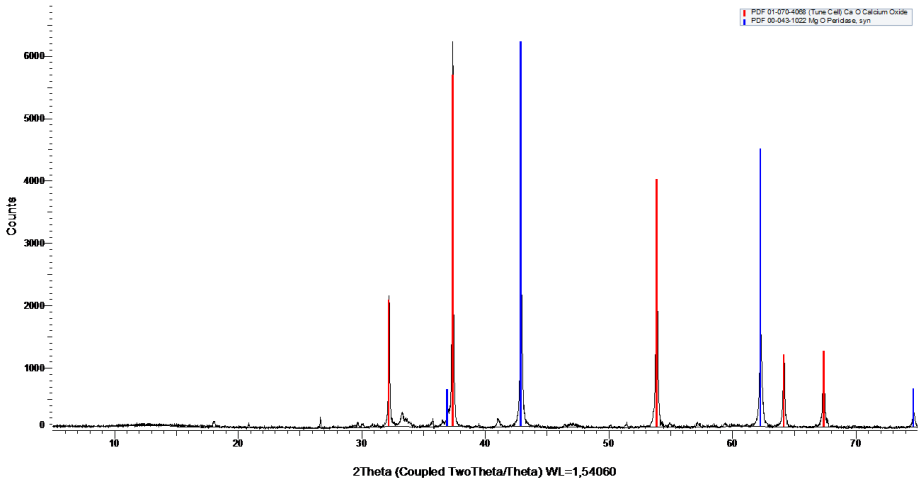

Figure A7.14: Phases measured by XRD of calcined sample NO-8. Red and blue peak indicates that the phase can be CaO and MgO respectively.

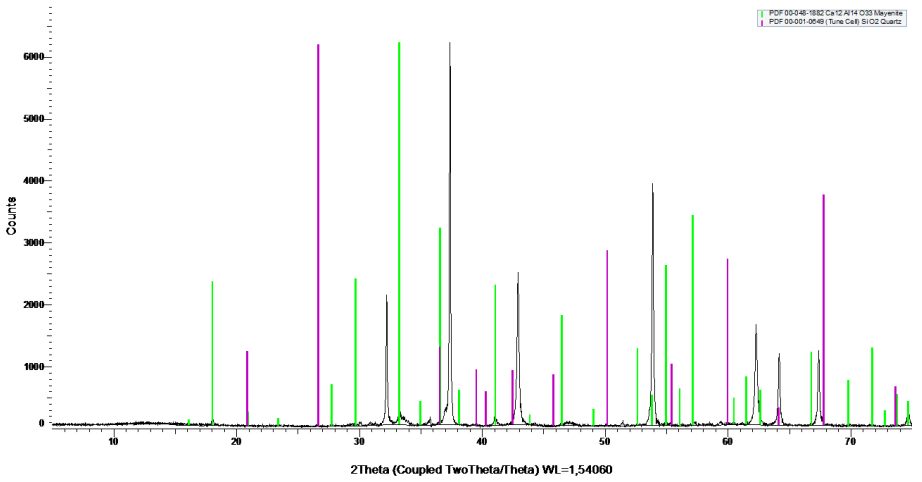

Figure A7.15: Phases measured by XRD of calcined sample NO-8. Limegreen peak indicates that the phase can be $CaZrO_3$, and pink peak might be mayenite ($Ca_{12}Al_{14}O_{33}$).

NO-10

Phase identification for NO-10 at 30 minutes measurement.

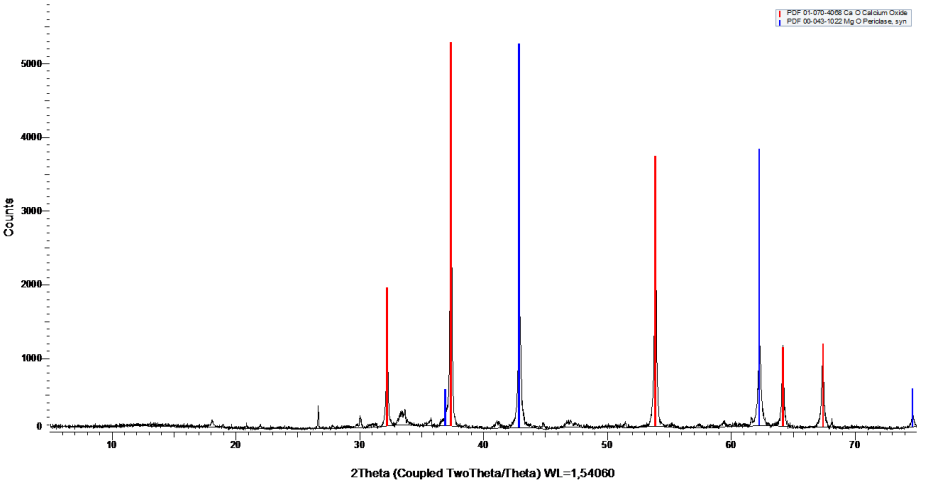

Figure A7.16: Phases measured by XRD of calcined sample NO-10. 30 minutes XRD measurement time. Red and blue peak indicates that the phase can be CaO and MgO respectively.

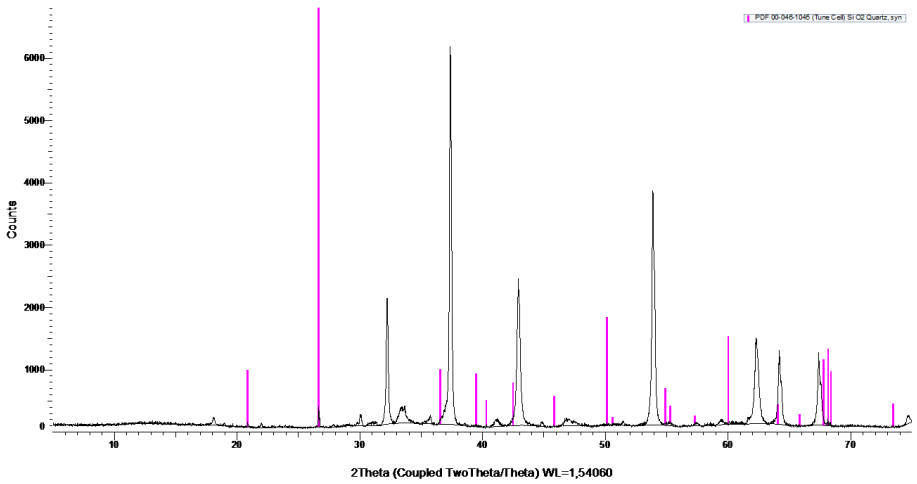

Figure A7.17: Phases measured by XRD of calcined sample NO-10. 30 minutes XRD measurement time. Pink peak indicates that the phase can be SiO_2.

Phase identification for NO-10 at 60 minutes measurement.

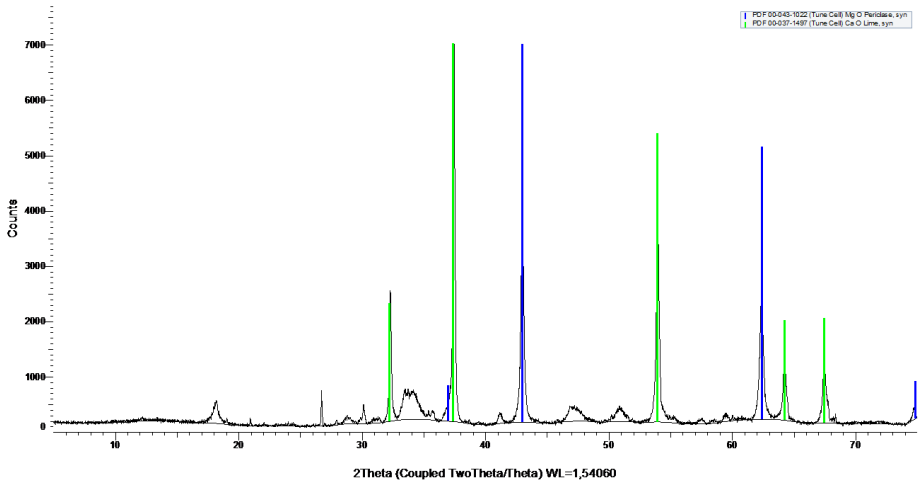

Figure A7.18: Phases measured by XRD of calcined sample NO-10. 60 minutes XRD measurement time. Limegreen and blue peak indicates that the phase can be CaO and MgO respectively.

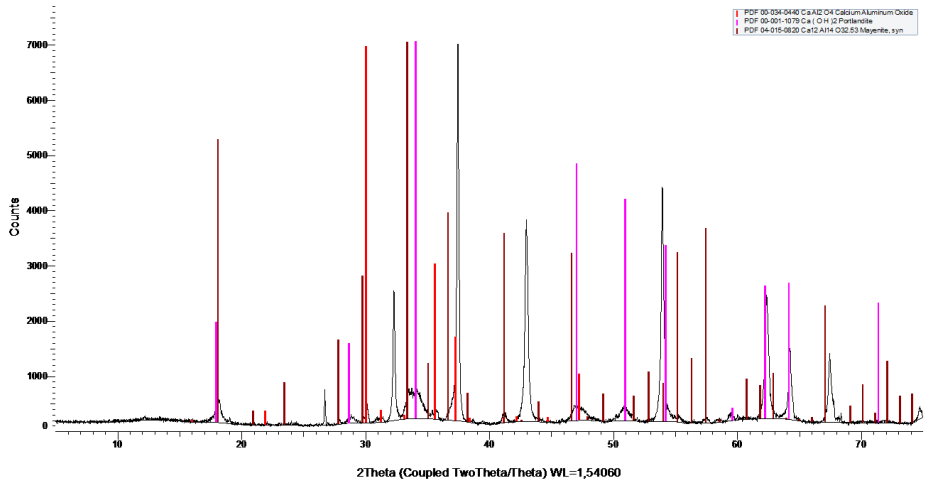

Figure A7.19: Phases measured by XRD of calcined sample NO-10. 60 minutes XRD measurement time. Red, pink and xx peak indicates that the phase can be $CaAl_2O_4$ or $Ca(OH)_2$ or mayenite ($Ca_{12}Al_{14}O_{33}$) respectively.

NO-12

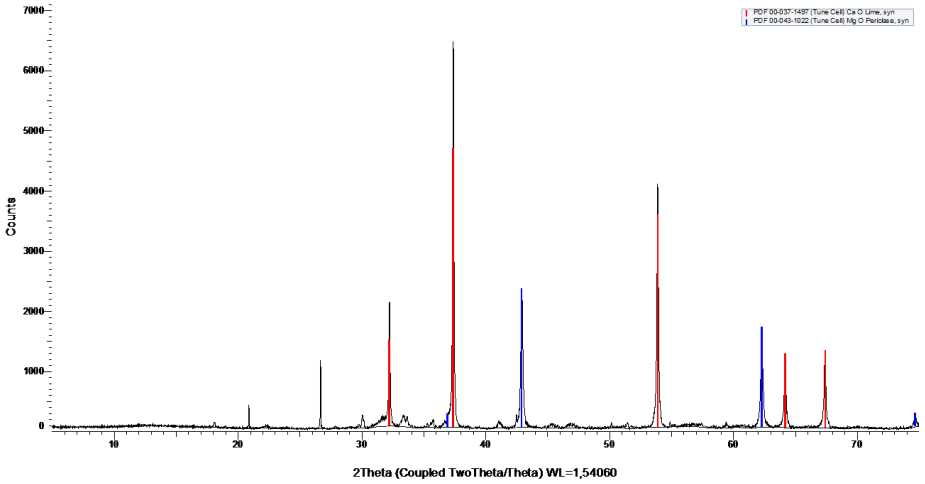

Figure A7.20: Phases measured by XRD of calcined sample NO-12. Red and blue peak indicates that the phase can be CaO and MgO respectively.

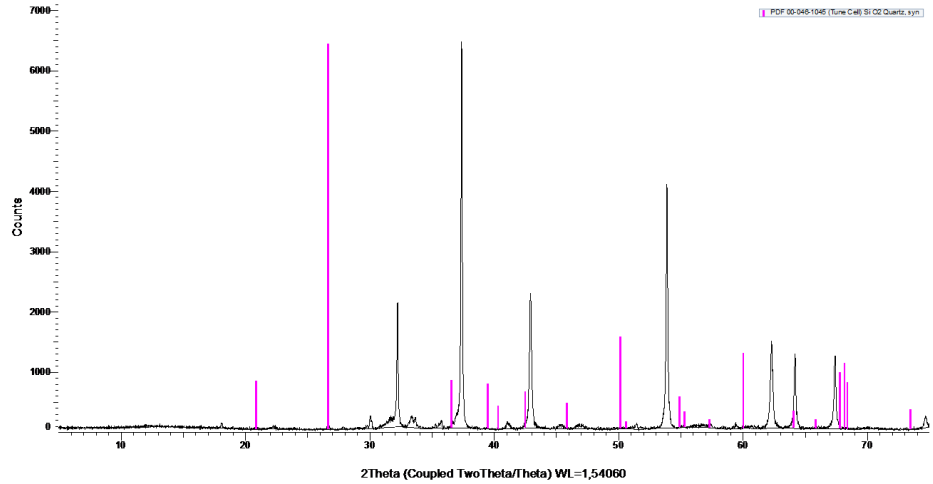

Figure A7.21: Phases measured by XRD of calcined sample NO-12. Pink peak indicates that the phase can be SiO_2.

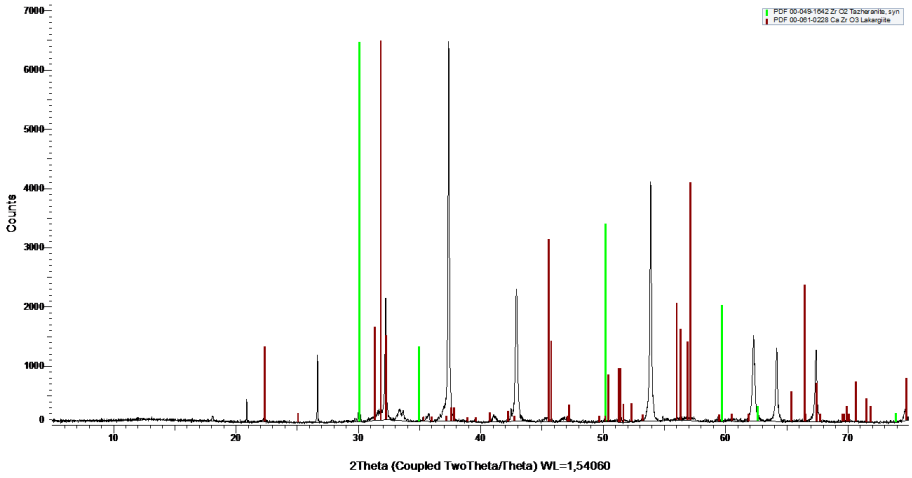

Figure A7.22: Phases measured by XRD of calcined sample NO-12. Lime green peak indicates that the phase can be ZrO_2, and brown peak can be assigned to $CaZrO_3$

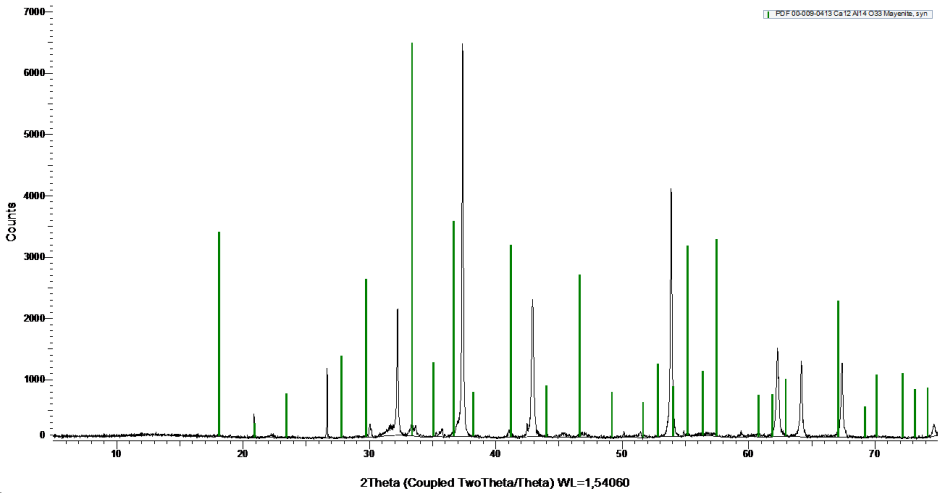

Figure A7.23: Phases measured by XRD of calcined sample NO-12. Green peak indicates that the phase might be Mayenite ($Ca_{12}Al_{14}O_{33}$)

NO-20

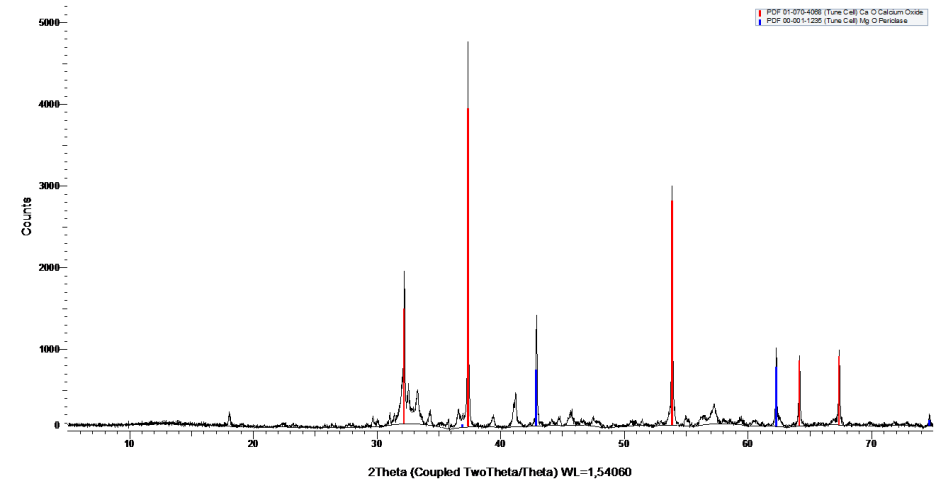

Figure A7.24: Phases measured by XRD of calcined sample NO-20. Red and blue peak indicates that the phase can be CaO and MgO respectively.

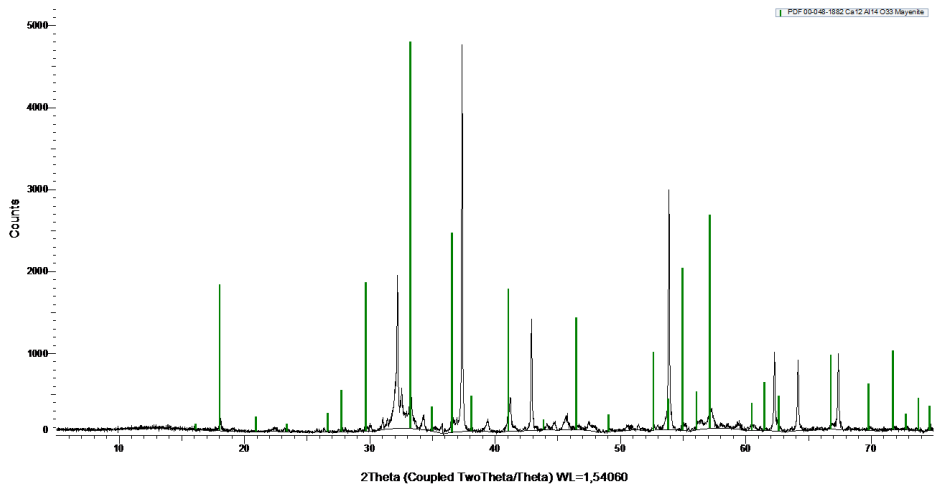

Figure A7.25: Phases measured by XRD of calcined sample NO-20. Green peak indicates that the phase might be Mayenite (($Ca_{12}Al_{14}O_{33}$)

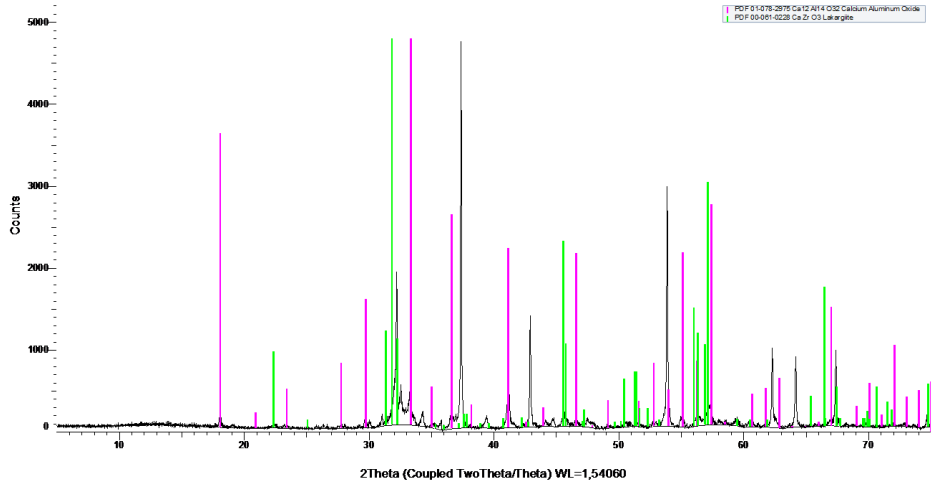

Figure A7.26: Phases measured by XRD of calcined sample NO-20. Green peak indicates that the phase can be $CaZrO_3$, and pink peak can be calsium aluminum oxide ($Ca_{12}Al_{14}O_{32}$).

NO-21

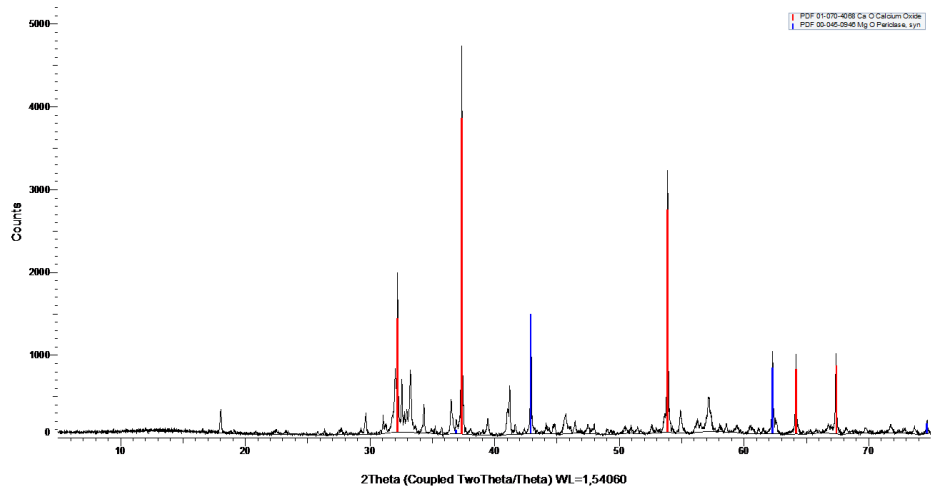

Figure A7.27: Phases measured by XRD of calcined sample NO-21. Red and blue peak indicates that the phase can be CaO and MgO respectively.

NO-22

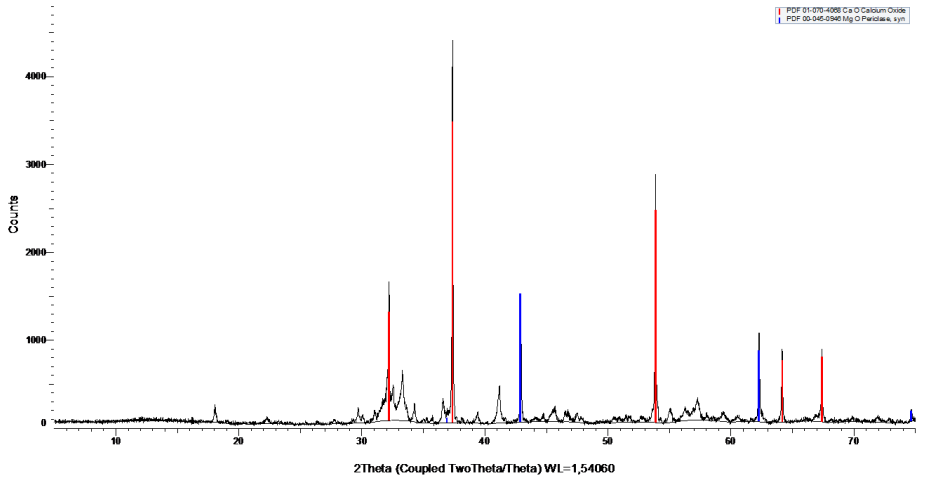

Figure A7.28: Phases measured by XRD of calcined sample NO-22. Red and blue peak indicates that the phase can be CaO and MgO respectively.

NO-23

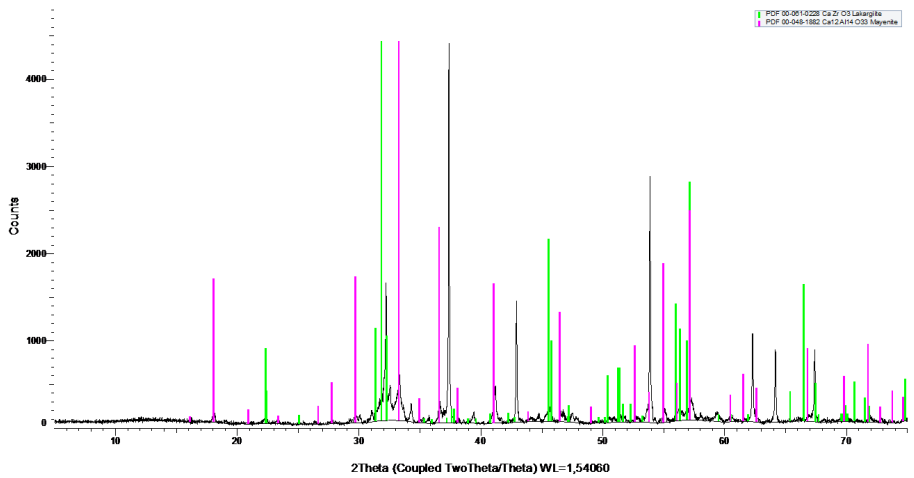

Figure A7.29: Phases measured by XRD of calcined sample NO-22. Green peak indicates that the phase can be $CaZrO_3$, and pink peak can be mayenite ($Ca_{12}Al_{14}O_{33}$).

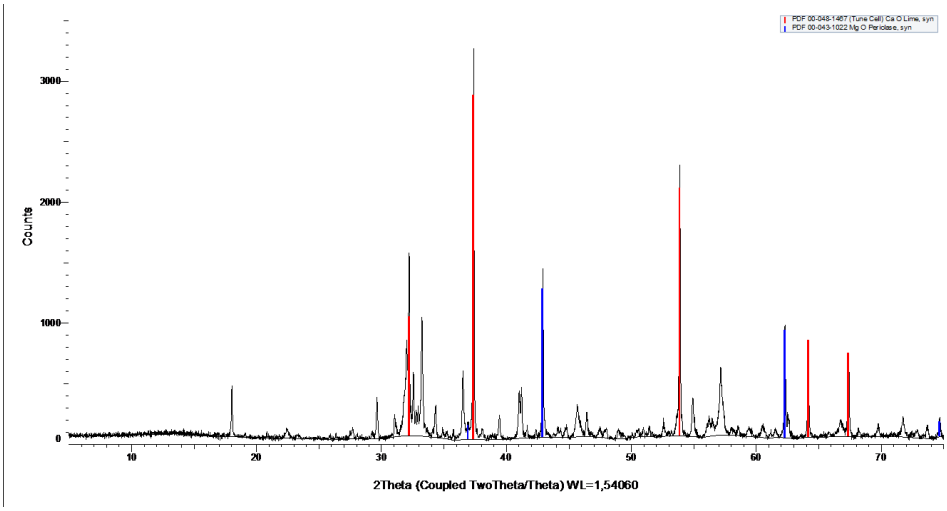

Figure A7.30: Phases measured by XRD of calcined sample NO-23. Red and blue peak indicates that the phase can be CaO and MgO respectively.

A7.4.4 Morphology and Surface of Pellets

Cement ADDA based samples

SEM pictures of calcined pellets NO-20, NO-21, NO-22 and NO-23 is given in figure **??**. The pictures, in figure **??**, are taken with resolution x50.

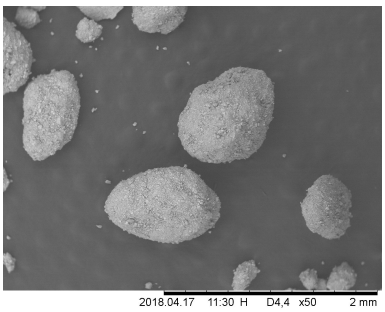

(a) NO-20 500-850um

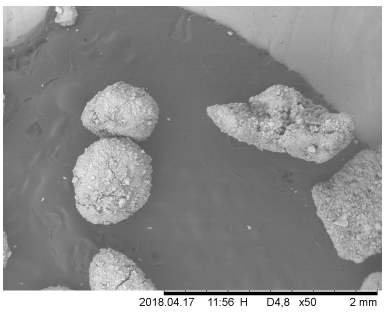

(b) NO-21 500-850um

Figure A7.31: Calcined cement ADDA pellets. Resolution x50.

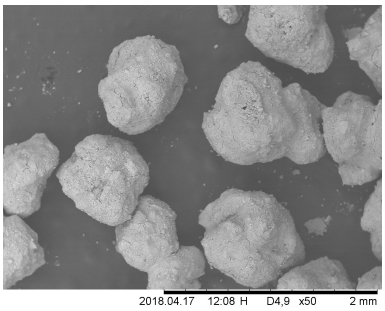

(a) NO-22 500-850um

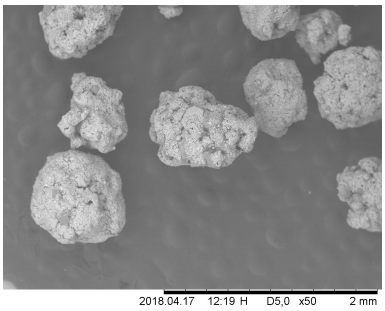

(b) NO-23 500-850um

Figure A7.32: Calcined cement ADDA pellets. Resolution x50.

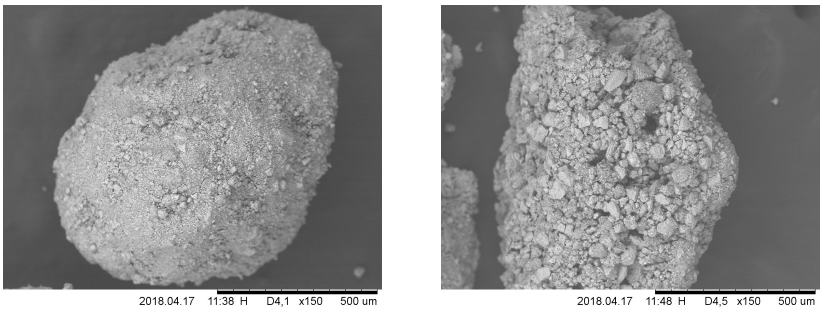

(a) NO-20 500-850um **(b)** NO-21 500-850um

Figure A7.33: Calcined cement ADDA pellets. Resolution x150.

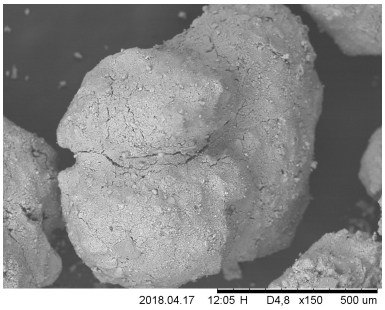

(a) NO-22 500-850um

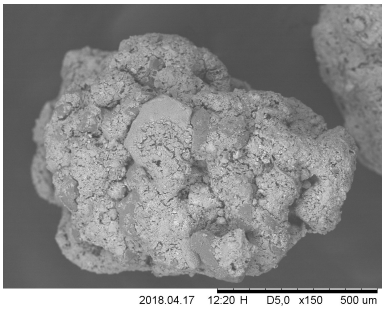

(b) NO-23 500-850um

Figure A7.34: Uncalcined cement ADDA pellets. Resolution x150.

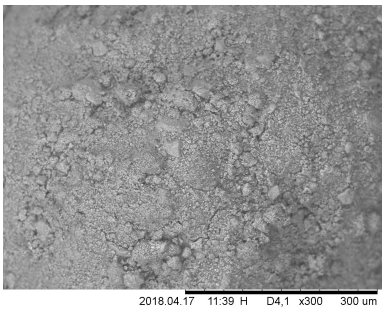

(a) NO-20 500-850um

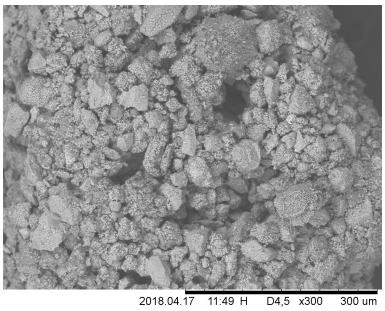

(b) NO-21 500-850um

Figure A7.35: Calcined cement ADDA pellets. Resolution x300.

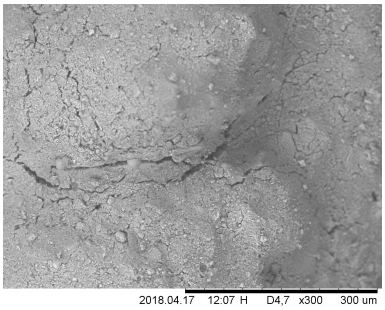

(a) NO-22 500-850um

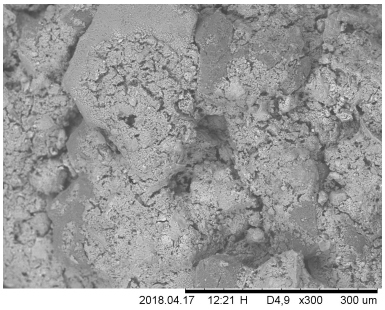

(b) NO-23 500-850um

Figure A7.36: Uncalcined cement ADDA pellets. Resolution x300.

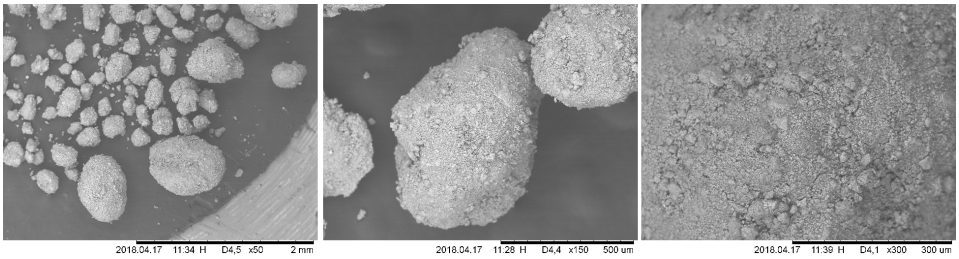

Figure A7.37: NO-20 SEM pictures of calcined pellets. (left) magnification x50 (middle) magnification x150 (right) magnification x300

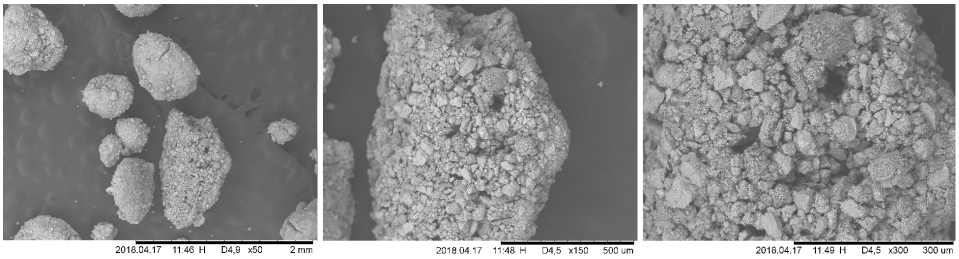

Figure A7.38: NO-21 SEM pictures of calcined pellets. (left) magnification x50 (middle) magnification x150 (right) magnification x300

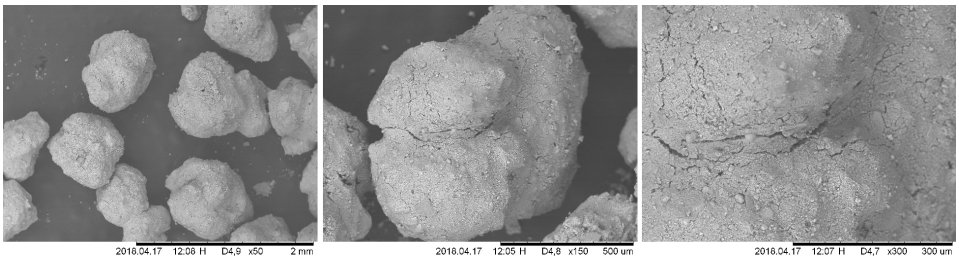

Figure A7.39: NO-22 SEM pictures of calcined pellets. (left) magnification x50 (middle) magnification x150 (right) magnification x300

Dolomite based samples

More SEM pictures of dolomide-based pellets.

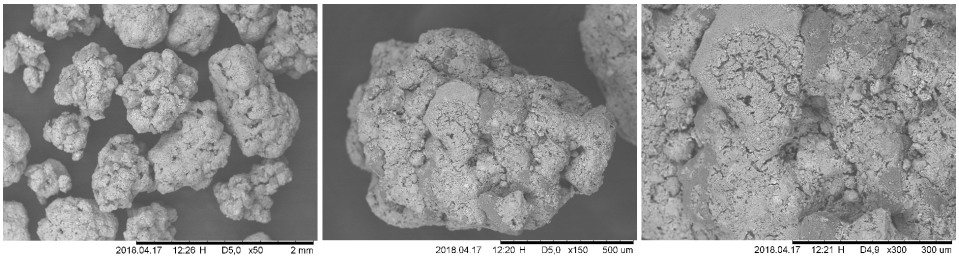

Figure A7.40: NO-23 SEM pictures of calcined pellets. (left) magnification x50 (middle) magnification x150 (right) magnification x300

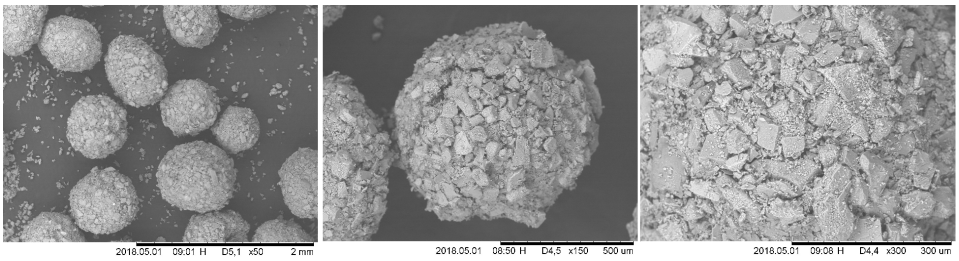

Figure A7.41: NO-1 SEM pictures of calcined pellets. (left) magnification x50 (middle) magnification x150 (right) magnification x300

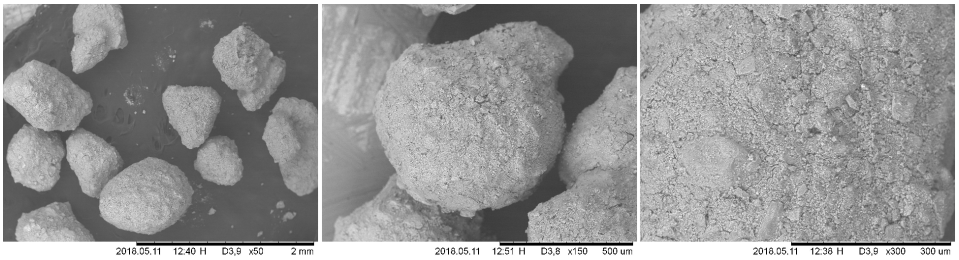

Figure A7.42: NO-3 SEM pictures of calcined pellets. (left) magnification x50 (middle) magnification x150 (right) magnification x300

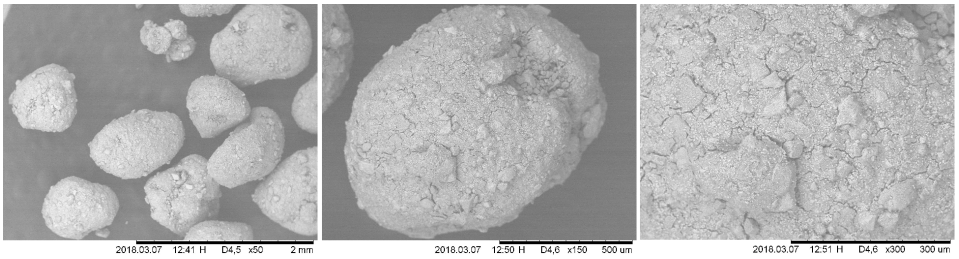

Figure A7.43: NO-6 SEM pictures of calcined pellets. (left) magnification x50 (middle) magnification x150 (right) magnification x300

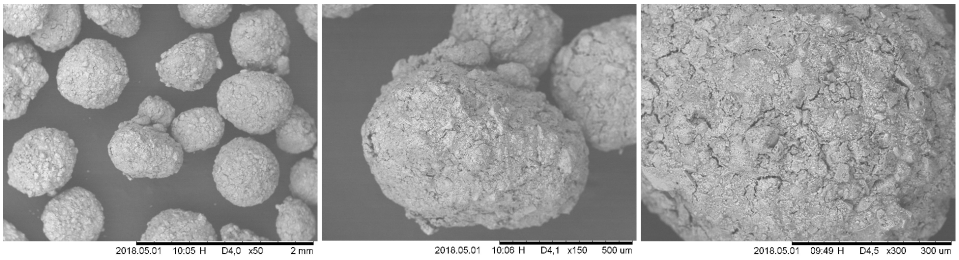

Figure A7.44: NO-8 SEM pictures of calcined pellets. (left) magnification x50 (middle) magnification x150 (right) magnification x300

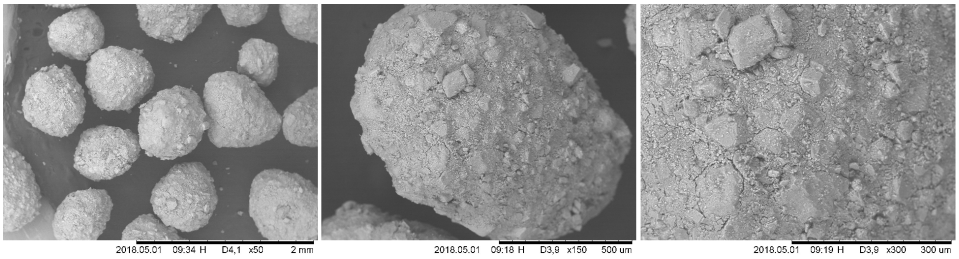

Figure A7.45: NO-10 SEM pictures of calcined pellets. (left) magnification x50 (middle) magnification x150 (right) magnification x300

A7.4.5 BET SA vs. CO2-capacity

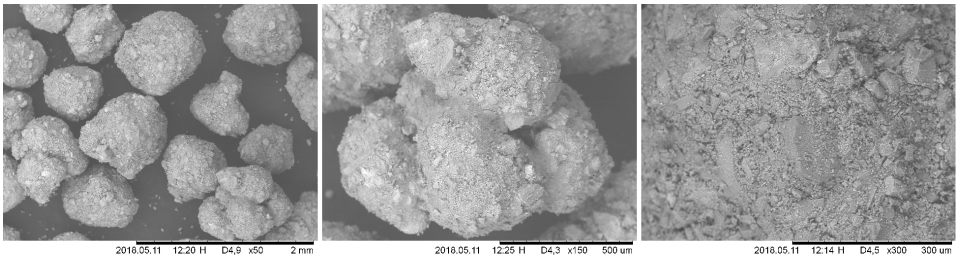

Figure A7.46: NO-12 SEM pictures of calcined pellets. (left) magnification x50 (middle) magnification x150 (right) magnification x300

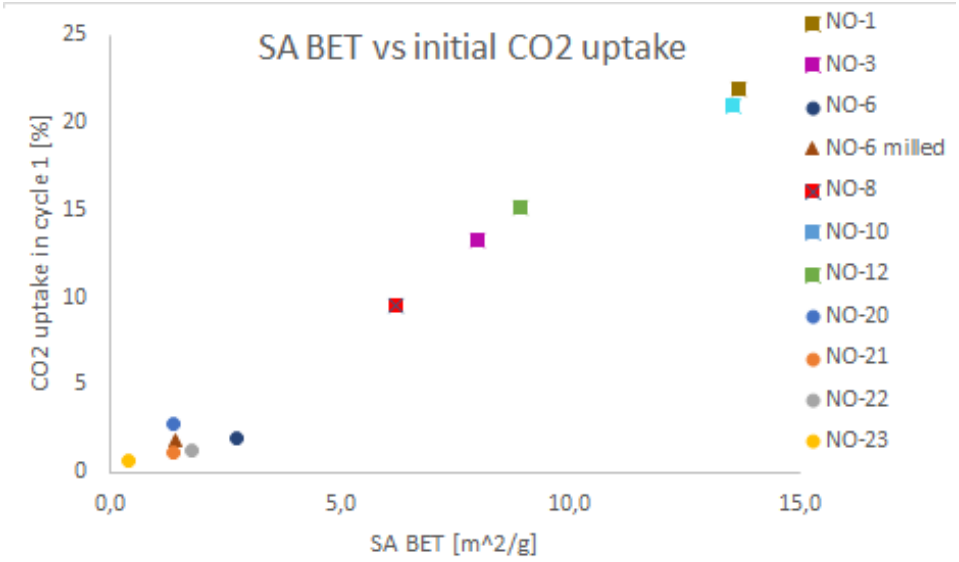

Figure A7.47: BET surface area vs. CO2 sorption capacity in cycle 1.

A7.4.6 TGA (dry) - NO-1 vs. Raw Material of Calcined Dolomite (500-850um)

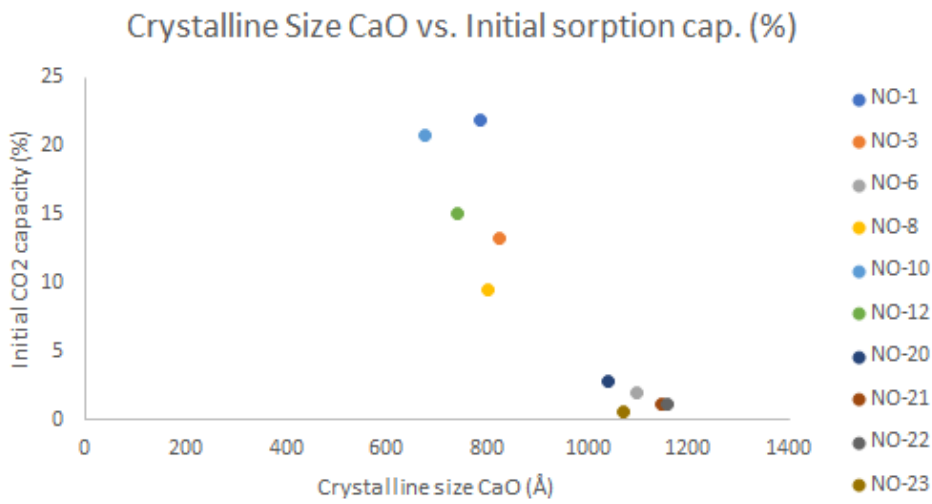

Figure A7.48: Crystalline size of CaO vs. CO2 sorption capacity in cycle 1.

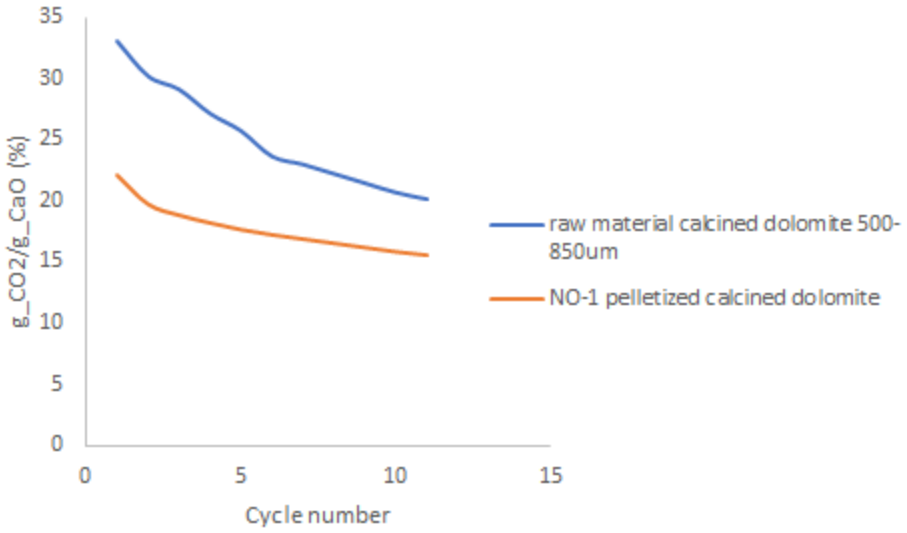

Figure A7.49: 11 sorption cycles for NO-1 compared to grains of raw calcined dolomite with size 500-850um.

A7.4.7 Mechanical strength test

SEM pictures of attrition residue for all samples. Pictures taken with resolution x50.

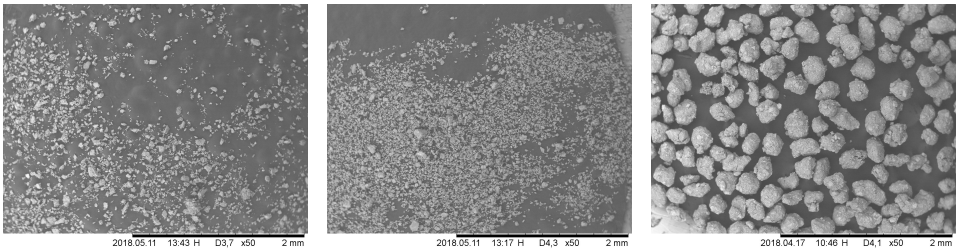

Figure A7.50: (left) NO-1 , (middle) NO-3, (right) NO-6. All SEM photos taken at resolution x50.

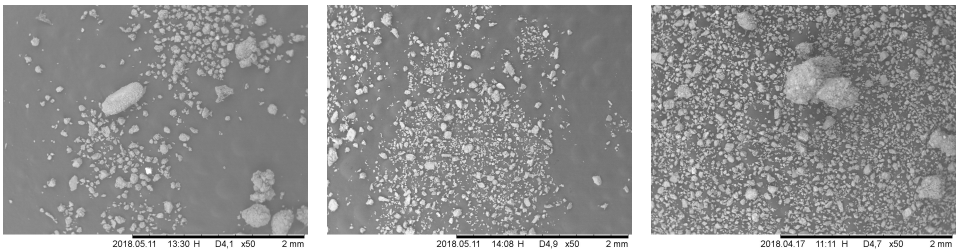

Figure A7.51: (left) NO-8 , (middle) NO-10, (right) NO-12. All SEM photos taken at resolution x50.

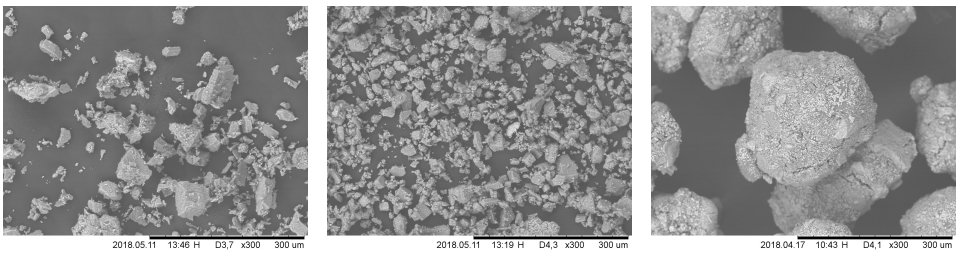

Figure A7.52: (left) NO-1 , (middle) NO-3, (right) NO-6. All SEM photos taken at resolution x300.

A7.5 Investigation of NO-6

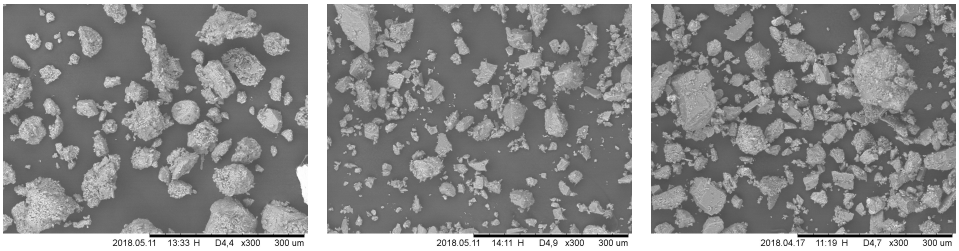

Figure A7.53: (left) NO-8 , (middle) NO-10, (right) NO-12. All SEM photos taken at resolution x300.

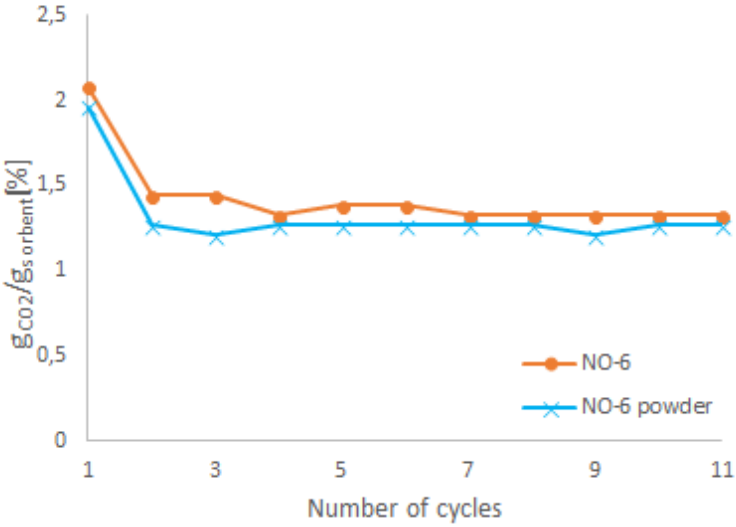

Figure A7.54: TGA: 11 cycles of NO-6 pellets vs. milled pellets (5 min)

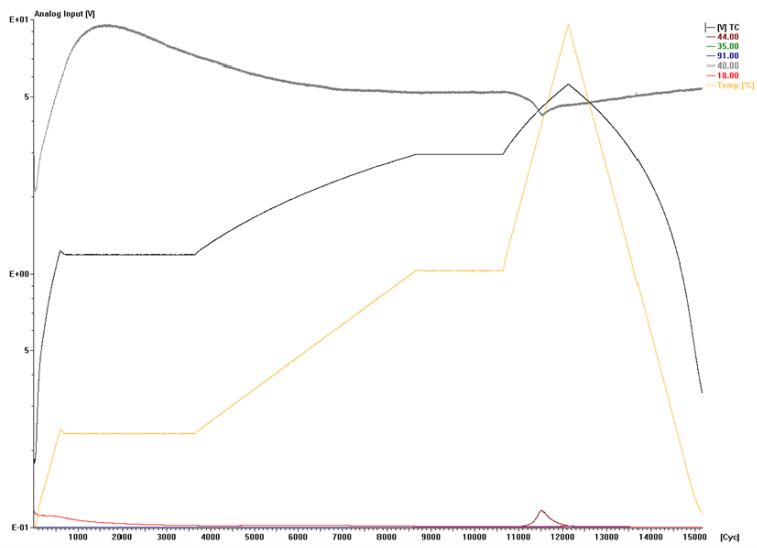

Figure A7.55: Calcination Check of pellet NO-6 using TGA with MS to detect gases leaving the pellets during calcination. Red curve is water, brown curve is carbon dioxide, yellow curve is temperature, grey curve is argon as balance gas.

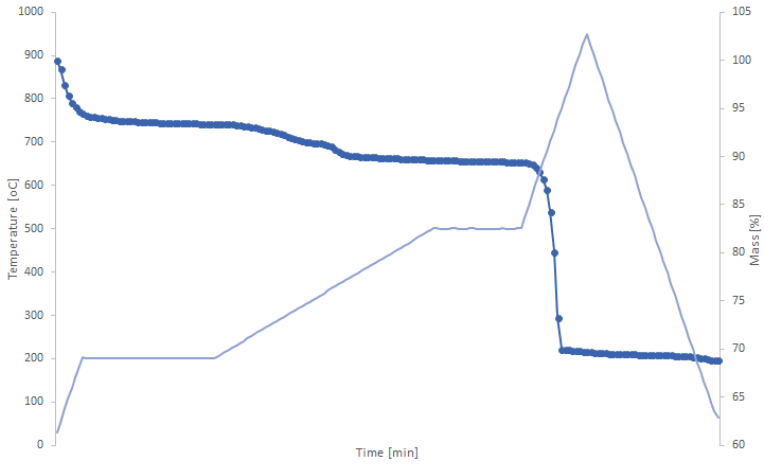

Figure A7.56: Calcination Check of pellet NO-6 using TGA with MS to detect gases leaving the pellets during calcination. Dark blue is mass percentage and ligt blue curve is temperature.

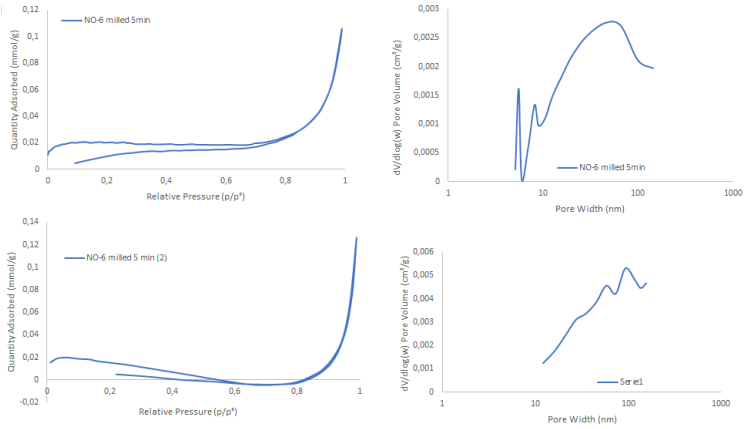

Figure A7.57: (left) BET isotherms for sample NO-6, (right) BJH pore size distribution

A7.6 Results- Kinetic study of sample NO-12

Kinetic study performed on both granulated and extruded pellets.

	CO2 partial pressure (%)	Time derivative (mg/min)		
Cycle		15mg 250um 620degC	5mg 250um 620degC	30mg 250um 620degC
1	2	0,04	0,05	0,03
2	11,3	0,34	0,45	0,26
3	15,6	0,54	0,58	0,47
4	3,3	0,19	0,31	0,13
5	2	0,15	0,26	0,10
6	2	0,16	0,26	0,10
7	11,3	0,37	0,50	0,27
8	15,6	0,53	0,59	0,47
9	3,3	0,19	0,30	0,13
10	2	0,15	0,25	0,10
MASS		*15,03*	*5,14*	*29,65*

Figure A7.58: CO_2-sorption at 620°C. Cycles at different CO_2 pressure for size 250um. Using 5mg, 15mg and 30mg sample load

	CO2 partial pressure (%)	Time derivative (mg/min)		
Cycle		15mg 250um 550degC	15mg 250um 620degC	15mg 250um 650degC
1	2	0,03	0,04	0,03
2	11,3	0,14	0,34	0,35
3	15,6	0,17	0,54	0,66
4	3,3	0,11	0,19	0,17
5	2	0,09	0,15	0,13
6	2	0,09	0,16	0,13
7	11,3	0,14	0,37	0,39
8	15,6	0,15	0,53	0,64
9	3,3	0,10	0,19	0,17
10	2	0,09	0,15	0,13
MASS		*15,5*	*15,03*	*15,1*

Figure A7.59: CO_2-sorption at 550°C, 620°C and 650°C. Cycles at different CO_2 pressure for size 250um.

	CO2 partial pressure (%)	Time derivative (mg/min)					
Cycle		15mg 250um 650degC	15mg 1.2mm 650degC	9mg 2mm 650degC	22mg 2mm 650degC	19mg 3mm 650degC	28mg 4mm 650degC
1	2	0,03	0,03	0,05	0,01	0,01	0,01
2	11,3	0,35	0,32	0,18	0,15	0,13	0,12
3	15,6	0,66	0,66	0,34	0,34	0,30	0,26
4	3,3	0,17	0,15	0,08	0,07	0,06	0,05
5	2	0,13	0,12	0,07	0,05	0,05	0,04
6	2	0,13	0,12	0,07	0,06	0,05	0,04
7	11,3	0,39	0,34	0,18	0,17	0,14	0,12
8	15,6	0,64	0,63	0,33	0,35	0,30	0,26
9	3,3	0,17	0,15	0,08	0,07	0,06	0,05
10	2	0,13	0,12	0,07	0,05	0,05	0,04
MASS		*15,1*	*15*	*9*	*22,56*	*18,85*	*28,13*
					en kule	2 kuler	

Figure A7.60: CO_2-sorption 650deg , cycles different co2 pressure size 250um, 1.2mm, 2mm, 3mm, 4mm

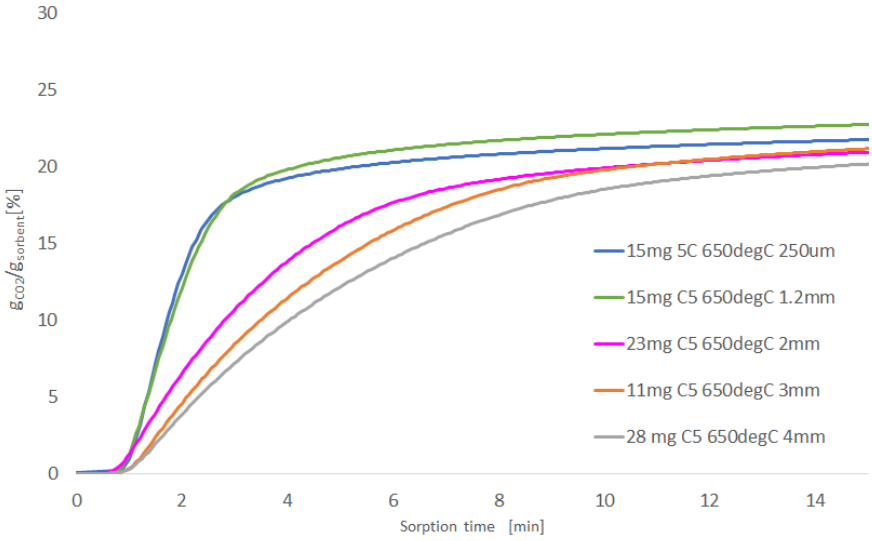

Figure A7.61: CO_2-sorption at 650°C for size 250μm, 1.2mm,2mm, 3mm and 4mm. Cycle 5 (C5) is applied in this plus using 2% CO_2 concentration. First 15 minutes.

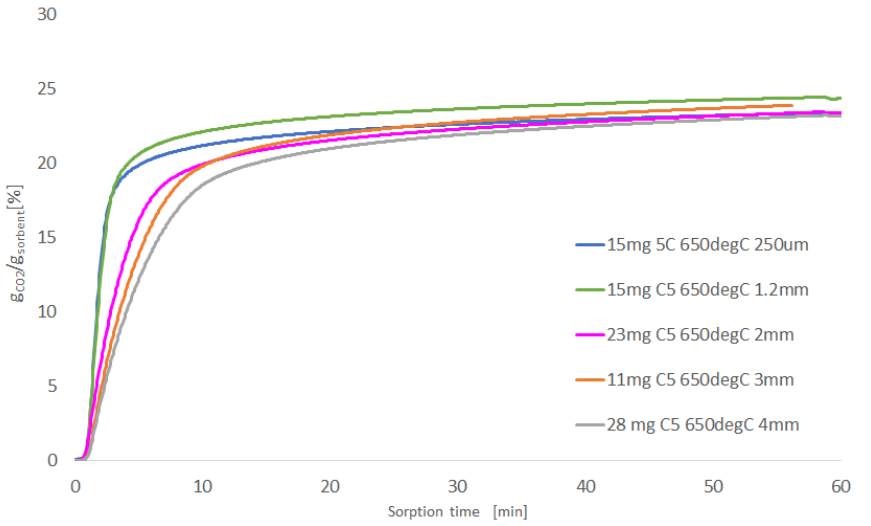

Figure A7.62: CO_2-sorption at 650°C for size 250μm, 1.2mm,2mm, 3mm and 4mm. Cycle 5 (C5) is applied in this plus using 2% CO_2 concentration. 60 minutes.

% of max cap.	250um time (min)	1.2 mm time (min)	2mm time (min)	3mm time (min)	4mm time (min)
100	48	49,2	49,3	49,1	48,7
90	8,1	8,48	14,24	15,67	17,11
80	3,3	3,63	6,87	8,5	9,62
70	2,42	2,66	5,03	6,42	7,3
60	2,09	2,27	3,94	5,13	5,75
50	1,85	2	3,2	4,13	4,65
40	1,65	1,76	2,63	3,33	3,67
30	1,49	1,53	2	2,63	2,89
20	1,33	1,35	1,6	2,03	2,18

Figure A7.63: Table of percentage of max capacity at different time (min)

A7.7 Granulation with GMX-LAB Micro GRANUMEIST® Granulator

During the specializaition project fall 2017, a GMX-LAB Micro GRANUMEIST® Granulator/Mixer was used to make pellets with solid cement powder, calcined dolomite, water and flowing air at a pressure of about 1-2 barg in ambient temperature. The GMX GRANUMEIST® High Shear Granulator and Mixer is designed for efficient and homogeneous wet granulation of powders to form a medium to high density granule. The granulator is equipped with a high-speed impeller and rotor to make small pellets with a uniform size and shape. Water is pumped and spread by flowing air into the bowl in the granulator and mixed with fine solid powder. The granulator is equipped with a motor rated at 1.4kW which supplies high shear stirring to ensure mixing of water and solid. A control system is used to interface with the granulator/mixer and control the process. Specifications for the GMX-Lab Micro Granulator is given in table A7.2.

Table A7.2: Specifications for GMX-LAB Micro GRANUMEIST® Granulator/Mixer.

Specification	Value of specification
Height	30" (776 mm)
Width	35" (894 mm)
Depth	24" (602 mm)
Voltage	220V/50-60/1 30 amp
Mixer Bowl Capacity	1 L working capacity 0.33L - 0.7L

Agitation supplied by impeller at high rpm can lead to a temperature increase in the bowl, in addition, the reaction between the cement/dolomite and water is an exothermic reaction, and will give a temperature increase in the bowl (reaction between water and active calcium oxide is given in equation 1.5). Therefore, the bowl is equipped with a thermal

jacket to control the temperature with water recirculating by Julabo Refrigerating Heating system.

In order to use using the 1L bowl, the mixer blade with short arms and the chopper blades with 2 blades are used. The granulation procedures are given as a part of the result because the main task was to develop a procedure for making the CaO-based pellets with cement binder.

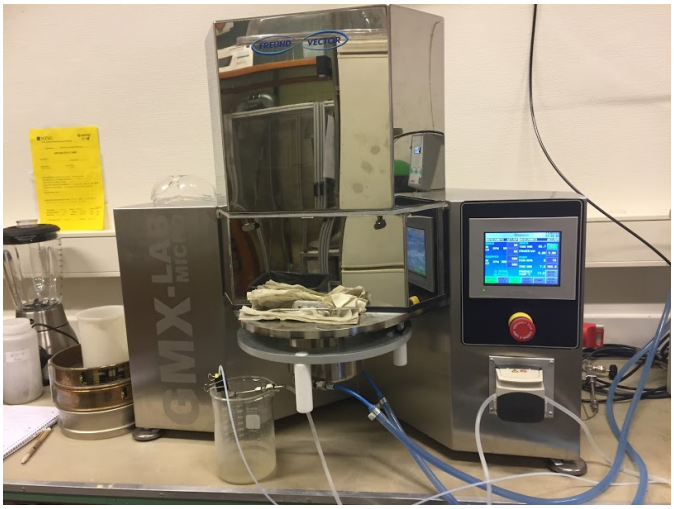

Figure A7.64: GMX-LAB Micro GRANUMEIST® Granulator/Mixer

Stirring was an issue for all procedures and stirring had to be stopped after a while. A picture of the granulation bowl with mixed material is given in figure A7.65, which clearly show the dry powder on the wall of the bowl. The well mixed material also sticks to the wall of the bowl forming a hard, tick layer of dolomite and cement. This layer is causing a high noise and unstable stirring after the water is added. This problem occurred during granulation in a 4L bowl using cement types Adda and Fondu, and also in granulation using pure calcined dolomite (800°C,6h, <106μm), calcined dolomite mixed with 2-3 % cement fondu and 11% cement fondu. A figure of the experiment mixing calcined dolomite with 2-3 % cement fondu and 11% fondu is given in figure A7.66. Without the cement the granules seem to posses more preferable morphology, but stirring was also an issue for this procedure.

Figure A7.65: A figure of one of the experiments indicating bad stirring of water, dolomite and cement. The light grey material is dry dolomite/cement while the dark gray dolomite/cement is mixed with water.

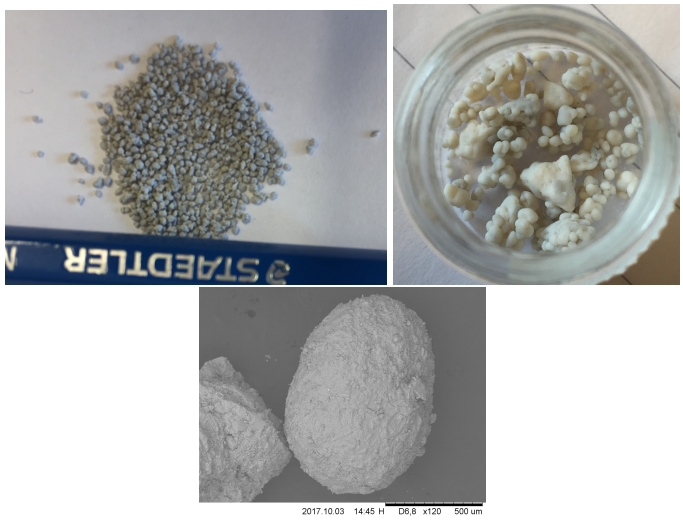

Figure A7.66: (top left) Calcined dolomite and 2-3 % cement Fondu pellets. Particle size between 850-250 μm. (top right) pure calcined dolomite (bottom) SEM picture of sample with only pure calcined dolomite. Resolution x120.

A7.7.1 Method - GMX-LAB Micro GRANUMEIST® Granulator

A 1L bowl was used and a certain volume of material was necessary to get the chopper in contact with the powder. Therefore, 250g dolomite powder was used to obtain a volume of approximately 1/3 (350mL) of the bowl. After water addition, the volume increased to fill about half the bowl. The pump used to introduce water to the bowl were set to 10rpm.

The pellets were prepared by mixing three different raw material:

- **50/50 Size**: mix of 125g calcined dolomite (800°C, 6h) at size <106μm, 125g calcined dolomite (800°C,6h) at size 106-212μm, 27.5g cement Fondu and water.
- **80/20 Cal/Uncal**: mix of 200g calcined dolomite (800°C, 6h, <106μm), 50g uncalcined dolomite (<106μm), 27.5g cement Fondu and water.
- **50/50 Cal800/Cal650**: mix of 125g calcined dolomite (800°C, 6h, <106μm) and 125g partly calcined dolomite (650°C, 6h, <106μm), 27.5g cement Fondu and water.

A picture of the resulting pellets is shown in figure A7.67

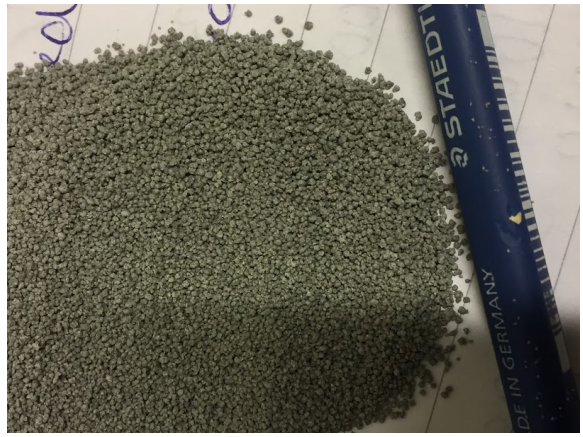

Figure A7.67: Sample 50/50 Size pellets with size ranging from 850μm-250μm

A7.7.2 Result from Characterization using GMX-LAB Micro GRANUMEIST® Granulator

Surface Area and Pore Size

The surface area [m^2/g] measurements from the BET for all 3 pellets are given in table A7.3. BJH desorption average pore diameter and BJH desorption cumulative volume of pores are also given.

The isotherms for pellets 50/50 Size is given in figure A7.68.

Table A7.3: BET surface area, BJH average pore size and BJH pore volume for calcined pellets (1000°C, 3h, 850-250 μm).

Sample	S_{BET} (m^2/g)	d_p (nm)	V_p (cm^3/g)
50/50 Size	12	22.4	0.06
80/20 Cal/Uncal	13	20.6	0.06
50/50 Cal800/Cal650	12	18.3	0.05

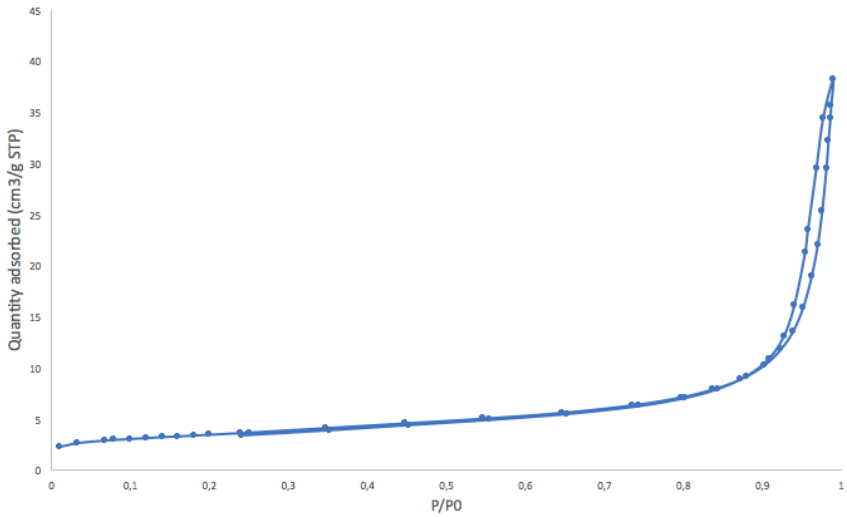

Figure A7.68: Adsorption isotherm for sample 50/50 Size (calcined at 1000°C for 3h).

Composition of Dolomite and Cement Based Pellets

X-Ray Fluorescence (XRF) X-ray fluorescence spectrometry is used to determine the bulk specimen [92].

Measured amount of the different component in the dolomite and cement based pellets measured from the X-ray fluorescence. The molar amount of CaO and MgO are given for the three pellets (calcined at 1000 °C 3h) in table A7.4.

Table A7.4: Molar percentage of CaO and MgO for the 3 pellets (calcined at 1000°C for 3h) measured with XRF.

Sample	CaO mole %	MgO mole %
50/50 Size	51.83	42.94
80/20 Cal/Uncal	52.53	43.35
50/50 Cal800/Cal650	45.32	49.72

Table A7.5: XRF elemental composition for pellets 50/50 Cal800/Cal650.

Component	**weight** %	**mole** %
MgO	0.40	49.72
Al_2O_3	0.04	2.06
SiO_2	0.02	1.45
P_2O_5	$8{\cdot}10^{-4}$	0.01
SO_3	$2{\cdot}10^{-3}$	0.14
Cl	$4{\cdot}10^{-4}$	0.05
K_2O	$6{\cdot}10^{-3}$	0.32
CaO	0.51	45.32
Fe_2O3	$3{\cdot}10^{-3}$	0.10
SrO	0.02	0.83
H_3BO_3	0.15	-

Table A7.6: XRF elemental composition for pellet 80/20 Cal/Uncal.

Component	**weight** %	**mole** %
MgO	0.35	43.35
Al_2O_3	0.03	1.47
SiO_2	0.02	1.72
K_2O	$6{\cdot}10^{-3}$	0.37
CaO	0.58	52.53
Fe_2O3	0.02	0.55
SrO	$3{\cdot}10^{-4}$	0.02
H_3BO_3	0.15	-

Table A7.7: XRF elemental composition for sample 50/50 Size.

Component	**weight** %	**mole** %
MgO	0.34	42.94
Al_2O_3	0.03	1.68
SiO_2	0.03	2.54
K_2O	$8{\cdot}10^{-3}$	0.44
CaO	0.57	51.83
Fe_2O3	0.02	0.57
H_3BO_3	0.16	-

Phase Identification of Dolomite and Cement Based Pellets

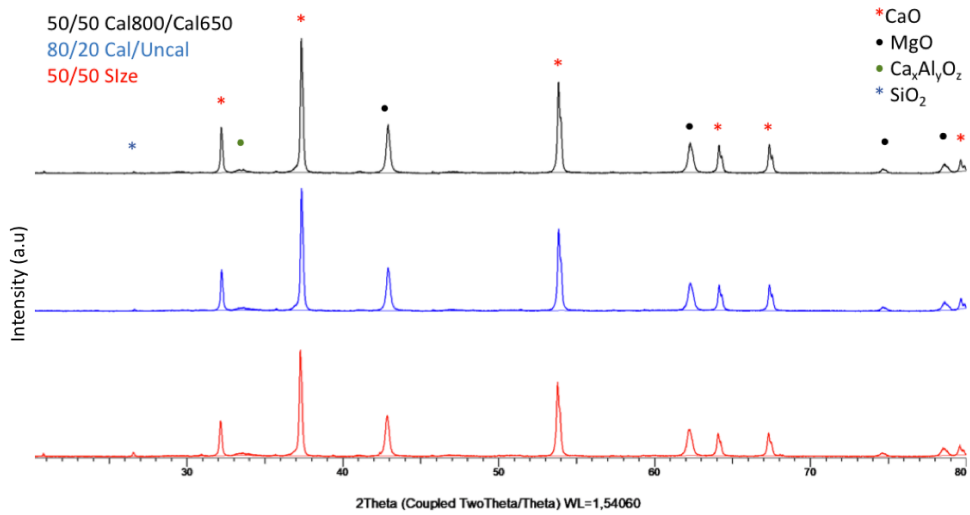

Figure A7.69: XRD phases of the three calcined dolomite/cement pellets (calcined at 1000°C, 3h). Red phase is the 50/50 Size pellets, blue phase is 80/20 Cal/Uncal pellets and black phase is 50/50 Cal800/Cal650. Red star, black dot, green dot and blue star can be identified as CaO, MgO, $Ca_xAl_yO_z$ and SiO_2 respectively.

Morphology and Surface of Pellets

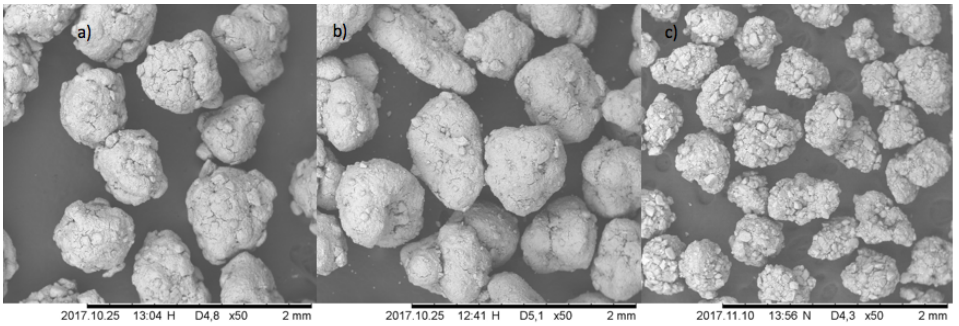

Figure A7.70: SEM pictures of calcined pellets. a) 50/50 Size, b) 80/20 Cal/Uncal, c) 50/50 cal800/cal650. Resolution x50.

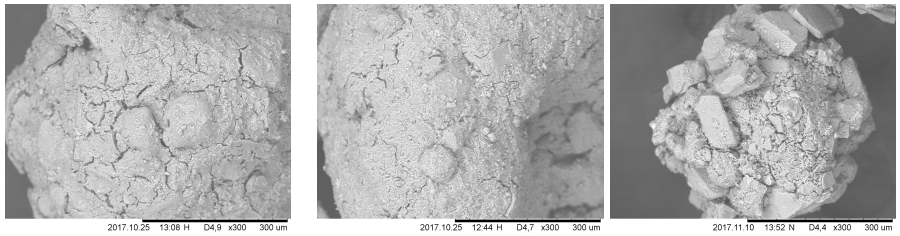

Figure A7.71: SEM pictures of calcined pellets (1000°C, 3h) taken at resolution x300. (left) 50/50 Size, (middle) 80/20 Cal/Uncal, (right) 50/50 Cal800/Cal650.

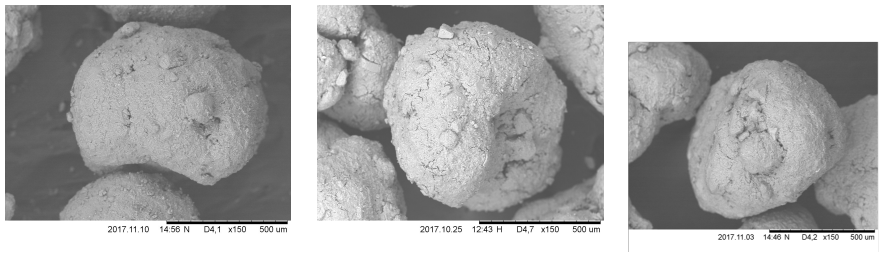

Figure A7.72: (top left) Uncalcined 80/20 Cal/Uncal, (top right) 80/20 Cal/Uncal calcined (1000°C,3h), (bottom) attrition tested 80/20 Cal/Uncal calcined (1000 °C 3h). Resolution x150

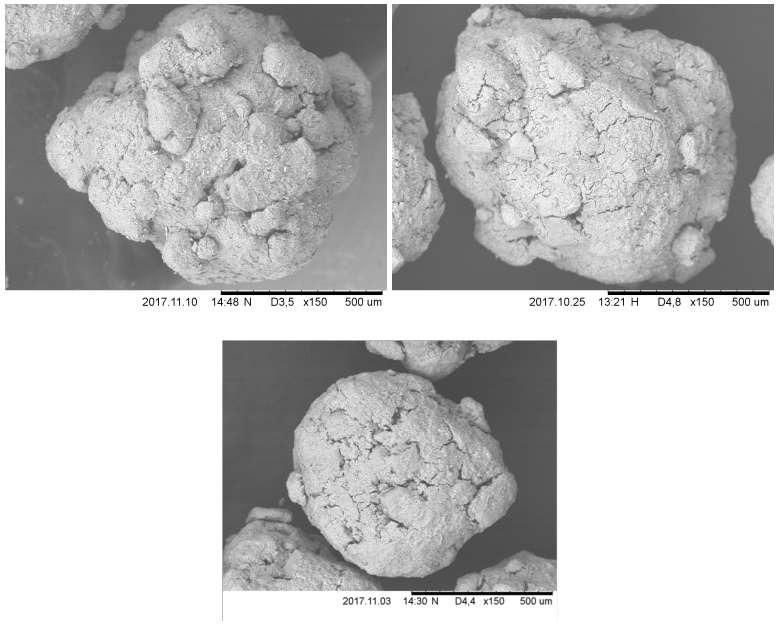

Figure A7.73: (top left) uncalcined 50/50 Size, (top right) 50/50 Size calcined (1000°C, 3h), (bottom) attrition tested 50/50 Size calcined (1000°C, 3h). Resolution x150

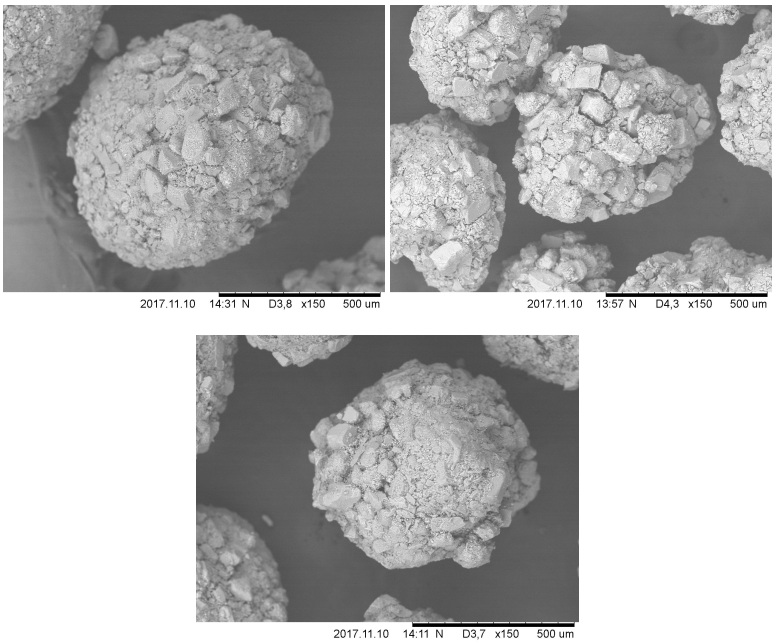

Figure A7.74: (top left) uncalcined 50/50 Cal800/Cal650, (top right) 50/50 Cal800/Cal650 calcined (1000, °C, 3h), (bottom) attrition tested 50/50 Cal800/Cal650 calcined (1000°C, 3h). Resolution x150

10 randomly chosen pellets from sample sample 80/20 Cal/Uncal. The width and height of pellet is measured from SEM pictures. The ratio between width and height should be as close to 1 as possible to have spherical pellets. The average of the size of the 10 pellets are 0.87.

Table A7.8: Width and height of 10 pellets (sample 80/20 Cal/Uncal) measured from SEM pictures and ratio between width and height

Pellet	Width	Height	H/W
Pellet 1	900	800	0.89
Pellet 2	1200	700	0.58
Pellet 3	1000	800	0.8
Pellet 4	1000	800	0.8
Pellet 5	800	800	1
Pellet 6	700	700	1
Pellet 7	1100	600	0.54
Pellet 8	700	650	0.93
Pellet 9	600	600	1
Pellet 10	850	700	0.82

Attrition Test

Falling Test

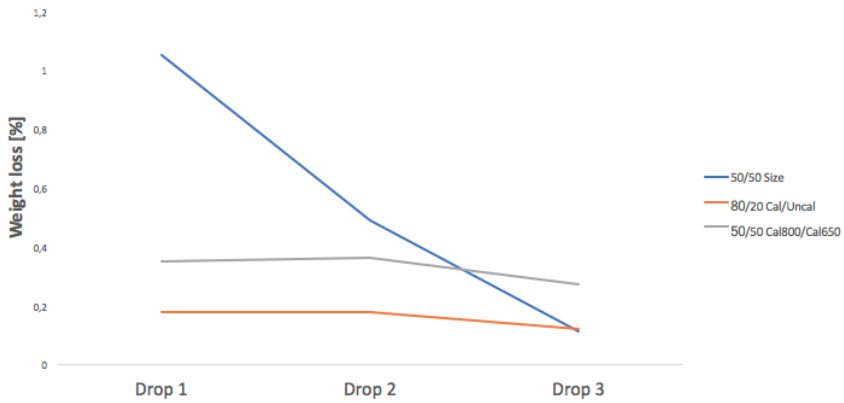

Figure A7.76: Weight loss (%) of each drop for the 3 calcined pellets (1000°C, 3h) after 1,2 and 3 throws.

A7.8 Raw data files - BET

Sample: Fondu
Operator: Maria Olsvik
Submitter:
File: C:\...\MARIAO~1\000-324.SMP

Started:	07.03.2018 14:17:21	Analysis Adsorptive:	N2
Completed:	07.03.2018 16:12:38	Analysis Bath Temp.:	-195.850 °C
Report Time:	08.03.2018 7:27:02	Sample Mass:	0.0891 g
Warm Free Space:	10.0188 cm^3 Measured	Cold Free Space:	30.3710 cm^3 Measured
Equilibration Interval:	5 s	Low Pressure Dose:	None
Sample Density:	1.000 g/cm^3	Automatic Degas:	No

Summary Report

Surface Area

Single point surface area at P/Po = 0.068886553: 0.0100 m^2/g

Pore Volume

Single point adsorption total pore volume of pores less than 129.6772 nm diameter at P/Po = 0.984844423: 0.000150 cm^3/g

Pore Size

Adsorption average pore width (4V/A by single point): 60.18762 nm

Sample: Fondu
Operator: Maria Olsvik
Submitter:
File: C:\...\MARIAO~1\000-324.SMP

Started:	07.03.2018 14:17:21	Analysis Adsorptive:	N2
Completed:	07.03.2018 16:12:38	Analysis Bath Temp.:	-195.850 °C
Report Time:	08.03.2018 7:27:02	Sample Mass:	0.0891 g
Warm Free Space:	10.0188 cm³ Measured	Cold Free Space:	30.3710 cm³ Measured
Equilibration Interval:	5 s	Low Pressure Dose:	None
Sample Density:	1.000 g/cm³	Automatic Degas:	No

Isotherm Tabular Report

Relative Pressure (P/Po)	Absolute Pressure (kPa)	Quantity Adsorbed (cm³/g STP)	Elapsed Time (h:min)	Saturation Pressure (kPa)
			00:42	99.1024930
0.011362642	1.1267317	0.0189	00:44	99.1610657
0.034417647	3.4141800	0.0175	00:45	99.1985301
0.068886553	6.8352773	0.0025	00:46	99.2251311
0.091920662	9.1225938	-0.0248	00:48	99.2442132
0.115294219	11.4450799	-0.0565	00:49	99.2684625
0.138599710	13.7607907	-0.0903	00:50	99.2844117
0.160946642	15.9819352	-0.1188	00:51	99.2995879
0.201049681	19.9633897	-0.1633	00:53	99.2958040
0.260198273	25.8392730	-0.2423	00:54	99.3060896
0.368621267	36.6092252	-0.3758	00:55	99.3139259
0.468215931	46.5017529	-0.5099	00:57	99.3168960
0.567724399	56.3829250	-0.6415	00:58	99.3139015
0.667151123	66.2576035	-0.7718	00:59	99.3142351
0.756863993	75.1640427	-0.8417	01:00	99.3098410
0.817667664	81.1951400	-0.8516	01:02	99.3009061
0.858258293	85.2227882	-0.8122	01:03	99.2973664
0.874386475	86.8198415	-0.7924	01:04	99.2922968
0.903629364	89.7134274	-0.7077	01:06	99.2812219
0.924125331	91.7407270	-0.6111	01:07	99.2730357
0.939833213	93.2896722	-0.5314	01:08	99.2619445
0.953022888	94.5873034	-0.4247	01:09	99.2497710
0.964223851	95.6946182	-0.3019	01:11	99.2452304
0.971751697	96.4177930	-0.1969	01:12	99.2206067
0.977650923	96.9965704	-0.0893	01:13	99.2139097
0.982650132	97.4885873	0.0253	01:14	99.2098654
0.984844423	97.6833305	0.0971	01:16	99.1865600
0.986693484	97.8554436	0.1451	01:17	99.1751189
0.988657961	98.0313569	0.2004	01:18	99.1559880
0.989779658	98.1269790	0.2272	01:20	99.1402260
0.970092743	96.1594889	-0.1627	01:21	99.1240163
0.945996272	93.7564471	-0.4163	01:22	99.1086856
0.921798578	91.3341522	-0.5562	01:24	99.0825484
0.887054579	87.8813999	-0.6698	01:25	99.0710178
0.856722014	84.8600087	-0.7314	01:27	99.0519764
0.821771766	81.3877593	-0.7775	01:28	99.0393716
0.801264410	79.3387736	-0.7913	01:29	99.0169695
0.723300356	71.6040889	-0.8049	01:31	98.9963413
0.633204991	62.6727657	-0.7706	01:32	98.9770557
0.532945070	52.7382492	-0.7008	01:33	98.9562567
0.432489748	42.7877265	-0.6851	01:35	98.9335046
0.331766748	32.8163111	-0.6109	01:36	98.9138041
0.221261428	21.8832294	-0.5477	01:38	98.9021433

Sample: Fondu
Operator: Maria Olsvik
Submitter:
File: C:\...\MARIAO~1\000-324.SMP

Started:	07.03.2018 14:17:21	Analysis Adsorptive:	N2
Completed:	07.03.2018 16:12:38	Analysis Bath Temp.:	-195.850 °C
Report Time:	08.03.2018 7:27:02	Sample Mass:	0.0891 g
Warm Free Space:	10.0188 cm³ Measured	Cold Free Space:	30.3710 cm³ Measured
Equilibration Interval:	5 s	Low Pressure Dose:	None
Sample Density:	1.000 g/cm³	Automatic Degas:	No

Isotherm Linear Plot

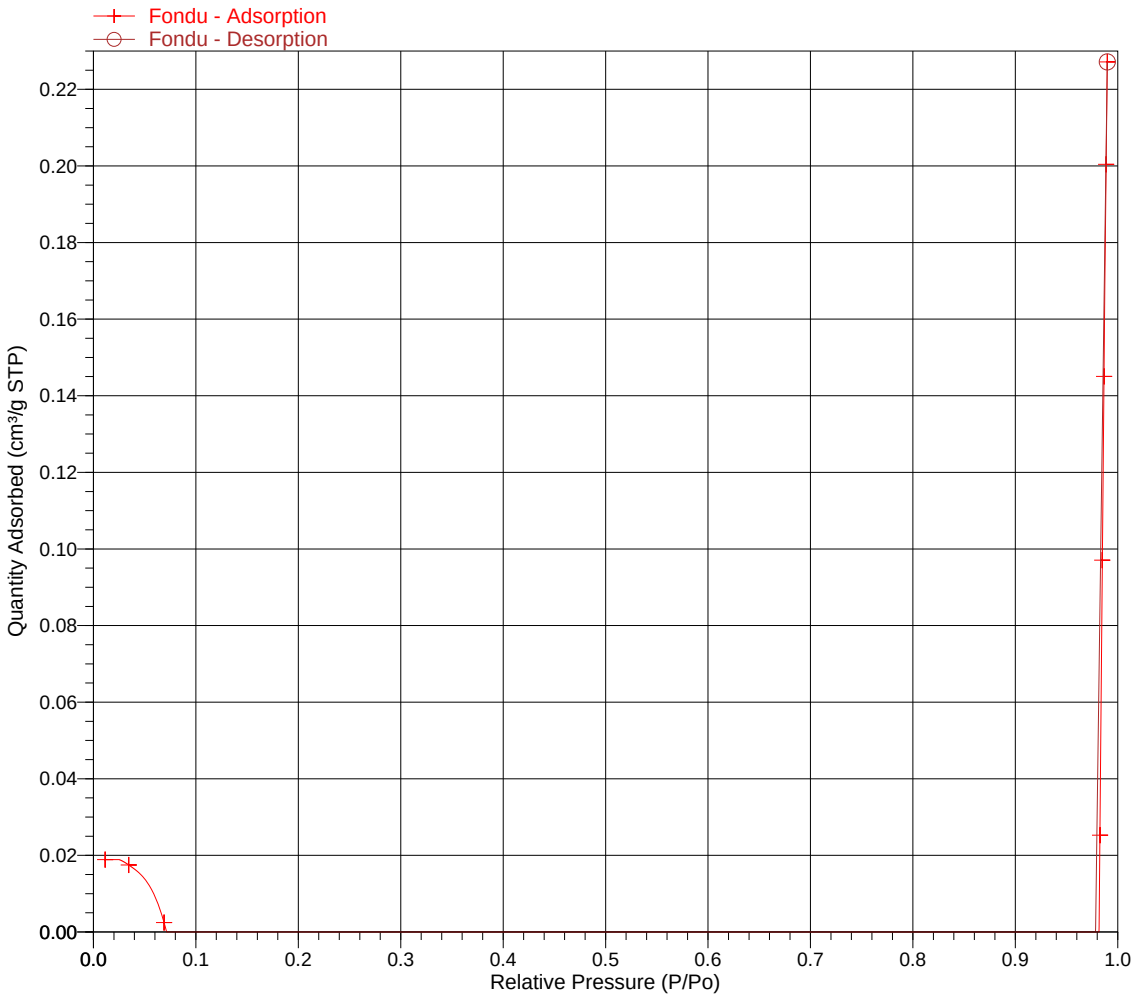

Full Report Set

Sample: NO-1
Operator: Maria Olsvik
File: C:\TriStar II 3020\data\Maria Olsvik\NO-1.SMP

Started:	08.05.2018 09:58:11	Analysis Adsorptive:	N2
Completed:	08.05.2018 16:06:32	Analysis Bath Temp.:	-195,850 °C
Report Time:	08.05.2018 21:19:08	Thermal Correction:	No
Sample Mass:	0,0733 g	Warm Free Space:	9,9746 cm³ Measured
Cold Free Space:	30,2745 cm³	Equilibration Interval:	10 s
Low Pressure Dose:	None	Sample Density:	1,000 g/cm³
Automatic Degas:	No		

Summary Report

Surface Area

Single point surface area at p/p° = 0,257211883:	14,1558 m²/g
BET Surface Area:	14,1385 m²/g
t-Plot Micropore Area:	4,4579 m²/g
t-Plot External Surface Area:	9,6806 m²/g
BJH Adsorption cumulative surface area of pores between 17,000 Å and 3 000,000 Å width:	9.421 m²/g
BJH Desorption cumulative surface area of pores between 17,000 Å and 3 000,000 Å width:	12,9569 m²/g

Pore Volume

t-Plot micropore volume:	0,002223 cm³/g
BJH Adsorption cumulative volume of pores between 17,000 Å and 3 000,000 Å width:	0,029996 cm³/g
BJH Desorption cumulative volume of pores between 17,000 Å and 3 000,000 Å width:	0,033471 cm³/g

Pore Size

BJH Adsorption average pore width (4V/A):	127,354 Å
BJH Desorption average pore width (4V/A):	103,330 Å

DFT Pore Size

Volume in Pores	<	9,51 Å	:	0,00394 cm³/g
Total Volume in Pores	<=	448,83 Å	:	0,02685 cm³/g
Total Area in Pores	>=	9,51 Å	:	10,014 m²/g

Nanoparticle Size:

Average Particle Size 4 243,743 Å

Sample: NO-1
Operator: Maria Olsvik
File: C:\TriStar II 3020\data\Maria Olsvik\NO-1.SMP

Started:	08.05.2018 09:58:11	Analysis Adsorptive:	N2
Completed:	08.05.2018 16:06:32	Analysis Bath Temp.:	-195,850 °C
Report Time:	08.05.2018 21:19:09	Thermal Correction:	No
Sample Mass:	0,0733 g	Warm Free Space:	9,9746 cm³ Measured
Cold Free Space:	30,2745 cm³	Equilibration Interval:	10 s
Low Pressure Dose:	None	Sample Density:	1,000 g/cm³
Automatic Degas:	No		

Isotherm Linear Plot

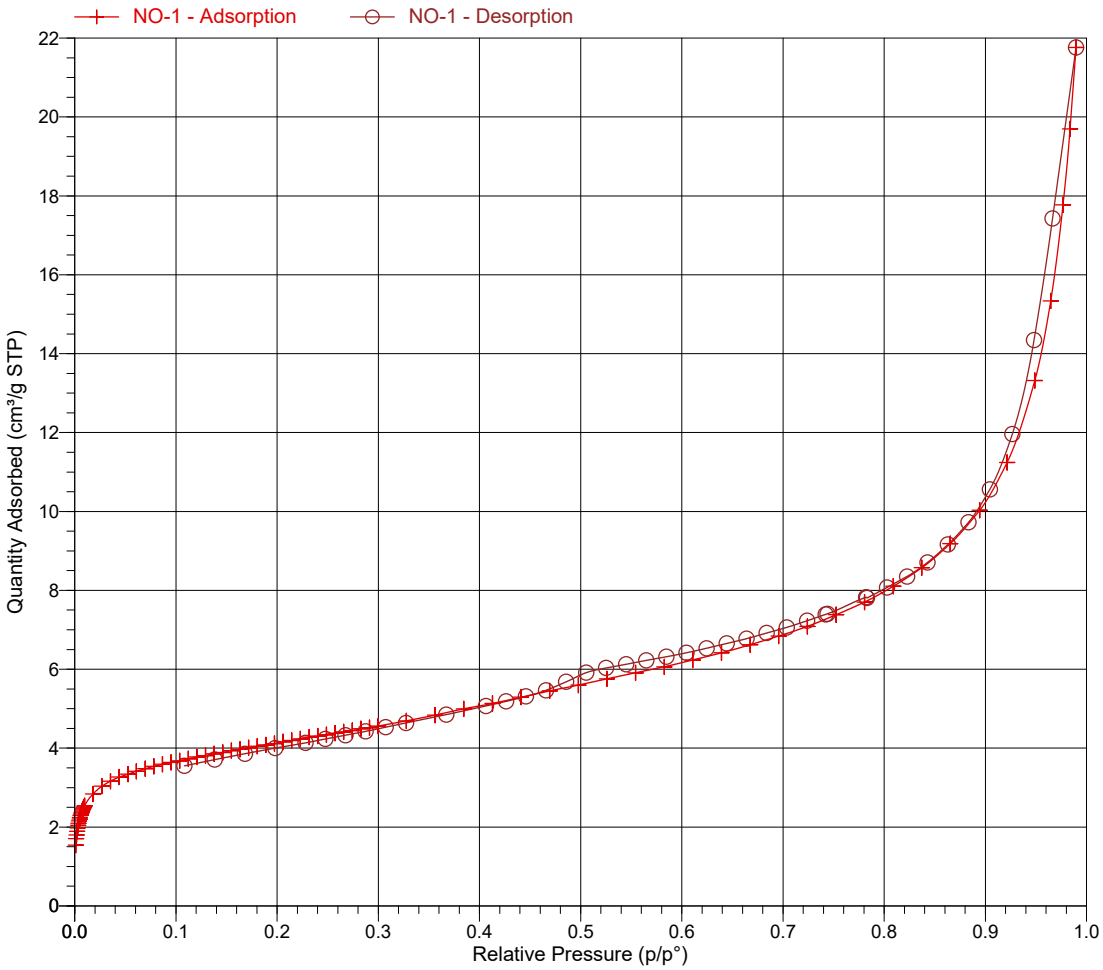

Sample: NO-1
Operator: Maria Olsvik
File: C:\TriStar II 3020\data\Maria Olsvik\NO-1.SMP

Started:	08.05.2018 09:58:11	Analysis Adsorptive:	N2
Completed:	08.05.2018 16:06:32	Analysis Bath Temp.:	-195,850 °C
Report Time:	08.05.2018 21:19:09	Thermal Correction:	No
Sample Mass:	0,0733 g	Warm Free Space:	9,9746 cm³ Measured
Cold Free Space:	30,2745 cm³	Equilibration Interval:	10 s
Low Pressure Dose:	None	Sample Density:	1,000 g/cm³
Automatic Degas:	No		

BJH Adsorption dV/dw Pore Volume

Halsey : Faas Correction

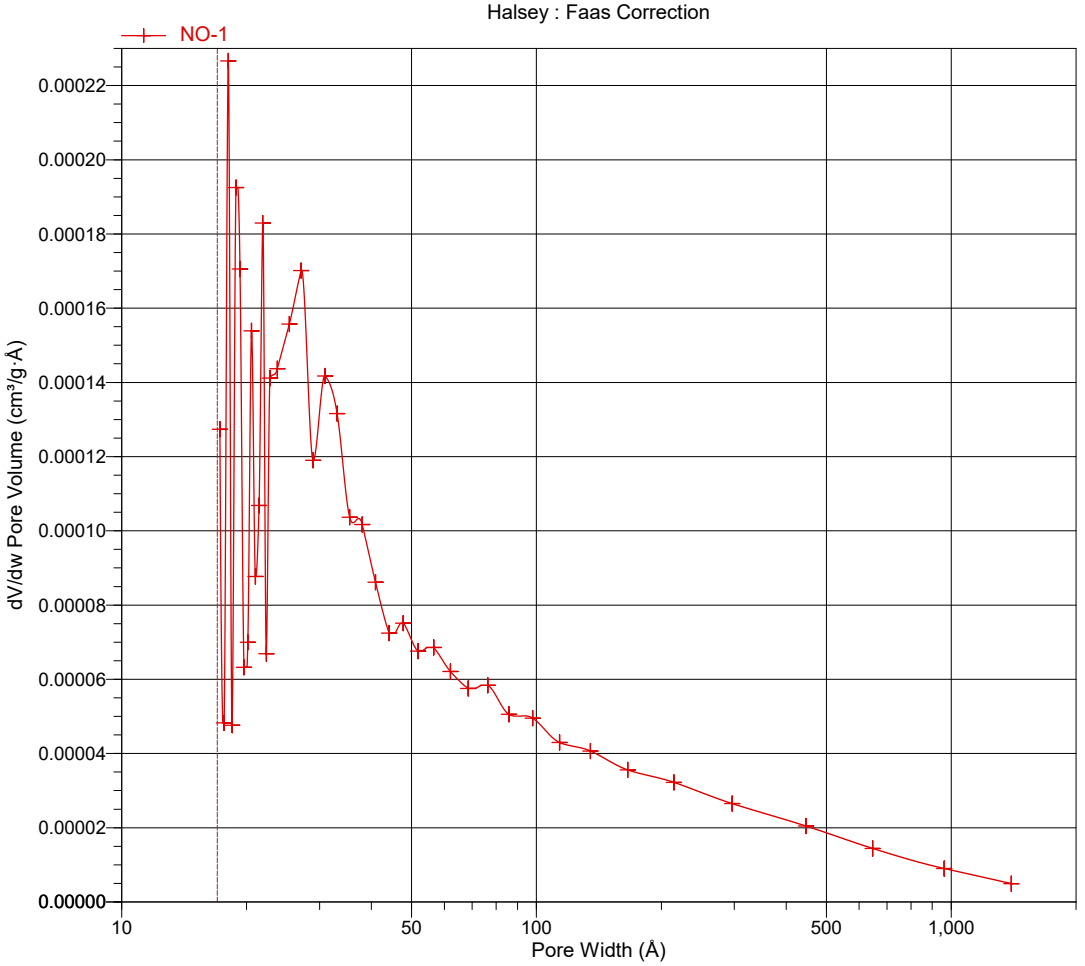

Full Report Set

Sample: NO-1
Operator: Maria Olsvik
File: C:\TriStar II 3020\data\Maria Olsvik\NO-1 test2.SMP

Started:	08.05.2018 21:24:25	Analysis Adsorptive:	N2
Completed:	09.05.2018 03:26:30	Analysis Bath Temp.:	-195,850 °C
Report Time:	23.05.2018 09:23:16	Thermal Correction:	No
Sample Mass:	0,0733 g	Warm Free Space:	9,9498 cm³ Measured
Cold Free Space:	30,2593 cm³	Equilibration Interval:	10 s
Low Pressure Dose:	None	Sample Density:	1,000 g/cm³
Automatic Degas:	No		

Summary Report

Surface Area

Single point surface area at p/p° = 0,257167042:	13,1032 m²/g
BET Surface Area:	12,9899 m²/g
t-Plot Micropore Area:	4,9018 m²/g
t-Plot External Surface Area:	8,0881 m²/g
BJH Adsorption cumulative surface area of pores between 1,7000 nm and 300,0000 nm diameter:	8.561 m²/g
BJH Desorption cumulative surface area of pores between 1,7000 nm and 300,0000 nm diameter:	13,0428 m²/g

Pore Volume

t-Plot micropore volume:	0,002461 cm³/g
BJH Adsorption cumulative volume of pores between 1,7000 nm and 300,0000 nm diameter:	0,035233 cm³/g
BJH Desorption cumulative volume of pores between 1,7000 nm and 300,0000 nm diameter:	0,039373 cm³/g

Pore Size

BJH Adsorption average pore diameter (4V/A):	16,4627 nm
BJH Desorption average pore diameter (4V/A):	12,0751 nm

DFT Pore Size

Volume in Pores	<	0,951 nm	:	0,00252 cm³/g
Total Volume in Pores	<=	44,883 nm	:	0,02893 cm³/g
Total Area in Pores	>=	0,951 nm	:	13,735 m²/g

Nanoparticle Size:

Average Particle Size	461,8977 nm

Sample: NO-1
Operator: Maria Olsvik
File: C:\TriStar II 3020\data\Maria Olsvik\NO-1 test2.SMP

Started:	08.05.2018 21:24:25	Analysis Adsorptive:	N2
Completed:	09.05.2018 03:26:30	Analysis Bath Temp.:	-195,850 °C
Report Time:	23.05.2018 09:23:16	Thermal Correction:	No
Sample Mass:	0,0733 g	Warm Free Space:	9,9498 cm³ Measured
Cold Free Space:	30,2593 cm³	Equilibration Interval:	10 s
Low Pressure Dose:	None	Sample Density:	1,000 g/cm³
Automatic Degas:	No		

Isotherm Linear Plot

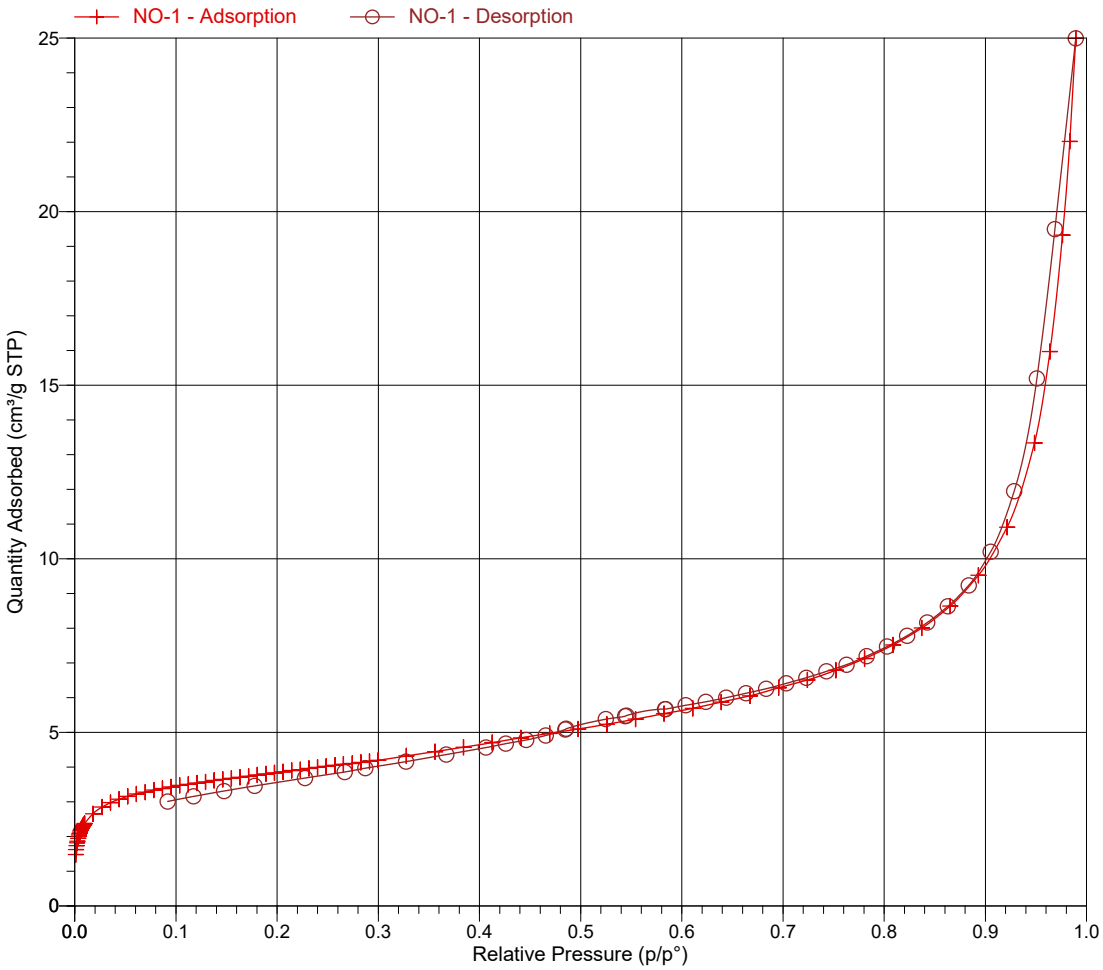

Sample: NO-1
Operator: Maria Olsvik
File: C:\TriStar II 3020\data\Maria Olsvik\NO-1 test2.SMP

Started:	08.05.2018 21:24:25	Analysis Adsorptive:	N2
Completed:	09.05.2018 03:26:30	Analysis Bath Temp.:	-195,850 °C
Report Time:	23.05.2018 09:23:16	Thermal Correction:	No
Sample Mass:	0,0733 g	Warm Free Space:	9,9498 cm³ Measured
Cold Free Space:	30,2593 cm³	Equilibration Interval:	10 s
Low Pressure Dose:	None	Sample Density:	1,000 g/cm³
Automatic Degas:	No		

BJH Adsorption dV/dD Pore Volume

Halsey : Faas Correction

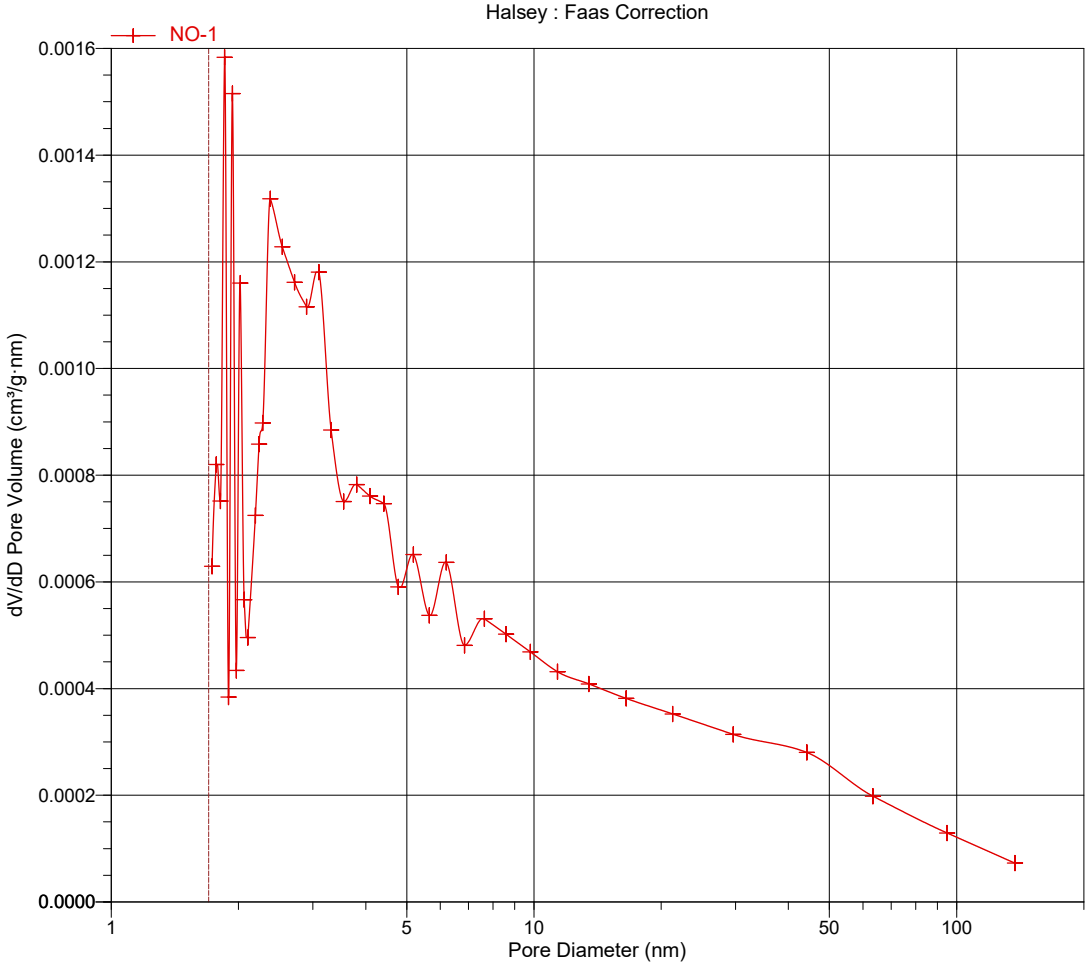

Full Report Set

Sample: NO-1 test3
Operator: Maria Olsvik
File: C:\TriStar II 3020\data\Maria Olsvik\NO-1 test3.SMP

Started:	04.06.2018 12:00:13	Analysis Adsorptive:	N2
Completed:	04.06.2018 18:36:30	Analysis Bath Temp.:	-195,850 °C
Report Time:	04.06.2018 20:13:08	Thermal Correction:	No
Sample Mass:	0,0911 g	Warm Free Space:	10,1607 cm³ Measured
Cold Free Space:	30,4992 cm³	Equilibration Interval:	10 s
Low Pressure Dose:	None	Sample Density:	1,000 g/cm³
Automatic Degas:	No		

Summary Report

Surface Area

Single point surface area at p/p° = 0,257409602:	13,9115 m²/g
BET Surface Area:	14,0471 m²/g
t-Plot Micropore Area:	2,1299 m²/g
t-Plot External Surface Area:	11,9172 m²/g
BJH Adsorption cumulative surface area of pores between 17,000 Å and 3 000,000 Å width:	10.633 m²/g
BJH Desorption cumulative surface area of pores between 17,000 Å and 3 000,000 Å width:	14,0400 m²/g

Pore Volume

t-Plot micropore volume:	0,001063 cm³/g
BJH Adsorption cumulative volume of pores between 17,000 Å and 3 000,000 Å width:	0,025793 cm³/g
BJH Desorption cumulative volume of pores between 17,000 Å and 3 000,000 Å width:	0,030014 cm³/g

Pore Size

BJH Adsorption average pore width (4V/A):	97,031 Å
BJH Desorption average pore width (4V/A):	85,510 Å

DFT Pore Size

Volume in Pores	<	10,22 Å	:	0,00349 cm³/g
Total Volume in Pores	<=	448,83 Å	:	0,02470 cm³/g
Total Area in Pores	>=	10,22 Å	:	11,308 m²/g

Nanoparticle Size:

Average Particle Size 4 271,357 Å

Sample: NO-1 test3
Operator: Maria Olsvik
File: C:\TriStar II 3020\data\Maria Olsvik\NO-1 test3.SMP

Started:	04.06.2018 12:00:13	Analysis Adsorptive:	N2
Completed:	04.06.2018 18:36:30	Analysis Bath Temp.:	-195,850 °C
Report Time:	04.06.2018 20:13:09	Thermal Correction:	No
Sample Mass:	0,0911 g	Warm Free Space:	10,1607 cm³ Measured
Cold Free Space:	30,4992 cm³	Equilibration Interval:	10 s
Low Pressure Dose:	None	Sample Density:	1,000 g/cm³
Automatic Degas:	No		

Isotherm Linear Plot

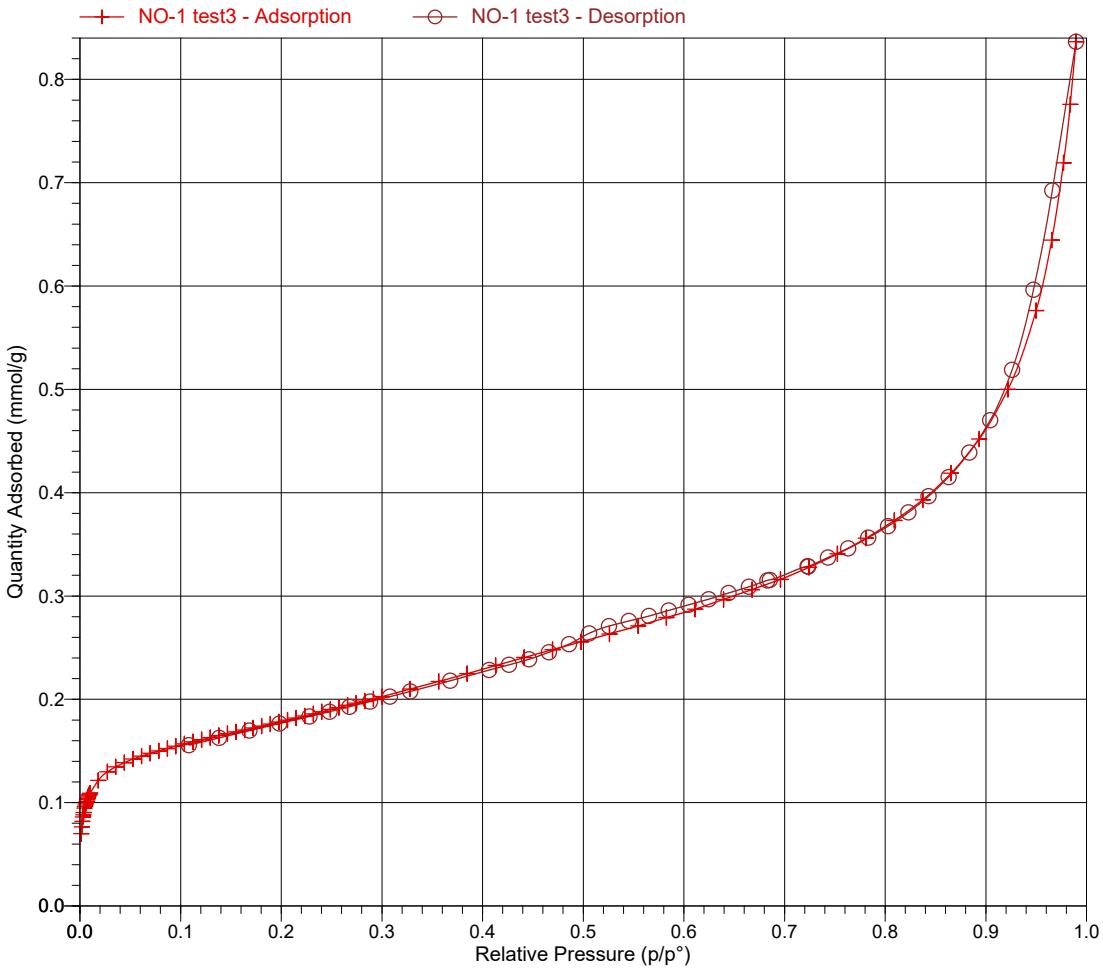

Sample: NO-1 test3
Operator: Maria Olsvik
File: C:\TriStar II 3020\data\Maria Olsvik\NO-1 test3.SMP

Started:	04.06.2018 12:00:13	Analysis Adsorptive:	N2
Completed:	04.06.2018 18:36:30	Analysis Bath Temp.:	-195,850 °C
Report Time:	04.06.2018 20:13:09	Thermal Correction:	No
Sample Mass:	0,0911 g	Warm Free Space:	10,1607 cm³ Measured
Cold Free Space:	30,4992 cm³	Equilibration Interval:	10 s
Low Pressure Dose:	None	Sample Density:	1,000 g/cm³
Automatic Degas:	No		

BJH Adsorption dV/dw Pore Volume

Halsey : Faas Correction

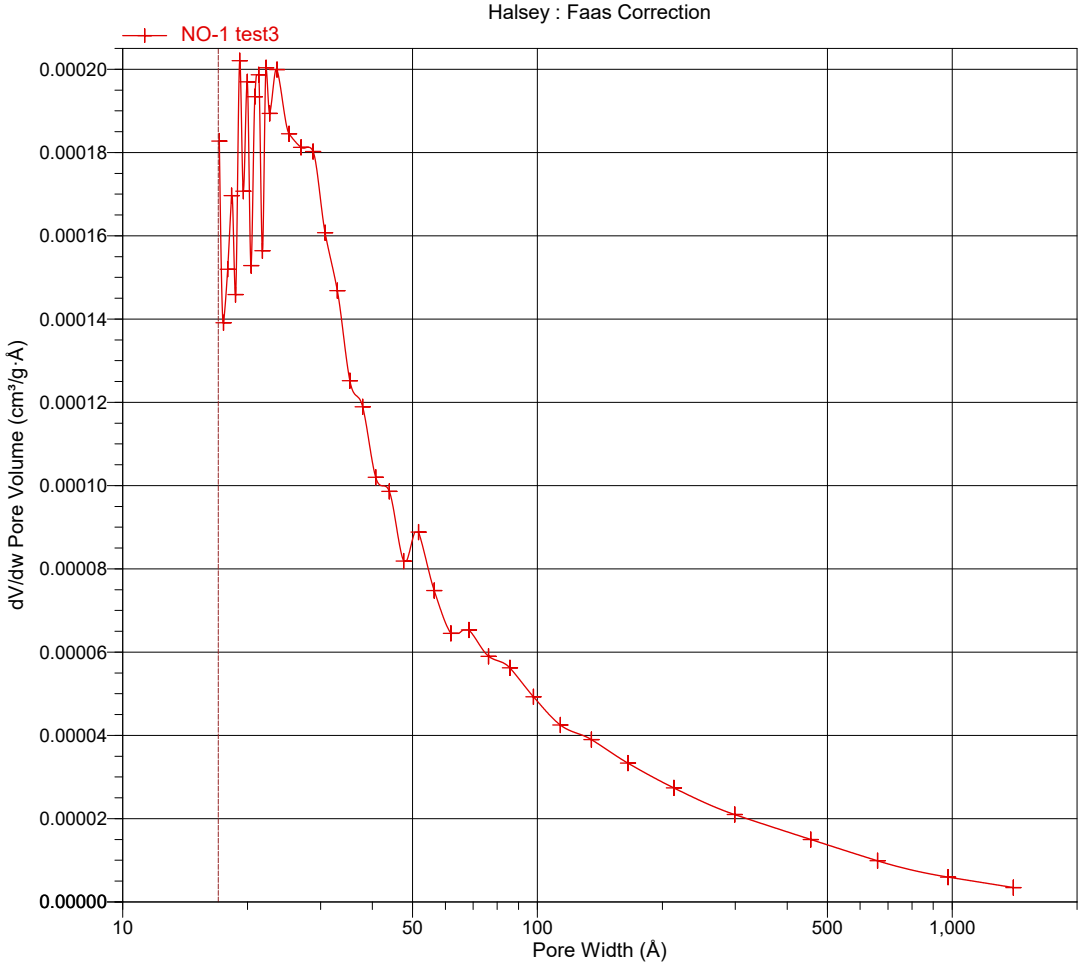

Full Report Set

Sample: NO-3
Operator: Maria Olsvik
File: C:\TriStar II 3020\data\Maria Olsvik\NO-3.SMP

Started:	27.03.2018 19:44:43	Analysis Adsorptive:	N2
Completed:	28.03.2018 01:50:55	Analysis Bath Temp.:	-195,850 °C
Report Time:	28.03.2018 08:28:32	Thermal Correction:	No
Sample Mass:	0,0846 g	Warm Free Space:	10,4897 cm³ Measured
Cold Free Space:	31,9619 cm³	Equilibration Interval:	10 s
Low Pressure Dose:	None	Sample Density:	1,000 g/cm³
Automatic Degas:	No		

Summary Report

Surface Area

Single point surface area at p/p° = 0,257999182:	7,8657 m²/g
BET Surface Area:	8,0035 m²/g
t-Plot Micropore Area:	0,9794 m²/g
t-Plot External Surface Area:	7,0241 m²/g
BJH Adsorption cumulative surface area of pores between 17,000 Å and 3 000,000 Å width:	6.384 m²/g
BJH Desorption cumulative surface area of pores between 17,000 Å and 3 000,000 Å width:	8,3318 m²/g

Pore Volume

t-Plot micropore volume:	0,000468 cm³/g
BJH Adsorption cumulative volume of pores between 17,000 Å and 3 000,000 Å width:	0,013670 cm³/g
BJH Desorption cumulative volume of pores between 17,000 Å and 3 000,000 Å width:	0,015529 cm³/g

Pore Size

BJH Adsorption average pore width (4V/A):	85,644 Å
BJH Desorption average pore width (4V/A):	74,554 Å

DFT Pore Size

Volume in Pores	<	9,51 Å	:	0,00189 cm³/g
Total Volume in Pores	<=	448,83 Å	:	0,01349 cm³/g
Total Area in Pores	>=	9,51 Å	:	6,620 m²/g

Nanoparticle Size:

Average Particle Size 7 496,722 Å

Sample: NO-3
Operator: Maria Olsvik
File: C:\TriStar II 3020\data\Maria Olsvik\NO-3.SMP

Started:	27.03.2018 19:44:43	Analysis Adsorptive:	N2
Completed:	28.03.2018 01:50:55	Analysis Bath Temp.:	-195,850 °C
Report Time:	28.03.2018 08:28:32	Thermal Correction:	No
Sample Mass:	0,0846 g	Warm Free Space:	10,4897 cm³ Measured
Cold Free Space:	31,9619 cm³	Equilibration Interval:	10 s
Low Pressure Dose:	None	Sample Density:	1,000 g/cm³
Automatic Degas:	No		

Isotherm Linear Plot

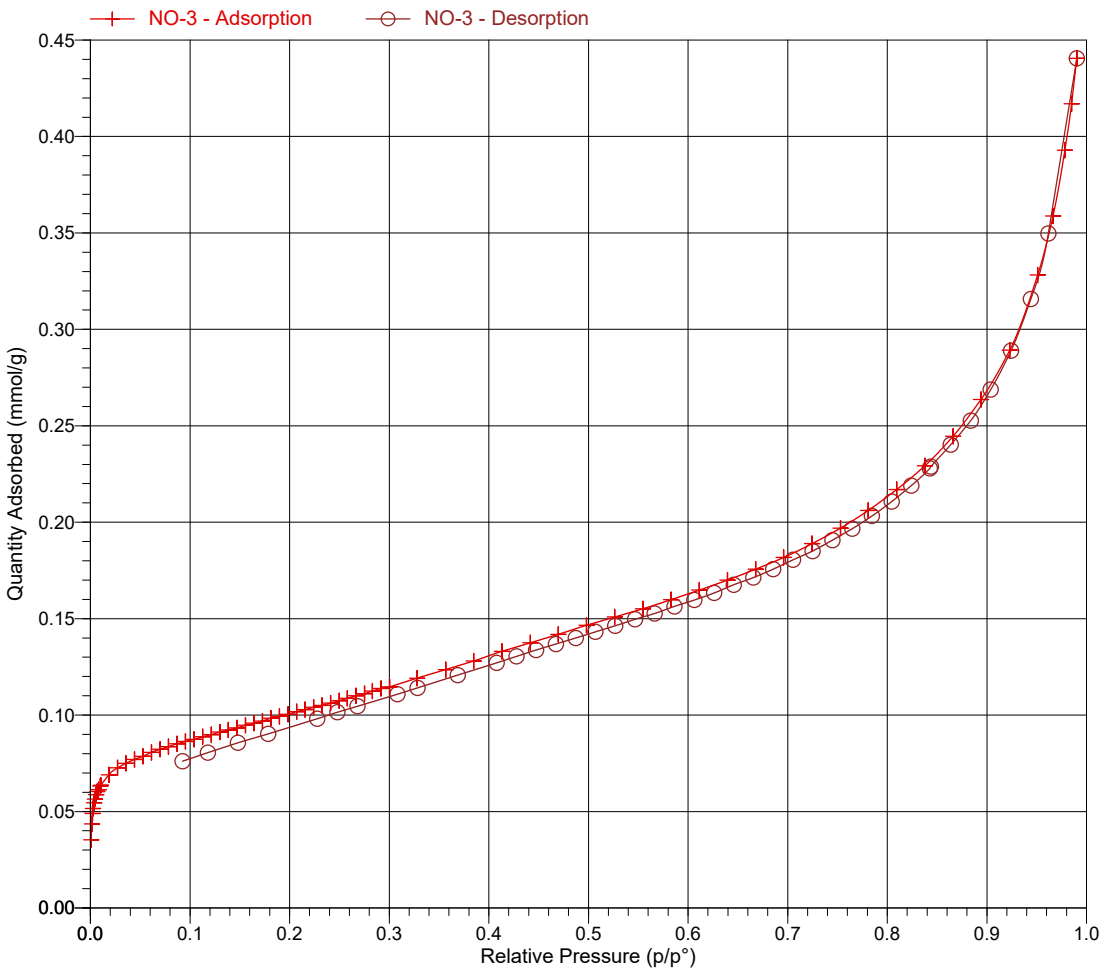

Sample: NO-3
Operator: Maria Olsvik
File: C:\TriStar II 3020\data\Maria Olsvik\NO-3.SMP

Started:	27.03.2018 19:44:43	Analysis Adsorptive:	N2
Completed:	28.03.2018 01:50:55	Analysis Bath Temp.:	-195,850 °C
Report Time:	28.03.2018 08:28:32	Thermal Correction:	No
Sample Mass:	0,0846 g	Warm Free Space:	10,4897 cm³ Measured
Cold Free Space:	31,9619 cm³	Equilibration Interval:	10 s
Low Pressure Dose:	None	Sample Density:	1,000 g/cm³
Automatic Degas:	No		

BJH Adsorption dV/dw Pore Volume

Halsey : Faas Correction

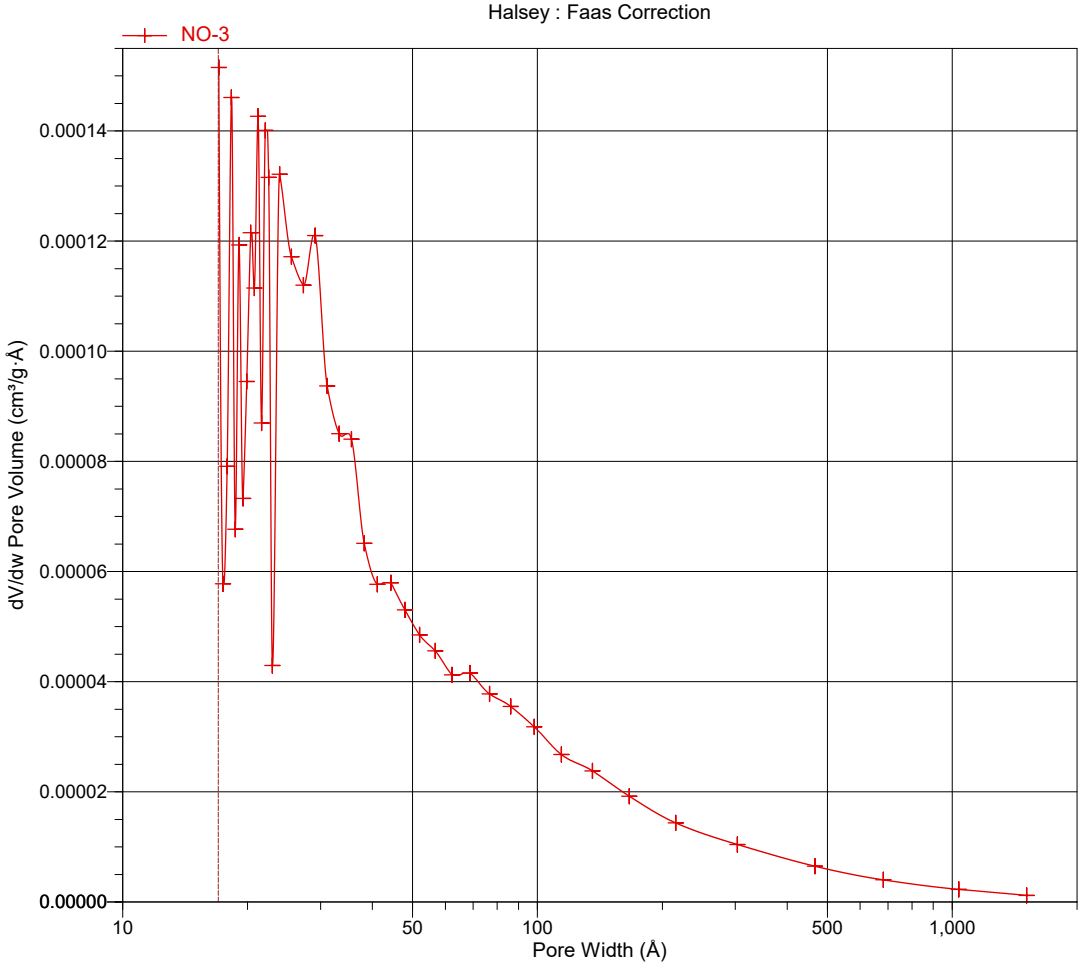

Full Report Set

Sample: NO-3 test2
Operator: Maria Olsvik
File: C:\TriStar II 3020\data\Maria Olsvik\NO-3 test2.SMP

Started:	19.04.2018 11:16:53	Analysis Adsorptive:	N2
Completed:	19.04.2018 17:10:06	Analysis Bath Temp.:	-195,850 °C
Report Time:	20.04.2018 09:00:10	Thermal Correction:	No
Sample Mass:	0,0816 g	Warm Free Space:	9,6034 cm³ Measured
Cold Free Space:	28,9941 cm³	Equilibration Interval:	10 s
Low Pressure Dose:	None	Sample Density:	1,000 g/cm³
Automatic Degas:	No		

Summary Report

Surface Area

Single point surface area at p/p° = 0,257914857:	7,9287 m²/g
BET Surface Area:	7,7902 m²/g
t-Plot Micropore Area:	3,4070 m²/g
t-Plot External Surface Area:	4,3832 m²/g
BJH Adsorption cumulative surface area of pores between 17,000 Å and 3 000,000 Å width:	4.647 m²/g
BJH Desorption cumulative surface area of pores between 17,000 Å and 3 000,000 Å width:	6,9648 m²/g

Pore Volume

t-Plot micropore volume:	0,001749 cm³/g
BJH Adsorption cumulative volume of pores between 17,000 Å and 3 000,000 Å width:	0,012848 cm³/g
BJH Desorption cumulative volume of pores between 17,000 Å and 3 000,000 Å width:	0,014875 cm³/g

Pore Size

BJH Adsorption average pore width (4V/A):	110,583 Å
BJH Desorption average pore width (4V/A):	85,428 Å

DFT Pore Size

Volume in Pores	<	10,22 Å	:	0,00282 cm³/g
Total Volume in Pores	<=	448,83 Å	:	0,01256 cm³/g
Total Area in Pores	>=	10,22 Å	:	3,720 m²/g

Nanoparticle Size:

Average Particle Size 7 701,996 Å

Sample: NO-3 test2
Operator: Maria Olsvik
File: C:\TriStar II 3020\data\Maria Olsvik\NO-3 test2.SMP

Started:	19.04.2018 11:16:53	Analysis Adsorptive:	N2
Completed:	19.04.2018 17:10:06	Analysis Bath Temp.:	-195,850 °C
Report Time:	20.04.2018 09:00:10	Thermal Correction:	No
Sample Mass:	0,0816 g	Warm Free Space:	9,6034 cm³ Measured
Cold Free Space:	28,9941 cm³	Equilibration Interval:	10 s
Low Pressure Dose:	None	Sample Density:	1,000 g/cm³
Automatic Degas:	No		

Isotherm Linear Plot

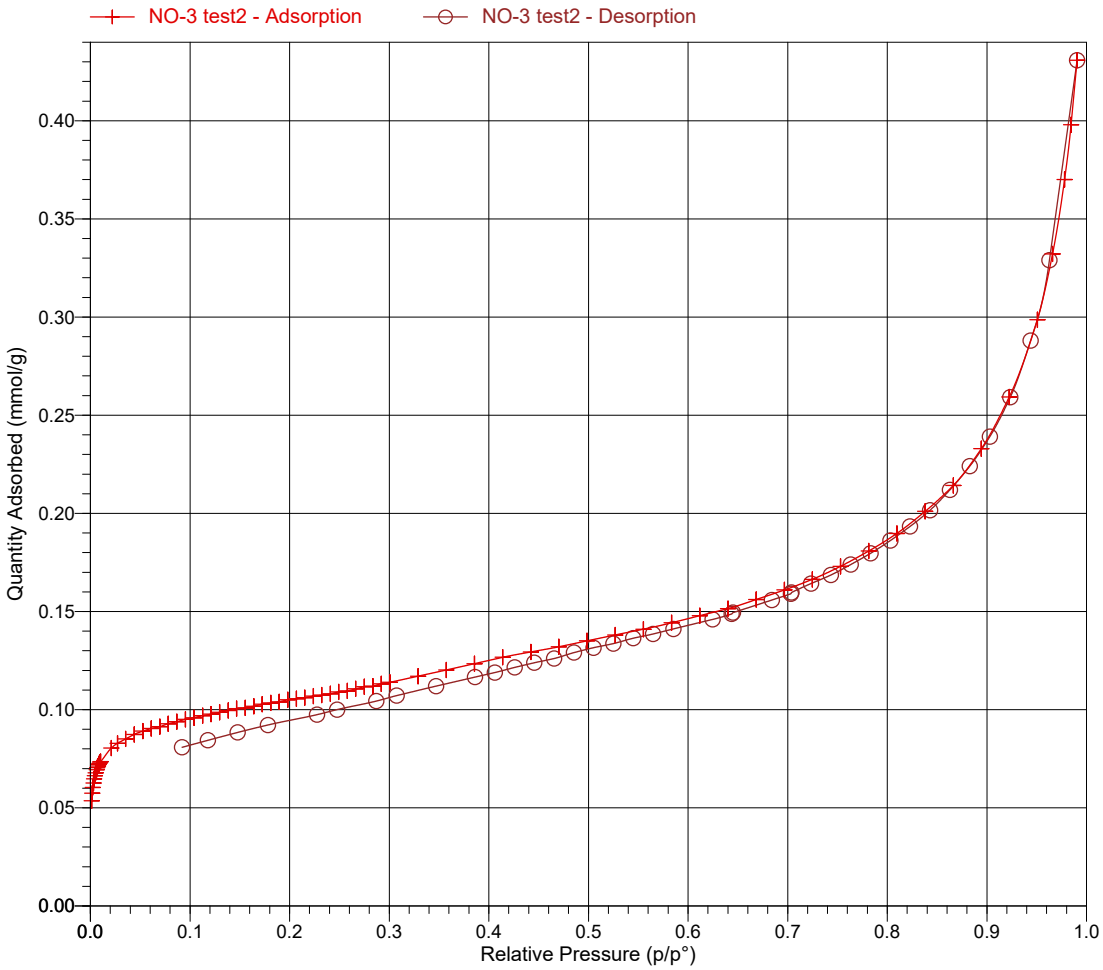

Sample: NO-3 test2
Operator: Maria Olsvik
File: C:\TriStar II 3020\data\Maria Olsvik\NO-3 test2.SMP

Started:	19.04.2018 11:16:53	Analysis Adsorptive:	N2
Completed:	19.04.2018 17:10:06	Analysis Bath Temp.:	-195,850 °C
Report Time:	20.04.2018 09:00:10	Thermal Correction:	No
Sample Mass:	0,0816 g	Warm Free Space:	9,6034 cm³ Measured
Cold Free Space:	28,9941 cm³	Equilibration Interval:	10 s
Low Pressure Dose:	None	Sample Density:	1,000 g/cm³
Automatic Degas:	No		

BJH Adsorption dV/dw Pore Volume

Halsey : Faas Correction

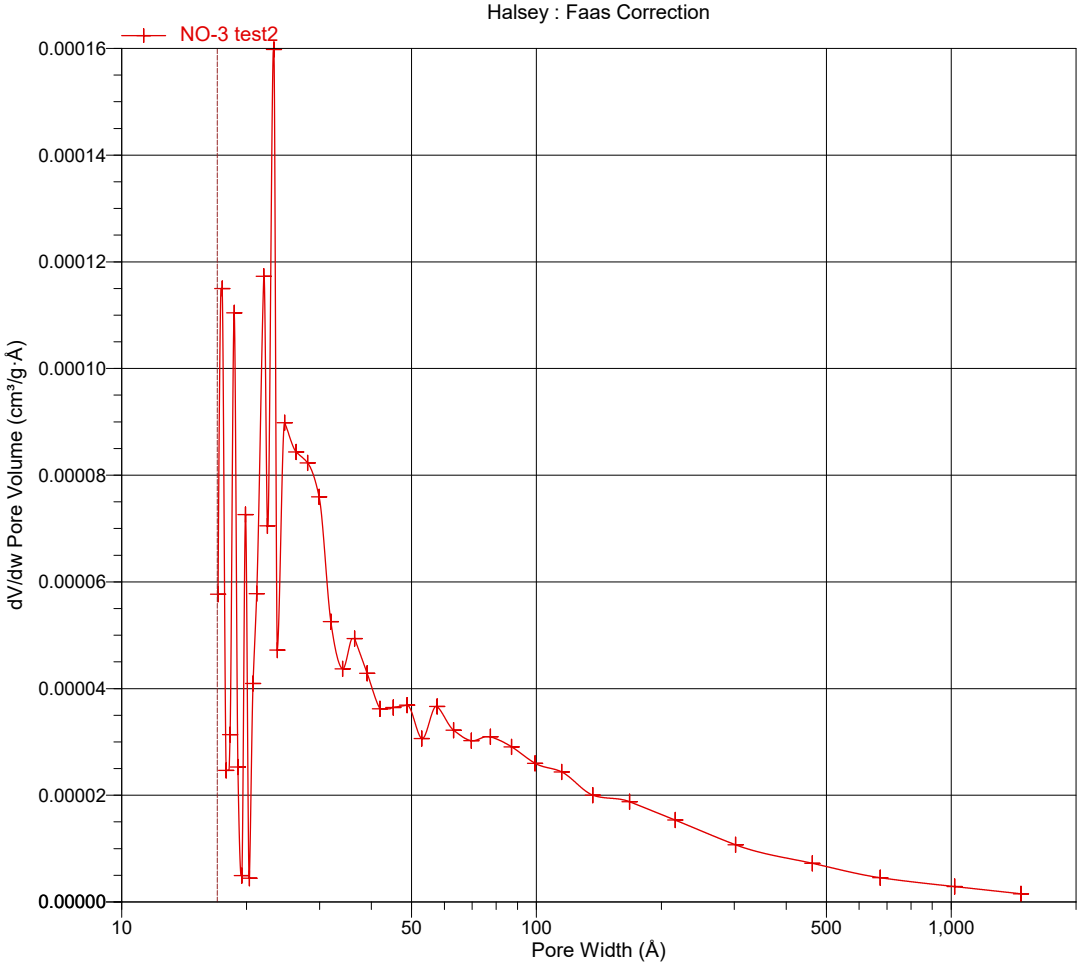

Full Report Set

Sample: NO-3 test4
Operator: Maria Olsvik
File: C:\TriStar II 3020\data\Maria Olsvik\NO-3 test4.SMP

Started:	04.06.2018 12:00:13	Analysis Adsorptive:	N2
Completed:	04.06.2018 18:36:30	Analysis Bath Temp.:	-195,850 °C
Report Time:	04.06.2018 20:13:50	Thermal Correction:	No
Sample Mass:	0,0802 g	Warm Free Space:	10,1222 cm³ Measured
Cold Free Space:	30,3504 cm³	Equilibration Interval:	10 s
Low Pressure Dose:	None	Sample Density:	1,000 g/cm³
Automatic Degas:	No		

Summary Report

Surface Area

Single point surface area at p/p° = 0,257844871:	9,6231 m²/g
BET Surface Area:	9,5385 m²/g
t-Plot Micropore Area:	3,1418 m²/g
t-Plot External Surface Area:	6,3967 m²/g
BJH Adsorption cumulative surface area of pores between 17,000 Å and 3 000,000 Å width:	5.437 m²/g
BJH Desorption cumulative surface area of pores between 17,000 Å and 3 000,000 Å width:	7,2526 m²/g

Pore Volume

t-Plot micropore volume:	0,001605 cm³/g
BJH Adsorption cumulative volume of pores between 17,000 Å and 3 000,000 Å width:	0,011307 cm³/g
BJH Desorption cumulative volume of pores between 17,000 Å and 3 000,000 Å width:	0,013178 cm³/g

Pore Size

BJH Adsorption average pore width (4V/A):	83,187 Å
BJH Desorption average pore width (4V/A):	72,682 Å

DFT Pore Size

Volume in Pores	<	10,22 Å	:	0,00277 cm³/g
Total Volume in Pores	<=	448,83 Å	:	0,01250 cm³/g
Total Area in Pores	>=	10,22 Å	:	5,842 m²/g

Nanoparticle Size:

Average Particle Size 6 290,292 Å

Sample: NO-3 test4
Operator: Maria Olsvik
File: C:\TriStar II 3020\data\Maria Olsvik\NO-3 test4.SMP

Started:	04.06.2018 12:00:13	Analysis Adsorptive:	N2
Completed:	04.06.2018 18:36:30	Analysis Bath Temp.:	-195,850 °C
Report Time:	04.06.2018 20:13:50	Thermal Correction:	No
Sample Mass:	0,0802 g	Warm Free Space:	10,1222 cm³ Measured
Cold Free Space:	30,3504 cm³	Equilibration Interval:	10 s
Low Pressure Dose:	None	Sample Density:	1,000 g/cm³
Automatic Degas:	No		

Isotherm Linear Plot

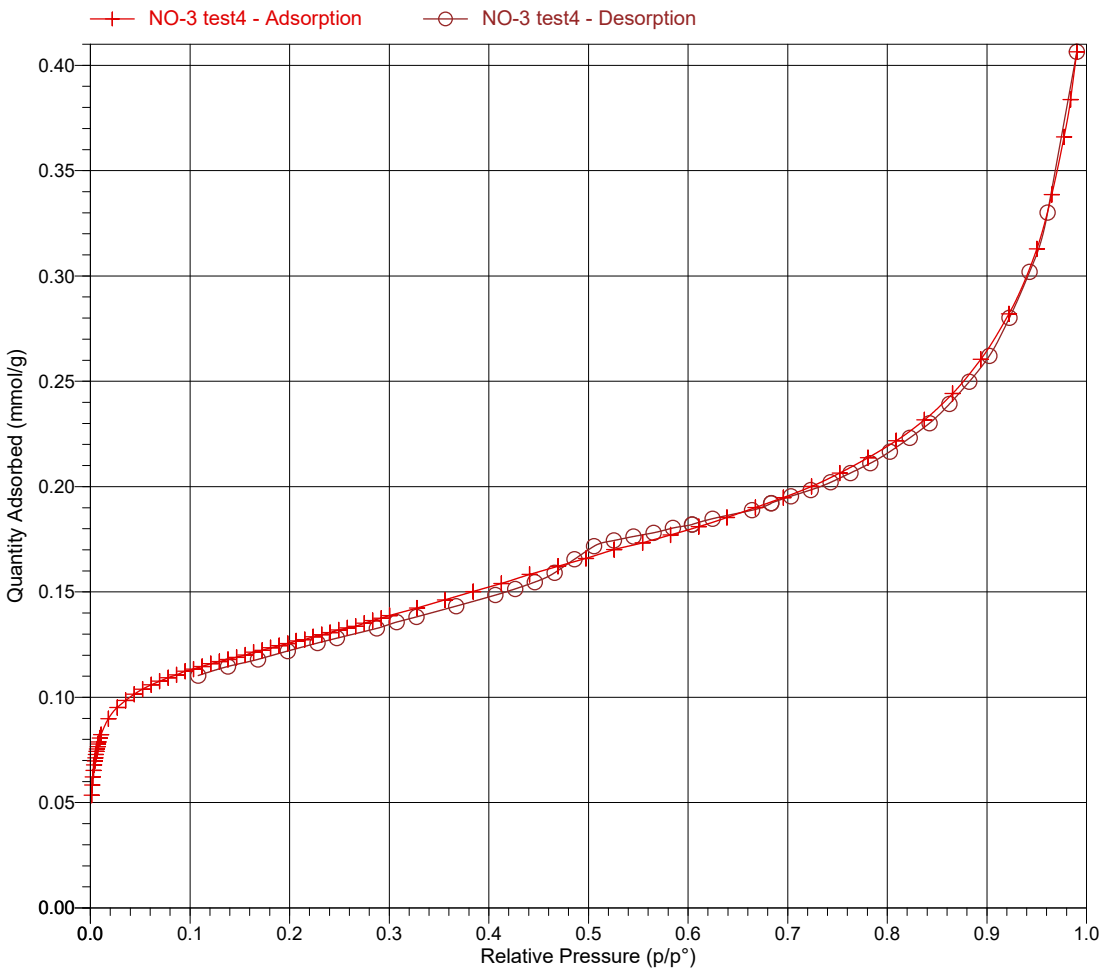

Sample: NO-3 test4
Operator: Maria Olsvik
File: C:\TriStar II 3020\data\Maria Olsvik\NO-3 test4.SMP

Started:	04.06.2018 12:00:13	Analysis Adsorptive:	N2
Completed:	04.06.2018 18:36:30	Analysis Bath Temp.:	-195,850 °C
Report Time:	04.06.2018 20:13:50	Thermal Correction:	No
Sample Mass:	0,0802 g	Warm Free Space:	10,1222 cm³ Measured
Cold Free Space:	30,3504 cm³	Equilibration Interval:	10 s
Low Pressure Dose:	None	Sample Density:	1,000 g/cm³
Automatic Degas:	No		

BJH Adsorption dV/dw Pore Volume

Halsey : Faas Correction

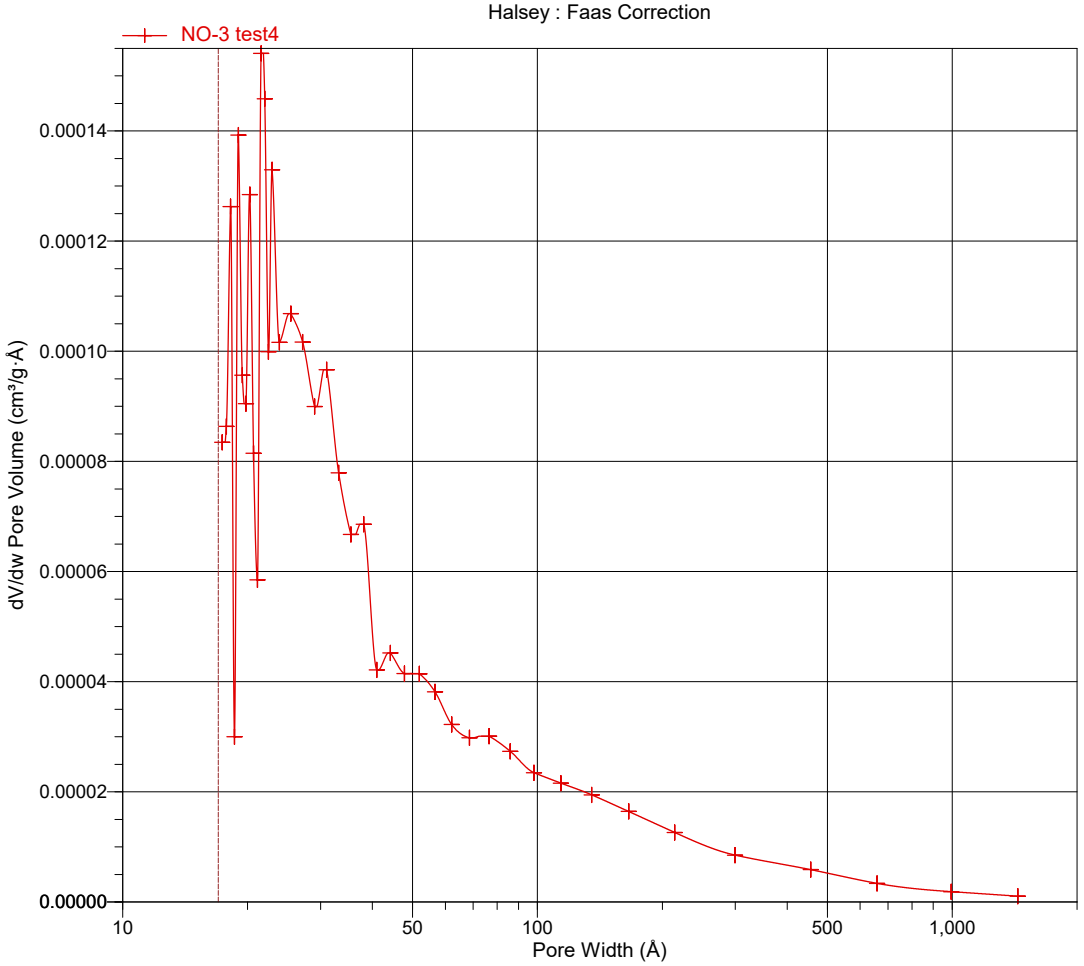

Sample: NO6
Operator: Maria Olsvik
Submitter:
File: C:\...\MARIAO~1\000-323.SMP

Started:	07.03.2018 14:17:21	Analysis Adsorptive:	N2
Completed:	07.03.2018 16:12:38	Analysis Bath Temp.:	-195.850 °C
Report Time:	08.03.2018 7:27:04	Sample Mass:	0.0792 g
Warm Free Space:	10.0247 cm^3 Measured	Cold Free Space:	30.3183 cm^3 Measured
Equilibration Interval:	5 s	Low Pressure Dose:	None
Sample Density:	1.000 g/cm^3	Automatic Degas:	No

Summary Report

Surface Area

Single point surface area at P/Po = 0.138279068: 2.6244 m^2/g

BJH Desorption cumulative surface area of pores between 1.7000 nm and 300.0000 nm diameter: 0.6936 m^2/g

Pore Volume

Single point adsorption total pore volume of pores less than 129.6136 nm diameter at P/Po = 0.984836858: 0.005298 cm^3/g

BJH Desorption cumulative volume of pores between 1.7000 nm and 300.0000 nm diameter: 0.005977 cm^3/g

Pore Size

Adsorption average pore width (4V/A by BET): 8.81458 nm

BJH Desorption average pore diameter (4V/A): 34.4694 nm

Sample: NO6
Operator: Maria Olsvik
Submitter:
File: C:\...\MARIAO~1\000-323.SMP

Started:	07.03.2018 14:17:21	Analysis Adsorptive:	N2
Completed:	07.03.2018 16:12:38	Analysis Bath Temp.:	-195.850 °C
Report Time:	08.03.2018 7:27:04	Sample Mass:	0.0792 g
Warm Free Space:	10.0247 cm³ Measured	Cold Free Space:	30.3183 cm³ Measured
Equilibration Interval:	5 s	Low Pressure Dose:	None
Sample Density:	1.000 g/cm³	Automatic Degas:	No

Isotherm Linear Plot

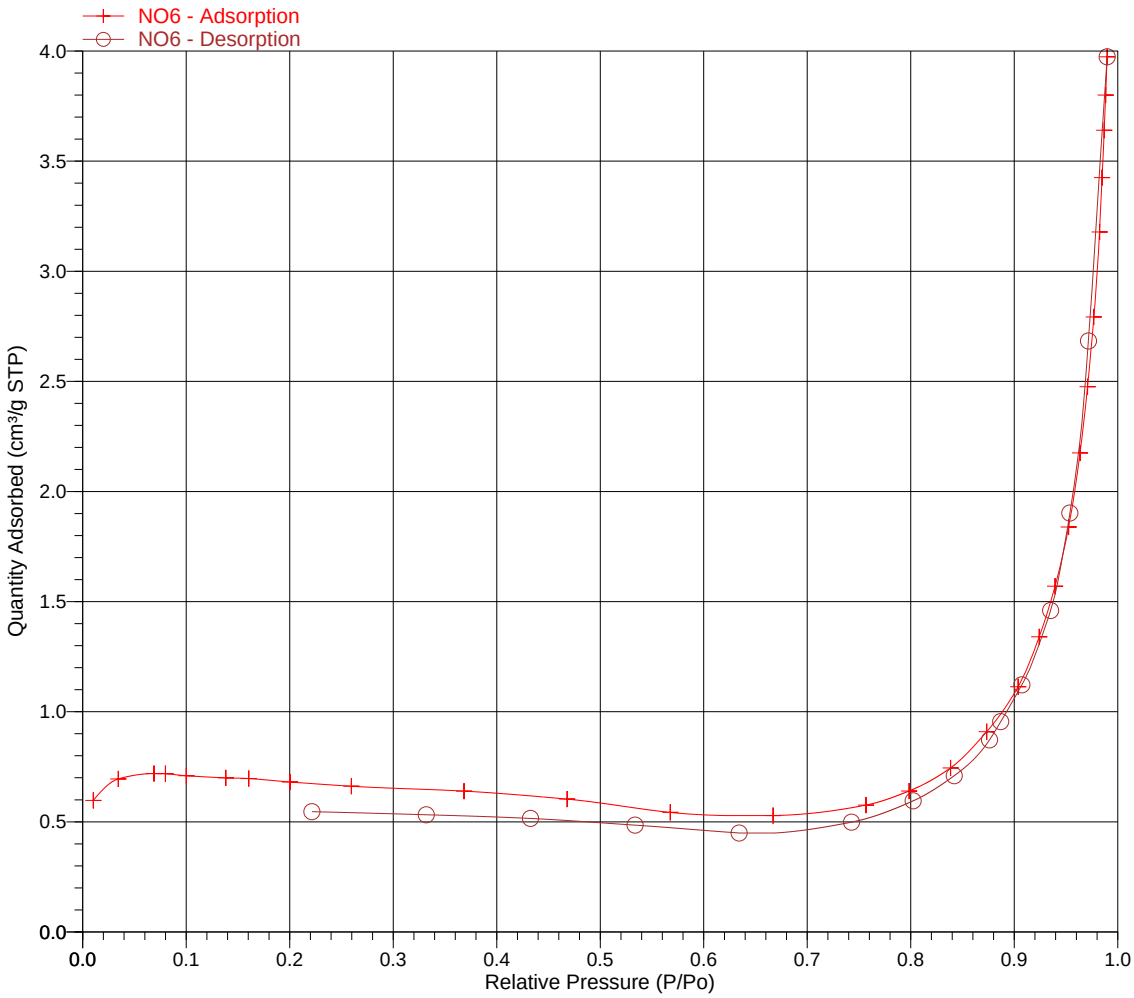

Sample: NO6
Operator: Maria Olsvik
Submitter:
File: C:\...\MARIAO~1\000-323.SMP

Started:	07.03.2018 14:17:21	Analysis Adsorptive:	N2
Completed:	07.03.2018 16:12:38	Analysis Bath Temp.:	-195.850 °C
Report Time:	08.03.2018 7:27:04	Sample Mass:	0.0792 g
Warm Free Space:	10.0247 cm³ Measured	Cold Free Space:	30.3183 cm³ Measured
Equilibration Interval:	5 s	Low Pressure Dose:	None
Sample Density:	1.000 g/cm³	Automatic Degas:	No

BJH Adsorption dV/dlog(D) Pore Volume

Halsey : Faas Correction

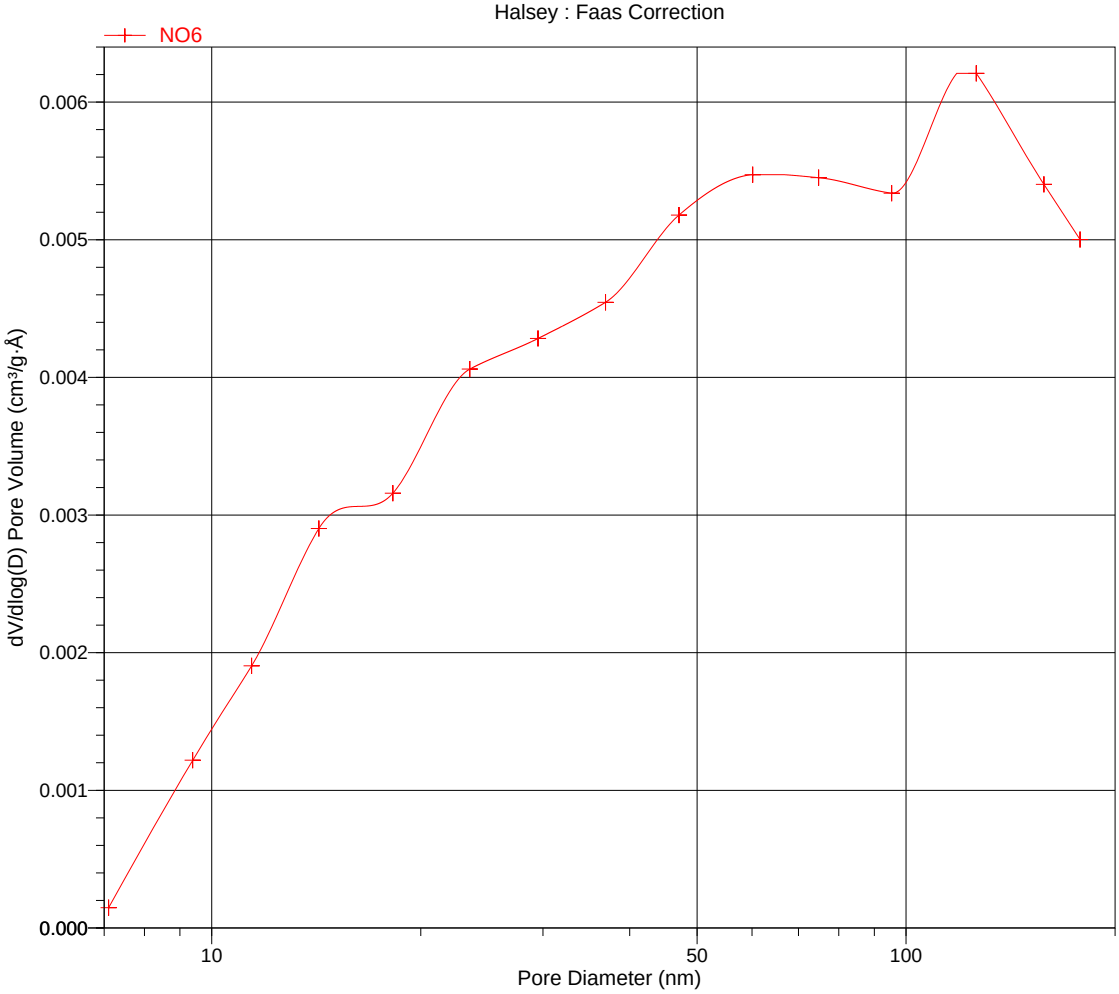

Sample: NO6
Operator: Maria Olsvik
Submitter:
File: C:\...\MARIAO~1\000-322.SMP

Started:	07.03.2018 9:38:14	Analysis Adsorptive:	N2
Completed:	07.03.2018 12:00:54	Analysis Bath Temp.:	-195.850 °C
Report Time:	07.03.2018 13:57:43	Sample Mass:	0.0803 g
Warm Free Space:	10.0306 cm^3 Measured	Cold Free Space:	30.1966 cm^3 Measured
Equilibration Interval:	5 s	Low Pressure Dose:	None
Sample Density:	1.000 g/cm^3	Automatic Degas:	No

Summary Report

Surface Area

Single point surface area at P/Po = 0.200821456: 2.8235 m^2/g

BJH Desorption cumulative surface area of pores between 1.7000 nm and 300.0000 nm diameter: 1.2834 m^2/g

Pore Volume

Single point adsorption total pore volume of pores less than 126.5527 nm diameter at P/Po = 0.984463430: 0.005736 cm^3/g

BJH Desorption cumulative volume of pores between 1.7000 nm and 300.0000 nm diameter: 0.005841 cm^3/g

Pore Size

Adsorption average pore width (4V/A by BET): 8.38675 nm

BJH Desorption average pore diameter (4V/A): 18.2058 nm

Sample: NO6
Operator: Maria Olsvik
Submitter:
File: C:\...\MARIAO~1\000-322.SMP

Started:	07.03.2018 9:38:14	Analysis Adsorptive:	N2
Completed:	07.03.2018 12:00:54	Analysis Bath Temp.:	-195.850 °C
Report Time:	07.03.2018 13:57:43	Sample Mass:	0.0803 g
Warm Free Space:	10.0306 cm³ Measured	Cold Free Space:	30.1966 cm³ Measured
Equilibration Interval:	5 s	Low Pressure Dose:	None
Sample Density:	1.000 g/cm³	Automatic Degas:	No

Isotherm Linear Plot

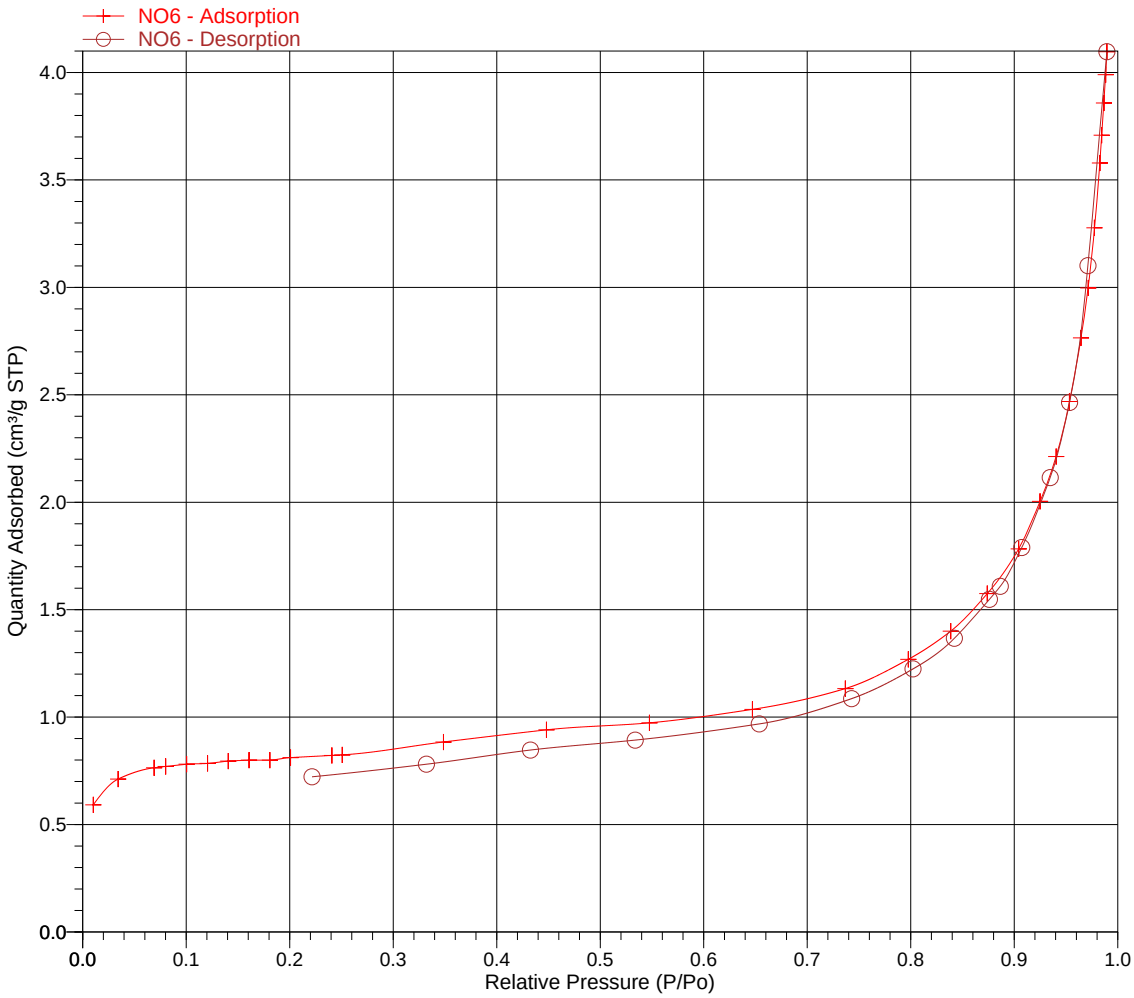

Sample: NO6
Operator: Maria Olsvik
Submitter:
File: C:\...\MARIAO~1\000-322.SMP

Started:	07.03.2018 9:38:14	Analysis Adsorptive:	N2
Completed:	07.03.2018 12:00:54	Analysis Bath Temp.:	-195.850 °C
Report Time:	07.03.2018 13:57:43	Sample Mass:	0.0803 g
Warm Free Space:	10.0306 cm³ Measured	Cold Free Space:	30.1966 cm³ Measured
Equilibration Interval:	5 s	Low Pressure Dose:	None
Sample Density:	1.000 g/cm³	Automatic Degas:	No

BJH Adsorption dV/dlog(D) Pore Volume

Halsey : Faas Correction

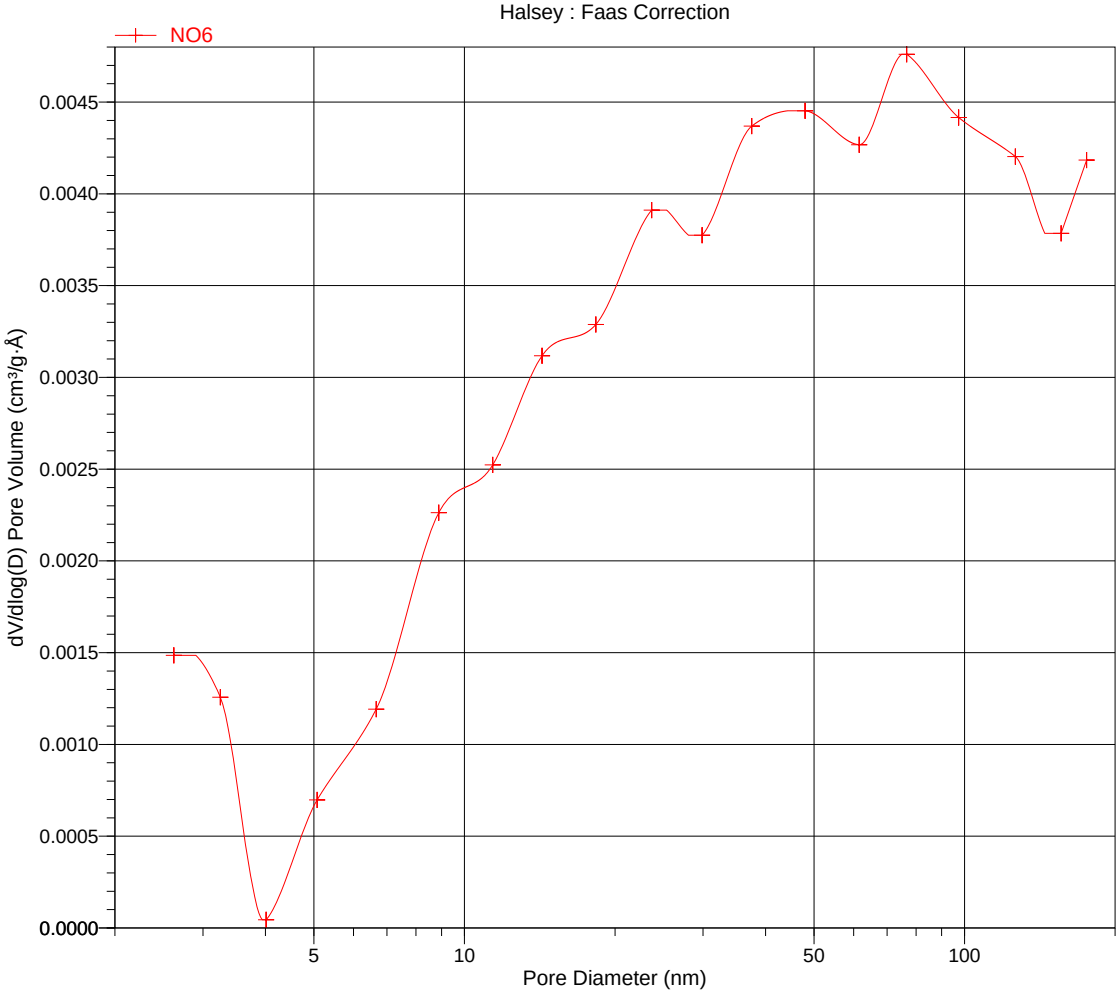

Full Report Set

Sample: NO-6
Operator: maria olsvik
Submitter: MO
File: C:\TriStar II 3020\data\Maria Olsvik\NO-6 test3.SMP

Started:	04.06.2018 20:18:55	Analysis Adsorptive:	N2
Completed:	05.06.2018 10:25:58	Analysis Bath Temp.:	-195,850 °C
Report Time:	06.06.2018 09:53:11	Thermal Correction:	No
Sample Mass:	0,0752 g	Warm Free Space:	10,6036 cm³ Measured
Cold Free Space:	32,1280 cm³	Equilibration Interval:	5 s
Low Pressure Dose:	None	Sample Density:	1,000 g/cm³
Automatic Degas:	No		

Summary Report

Surface Area

Single point surface area at p/p° = 0,200912736: 2,7444 m²/g

BJH Desorption cumulative surface area of pores between 17,000 Å and 3 000,000 Å width: 0,6401 m²/g

Pore Volume

Single point adsorption total pore volume of pores less than 1 226,495 Å width at p/p° = 0,983959817: 0,005274 cm³/g

BJH Desorption cumulative volume of pores between 17,000 Å and 3 000,000 Å width: 0,005109 cm³/g

Pore Size

Adsorption average pore diameter (4V/A by BET): 78,7718 Å

BJH Desorption average pore width (4V/A): 319,289 Å

Sample: NO-6
Operator: maria olsvik
Submitter: MO
File: C:\TriStar II 3020\data\Maria Olsvik\NO-6 test3.SMP

Started:	04.06.2018 20:18:55	Analysis Adsorptive:	N2
Completed:	05.06.2018 10:25:58	Analysis Bath Temp.:	-195,850 °C
Report Time:	06.06.2018 09:53:11	Thermal Correction:	No
Sample Mass:	0,0752 g	Warm Free Space:	10,6036 cm³ Measured
Cold Free Space:	32,1280 cm³	Equilibration Interval:	5 s
Low Pressure Dose:	None	Sample Density:	1,000 g/cm³
Automatic Degas:	No		

Isotherm Linear Plot

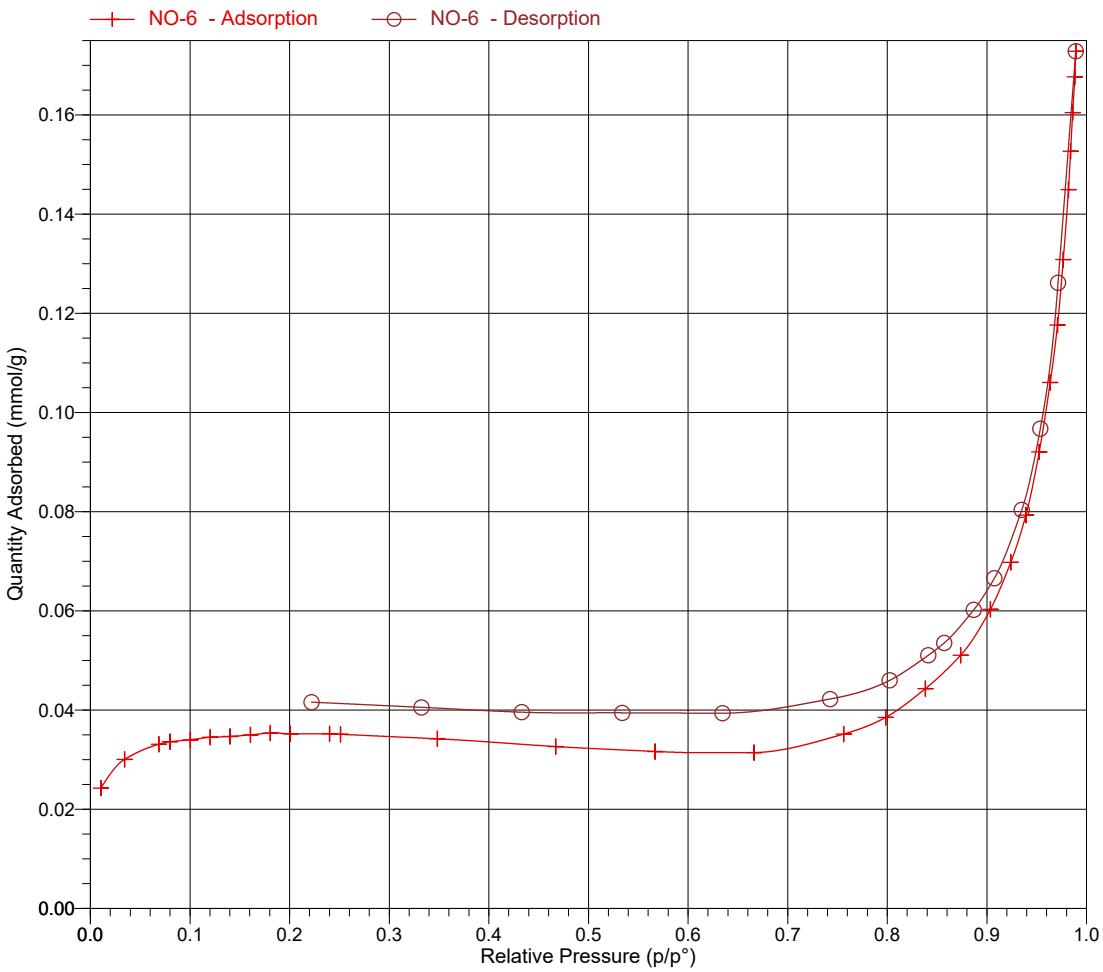

Sample: NO-6
Operator: maria olsvik
Submitter: MO
File: C:\TriStar II 3020\data\Maria Olsvik\NO-6 test3.SMP

Started:	04.06.2018 20:18:55	Analysis Adsorptive:	N2
Completed:	05.06.2018 10:25:58	Analysis Bath Temp.:	-195,850 °C
Report Time:	06.06.2018 09:53:11	Thermal Correction:	No
Sample Mass:	0,0752 g	Warm Free Space:	10,6036 cm³ Measured
Cold Free Space:	32,1280 cm³	Equilibration Interval:	5 s
Low Pressure Dose:	None	Sample Density:	1,000 g/cm³
Automatic Degas:	No		

BJH Adsorption dV/dw Pore Volume

Halsey : Faas Correction

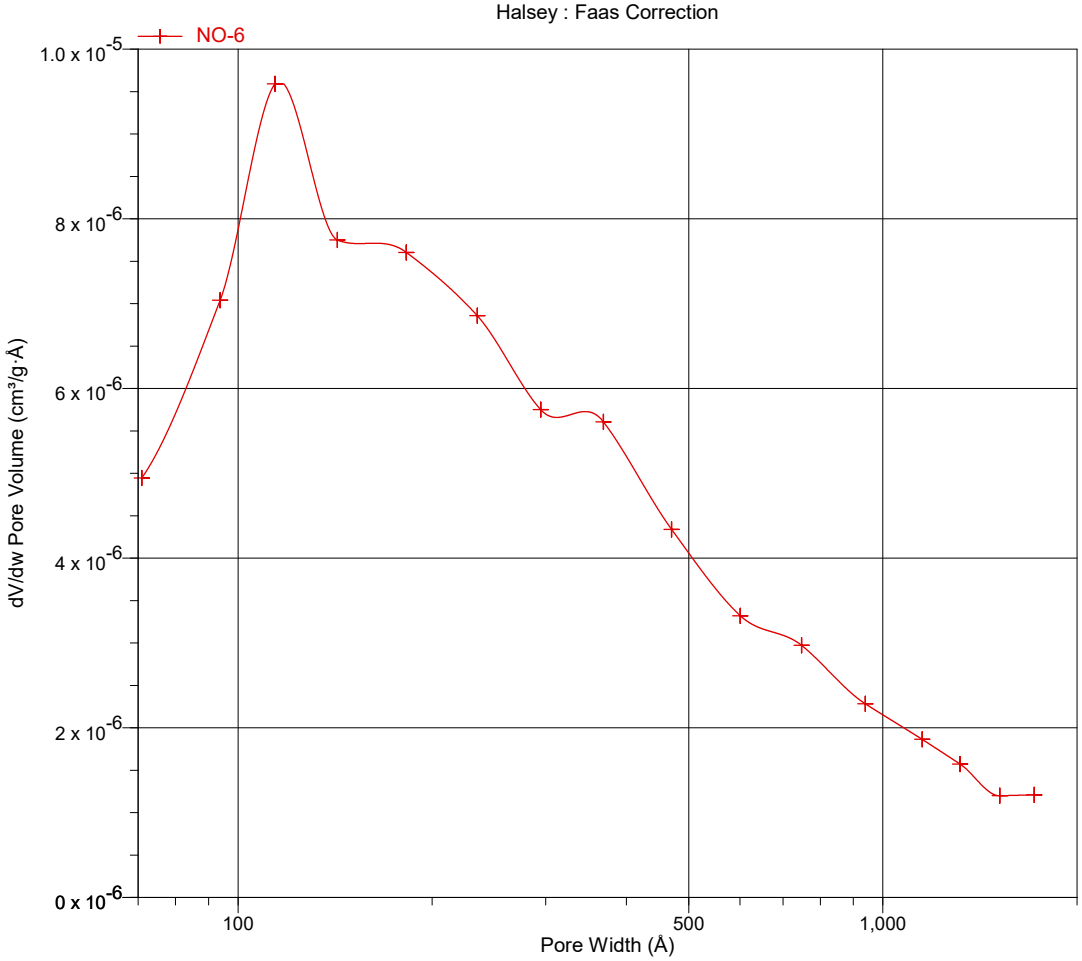

Full Report Set

Sample: NO-6 milled5min
Operator: Maria Olsvik
File: C:\TriStar II 3020\data\Maria O...\NO-6 milled5min.SMP

Started:	27.03.2018 13:10:11	Analysis Adsorptive:	N2
Completed:	27.03.2018 18:49:52	Analysis Bath Temp.:	-195,850 °C
Report Time:	27.03.2018 19:37:03	Thermal Correction:	No
Sample Mass:	0,0698 g	Warm Free Space:	10,0938 cm³ Measured
Cold Free Space:	30,4395 cm³	Equilibration Interval:	10 s
Low Pressure Dose:	None	Sample Density:	1,000 g/cm³
Automatic Degas:	No		

Summary Report

Surface Area

Single point surface area at p/p° = 0,260063327:	1,4756 m²/g
BET Surface Area:	1,3646 m²/g
t-Plot Micropore Area:	1,7634 m²/g
t-Plot External Surface Area:	-0,3988 m²/g
BJH Adsorption cumulative surface area of pores between 17,000 Å and 3 000,000 Å width:	0.454 m²/g
BJH Desorption cumulative surface area of pores between 17,000 Å and 3 000,000 Å width:	0,7440 m²/g

Pore Volume

t-Plot micropore volume:	0,000876 cm³/g
BJH Adsorption cumulative volume of pores between 17,000 Å and 3 000,000 Å width:	0,003077 cm³/g
BJH Desorption cumulative volume of pores between 17,000 Å and 3 000,000 Å width:	0,003408 cm³/g

Pore Size

BJH Adsorption average pore width (4V/A):	271,071 Å
BJH Desorption average pore width (4V/A):	183,253 Å

DFT Pore Size

Volume in Pores	<	10,22 Å	:	0,00043 cm³/g
Total Volume in Pores	<=	448,83 Å	:	0,00279 cm³/g
Total Area in Pores	>=	10,22 Å	:	0,695 m²/g

Nanoparticle Size:

Average Particle Size 43 967,972 Å

Sample: NO-6 milled5min
Operator: Maria Olsvik
File: C:\TriStar II 3020\data\Maria O...\NO-6 milled5min.SMP

Started:	27.03.2018 13:10:11	Analysis Adsorptive:	N2
Completed:	27.03.2018 18:49:52	Analysis Bath Temp.:	-195,850 °C
Report Time:	27.03.2018 19:37:03	Thermal Correction:	No
Sample Mass:	0,0698 g	Warm Free Space:	10,0938 cm³ Measured
Cold Free Space:	30,4395 cm³	Equilibration Interval:	10 s
Low Pressure Dose:	None	Sample Density:	1,000 g/cm³
Automatic Degas:	No		

Isotherm Linear Plot

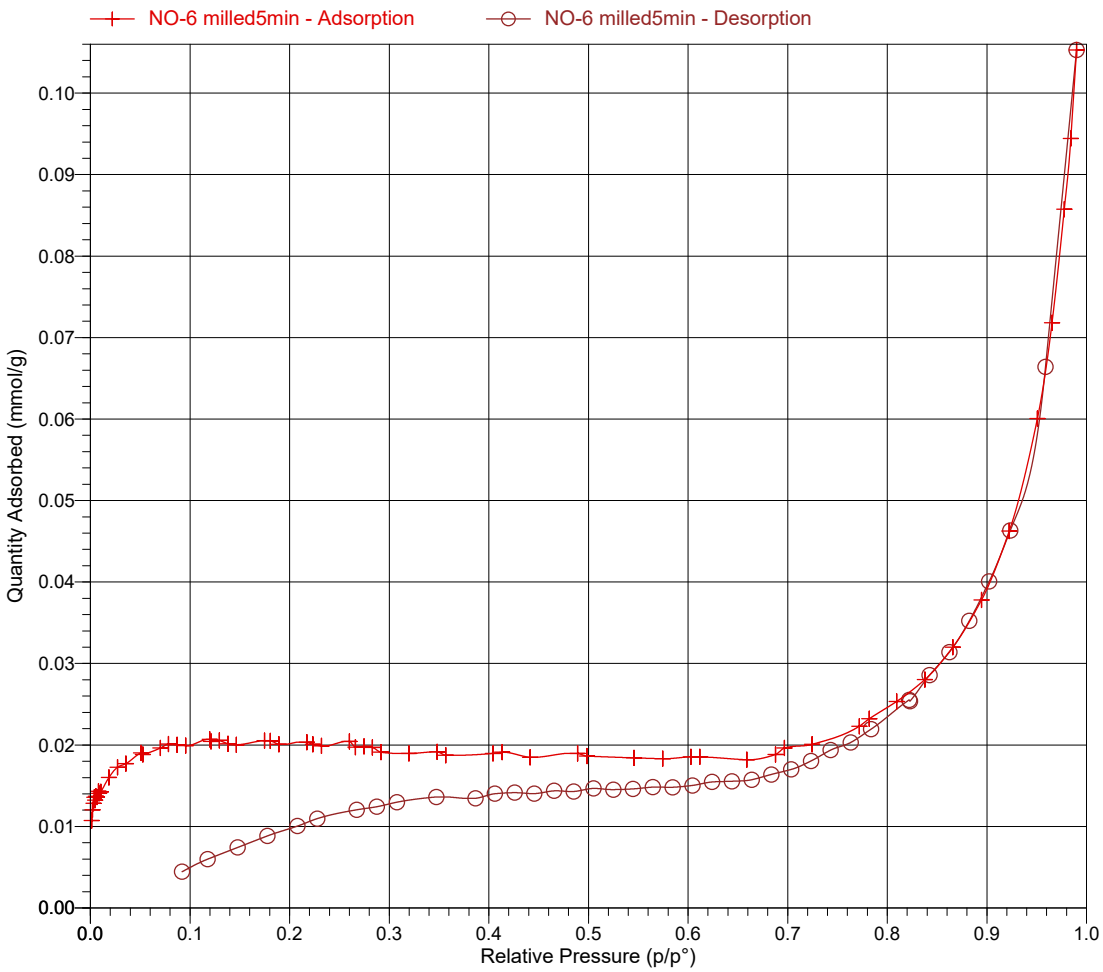

Sample: NO-6 milled5min
Operator: Maria Olsvik
File: C:\TriStar II 3020\data\Maria O...\NO-6 milled5min.SMP

Started:	27.03.2018 13:10:11	Analysis Adsorptive:	N2
Completed:	27.03.2018 18:49:52	Analysis Bath Temp.:	-195,850 °C
Report Time:	27.03.2018 19:37:03	Thermal Correction:	No
Sample Mass:	0,0698 g	Warm Free Space:	10,0938 cm³ Measured
Cold Free Space:	30,4395 cm³	Equilibration Interval:	10 s
Low Pressure Dose:	None	Sample Density:	1,000 g/cm³
Automatic Degas:	No		

BJH Adsorption dV/dlog(w) Pore Volume

Halsey : Faas Correction

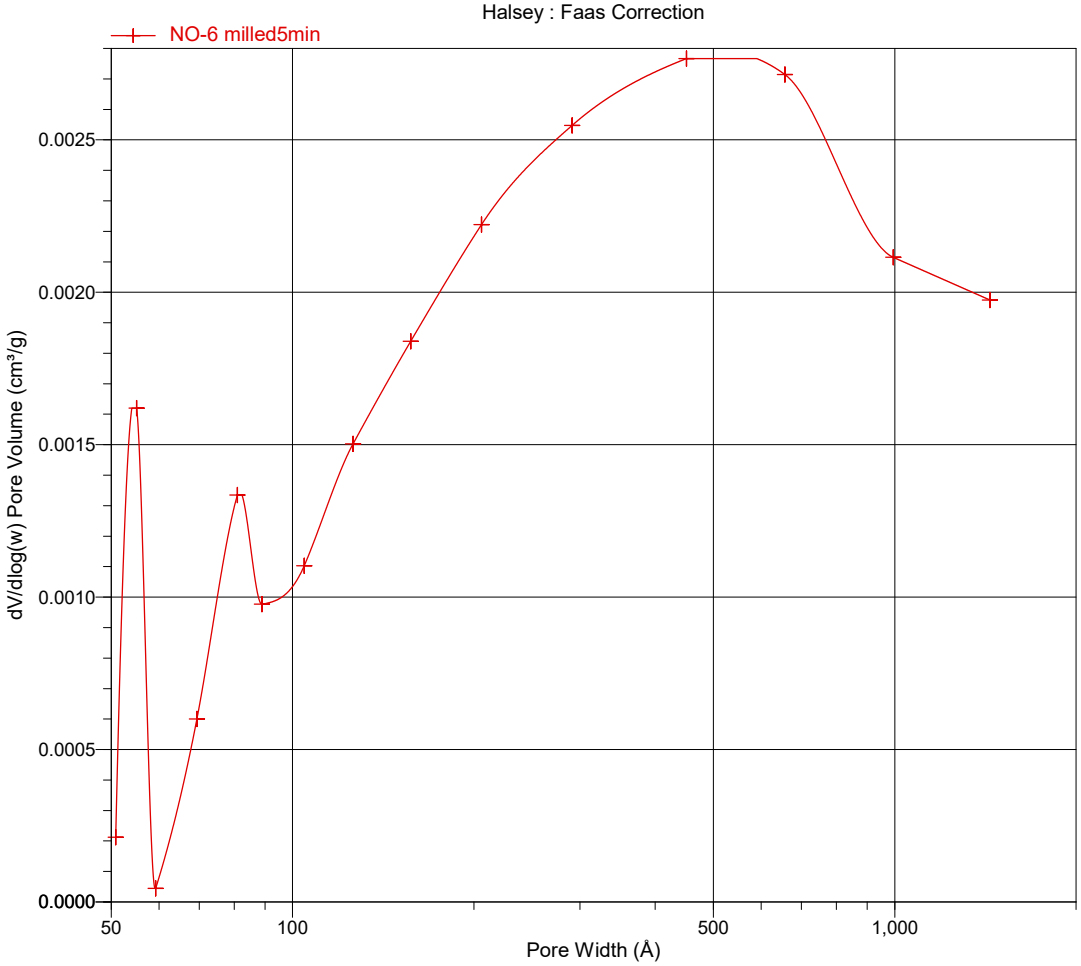

Full Report Set

Sample: NO-6 milled5min test2
Operator: maria olsvik
Submitter:
File: C:\TriStar II 3020\data\M...\NO-6 milled5min test2.SMP

Started:	05.04.2018 11:13:24	Analysis Adsorptive:	N2
Completed:	05.04.2018 13:23:19	Analysis Bath Temp.:	-195,850 °C
Report Time:	05.04.2018 18:16:39	Thermal Correction:	No
Sample Mass:	0,0671 g	Warm Free Space:	10,4573 cm³ Measured
Cold Free Space:	31,8492 cm³	Equilibration Interval:	5 s
Low Pressure Dose:	None	Sample Density:	1,000 g/cm³
Automatic Degas:	No		

Summary Report

Surface Area

Single point surface area at p/p° = 0,200205029: 1,1990 m²/g

BJH Desorption cumulative surface area of pores between 17,000 Å and 3 000,000 Å width: 0,4312 m²/g

Pore Volume

Single point adsorption total pore volume of pores less than 1 226,495 Å width at p/p° = 0,983959817: 0,003512 cm³/g

BJH Desorption cumulative volume of pores between 17,000 Å and 3 000,000 Å width: 0,004368 cm³/g

Pore Size

Adsorption average pore diameter (4V/A by BET): 130,2096 Å

BJH Desorption average pore width (4V/A): 405,176 Å

Sample: NO-6 milled5min test2
Operator: maria olsvik
Submitter:
File: C:\TriStar II 3020\data\M...\NO-6 milled5min test2.SMP

Started:	05.04.2018 11:13:24	Analysis Adsorptive:	N2
Completed:	05.04.2018 13:23:19	Analysis Bath Temp.:	-195,850 °C
Report Time:	05.04.2018 18:16:39	Thermal Correction:	No
Sample Mass:	0,0671 g	Warm Free Space:	10,4573 cm³ Measured
Cold Free Space:	31,8492 cm³	Equilibration Interval:	5 s
Low Pressure Dose:	None	Sample Density:	1,000 g/cm³
Automatic Degas:	No		

Isotherm Linear Plot

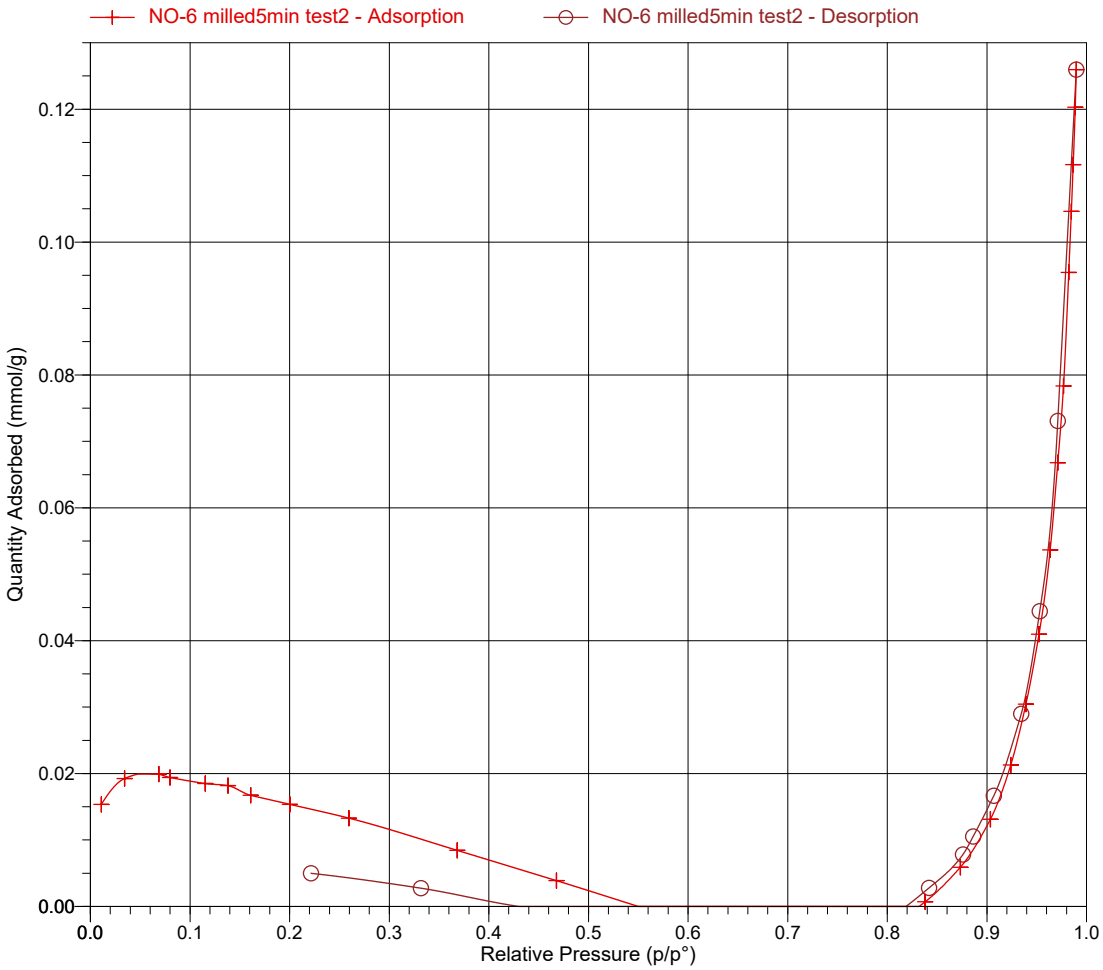

Sample: NO-6 milled5min test2
Operator: maria olsvik
Submitter:
File: C:\TriStar II 3020\data\M...\NO-6 milled5min test2.SMP

Started:	05.04.2018 11:13:24	Analysis Adsorptive:	N2
Completed:	05.04.2018 13:23:19	Analysis Bath Temp.:	-195,850 °C
Report Time:	05.04.2018 18:16:39	Thermal Correction:	No
Sample Mass:	0,0671 g	Warm Free Space:	10,4573 cm³ Measured
Cold Free Space:	31,8492 cm³	Equilibration Interval:	5 s
Low Pressure Dose:	None	Sample Density:	1,000 g/cm³
Automatic Degas:	No		

BJH Adsorption dV/dlog(w) Pore Volume

Halsey : Faas Correction

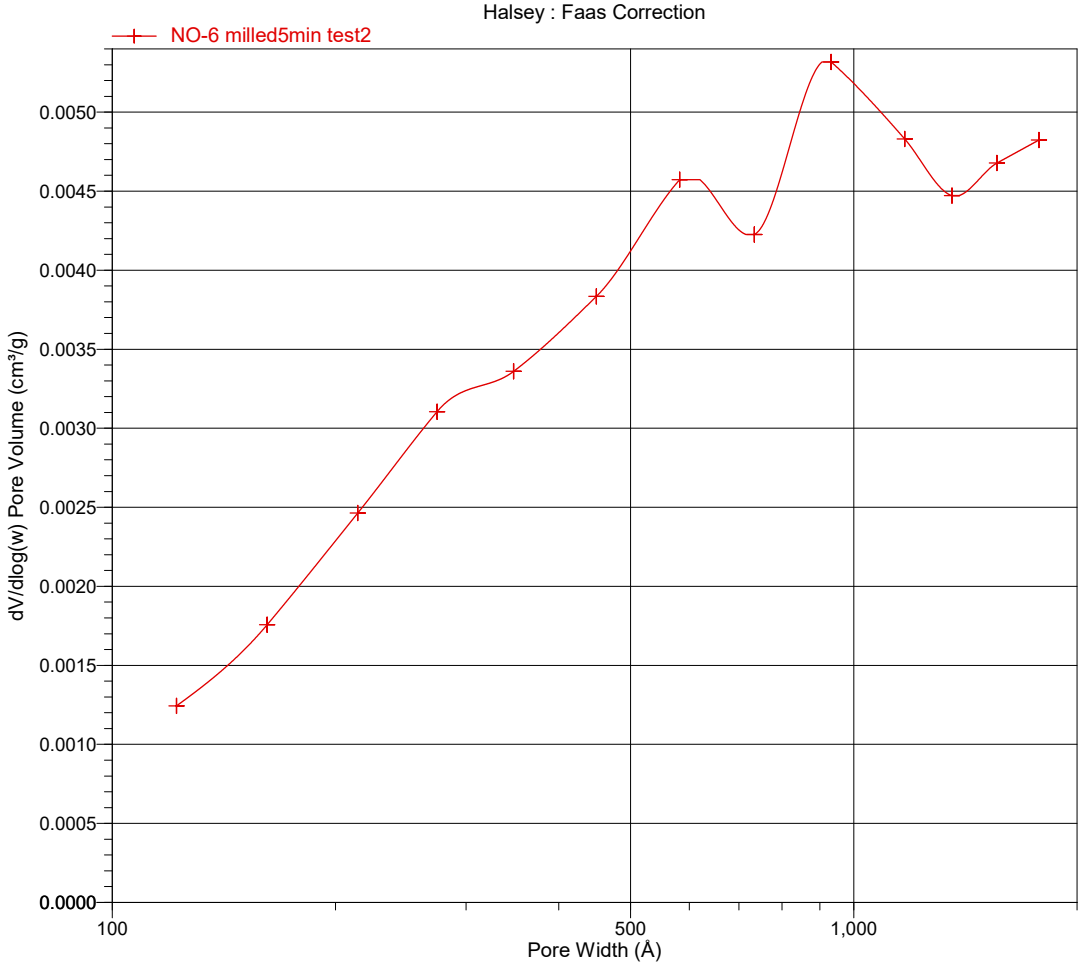

Full Report Set

Sample: NO-8
Operator: Maria Olsvik
File: C:\TriStar II 3020\data\Maria Olsvik\NO-8.SMP

Started:	08.05.2018 09:58:11	Analysis Adsorptive:	N2
Completed:	08.05.2018 16:06:32	Analysis Bath Temp.:	-195,850 °C
Report Time:	08.05.2018 21:19:46	Thermal Correction:	No
Sample Mass:	0,0802 g	Warm Free Space:	10,3297 cm³ Measured
Cold Free Space:	31,5689 cm³	Equilibration Interval:	10 s
Low Pressure Dose:	None	Sample Density:	1,000 g/cm³
Automatic Degas:	No		

Summary Report

Surface Area

Single point surface area at p/p° = 0,257866107:	6,3372 m²/g
BET Surface Area:	6,4720 m²/g
t-Plot Micropore Area:	0,7806 m²/g
t-Plot External Surface Area:	5,6914 m²/g
BJH Adsorption cumulative surface area of pores between 17,000 Å and 3 000,000 Å width:	4.947 m²/g
BJH Desorption cumulative surface area of pores between 17,000 Å and 3 000,000 Å width:	6,5236 m²/g

Pore Volume

t-Plot micropore volume:	0,000356 cm³/g
BJH Adsorption cumulative volume of pores between 17,000 Å and 3 000,000 Å width:	0,014563 cm³/g
BJH Desorption cumulative volume of pores between 17,000 Å and 3 000,000 Å width:	0,015969 cm³/g

Pore Size

BJH Adsorption average pore width (4V/A):	117,739 Å
BJH Desorption average pore width (4V/A):	97,914 Å

DFT Pore Size

Volume in Pores	<	9,51 Å	:	0,00000 cm³/g
Total Volume in Pores	<=	448,83 Å	:	0,01231 cm³/g
Total Area in Pores	>=	9,51 Å	:	11,116 m²/g

Nanoparticle Size:

Average Particle Size 9 270,706 Å

Sample: NO-8
Operator: Maria Olsvik
File: C:\TriStar II 3020\data\Maria Olsvik\NO-8.SMP

Started:	08.05.2018 09:58:11	Analysis Adsorptive:	N2
Completed:	08.05.2018 16:06:32	Analysis Bath Temp.:	-195,850 °C
Report Time:	08.05.2018 21:19:46	Thermal Correction:	No
Sample Mass:	0,0802 g	Warm Free Space:	10,3297 cm³ Measured
Cold Free Space:	31,5689 cm³	Equilibration Interval:	10 s
Low Pressure Dose:	None	Sample Density:	1,000 g/cm³
Automatic Degas:	No		

Isotherm Linear Plot

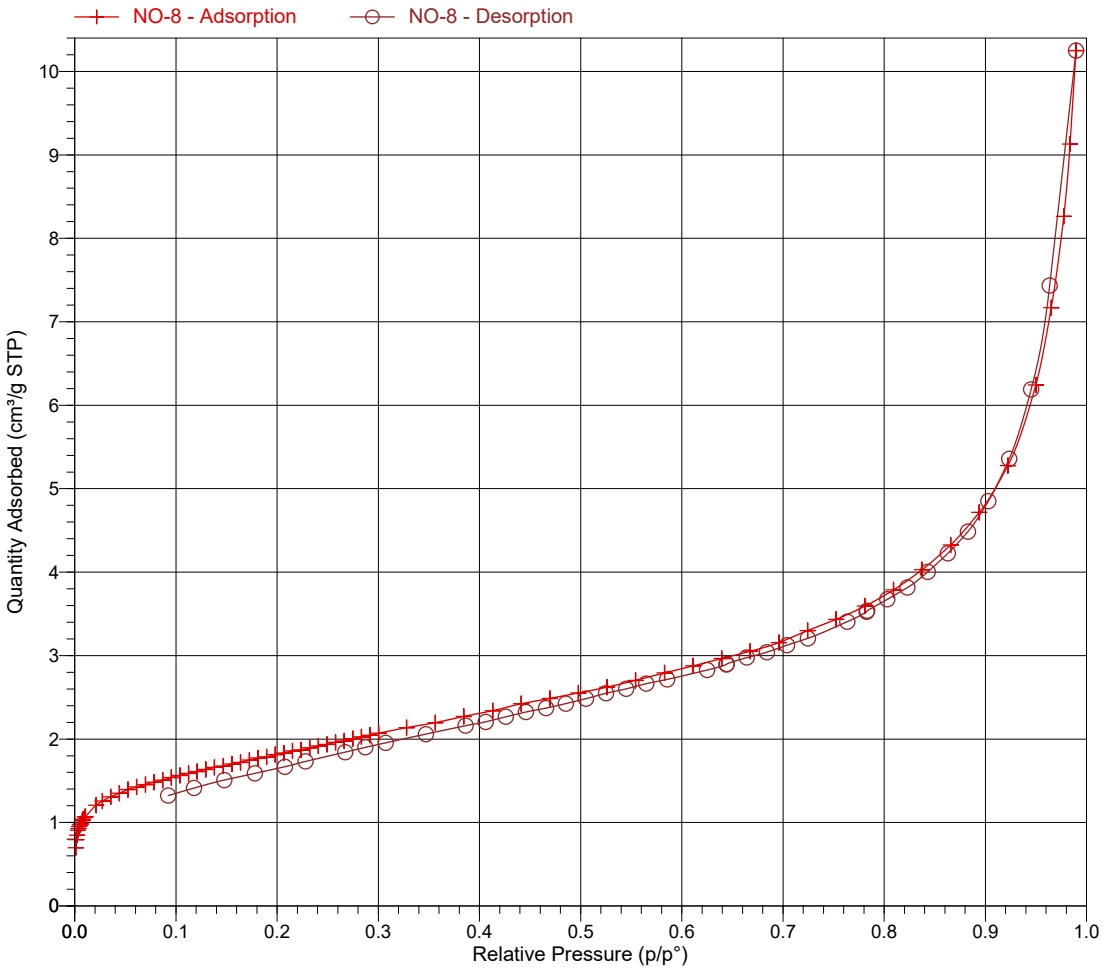

Sample: NO-8
Operator: Maria Olsvik
File: C:\TriStar II 3020\data\Maria Olsvik\NO-8.SMP

Started:	08.05.2018 09:58:11	Analysis Adsorptive:	N2
Completed:	08.05.2018 16:06:32	Analysis Bath Temp.:	-195,850 °C
Report Time:	08.05.2018 21:19:46	Thermal Correction:	No
Sample Mass:	0,0802 g	Warm Free Space:	10,3297 cm³ Measured
Cold Free Space:	31,5689 cm³	Equilibration Interval:	10 s
Low Pressure Dose:	None	Sample Density:	1,000 g/cm³
Automatic Degas:	No		

BJH Adsorption dV/dlog(w) Pore Volume

Halsey : Faas Correction

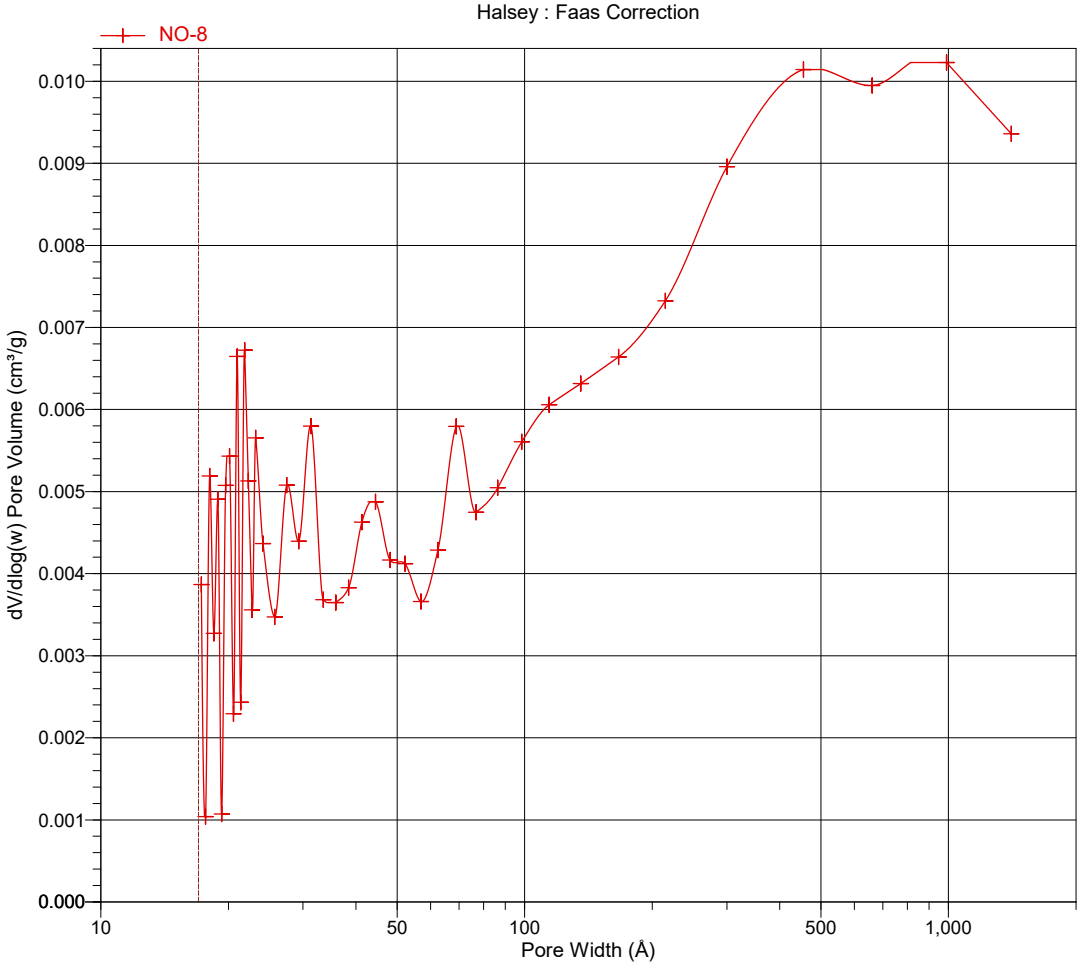

Full Report Set

Sample: NO-8
Operator: Maria Olsvik
File: C:\TriStar II 3020\data\Maria Olsvik\NO-8 test2.SMP

Started:	08.05.2018 21:24:25	Analysis Adsorptive:	N2
Completed:	09.05.2018 03:26:30	Analysis Bath Temp.:	-195,850 °C
Report Time:	23.05.2018 09:23:55	Thermal Correction:	No
Sample Mass:	0,0802 g	Warm Free Space:	10,2965 cm³ Measured
Cold Free Space:	31,5528 cm³	Equilibration Interval:	10 s
Low Pressure Dose:	None	Sample Density:	1,000 g/cm³
Automatic Degas:	No		

Summary Report

Surface Area

Single point surface area at p/p° = 0,257890880:	6,0095 m²/g
BET Surface Area:	6,1304 m²/g
t-Plot Micropore Area:	1,1363 m²/g
t-Plot External Surface Area:	4,9941 m²/g
BJH Adsorption cumulative surface area of pores between 1,7000 nm and 300,0000 nm diameter:	4.639 m²/g
BJH Desorption cumulative surface area of pores between 1,7000 nm and 300,0000 nm diameter:	5,6604 m²/g

Pore Volume

t-Plot micropore volume:	0,000536 cm³/g
BJH Adsorption cumulative volume of pores between 1,7000 nm and 300,0000 nm diameter:	0,016153 cm³/g
BJH Desorption cumulative volume of pores between 1,7000 nm and 300,0000 nm diameter:	0,017087 cm³/g

Pore Size

BJH Adsorption average pore diameter (4V/A):	13,9288 nm
BJH Desorption average pore diameter (4V/A):	12,0746 nm

DFT Pore Size

Volume in Pores	<	1,022 nm	:	0,00172 cm³/g
Total Volume in Pores	<=	44,883 nm	:	0,01314 cm³/g
Total Area in Pores	>=	1,022 nm	:	3,984 m²/g

Nanoparticle Size:

Average Particle Size	978,7303 nm

Sample: NO-8
Operator: Maria Olsvik
File: C:\TriStar II 3020\data\Maria Olsvik\NO-8 test2.SMP

Started:	08.05.2018 21:24:25	Analysis Adsorptive:	N2
Completed:	09.05.2018 03:26:30	Analysis Bath Temp.:	-195,850 °C
Report Time:	23.05.2018 09:23:55	Thermal Correction:	No
Sample Mass:	0,0802 g	Warm Free Space:	10,2965 cm³ Measured
Cold Free Space:	31,5528 cm³	Equilibration Interval:	10 s
Low Pressure Dose:	None	Sample Density:	1,000 g/cm³
Automatic Degas:	No		

Isotherm Linear Plot

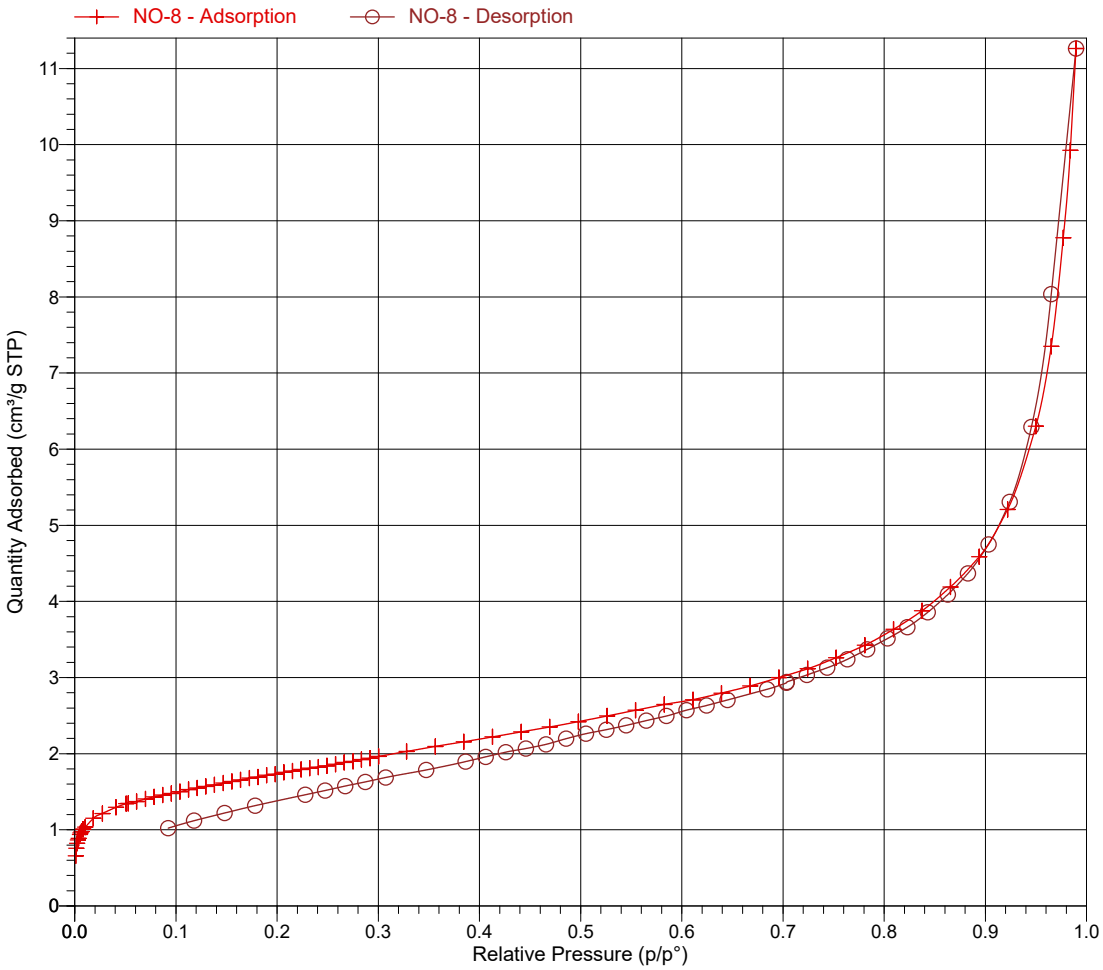

Sample: NO-8
Operator: Maria Olsvik
File: C:\TriStar II 3020\data\Maria Olsvik\NO-8 test2.SMP

Started:	08.05.2018 21:24:25	Analysis Adsorptive:	N2
Completed:	09.05.2018 03:26:30	Analysis Bath Temp.:	-195,850 °C
Report Time:	23.05.2018 09:23:55	Thermal Correction:	No
Sample Mass:	0,0802 g	Warm Free Space:	10,2965 cm³ Measured
Cold Free Space:	31,5528 cm³	Equilibration Interval:	10 s
Low Pressure Dose:	None	Sample Density:	1,000 g/cm³
Automatic Degas:	No		

BJH Adsorption dV/dlog(D) Pore Volume

Halsey : Faas Correction

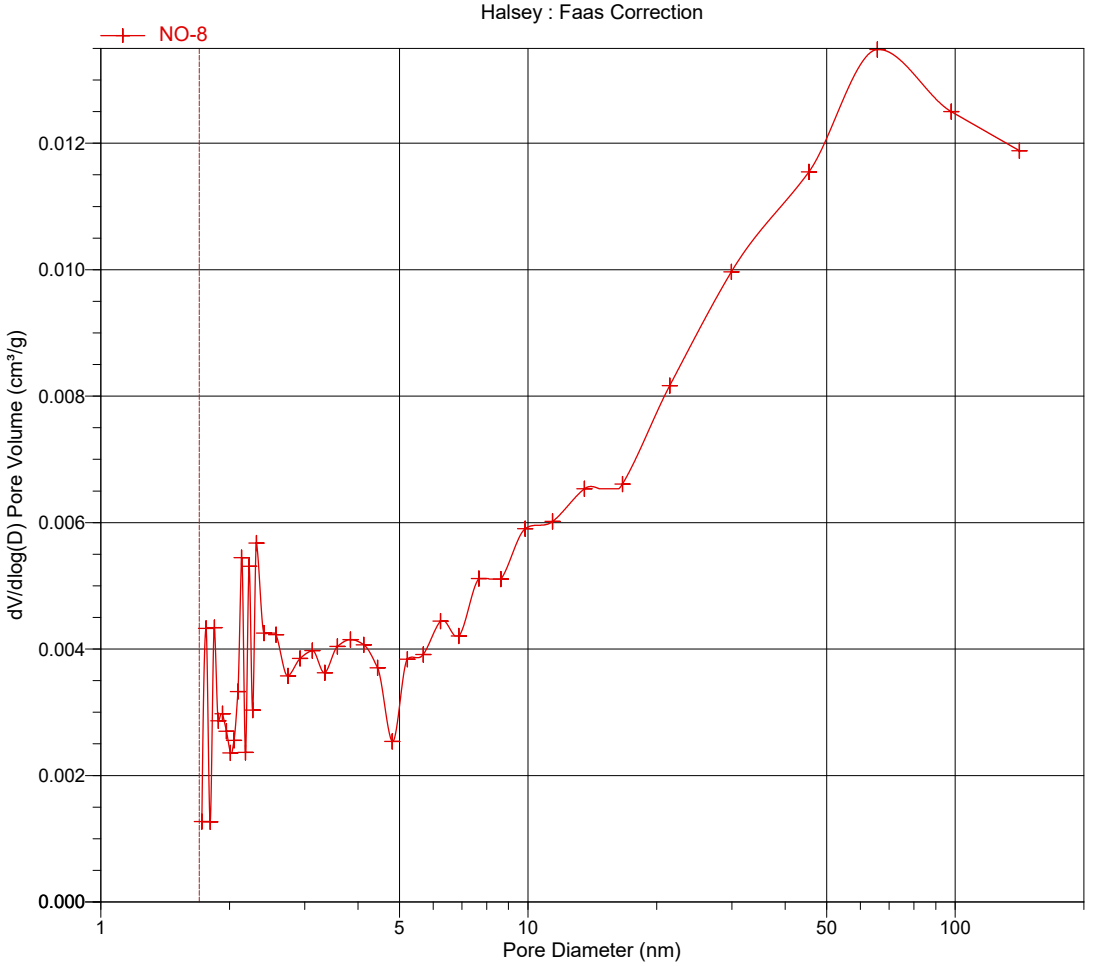

Full Report Set

Sample: NO-8 test3
Operator: Maria Olsvik
File: C:\TriStar II 3020\data\Maria Olsvik\NO-8 test3.SMP

Started:	04.06.2018 20:18:55	Analysis Adsorptive:	N2
Completed:	05.06.2018 10:25:58	Analysis Bath Temp.:	-195,850 °C
Report Time:	06.06.2018 09:53:51	Thermal Correction:	No
Sample Mass:	0,0726 g	Warm Free Space:	10,5208 cm³ Measured
Cold Free Space:	31,8838 cm³	Equilibration Interval:	10 s
Low Pressure Dose:	None	Sample Density:	1,000 g/cm³
Automatic Degas:	No		

Summary Report

Surface Area

Single point surface area at p/p° = 0,257352312:	8,4971 m²/g
BET Surface Area:	8,4875 m²/g
t-Plot Micropore Area:	3,0193 m²/g
t-Plot External Surface Area:	5,4682 m²/g
BJH Adsorption cumulative surface area of pores between 17,000 Å and 3 000,000 Å width:	5.488 m²/g
BJH Desorption cumulative surface area of pores between 17,000 Å and 3 000,000 Å width:	9,0132 m²/g

Pore Volume

t-Plot micropore volume:	0,001477 cm³/g
BJH Adsorption cumulative volume of pores between 17,000 Å and 3 000,000 Å width:	0,012240 cm³/g
BJH Desorption cumulative volume of pores between 17,000 Å and 3 000,000 Å width:	0,014835 cm³/g

Pore Size

BJH Adsorption average pore width (4V/A):	89,216 Å
BJH Desorption average pore width (4V/A):	65,838 Å

DFT Pore Size

Volume in Pores	<	10,22 Å	:	0,00230 cm³/g
Total Volume in Pores	<=	448,83 Å	:	0,01288 cm³/g
Total Area in Pores	>=	10,22 Å	:	5,567 m²/g

Nanoparticle Size:

Average Particle Size 7 069,190 Å

Sample: NO-8 test3
Operator: Maria Olsvik
File: C:\TriStar II 3020\data\Maria Olsvik\NO-8 test3.SMP

Started:	04.06.2018 20:18:55	Analysis Adsorptive:	N2
Completed:	05.06.2018 10:25:58	Analysis Bath Temp.:	-195,850 °C
Report Time:	06.06.2018 09:53:51	Thermal Correction:	No
Sample Mass:	0,0726 g	Warm Free Space:	10,5208 cm³ Measured
Cold Free Space:	31,8838 cm³	Equilibration Interval:	10 s
Low Pressure Dose:	None	Sample Density:	1,000 g/cm³
Automatic Degas:	No		

Isotherm Linear Plot

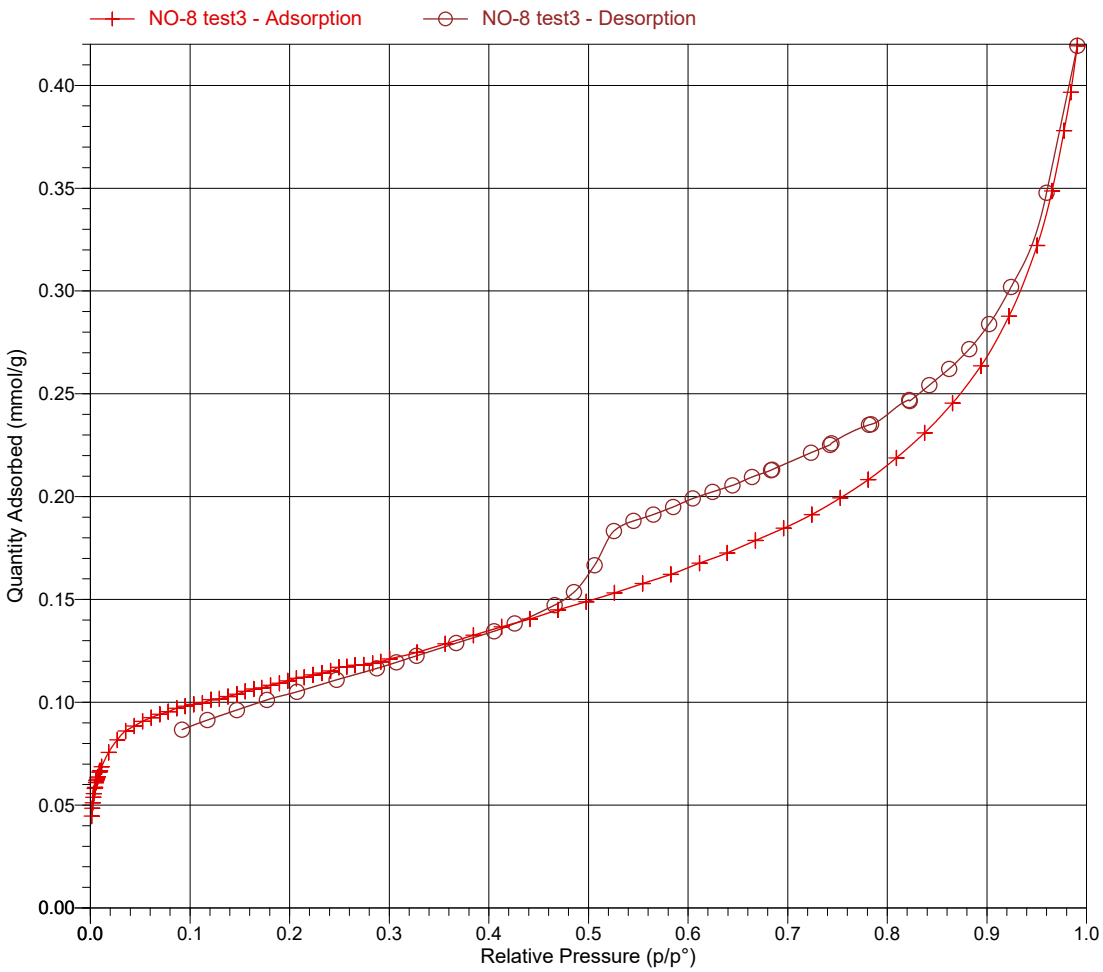

Sample: NO-8 test3
Operator: Maria Olsvik
File: C:\TriStar II 3020\data\Maria Olsvik\NO-8 test3.SMP

Started:	04.06.2018 20:18:55	Analysis Adsorptive:	N2
Completed:	05.06.2018 10:25:58	Analysis Bath Temp.:	-195,850 °C
Report Time:	06.06.2018 09:53:51	Thermal Correction:	No
Sample Mass:	0,0726 g	Warm Free Space:	10,5208 cm³ Measured
Cold Free Space:	31,8838 cm³	Equilibration Interval:	10 s
Low Pressure Dose:	None	Sample Density:	1,000 g/cm³
Automatic Degas:	No		

BJH Adsorption dV/dlog(w) Pore Volume

Halsey : Faas Correction

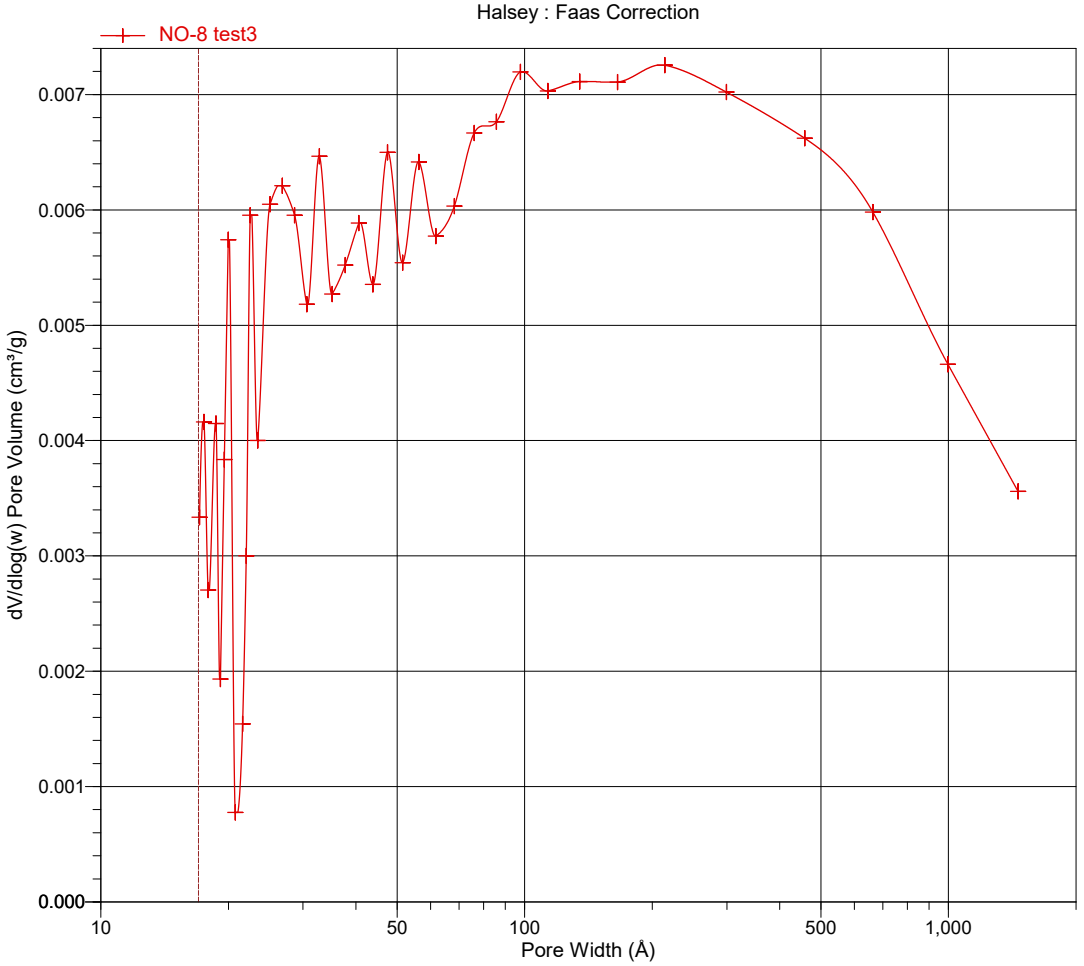

Sample: Mar_2
Operator: Maria Olsvik
Submitter:
File: C:\...\MARIAO~1\000-332.SMP

Started:	08.03.2018 10:54:39	Analysis Adsorptive:	N2
Completed:	08.03.2018 13:46:24	Analysis Bath Temp.:	-195.850 °C
Report Time:	09.03.2018 9:28:30	Sample Mass:	0.0877 g
Warm Free Space:	9.6686 cm³ Measured	Cold Free Space:	29.0230 cm³ Measured
Equilibration Interval:	5 s	Low Pressure Dose:	None
Sample Density:	1.000 g/cm³	Automatic Degas:	No

Summary Report

Surface Area

Single point surface area at P/Po = 0.200901996: 13.6498 m²/g

BJH Desorption cumulative surface area of pores between 1.7000 nm and 300.0000 nm diameter: 13.0148 m²/g

Pore Volume

Single point adsorption total pore volume of pores less than 120.9406 nm diameter at P/Po = 0.983728954: 0.050304 cm³/g

BJH Desorption cumulative volume of pores between 1.7000 nm and 300.0000 nm diameter: 0.060588 cm³/g

Pore Size

Adsorption average pore width (4V/A by BET): 14.60517 nm

BJH Desorption average pore diameter (4V/A): 18.6213 nm

Sample: Mar_2
Operator: Maria Olsvik
Submitter:
File: C:\...\MARIAO~1\000-332.SMP

Started:	08.03.2018 10:54:39	Analysis Adsorptive:	N2
Completed:	08.03.2018 13:46:24	Analysis Bath Temp.:	-195.850 °C
Report Time:	09.03.2018 9:28:30	Sample Mass:	0.0877 g
Warm Free Space:	9.6686 cm³ Measured	Cold Free Space:	29.0230 cm³ Measured
Equilibration Interval:	5 s	Low Pressure Dose:	None
Sample Density:	1.000 g/cm³	Automatic Degas:	No

Isotherm Linear Plot

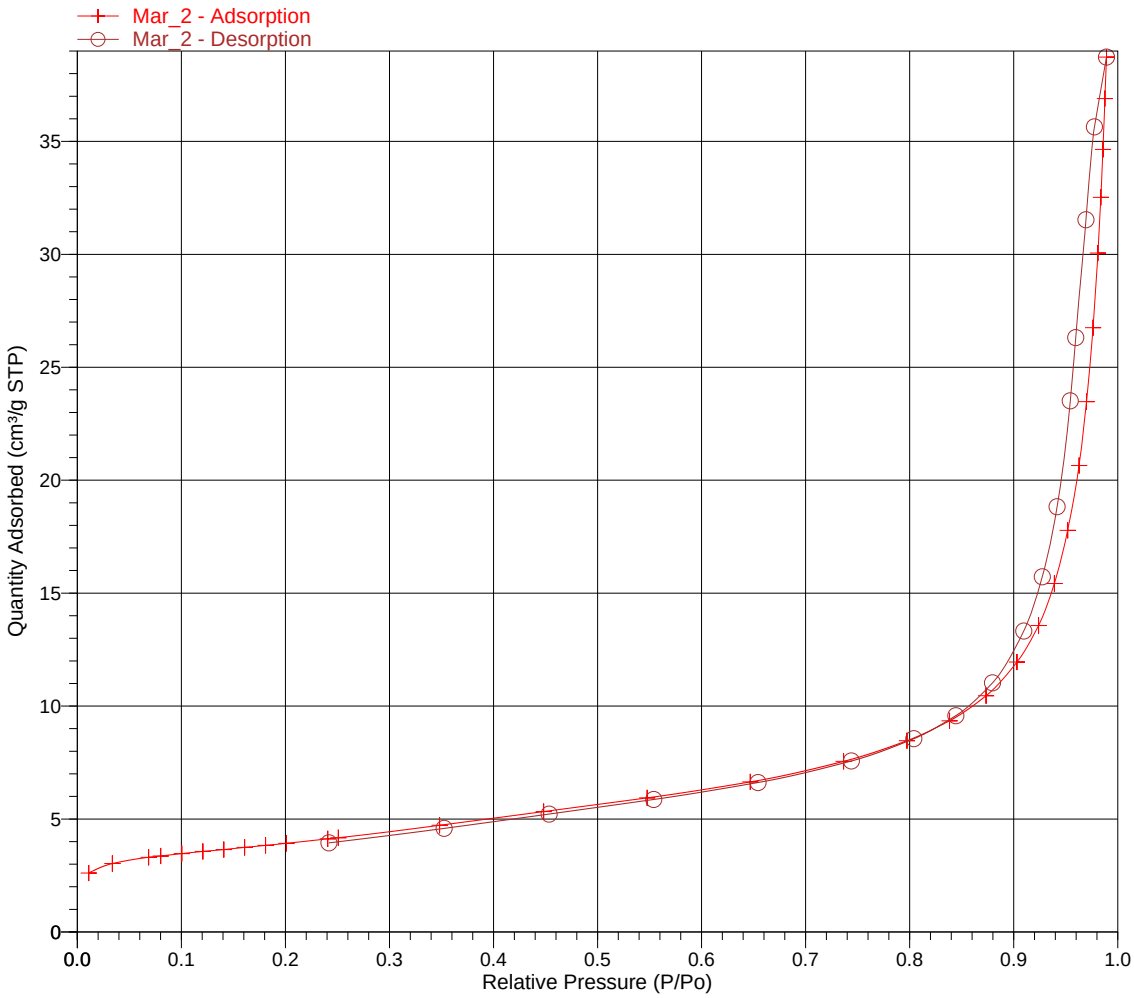

Sample: Mar_2
Operator: Maria Olsvik
Submitter:
File: C:\...\MARIAO~1\000-332.SMP

Started:	08.03.2018 10:54:39	Analysis Adsorptive:	N2
Completed:	08.03.2018 13:46:24	Analysis Bath Temp.:	-195.850 °C
Report Time:	09.03.2018 9:28:30	Sample Mass:	0.0877 g
Warm Free Space:	9.6686 cm³ Measured	Cold Free Space:	29.0230 cm³ Measured
Equilibration Interval:	5 s	Low Pressure Dose:	None
Sample Density:	1.000 g/cm³	Automatic Degas:	No

BJH Adsorption dV/dlog(D) Pore Volume

Halsey : Faas Correction

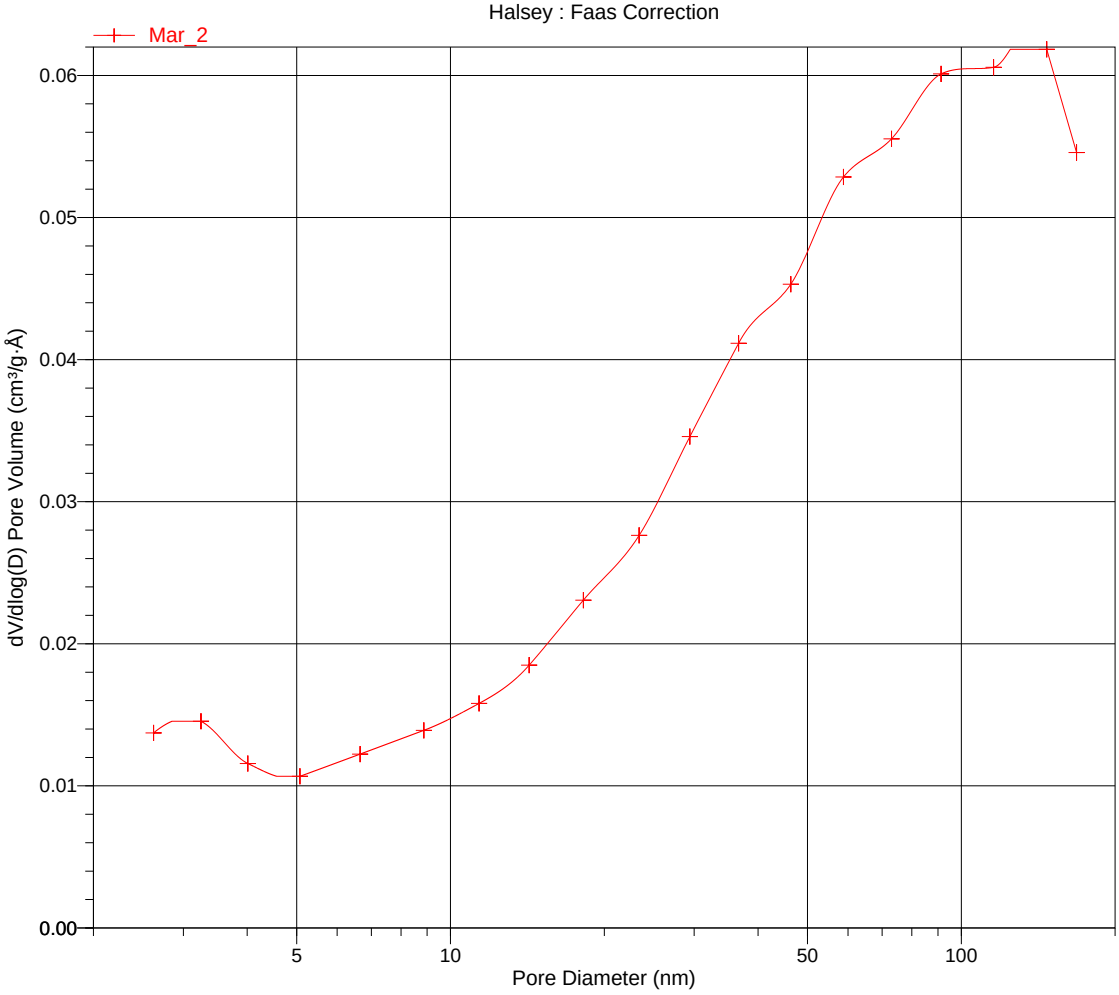

Full Report Set

Sample: Mar_2 test2
Operator: Maria Olsvik
File: C:\TriStar II 3020\data\Maria Olsvik\Mar_2 test2.SMP

Started:	19.04.2018 11:16:53	Analysis Adsorptive:	N2
Completed:	19.04.2018 17:10:06	Analysis Bath Temp.:	-195,850 °C
Report Time:	20.04.2018 08:59:05	Thermal Correction:	No
Sample Mass:	0,0867 g	Warm Free Space:	10,1327 cm³ Measured
Cold Free Space:	30,6156 cm³	Equilibration Interval:	10 s
Low Pressure Dose:	None	Sample Density:	1,000 g/cm³
Automatic Degas:	No		

Summary Report

Surface Area

Single point surface area at p/p° = 0,258264069:	13,5296 m²/g
BET Surface Area:	13,6155 m²/g
t-Plot Micropore Area:	3,1944 m²/g
t-Plot External Surface Area:	10,4211 m²/g
BJH Adsorption cumulative surface area of pores between 17,000 Å and 3 000,000 Å width:	9.944 m²/g
BJH Desorption cumulative surface area of pores between 17,000 Å and 3 000,000 Å width:	11,9976 m²/g

Pore Volume

t-Plot micropore volume:	0,001583 cm³/g
BJH Adsorption cumulative volume of pores between 17,000 Å and 3 000,000 Å width:	0,036477 cm³/g
BJH Desorption cumulative volume of pores between 17,000 Å and 3 000,000 Å width:	0,039238 cm³/g

Pore Size

BJH Adsorption average pore width (4V/A):	146,729 Å
BJH Desorption average pore width (4V/A):	130,822 Å

DFT Pore Size

Volume in Pores	<	9,51 Å	:	0,00000 cm³/g
Total Volume in Pores	<=	448,83 Å	:	0,03035 cm³/g
Total Area in Pores	>=	9,51 Å	:	24,129 m²/g

Nanoparticle Size:

Average Particle Size 4 406,751 Å

Sample: Mar_2 test2
Operator: Maria Olsvik
File: C:\TriStar II 3020\data\Maria Olsvik\Mar_2 test2.SMP

Started:	19.04.2018 11:16:53	Analysis Adsorptive:	N2
Completed:	19.04.2018 17:10:06	Analysis Bath Temp.:	-195,850 °C
Report Time:	20.04.2018 08:59:05	Thermal Correction:	No
Sample Mass:	0,0867 g	Warm Free Space:	10,1327 cm³ Measured
Cold Free Space:	30,6156 cm³	Equilibration Interval:	10 s
Low Pressure Dose:	None	Sample Density:	1,000 g/cm³
Automatic Degas:	No		

Isotherm Linear Plot

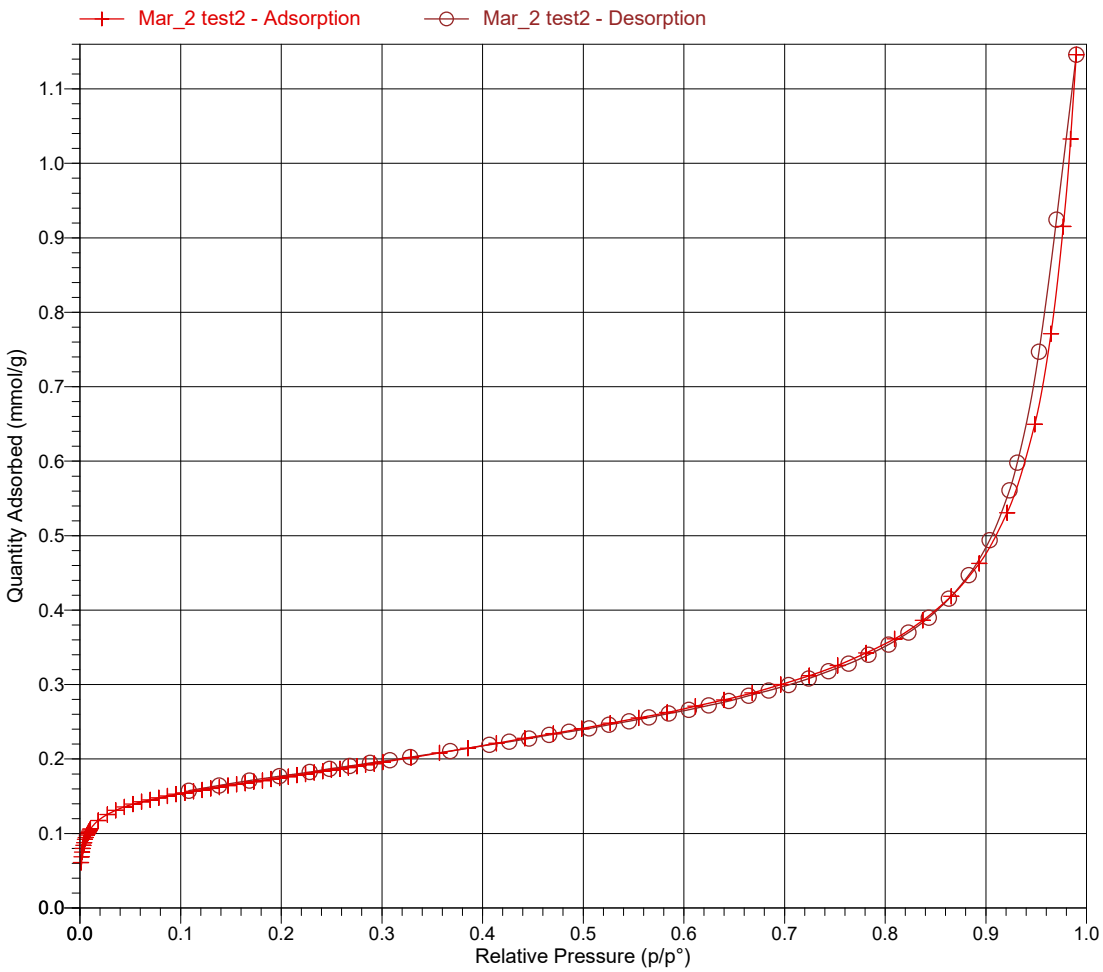

Sample: Mar_2 test2
Operator: Maria Olsvik
File: C:\TriStar II 3020\data\Maria Olsvik\Mar_2 test2.SMP

Started:	19.04.2018 11:16:53	Analysis Adsorptive:	N2
Completed:	19.04.2018 17:10:06	Analysis Bath Temp.:	-195,850 °C
Report Time:	20.04.2018 08:59:05	Thermal Correction:	No
Sample Mass:	0,0867 g	Warm Free Space:	10,1327 cm³ Measured
Cold Free Space:	30,6156 cm³	Equilibration Interval:	10 s
Low Pressure Dose:	None	Sample Density:	1,000 g/cm³
Automatic Degas:	No		

BJH Adsorption dV/dlog(w) Pore Volume

Halsey : Faas Correction

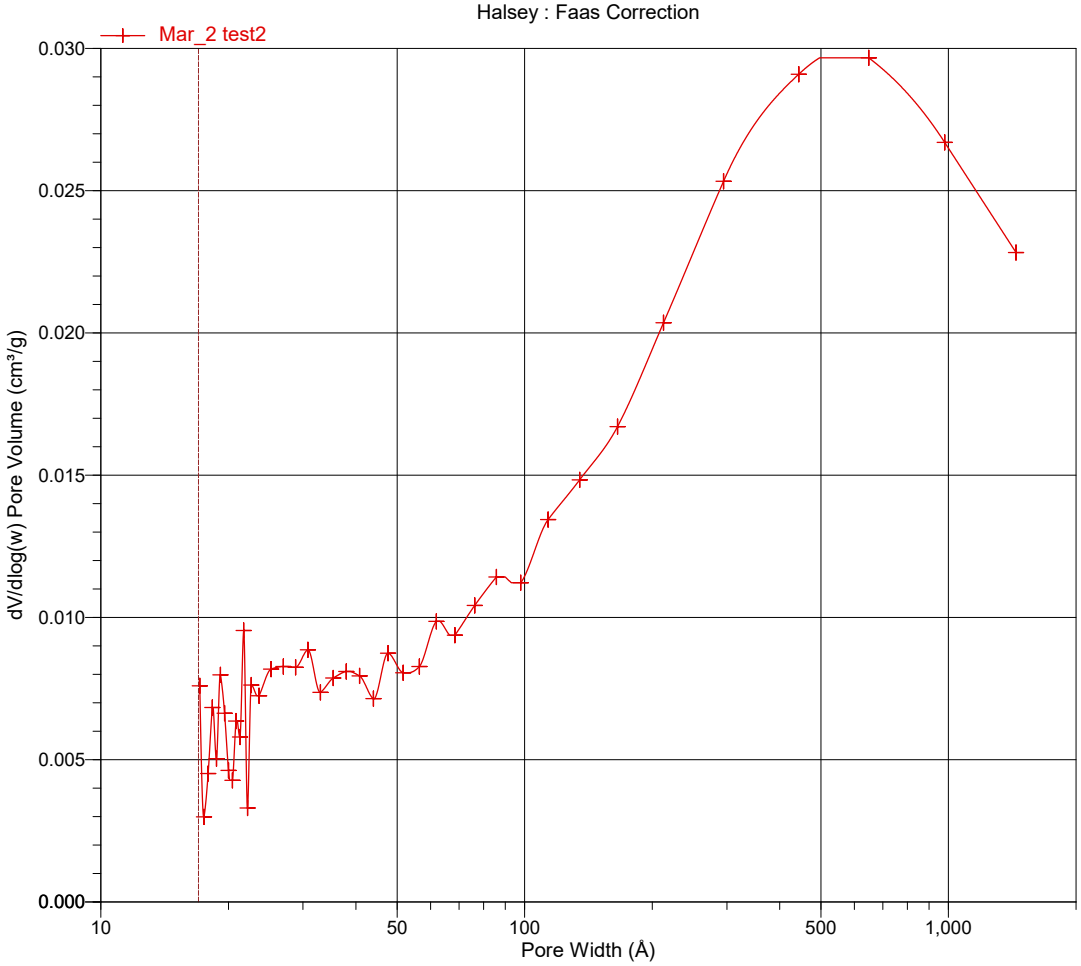

Sample: NO-12 (2)
Operator: Maria Olsvik
Submitter:
File: C:\...\MARIAO~1\000-330.SMP

Started:	08.03.2018 10:54:39	Analysis Adsorptive:	N2
Completed:	08.03.2018 13:46:24	Analysis Bath Temp.:	-195.850 °C
Report Time:	09.03.2018 9:27:35	Sample Mass:	0.0639 g
Warm Free Space:	10.3687 cm^3 Measured	Cold Free Space:	31.4272 cm^3 Measured
Equilibration Interval:	5 s	Low Pressure Dose:	None
Sample Density:	1.000 g/cm^3	Automatic Degas:	No

Summary Report

Surface Area

Single point surface area at P/Po = 0.200907892: 8.4766 m^2/g

BJH Desorption cumulative surface area of pores between 1.7000 nm and 300.0000 nm diameter: 7.0222 m^2/g

Pore Volume

Single point adsorption total pore volume of pores less than 126.2374 nm diameter at P/Po = 0.984423924: 0.024345 cm^3/g

BJH Desorption cumulative volume of pores between 1.7000 nm and 300.0000 nm diameter: 0.028661 cm^3/g

Pore Size

Adsorption average pore width (4V/A by BET): 11.40685 nm

BJH Desorption average pore diameter (4V/A): 16.3260 nm

Sample: NO-12 (2)
Operator: Maria Olsvik
Submitter:
File: C:\...\MARIAO~1\000-330.SMP

Started:	08.03.2018 10:54:39	Analysis Adsorptive:	N2
Completed:	08.03.2018 13:46:24	Analysis Bath Temp.:	-195.850 °C
Report Time:	09.03.2018 9:27:35	Sample Mass:	0.0639 g
Warm Free Space:	10.3687 cm³ Measured	Cold Free Space:	31.4272 cm³ Measured
Equilibration Interval:	5 s	Low Pressure Dose:	None
Sample Density:	1.000 g/cm³	Automatic Degas:	No

Isotherm Linear Plot

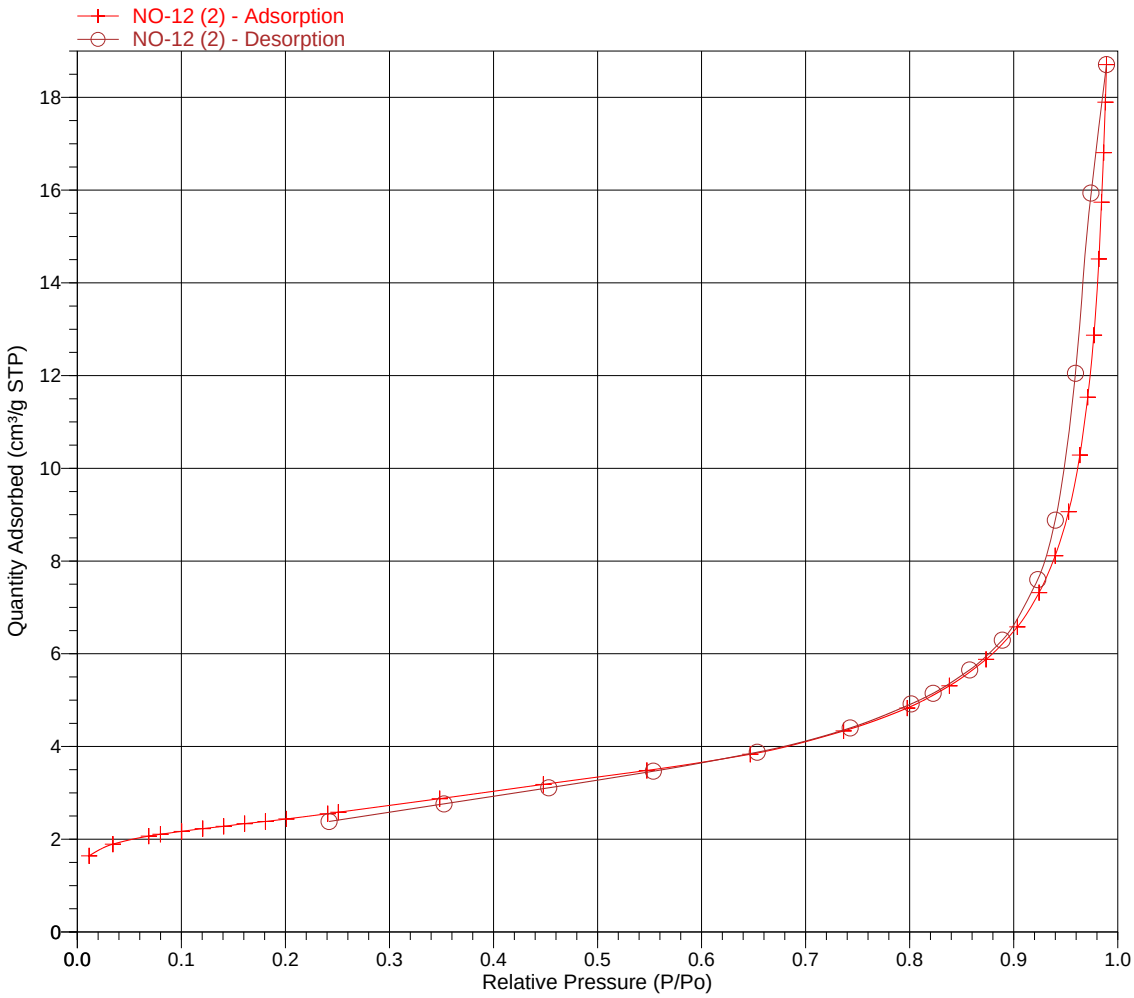

Sample: NO-12 (2)
Operator: Maria Olsvik
Submitter:
File: C:\...\MARIAO~1\000-330.SMP

Started:	08.03.2018 10:54:39	Analysis Adsorptive:	N2
Completed:	08.03.2018 13:46:24	Analysis Bath Temp.:	-195.850 °C
Report Time:	09.03.2018 9:27:35	Sample Mass:	0.0639 g
Warm Free Space:	10.3687 cm³ Measured	Cold Free Space:	31.4272 cm³ Measured
Equilibration Interval:	5 s	Low Pressure Dose:	None
Sample Density:	1.000 g/cm³	Automatic Degas:	No

BJH Adsorption dV/dlog(D) Pore Volume

Halsey : Faas Correction

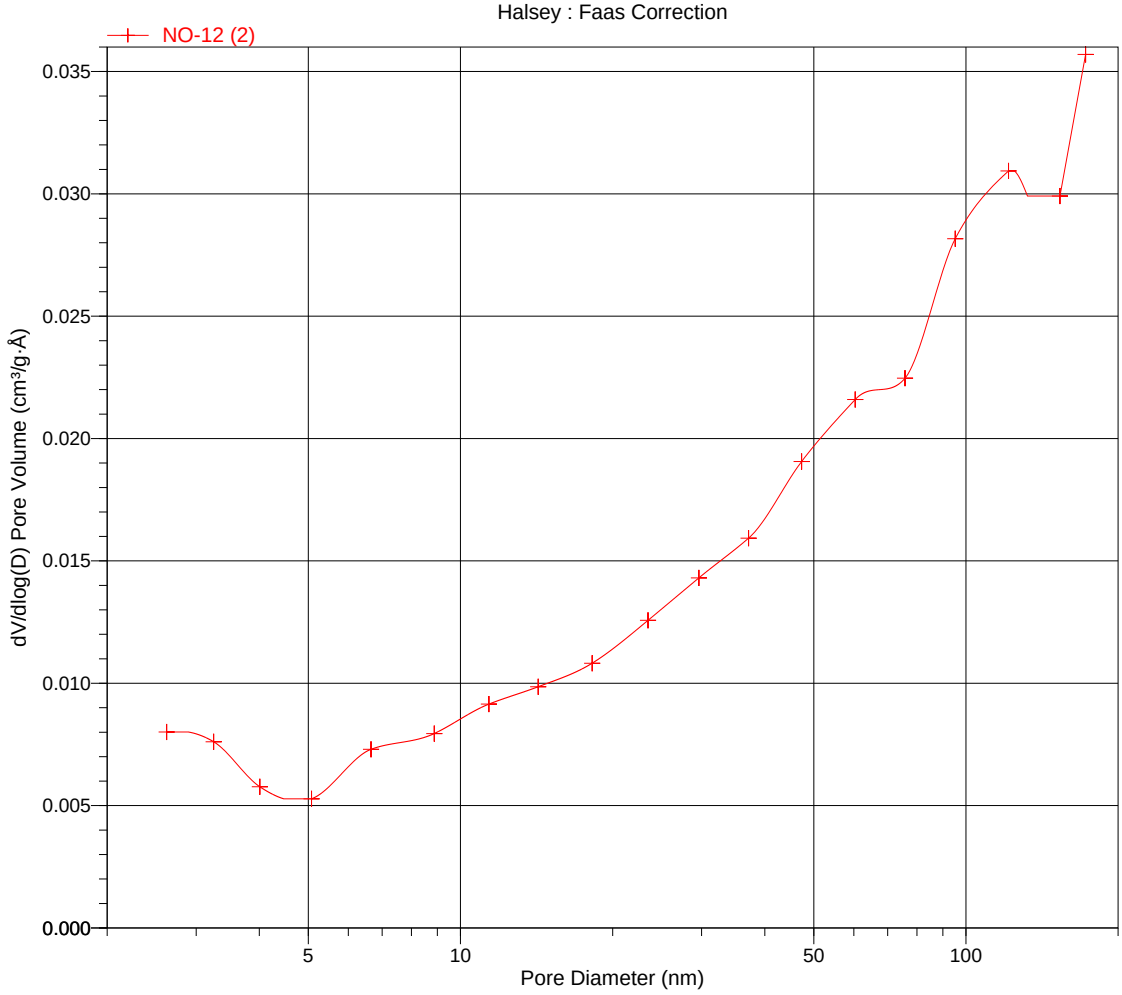

Sample: NO12
Operator: Maria Olsvik
Submitter:
File: C:\...\MARIAO~1\000-325.SMP

Started:	07.03.2018 14:17:21	Analysis Adsorptive:	N2
Completed:	07.03.2018 16:12:38	Analysis Bath Temp.:	-195.850 °C
Report Time:	08.03.2018 7:27:03	Sample Mass:	0.0791 g
Warm Free Space:	10.5044 cm³ Measured	Cold Free Space:	32.2802 cm³ Measured
Equilibration Interval:	5 s	Low Pressure Dose:	None
Sample Density:	1.000 g/cm³	Automatic Degas:	No

Summary Report

Surface Area

Single point surface area at P/Po = 0.199865491: 8.6066 m²/g

BJH Desorption cumulative surface area of pores between 1.7000 nm and 300.0000 nm diameter: 4.7778 m²/g

Pore Volume

Single point adsorption total pore volume of pores less than 121.5642 nm diameter at P/Po = 0.983813964: 0.023360 cm³/g

BJH Desorption cumulative volume of pores between 1.7000 nm and 300.0000 nm diameter: 0.026914 cm³/g

Pore Size

Adsorption average pore width (4V/A by BET): 10.99851 nm

BJH Desorption average pore diameter (4V/A): 22.5322 nm

Sample: NO12
Operator: Maria Olsvik
Submitter:
File: C:\...\MARIAO~1\000-325.SMP

Started:	07.03.2018 14:17:21	Analysis Adsorptive:	N2
Completed:	07.03.2018 16:12:38	Analysis Bath Temp.:	-195.850 °C
Report Time:	08.03.2018 7:27:03	Sample Mass:	0.0791 g
Warm Free Space:	10.5044 cm³ Measured	Cold Free Space:	32.2802 cm³ Measured
Equilibration Interval:	5 s	Low Pressure Dose:	None
Sample Density:	1.000 g/cm³	Automatic Degas:	No

Isotherm Linear Plot

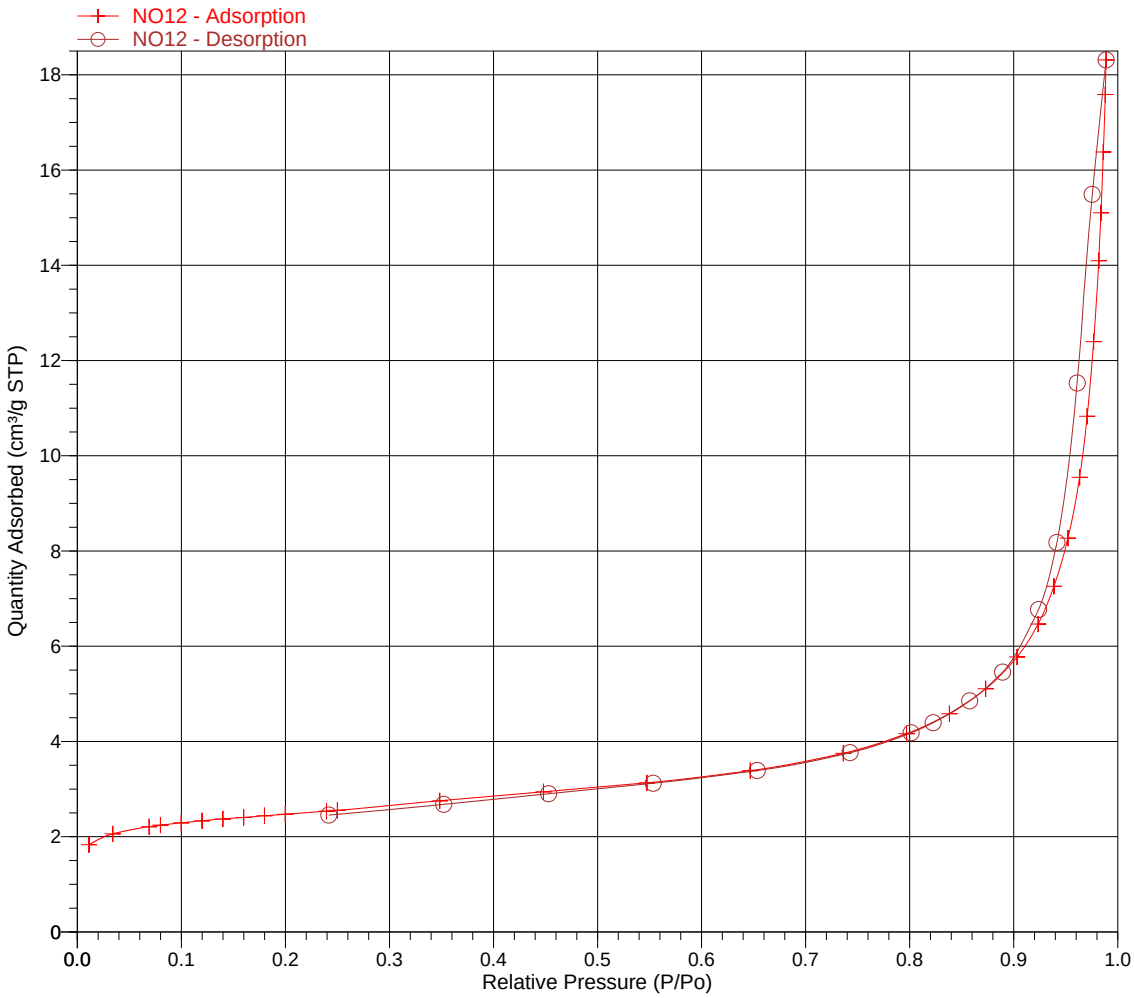

Sample: NO12
Operator: Maria Olsvik
Submitter:
File: C:\...\MARIAO~1\000-325.SMP

Started:	07.03.2018 14:17:21	Analysis Adsorptive:	N2
Completed:	07.03.2018 16:12:38	Analysis Bath Temp.:	-195.850 °C
Report Time:	08.03.2018 7:27:03	Sample Mass:	0.0791 g
Warm Free Space:	10.5044 cm³ Measured	Cold Free Space:	32.2802 cm³ Measured
Equilibration Interval:	5 s	Low Pressure Dose:	None
Sample Density:	1.000 g/cm³	Automatic Degas:	No

BJH Adsorption dV/dlog(D) Pore Volume

Halsey : Faas Correction

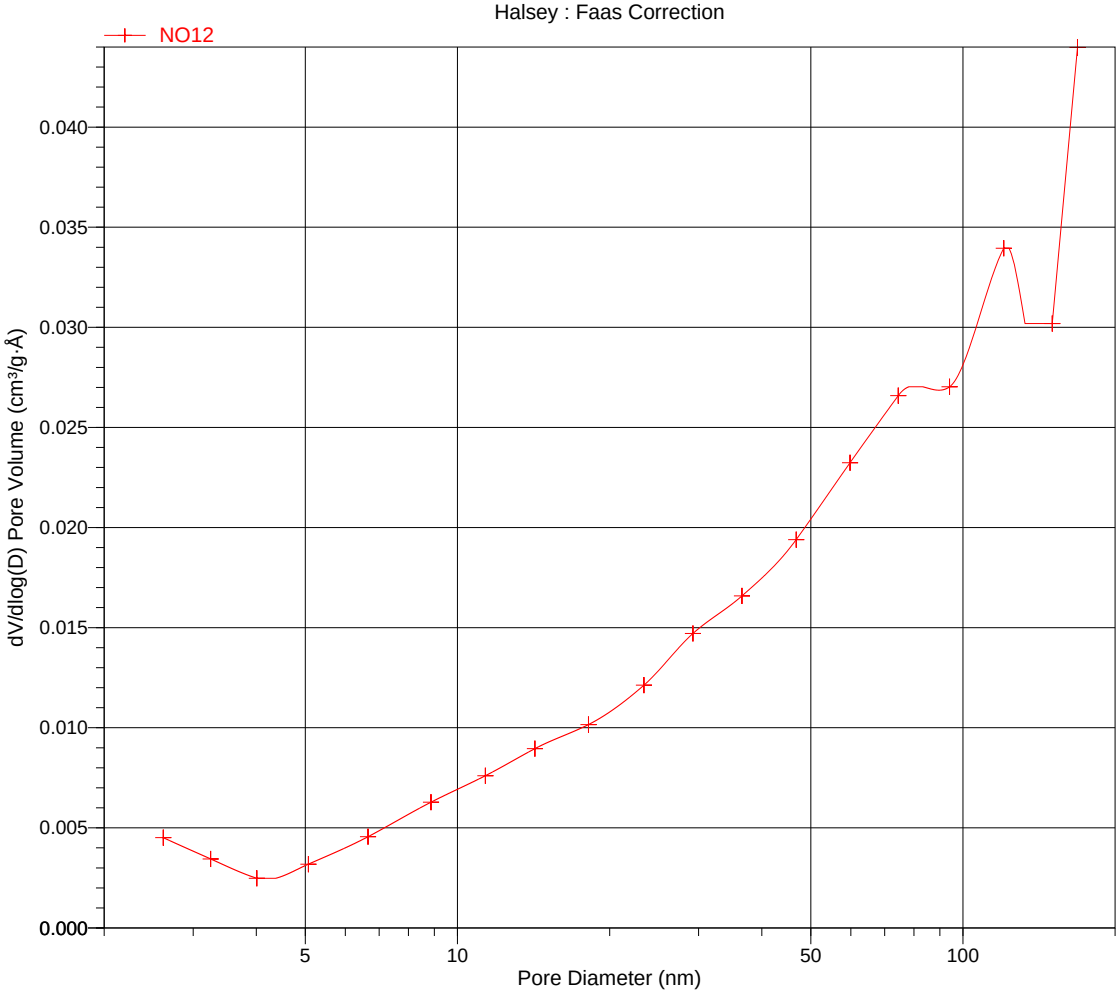

Sample: NO12
Operator: Maria Olsvik
Submitter:
File: C:\...\ANELIL~1\000-321.SMP

Started:	07.03.2018 9:38:14	Analysis Adsorptive:	N2
Completed:	07.03.2018 12:00:54	Analysis Bath Temp.:	-195.850 °C
Report Time:	07.03.2018 13:58:40	Sample Mass:	0.0796 g
Warm Free Space:	10.5110 cm^3 Measured	Cold Free Space:	32.1735 cm^3 Measured
Equilibration Interval:	5 s	Low Pressure Dose:	None
Sample Density:	1.000 g/cm^3	Automatic Degas:	No

Summary Report

Surface Area

Single point surface area at P/Po = 0.200762202: 9.2464 m^2/g

BJH Desorption cumulative surface area of pores between 1.7000 nm and 300.0000 nm diameter: 5.8845 m^2/g

Pore Volume

Single point adsorption total pore volume of pores less than 124.2255 nm diameter at P/Po = 0.984167025: 0.021946 cm^3/g

BJH Desorption cumulative volume of pores between 1.7000 nm and 300.0000 nm diameter: 0.023886 cm^3/g

Pore Size

Adsorption average pore width (4V/A by BET): 9.42653 nm

BJH Desorption average pore diameter (4V/A): 16.2368 nm

Sample: NO12
Operator: Maria Olsvik
Submitter:
File: C:\...\ANELIL~1\000-321.SMP

Started:	07.03.2018 9:38:14	Analysis Adsorptive:	N2
Completed:	07.03.2018 12:00:54	Analysis Bath Temp.:	-195.850 °C
Report Time:	07.03.2018 13:58:40	Sample Mass:	0.0796 g
Warm Free Space:	10.5110 cm³ Measured	Cold Free Space:	32.1735 cm³ Measured
Equilibration Interval:	5 s	Low Pressure Dose:	None
Sample Density:	1.000 g/cm³	Automatic Degas:	No

Isotherm Linear Plot

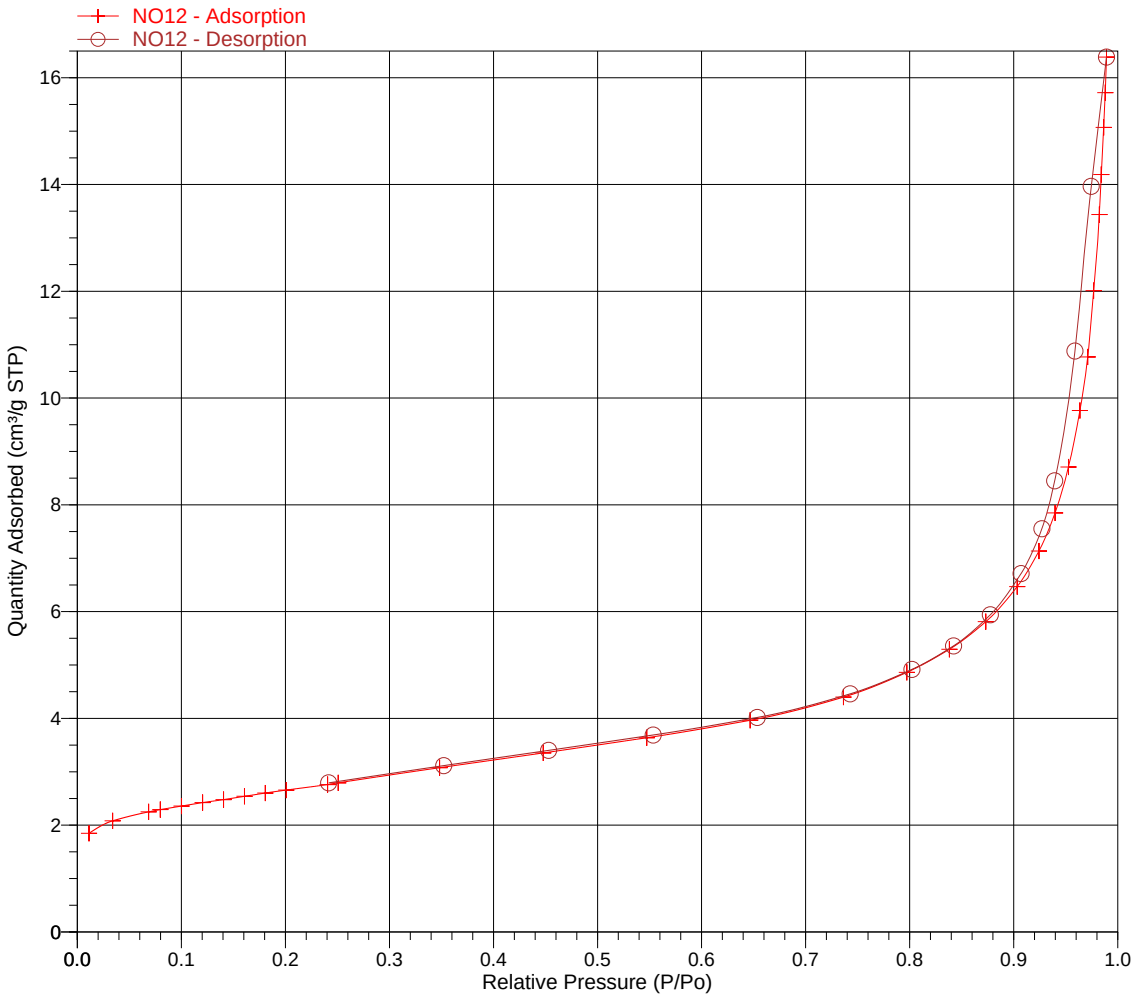

Sample: NO12
Operator: Maria Olsvik
Submitter:
File: C:\...\ANELIL~1\000-321.SMP

Started:	07.03.2018 9:38:14	Analysis Adsorptive:	N2
Completed:	07.03.2018 12:00:54	Analysis Bath Temp.:	-195.850 °C
Report Time:	07.03.2018 13:58:40	Sample Mass:	0.0796 g
Warm Free Space:	10.5110 cm³ Measured	Cold Free Space:	32.1735 cm³ Measured
Equilibration Interval:	5 s	Low Pressure Dose:	None
Sample Density:	1.000 g/cm³	Automatic Degas:	No

BJH Adsorption dV/dlog(D) Pore Volume

Halsey : Faas Correction

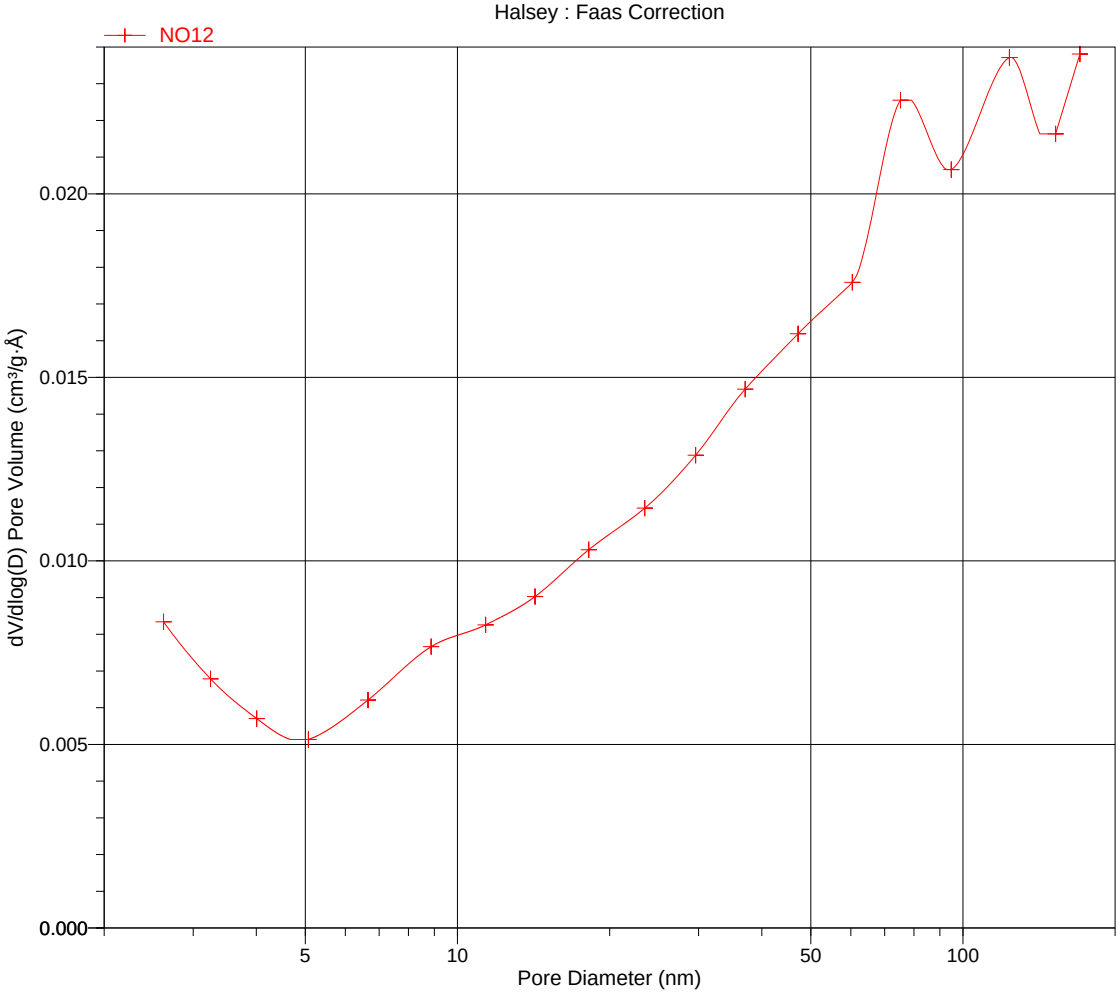

Full Report Set

Sample: NO-20
Operator: Maria Olsvik
File: C:\TriStar II 3020\data\Maria Olsvik\NO-20.SMP

Started:	27.03.2018 19:44:43	Analysis Adsorptive:	N2
Completed:	28.03.2018 01:50:55	Analysis Bath Temp.:	-195,850 °C
Report Time:	28.03.2018 08:27:36	Thermal Correction:	No
Sample Mass:	0,0898 g	Warm Free Space:	10,3704 cm³ Measured
Cold Free Space:	31,3692 cm³	Equilibration Interval:	10 s
Low Pressure Dose:	None	Sample Density:	1,000 g/cm³
Automatic Degas:	No		

Summary Report

Surface Area

Single point surface area at p/p° = 0,249990307:	0,8996 m²/g
BET Surface Area:	0,8375 m²/g
t-Plot Micropore Area:	0,6052 m²/g
t-Plot External Surface Area:	0,2323 m²/g
BJH Adsorption cumulative surface area of pores between 17,000 Å and 3 000,000 Å width:	0.536 m²/g
BJH Desorption cumulative surface area of pores between 17,000 Å and 3 000,000 Å width:	0,8495 m²/g

Pore Volume

t-Plot micropore volume:	0,000323 cm³/g
BJH Adsorption cumulative volume of pores between 17,000 Å and 3 000,000 Å width:	0,002274 cm³/g
BJH Desorption cumulative volume of pores between 17,000 Å and 3 000,000 Å width:	0,002534 cm³/g

Pore Size

BJH Adsorption average pore width (4V/A):	169,816 Å
BJH Desorption average pore width (4V/A):	119,328 Å

DFT Pore Size

Volume in Pores	<	10,22 Å	:	0,00036 cm³/g
Total Volume in Pores	<=	448,83 Å	:	0,00206 cm³/g
Total Area in Pores	>=	10,22 Å	:	0,281 m²/g

Nanoparticle Size:

Average Particle Size 71 641,663 Å

Sample: NO-20
Operator: Maria Olsvik
File: C:\TriStar II 3020\data\Maria Olsvik\NO-20.SMP

Started:	27.03.2018 19:44:43	Analysis Adsorptive:	N2
Completed:	28.03.2018 01:50:55	Analysis Bath Temp.:	-195,850 °C
Report Time:	28.03.2018 08:27:36	Thermal Correction:	No
Sample Mass:	0,0898 g	Warm Free Space:	10,3704 cm³ Measured
Cold Free Space:	31,3692 cm³	Equilibration Interval:	10 s
Low Pressure Dose:	None	Sample Density:	1,000 g/cm³
Automatic Degas:	No		

Isotherm Linear Plot

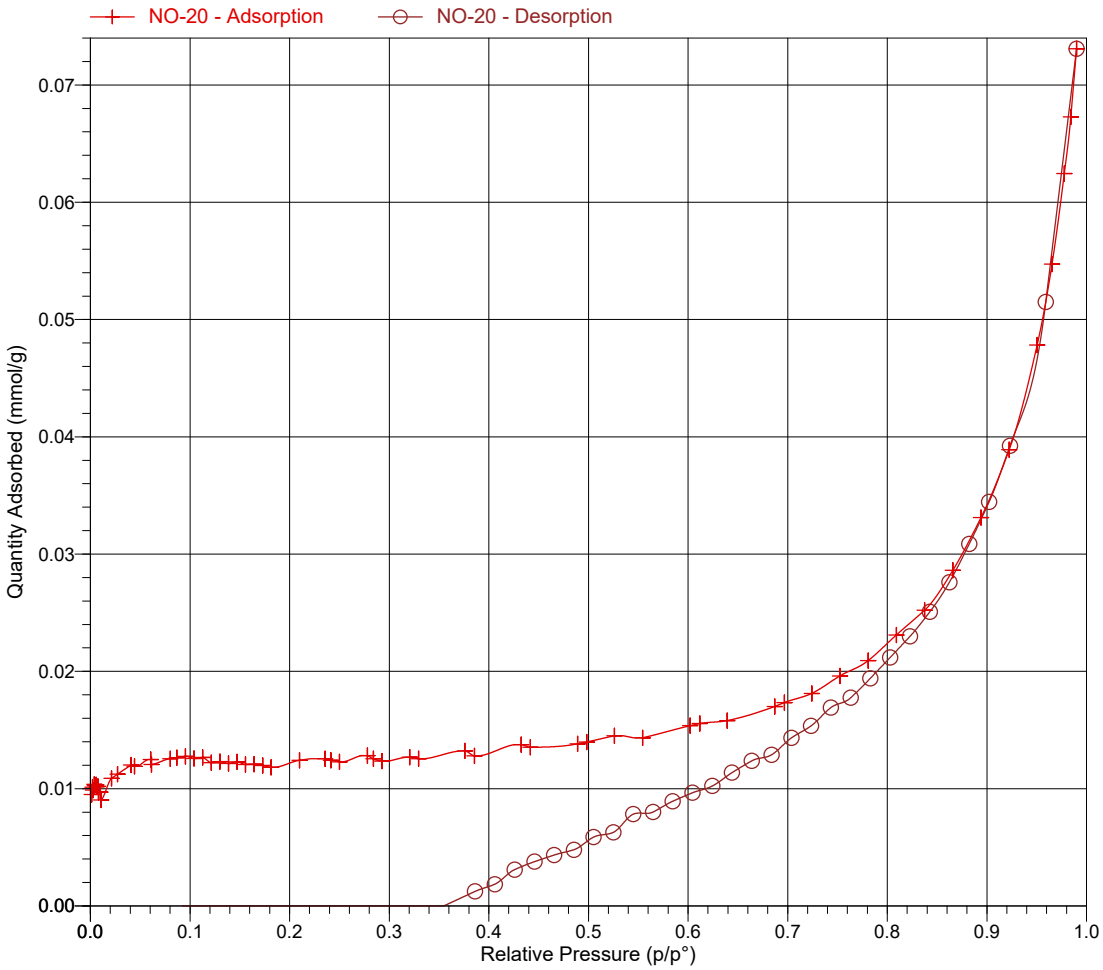

Sample: NO-20
Operator: Maria Olsvik
File: C:\TriStar II 3020\data\Maria Olsvik\NO-20.SMP

Started:	27.03.2018 19:44:43	Analysis Adsorptive:	N2
Completed:	28.03.2018 01:50:55	Analysis Bath Temp.:	-195,850 °C
Report Time:	28.03.2018 08:27:36	Thermal Correction:	No
Sample Mass:	0,0898 g	Warm Free Space:	10,3704 cm³ Measured
Cold Free Space:	31,3692 cm³	Equilibration Interval:	10 s
Low Pressure Dose:	None	Sample Density:	1,000 g/cm³
Automatic Degas:	No		

BJH Adsorption dV/dlog(w) Pore Volume

Halsey : Faas Correction

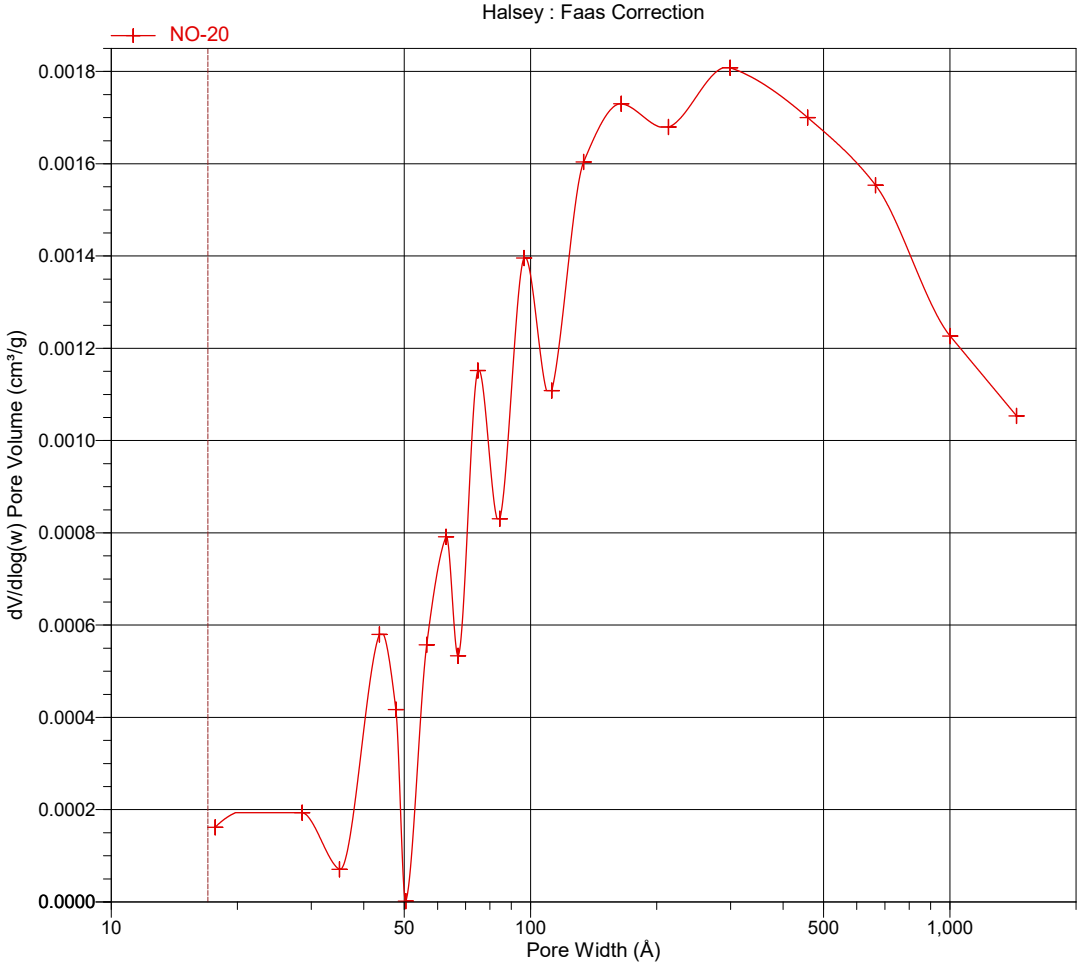

Full Report Set

Sample: NO-20 test2
Operator: maria olsvik
Submitter:
File: C:\TriStar II 3020\data\Maria Olsvik\NO-20 test2.SMP

Started:	05.04.2018 18:22:35	Analysis Adsorptive:	N2
Completed:	05.04.2018 20:00:47	Analysis Bath Temp.:	-195,850 °C
Report Time:	06.04.2018 10:14:07	Thermal Correction:	No
Sample Mass:	0,0743 g	Warm Free Space:	10,1156 cm³ Measured
Cold Free Space:	30,6678 cm³	Equilibration Interval:	5 s
Low Pressure Dose:	None	Sample Density:	1,000 g/cm³
Automatic Degas:	No		

Summary Report

Surface Area

Single point surface area at p/p° = 0,200333964: 1,8273 m²/g

BJH Desorption cumulative surface area of pores between 17,000 Å and 3 000,000 Å width: 0,3199 m²/g

Pore Volume

Single point adsorption total pore volume of pores less than 1 226,495 Å width at p/p° = 0,983959817: 0,002577 cm³/g

BJH Desorption cumulative volume of pores between 17,000 Å and 3 000,000 Å width: 0,003221 cm³/g

Pore Size

Adsorption average pore diameter (4V/A by BET): 59,5576 Å

BJH Desorption average pore width (4V/A): 402,753 Å

Sample: NO-20 test2
Operator: maria olsvik
Submitter:
File: C:\TriStar II 3020\data\Maria Olsvik\NO-20 test2.SMP

Started:	05.04.2018 18:22:35	Analysis Adsorptive:	N2
Completed:	05.04.2018 20:00:47	Analysis Bath Temp.:	-195,850 °C
Report Time:	06.04.2018 10:14:07	Thermal Correction:	No
Sample Mass:	0,0743 g	Warm Free Space:	10,1156 cm³ Measured
Cold Free Space:	30,6678 cm³	Equilibration Interval:	5 s
Low Pressure Dose:	None	Sample Density:	1,000 g/cm³
Automatic Degas:	No		

Isotherm Linear Plot

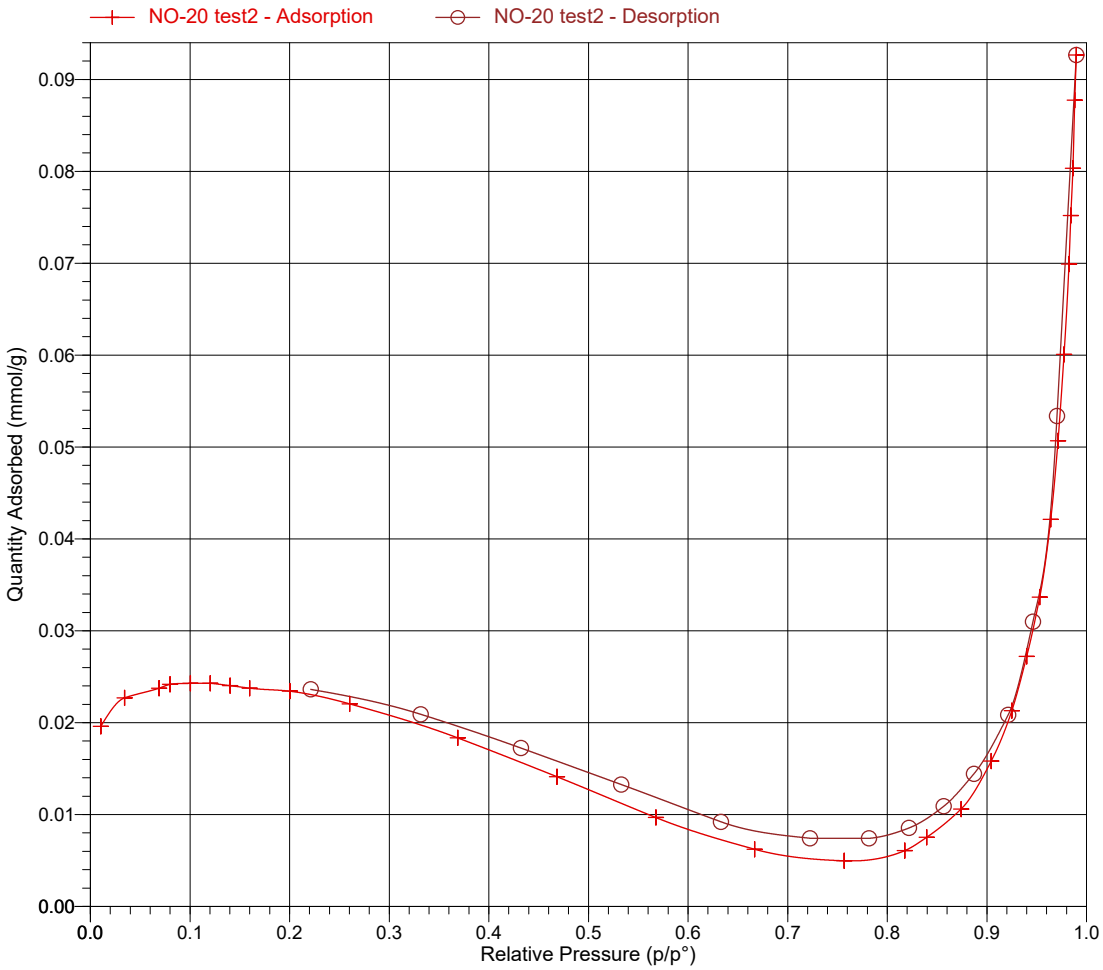

Sample: NO-20 test2
Operator: maria olsvik
Submitter:
File: C:\TriStar II 3020\data\Maria Olsvik\NO-20 test2.SMP

Started:	05.04.2018 18:22:35	Analysis Adsorptive:	N2
Completed:	05.04.2018 20:00:47	Analysis Bath Temp.:	-195,850 °C
Report Time:	06.04.2018 10:14:07	Thermal Correction:	No
Sample Mass:	0,0743 g	Warm Free Space:	10,1156 cm³ Measured
Cold Free Space:	30,6678 cm³	Equilibration Interval:	5 s
Low Pressure Dose:	None	Sample Density:	1,000 g/cm³
Automatic Degas:	No		

BJH Adsorption dV/dlog(w) Pore Volume

Halsey : Faas Correction

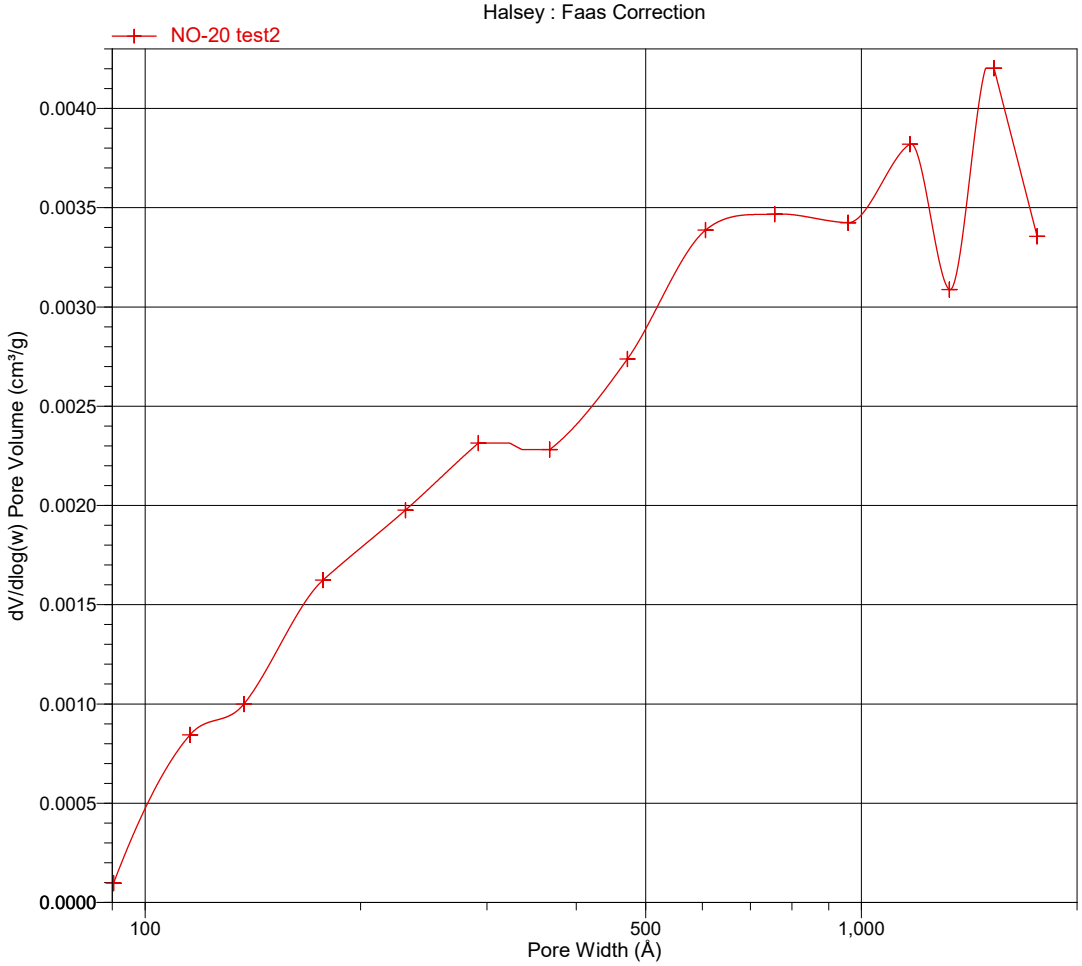

Full Report Set

Sample: NO-21
Operator: Maria Olsvik
File: C:\TriStar II 3020\data\Maria Olsvik\NO-21.SMP

Started:	27.03.2018 13:10:11	Analysis Adsorptive:	N2
Completed:	27.03.2018 18:49:52	Analysis Bath Temp.:	-195,850 °C
Report Time:	27.03.2018 19:37:40	Thermal Correction:	No
Sample Mass:	0,0781 g	Warm Free Space:	10,6379 cm³ Measured
Cold Free Space:	32,5513 cm³	Equilibration Interval:	10 s
Low Pressure Dose:	None	Sample Density:	1,000 g/cm³
Automatic Degas:	No		

Summary Report

Surface Area

Single point surface area at p/p° = 0,260662077:	0,0603 m²/g
BET Surface Area:	0,0607 m²/g
t-Plot Micropore Area:	1,5779 m²/g
t-Plot External Surface Area:	-1,5172 m²/g
BJH Adsorption cumulative surface area of pores between 17,000 Å and 3 000,000 Å width:	0.073 m²/g
BJH Desorption cumulative surface area of pores between 17,000 Å and 3 000,000 Å width:	0,1750 m²/g

Pore Volume

t-Plot micropore volume:	0,000751 cm³/g
BJH Adsorption cumulative volume of pores between 17,000 Å and 3 000,000 Å width:	0,001313 cm³/g
BJH Desorption cumulative volume of pores between 17,000 Å and 3 000,000 Å width:	0,001628 cm³/g

Pore Size

BJH Adsorption average pore width (4V/A):	718,573 Å
BJH Desorption average pore width (4V/A):	372,082 Å

DFT Pore Size

Volume in Pores	<	10,22 Å	:	0,00006 cm³/g
Total Volume in Pores	<=	448,83 Å	:	0,00098 cm³/g
Total Area in Pores	>=	10,22 Å	:	0,090 m²/g

Nanoparticle Size:

Average Particle Size 988 651,919 Å

Sample: NO-21
Operator: Maria Olsvik
File: C:\TriStar II 3020\data\Maria Olsvik\NO-21.SMP

Started:	27.03.2018 13:10:11	Analysis Adsorptive:	N2
Completed:	27.03.2018 18:49:52	Analysis Bath Temp.:	-195,850 °C
Report Time:	27.03.2018 19:37:40	Thermal Correction:	No
Sample Mass:	0,0781 g	Warm Free Space:	10,6379 cm³ Measured
Cold Free Space:	32,5513 cm³	Equilibration Interval:	10 s
Low Pressure Dose:	None	Sample Density:	1,000 g/cm³
Automatic Degas:	No		

Isotherm Linear Plot

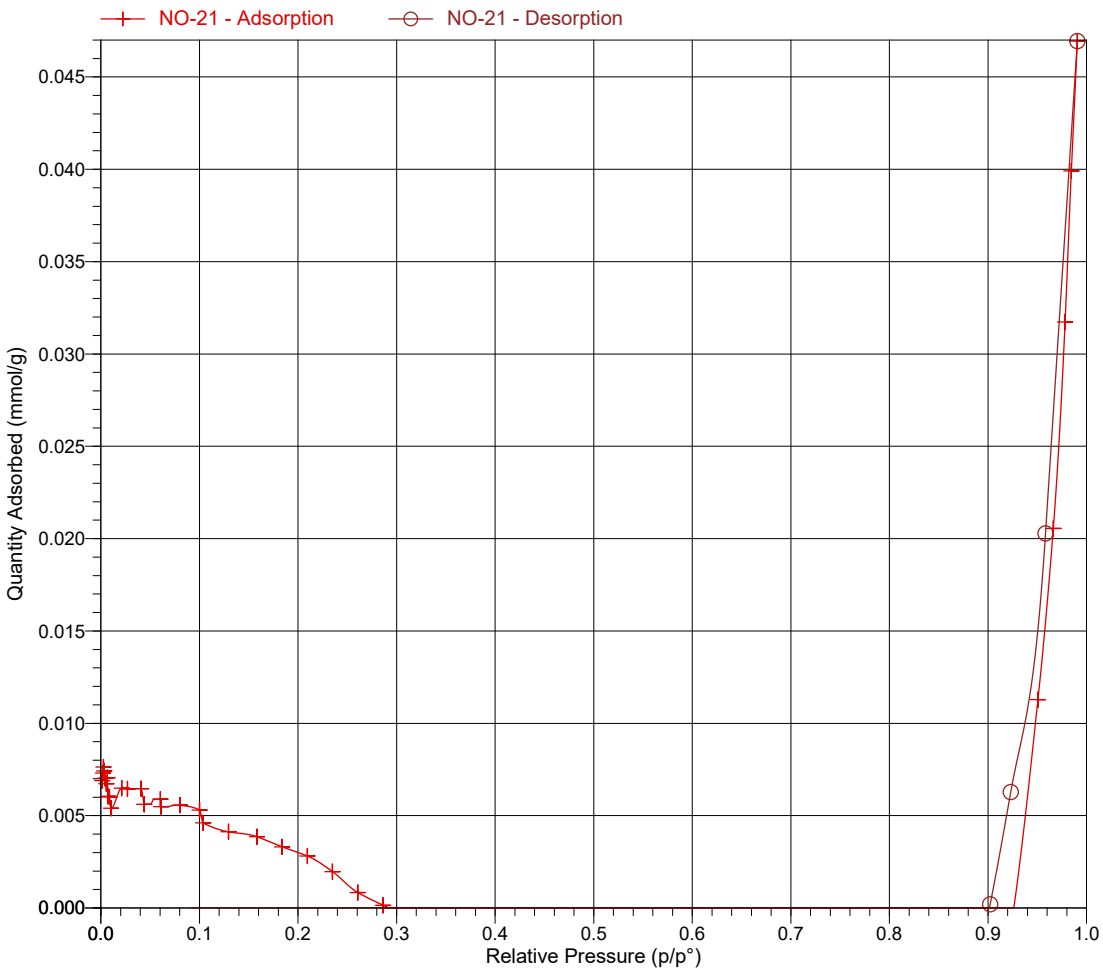

Sample: NO-21
Operator: Maria Olsvik
File: C:\TriStar II 3020\data\Maria Olsvik\NO-21.SMP

Started:	27.03.2018 13:10:11	Analysis Adsorptive:	N2
Completed:	27.03.2018 18:49:52	Analysis Bath Temp.:	-195,850 °C
Report Time:	27.03.2018 19:37:40	Thermal Correction:	No
Sample Mass:	0,0781 g	Warm Free Space:	10,6379 cm³ Measured
Cold Free Space:	32,5513 cm³	Equilibration Interval:	10 s
Low Pressure Dose:	None	Sample Density:	1,000 g/cm³
Automatic Degas:	No		

BJH Adsorption dV/dlog(w) Pore Volume

Halsey : Faas Correction

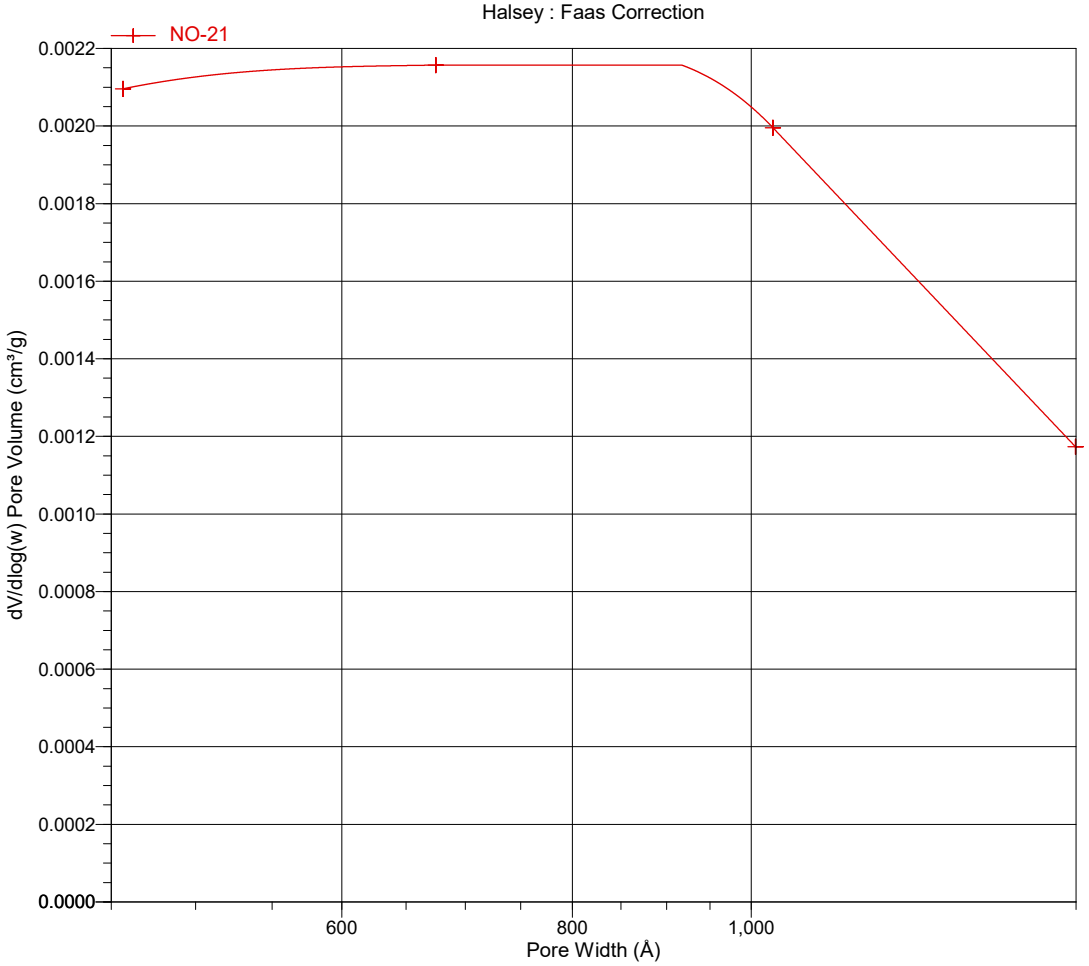

Full Report Set

Sample: NO-21 test2
Operator: maria olsvik
Submitter:
File: C:\TriStar II 3020\data\Maria Olsvik\NO-21 test2.SMP

Started:	05.04.2018 18:22:35	Analysis Adsorptive:	N2
Completed:	05.04.2018 20:00:47	Analysis Bath Temp.:	-195,850 °C
Report Time:	06.04.2018 10:15:56	Thermal Correction:	No
Sample Mass:	0,0709 g	Warm Free Space:	10,0335 cm³ Measured
Cold Free Space:	30,3337 cm³	Equilibration Interval:	5 s
Low Pressure Dose:	None	Sample Density:	1,000 g/cm³
Automatic Degas:	No		

Summary Report

Surface Area

Single point surface area at p/p° = 0,200972657: 0,8742 m²/g

BJH Desorption cumulative surface area of pores between 17,000 Å and 3 000,000 Å width: 0,3723 m²/g

Pore Volume

Single point adsorption total pore volume of pores less than 1 226,495 Å width at p/p° = 0,983959817: 0,002698 cm³/g

BJH Desorption cumulative volume of pores between 17,000 Å and 3 000,000 Å width: 0,003178 cm³/g

Pore Size

Adsorption average pore diameter (4V/A by BET): 134,5592 Å

BJH Desorption average pore width (4V/A): 341,474 Å

Sample: NO-21 test2
Operator: maria olsvik
Submitter:
File: C:\TriStar II 3020\data\Maria Olsvik\NO-21 test2.SMP

Started:	05.04.2018 18:22:35	Analysis Adsorptive:	N2
Completed:	05.04.2018 20:00:47	Analysis Bath Temp.:	-195,850 °C
Report Time:	06.04.2018 10:15:56	Thermal Correction:	No
Sample Mass:	0,0709 g	Warm Free Space:	10,0335 cm³ Measured
Cold Free Space:	30,3337 cm³	Equilibration Interval:	5 s
Low Pressure Dose:	None	Sample Density:	1,000 g/cm³
Automatic Degas:	No		

Isotherm Linear Plot

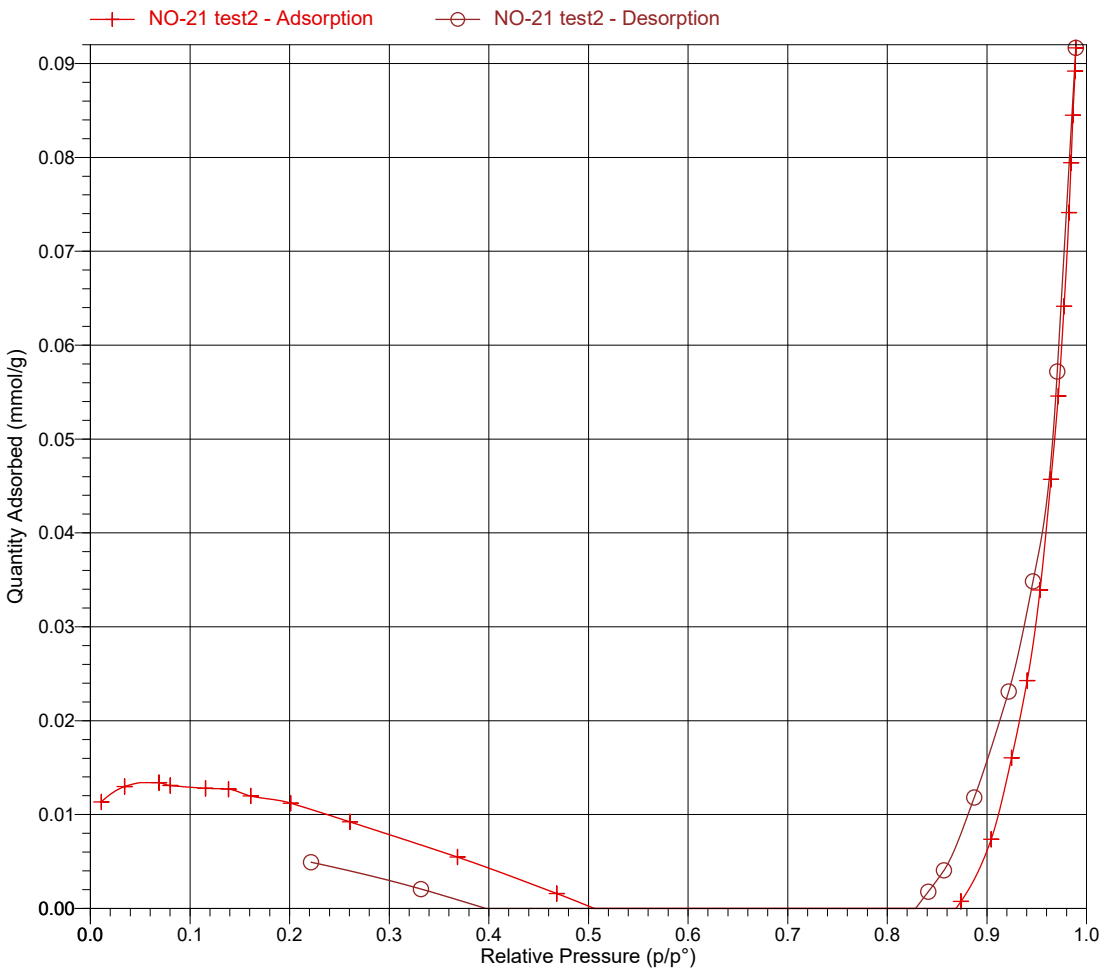

Sample: NO-21 test2
Operator: maria olsvik
Submitter:
File: C:\TriStar II 3020\data\Maria Olsvik\NO-21 test2.SMP

Started:	05.04.2018 18:22:35	Analysis Adsorptive:	N2
Completed:	05.04.2018 20:00:47	Analysis Bath Temp.:	-195,850 °C
Report Time:	06.04.2018 10:15:56	Thermal Correction:	No
Sample Mass:	0,0709 g	Warm Free Space:	10,0335 cm³ Measured
Cold Free Space:	30,3337 cm³	Equilibration Interval:	5 s
Low Pressure Dose:	None	Sample Density:	1,000 g/cm³
Automatic Degas:	No		

BJH Adsorption dV/dlog(w) Pore Volume

Halsey : Faas Correction

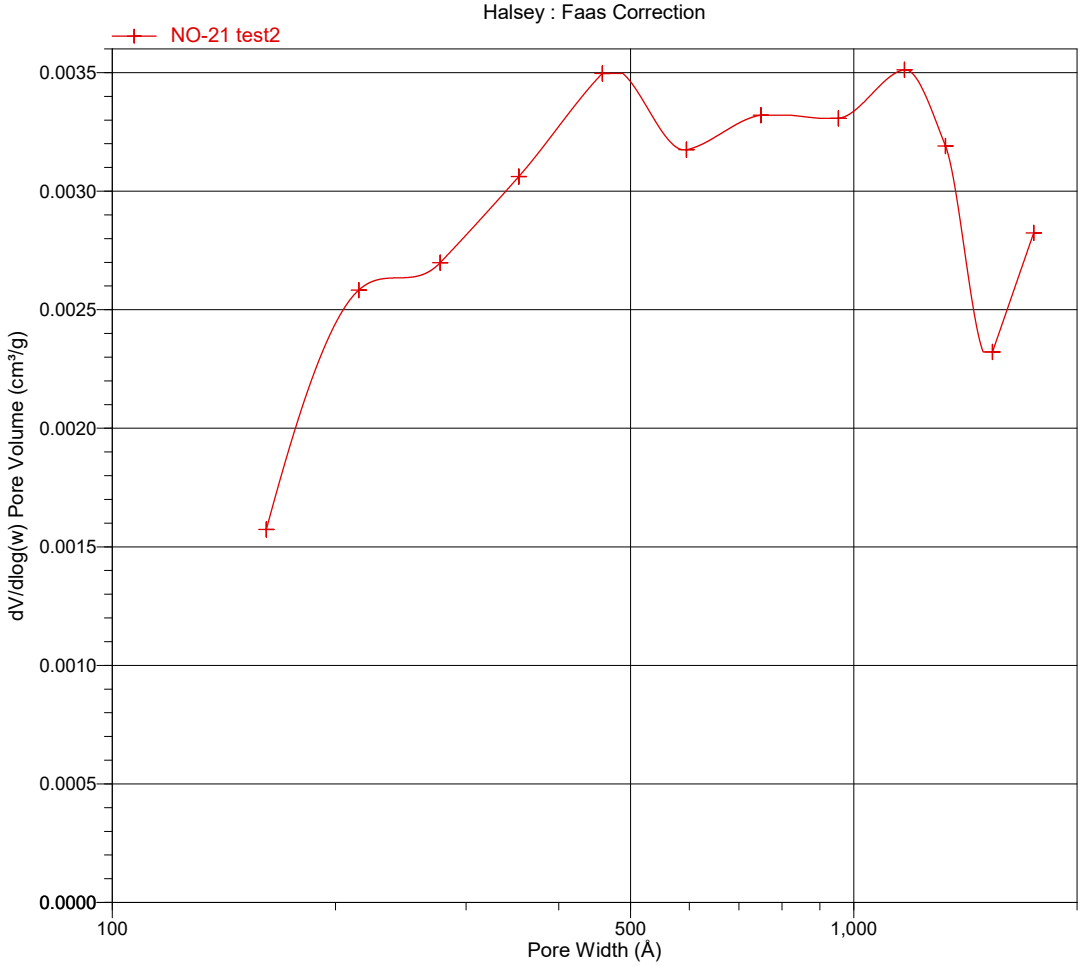

Full Report Set

Sample: NO-22
Operator: Maria Olsvik
File: C:\TriStar II 3020\data\Maria Olsvik\NO-22.SMP

Started:	27.03.2018 19:44:43	Analysis Adsorptive:	N2
Completed:	28.03.2018 01:50:55	Analysis Bath Temp.:	-195,850 °C
Report Time:	28.03.2018 08:28:09	Thermal Correction:	No
Sample Mass:	0,0849 g	Warm Free Space:	9,6642 cm³ Measured
Cold Free Space:	28,9447 cm³	Equilibration Interval:	10 s
Low Pressure Dose:	None	Sample Density:	1,000 g/cm³
Automatic Degas:	No		

Summary Report

Surface Area

Single point surface area at p/p° = 0,259922750:	1,7085 m²/g
BET Surface Area:	1,5658 m²/g
t-Plot Micropore Area:	2,0403 m²/g
t-Plot External Surface Area:	-0,4746 m²/g
BJH Adsorption cumulative surface area of pores between 17,000 Å and 3 000,000 Å width:	0.444 m²/g
BJH Desorption cumulative surface area of pores between 17,000 Å and 3 000,000 Å width:	0,7933 m²/g

Pore Volume

t-Plot micropore volume:	0,001027 cm³/g
BJH Adsorption cumulative volume of pores between 17,000 Å and 3 000,000 Å width:	0,002069 cm³/g
BJH Desorption cumulative volume of pores between 17,000 Å and 3 000,000 Å width:	0,002442 cm³/g

Pore Size

BJH Adsorption average pore width (4V/A):	186,207 Å
BJH Desorption average pore width (4V/A):	123,158 Å

DFT Pore Size

Volume in Pores	<	9,51 Å	:	0,00070 cm³/g
Total Volume in Pores	<=	448,83 Å	:	0,00222 cm³/g
Total Area in Pores	>=	9,51 Å	:	0,364 m²/g

Nanoparticle Size:

Average Particle Size	38 319,740 Å

Sample: NO-22
Operator: Maria Olsvik
File: C:\TriStar II 3020\data\Maria Olsvik\NO-22.SMP

Started:	27.03.2018 19:44:43	Analysis Adsorptive:	N2
Completed:	28.03.2018 01:50:55	Analysis Bath Temp.:	-195,850 °C
Report Time:	28.03.2018 08:28:09	Thermal Correction:	No
Sample Mass:	0,0849 g	Warm Free Space:	9,6642 cm³ Measured
Cold Free Space:	28,9447 cm³	Equilibration Interval:	10 s
Low Pressure Dose:	None	Sample Density:	1,000 g/cm³
Automatic Degas:	No		

Isotherm Linear Plot

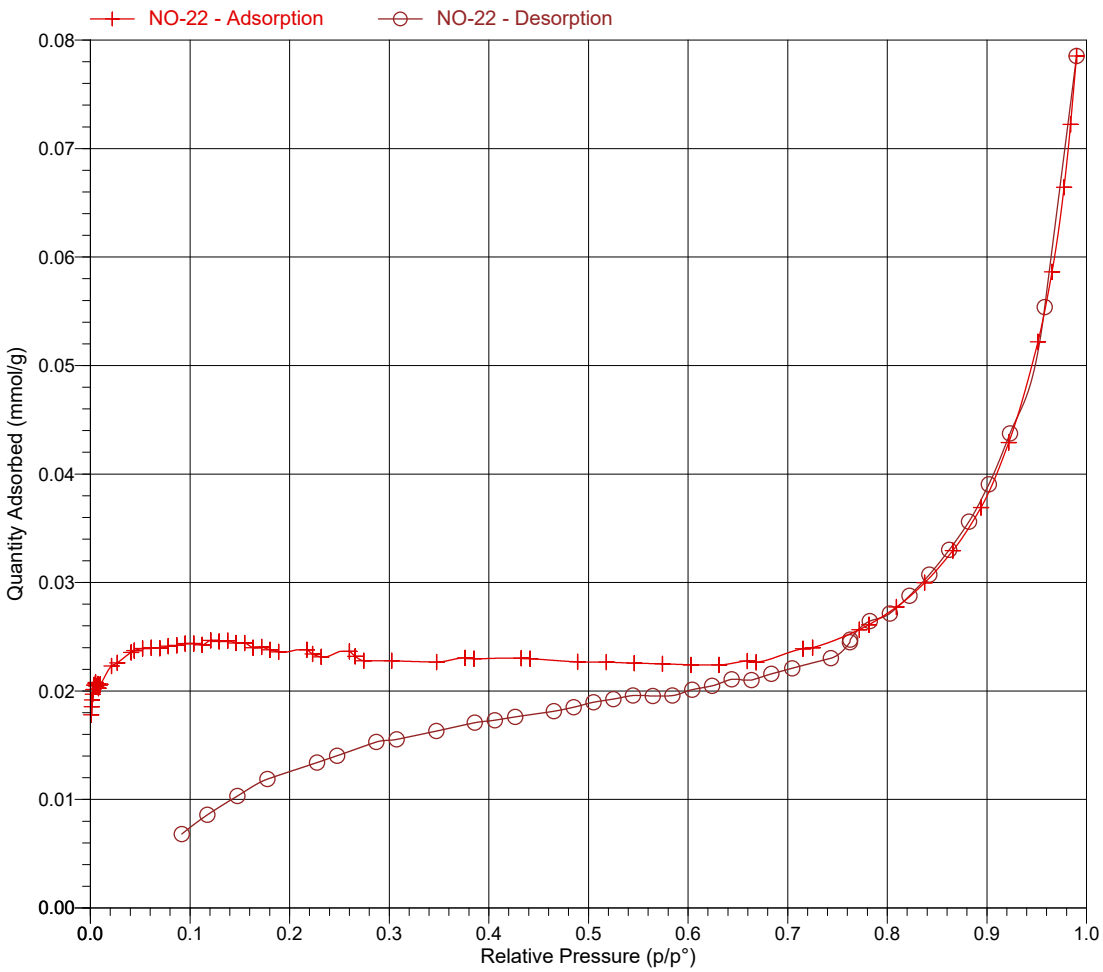

Sample: NO-22
Operator: Maria Olsvik
File: C:\TriStar II 3020\data\Maria Olsvik\NO-22.SMP

Started:	27.03.2018 19:44:43	Analysis Adsorptive:	N2
Completed:	28.03.2018 01:50:55	Analysis Bath Temp.:	-195,850 °C
Report Time:	28.03.2018 08:28:09	Thermal Correction:	No
Sample Mass:	0,0849 g	Warm Free Space:	9,6642 cm³ Measured
Cold Free Space:	28,9447 cm³	Equilibration Interval:	10 s
Low Pressure Dose:	None	Sample Density:	1,000 g/cm³
Automatic Degas:	No		

BJH Adsorption dV/dlog(w) Pore Volume

Halsey : Faas Correction

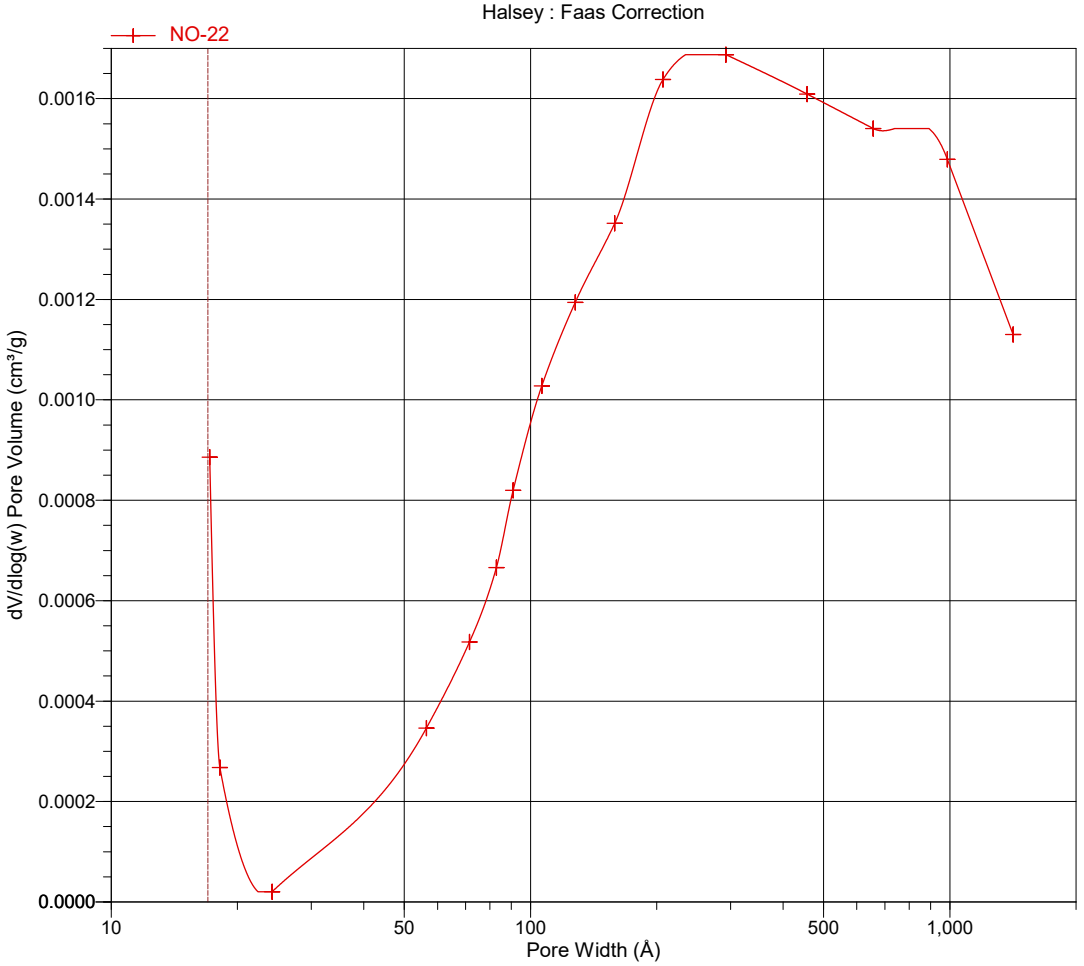

Full Report Set

Sample: NO-22 test2
Operator: maria olsvik
Submitter:
File: C:\TriStar II 3020\data\Maria Olsvik\NO-22 test2.SMP

Started:	05.04.2018 11:13:24	Analysis Adsorptive:	N2
Completed:	05.04.2018 13:23:19	Analysis Bath Temp.:	-195,850 °C
Report Time:	05.04.2018 18:17:28	Thermal Correction:	No
Sample Mass:	0,0885 g	Warm Free Space:	10,5032 cm³ Measured
Cold Free Space:	32,1829 cm³	Equilibration Interval:	5 s
Low Pressure Dose:	None	Sample Density:	1,000 g/cm³
Automatic Degas:	No		

Summary Report

Surface Area

Single point surface area at p/p° = 0,219761985: 1,8710 m²/g

BJH Desorption cumulative surface area of pores between 17,000 Å and 3 000,000 Å width: 0,3492 m²/g

Pore Volume

Single point adsorption total pore volume of pores less than 1 226,495 Å width at p/p° = 0,983959817: 0,002640 cm³/g

BJH Desorption cumulative volume of pores between 17,000 Å and 3 000,000 Å width: 0,003184 cm³/g

Pore Size

Adsorption average pore diameter (4V/A by BET): 59,2347 Å

BJH Desorption average pore width (4V/A): 364,778 Å

Sample: NO-22 test2
Operator: maria olsvik
Submitter:
File: C:\TriStar II 3020\data\Maria Olsvik\NO-22 test2.SMP

Started:	05.04.2018 11:13:24	Analysis Adsorptive:	N2
Completed:	05.04.2018 13:23:19	Analysis Bath Temp.:	-195,850 °C
Report Time:	05.04.2018 18:17:28	Thermal Correction:	No
Sample Mass:	0,0885 g	Warm Free Space:	10,5032 cm³ Measured
Cold Free Space:	32,1829 cm³	Equilibration Interval:	5 s
Low Pressure Dose:	None	Sample Density:	1,000 g/cm³
Automatic Degas:	No		

Isotherm Linear Plot

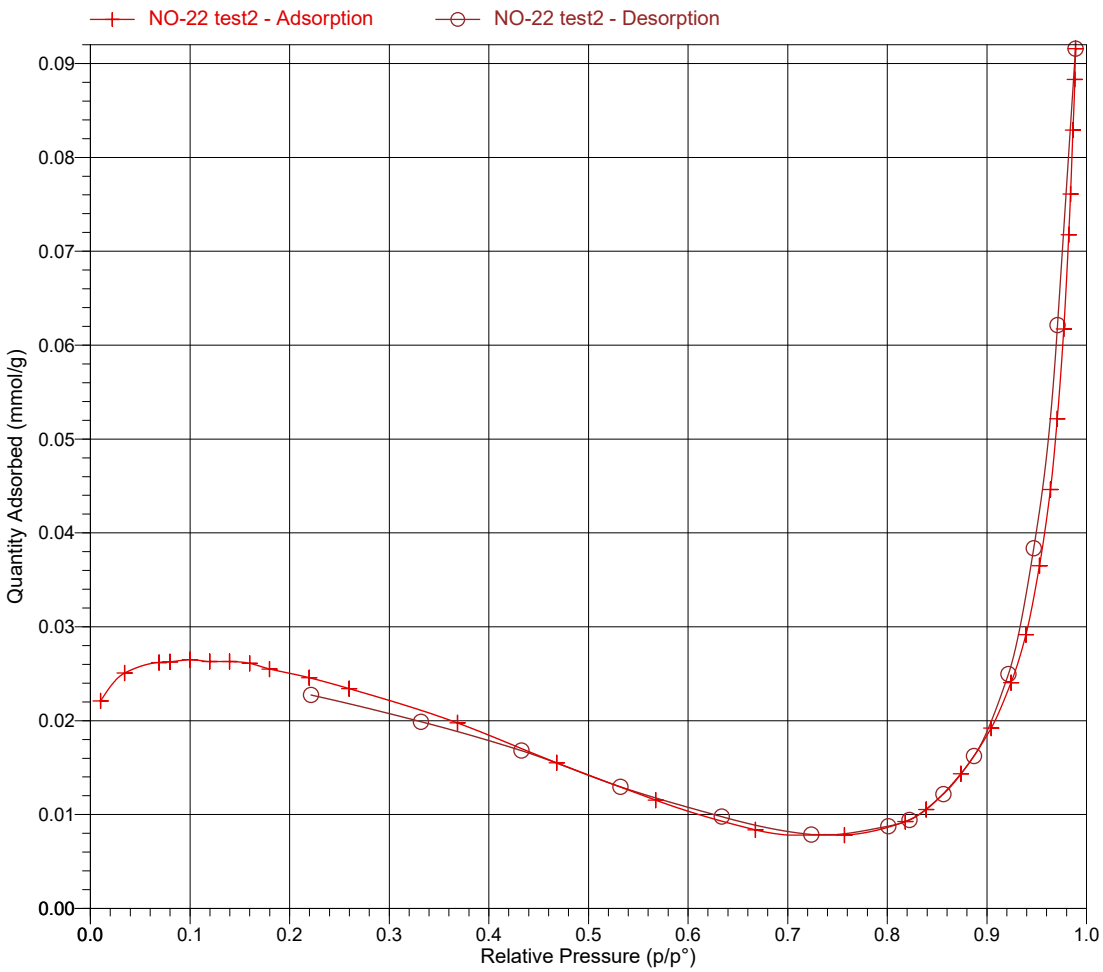

Sample: NO-22 test2
Operator: maria olsvik
Submitter:
File: C:\TriStar II 3020\data\Maria Olsvik\NO-22 test2.SMP

Started:	05.04.2018 11:13:24	Analysis Adsorptive:	N2
Completed:	05.04.2018 13:23:19	Analysis Bath Temp.:	-195,850 °C
Report Time:	05.04.2018 18:17:28	Thermal Correction:	No
Sample Mass:	0,0885 g	Warm Free Space:	10,5032 cm³ Measured
Cold Free Space:	32,1829 cm³	Equilibration Interval:	5 s
Low Pressure Dose:	None	Sample Density:	1,000 g/cm³
Automatic Degas:	No		

BJH Adsorption dV/dlog(w) Pore Volume

Halsey : Faas Correction

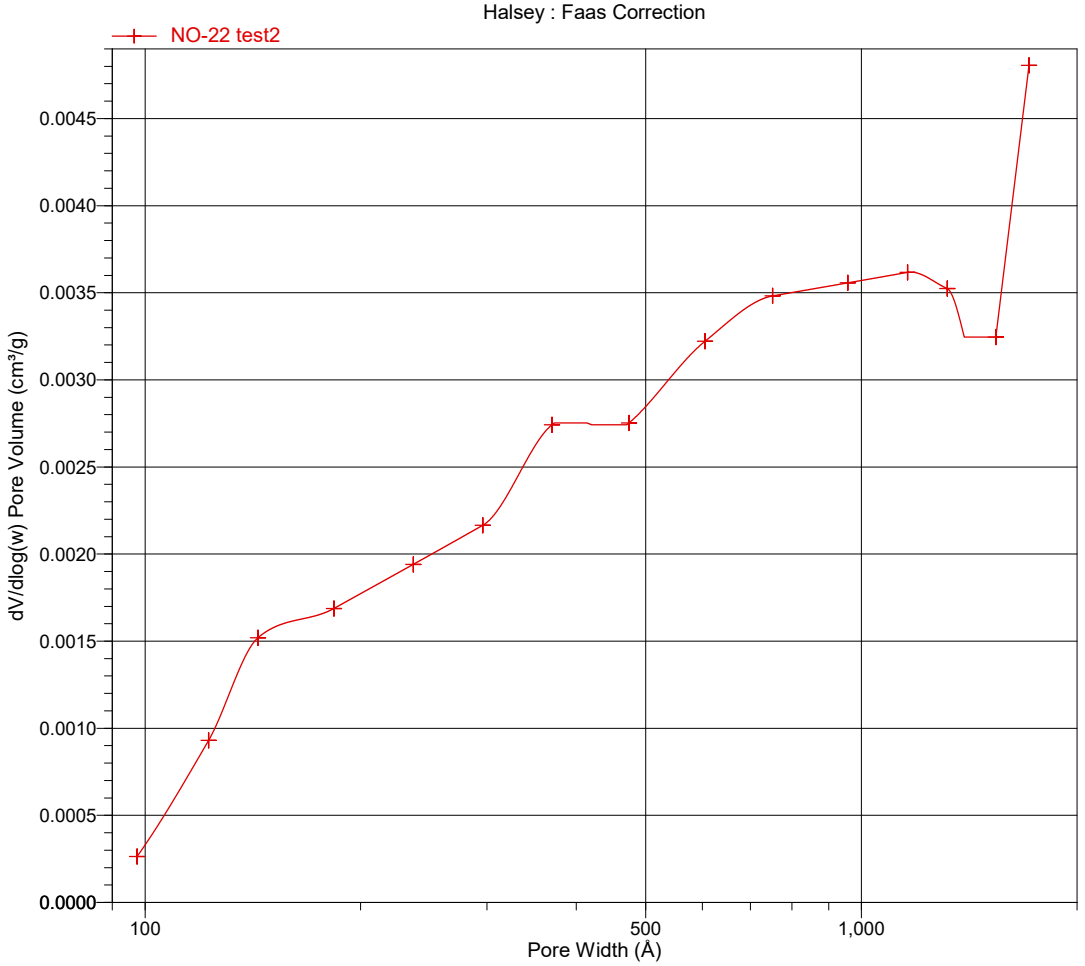

Full Report Set

Sample: NO-23
Operator: Maria Olsvik
File: C:\TriStar II 3020\data\Maria Olsvik\NO-23.SMP

Started:	27.03.2018 13:10:11	Analysis Adsorptive:	N2
Completed:	27.03.2018 18:49:52	Analysis Bath Temp.:	-195,850 °C
Report Time:	27.03.2018 19:37:58	Thermal Correction:	No
Sample Mass:	0,0816 g	Warm Free Space:	10,4271 cm³ Measured
Cold Free Space:	31,6327 cm³	Equilibration Interval:	10 s
Low Pressure Dose:	None	Sample Density:	1,000 g/cm³
Automatic Degas:	No		

Summary Report

Surface Area

BET Surface Area: -0,1074 m²/g

BJH Adsorption cumulative surface area of pores between 17,000 Å and 3 000,000 Å width: 0.333 m²/g

BJH Desorption cumulative surface area of pores between 17,000 Å and 3 000,000 Å width: 0,4605 m²/g

Pore Volume

BJH Adsorption cumulative volume of pores between 17,000 Å and 3 000,000 Å width: 0,002651 cm³/g

BJH Desorption cumulative volume of pores between 17,000 Å and 3 000,000 Å width: 0,002651 cm³/g

Pore Size

BJH Adsorption average pore width (4V/A): 318,314 Å

BJH Desorption average pore width (4V/A): 230,228 Å

DFT Pore Size

Volume in Pores	<	130,33 Å	:	0,00000 cm³/g
Total Volume in Pores	<=	448,83 Å	:	0,00188 cm³/g
Total Area in Pores	>=	130,33 Å	:	0,200 m²/g

Nanoparticle Size:

Average Particle Size -558 753,460 Å

Sample: NO-23
Operator: Maria Olsvik
File: C:\TriStar II 3020\data\Maria Olsvik\NO-23.SMP

Started:	27.03.2018 13:10:11	Analysis Adsorptive:	N2
Completed:	27.03.2018 18:49:52	Analysis Bath Temp.:	-195,850 °C
Report Time:	27.03.2018 19:37:58	Thermal Correction:	No
Sample Mass:	0,0816 g	Warm Free Space:	10,4271 cm³ Measured
Cold Free Space:	31,6327 cm³	Equilibration Interval:	10 s
Low Pressure Dose:	None	Sample Density:	1,000 g/cm³
Automatic Degas:	No		

Isotherm Linear Plot

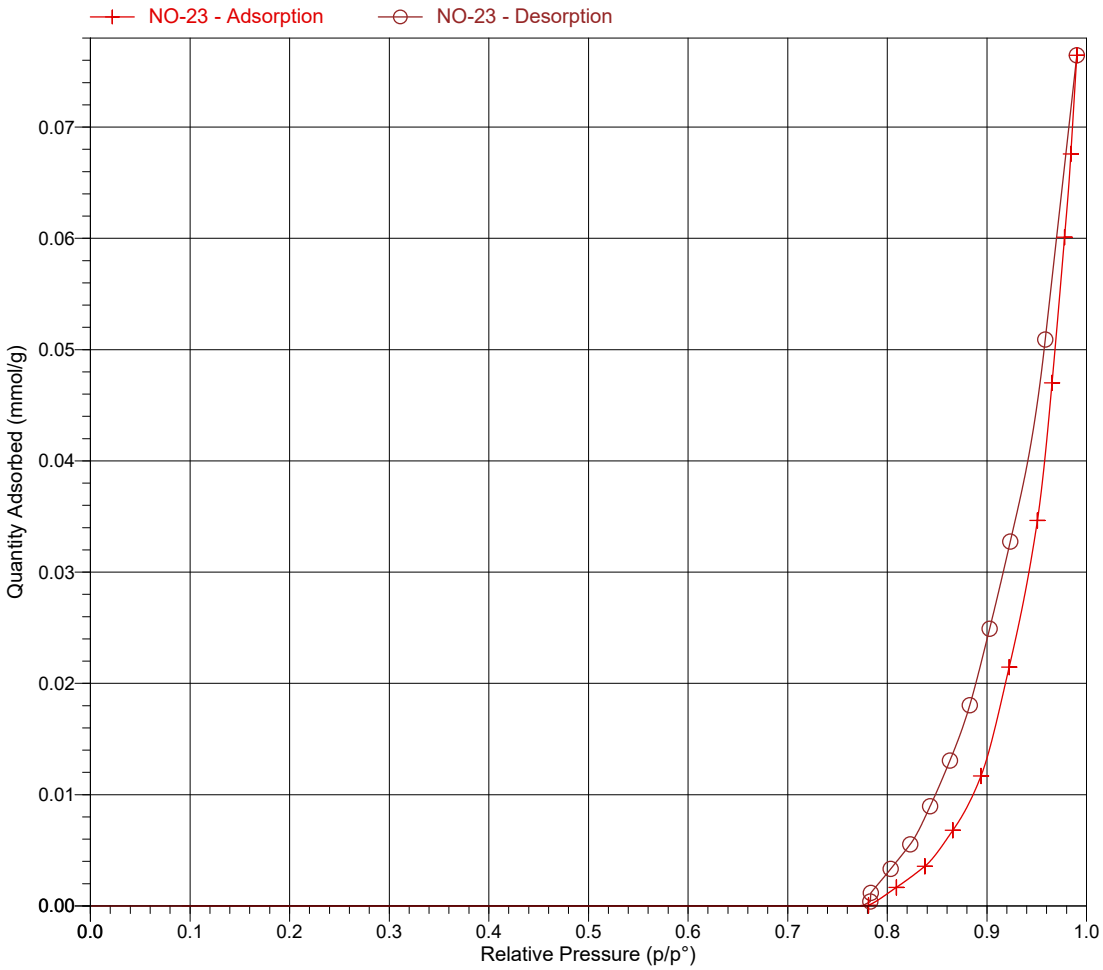

Sample: NO-23
Operator: Maria Olsvik
File: C:\TriStar II 3020\data\Maria Olsvik\NO-23.SMP

Started:	27.03.2018 13:10:11	Analysis Adsorptive:	N2
Completed:	27.03.2018 18:49:52	Analysis Bath Temp.:	-195,850 °C
Report Time:	27.03.2018 19:37:58	Thermal Correction:	No
Sample Mass:	0,0816 g	Warm Free Space:	10,4271 cm³ Measured
Cold Free Space:	31,6327 cm³	Equilibration Interval:	10 s
Low Pressure Dose:	None	Sample Density:	1,000 g/cm³
Automatic Degas:	No		

BJH Adsorption dV/dlog(w) Pore Volume

Halsey : Faas Correction

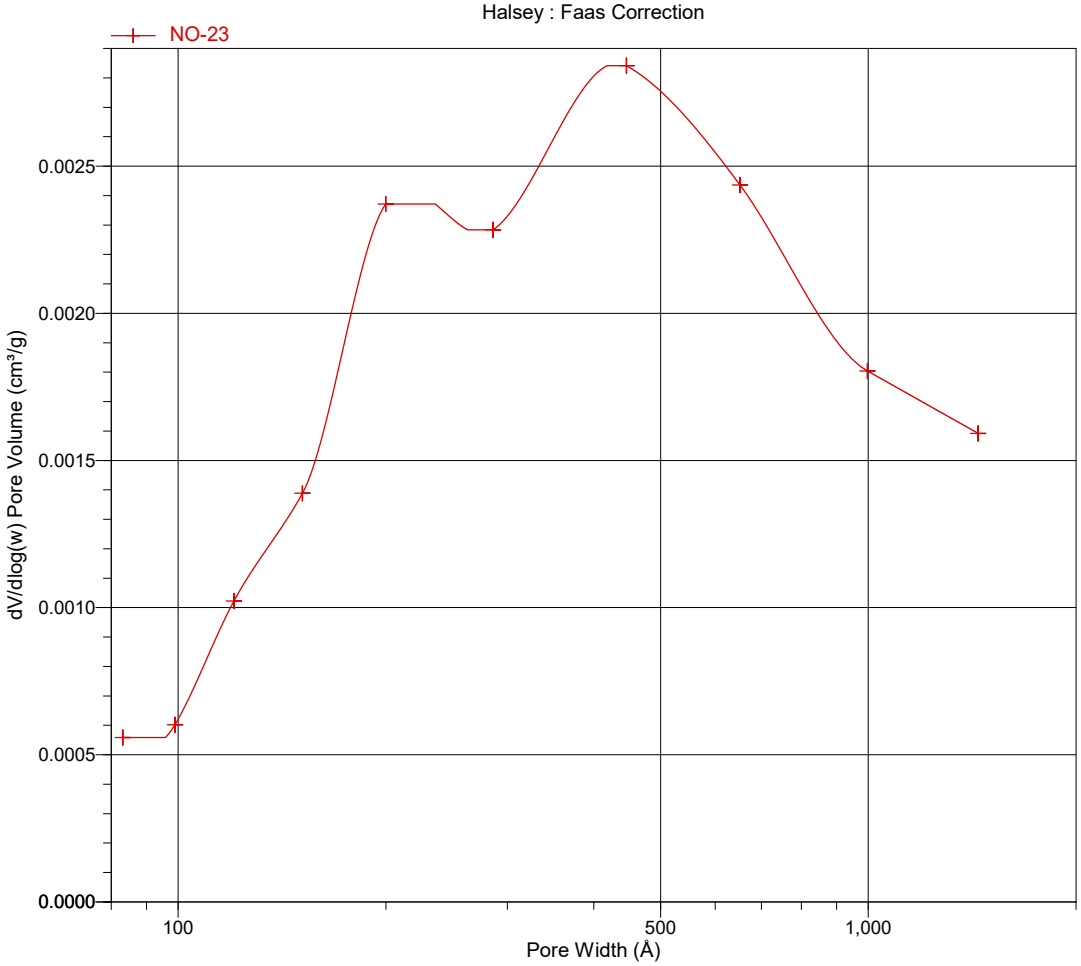

Full Report Set

Sample: NO-23 test2
Operator: maria olsvik
Submitter:
File: C:\TriStar II 3020\data\Maria Olsvik\NO-23 test2.SMP

Started:	05.04.2018 18:22:35	Analysis Adsorptive:	N2
Completed:	05.04.2018 20:00:47	Analysis Bath Temp.:	-195,850 °C
Report Time:	06.04.2018 10:13:14	Thermal Correction:	No
Sample Mass:	0,0624 g	Warm Free Space:	10,6324 cm³ Measured
Cold Free Space:	32,6436 cm³	Equilibration Interval:	5 s
Low Pressure Dose:	None	Sample Density:	1,000 g/cm³
Automatic Degas:	No		

Summary Report

Surface Area

Single point surface area at p/p° = 0,200873772: 0,5420 m²/g

BJH Desorption cumulative surface area of pores between 17,000 Å and 3 000,000 Å width: 0,2463 m²/g

Pore Volume

Single point adsorption total pore volume of pores less than 1 226,495 Å width at p/p° = 0,983959817: 0,002171 cm³/g

BJH Desorption cumulative volume of pores between 17,000 Å and 3 000,000 Å width: 0,002630 cm³/g

Pore Size

Adsorption average pore diameter (4V/A by BET): 180,2943 Å

BJH Desorption average pore width (4V/A): 427,203 Å

Sample: NO-23 test2
Operator: maria olsvik
Submitter:
File: C:\TriStar II 3020\data\Maria Olsvik\NO-23 test2.SMP

Started: 05.04.2018 18:22:35
Completed: 05.04.2018 20:00:47
Report Time: 06.04.2018 10:13:14
Sample Mass: 0,0624 g
Cold Free Space: 32,6436 cm³
Low Pressure Dose: None
Automatic Degas: No

Analysis Adsorptive: N2
Analysis Bath Temp.: -195,850 °C
Thermal Correction: No
Warm Free Space: 10,6324 cm³ Measured
Equilibration Interval: 5 s
Sample Density: 1,000 g/cm³

Isotherm Linear Plot

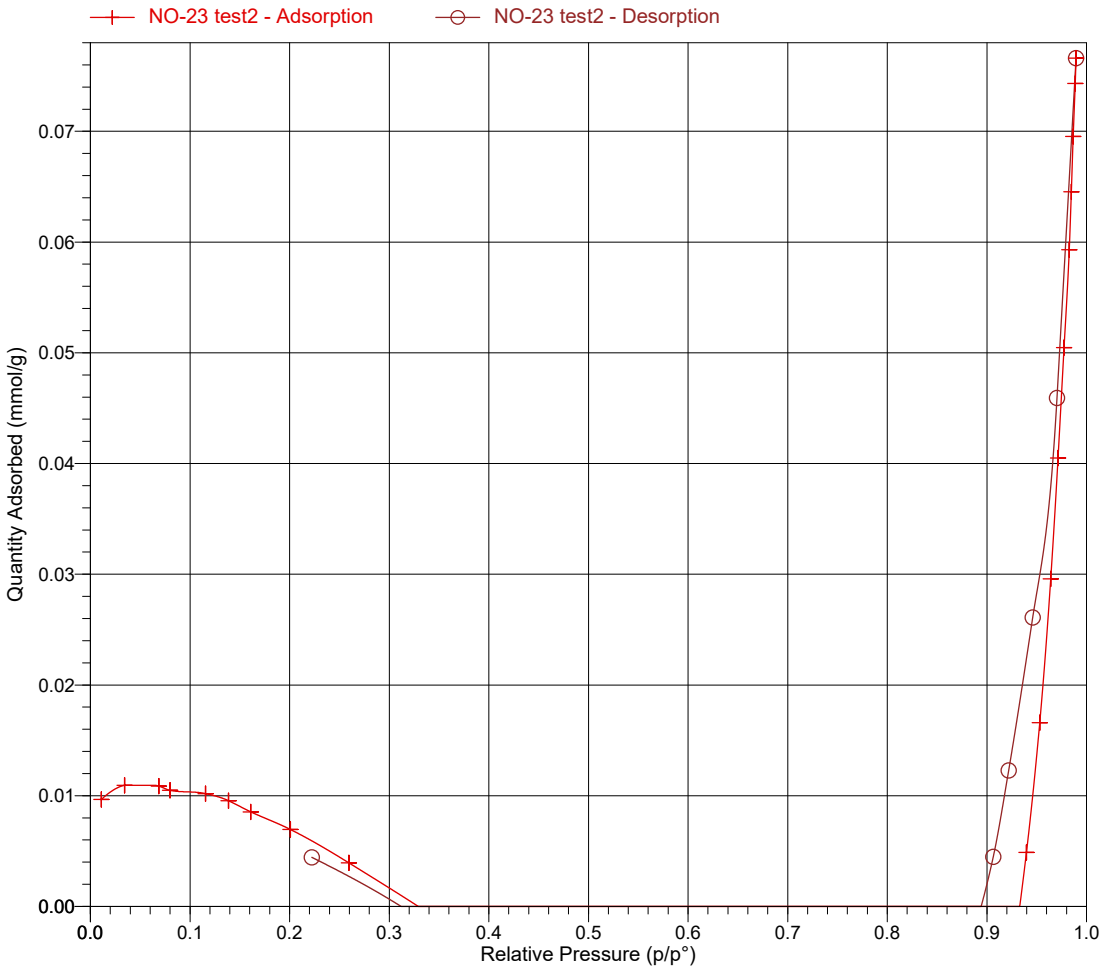

Sample: NO-23 test2
Operator: maria olsvik
Submitter:
File: C:\TriStar II 3020\data\Maria Olsvik\NO-23 test2.SMP

Started:	05.04.2018 18:22:35	Analysis Adsorptive:	N2
Completed:	05.04.2018 20:00:47	Analysis Bath Temp.:	-195,850 °C
Report Time:	06.04.2018 10:13:14	Thermal Correction:	No
Sample Mass:	0,0624 g	Warm Free Space:	10,6324 cm³ Measured
Cold Free Space:	32,6436 cm³	Equilibration Interval:	5 s
Low Pressure Dose:	None	Sample Density:	1,000 g/cm³
Automatic Degas:	No		

BJH Adsorption dV/dlog(w) Pore Volume

Halsey : Faas Correction

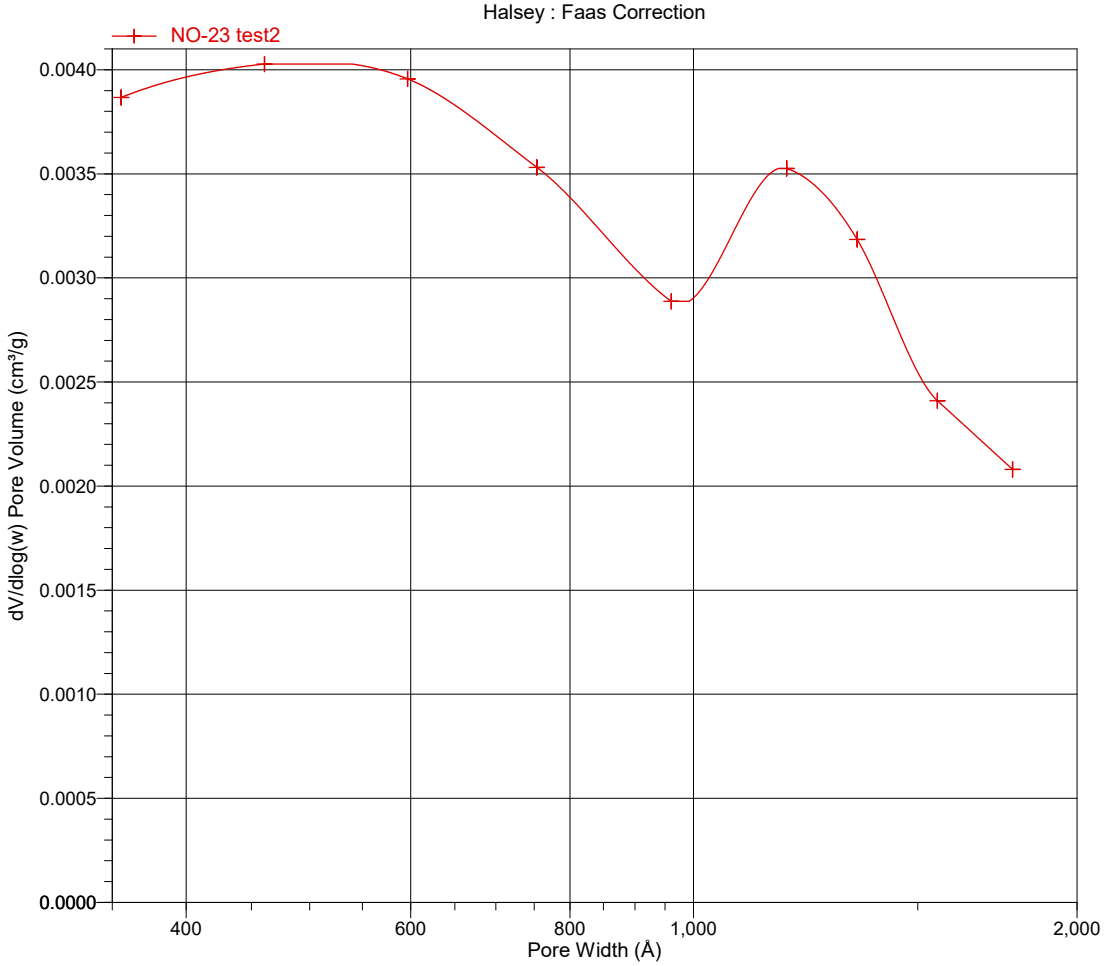

A7.9 PDF Overview of Granulation Experiments

Exp. No	Group*	Starting material	addtives	
		Calcined dolomite	Primary	Secondary
Jan_19	Macine/Operation	100g	n.a.	n.a.
Jan_23	Machine	100g, <106um	n.a.	n.a.
Jan_24	Operation	100g, <106um	n.a.	n.a.
Jan_25	Machine	only cement	n.a.	n.a.
Jan_26	Machine	100 g **ADDA** cement	n.a.	n.a.
Jan_26_A	Operation	99,2g <106um	n.a.	n.a.
Jan_26-B	Operation	99,2g <106um	n.a.	n.a.
Jan_29_A	Operation	99g <106um	n.a.	n.a.
Jan_29_B	Machine	99g <106um	n.a.	n.a.
Jan_30_A	Machine	100.9g <106um	n.a.	n.a.
Jan_30_B	Machine	100.9g <106um	n.a.	n.a.
Jan_31_A	Machine	100g, <106um	n.a.	n.a.
Jan_31_B	Machine	100g <106um	n.a.	n.a.
Feb_1_A	Machine	100,3 g <106um	n.a.	n.a.
Feb_1_B	Machine	100,3 g <106um	n.a.	n.a.

Feb_2_A	Machine	99,6g <106um	n.a.	n.a.
Feb_2_B	Machine		n.a.	n.a.
Feb_5_A	material	96,7g calcined ADDA	n.a.	n.a.
Feb_5_B	material	96,7g calcined ADDA	n.a.	n.a.
Feb_6_A	Machine	100g calcined dolomite		
Feb_6_B	Machine	100g calcined dolomite	n.a.	n.a.
Feb_6_C	material	100g calcined ADDA	n.a.	n.a.
Feb_6_D	material	100g calcined ADDA	n.a.	n.a.
Feb_7	upscaling	523g ADDA (not calc.)	n.a.	n.a.
Feb_11_A	upscaling	502g calcinert ADDA	n.a.	n.a.
Feb_11_B	upscaling	502g calcinert ADDA	n.a.	n.a.
Feb_21_A	upscaling	504g calcinert ADDA	n.a.	n.a.
Feb_21_B	upscaling	504g calcinert ADDA	n.a.	n.a.
Feb_22_A	Operation	100g calcined dolomite	n.a.	n.a.
Feb_22_B	Operation	100g calcined dolomite	n.a.	n.a.
Feb_26_A	Operation	100g	..	ZrN2O7
Feb_26_B	Operation	100g	..	ZrN2O7

Feb_28_A	Operation	100g	20g Fondu	ZrN2O7
Feb_28_B	Operation	100g	20g Fondu	ZrN2O7
Mar_1_A	Operation	100g	20g Fondu	ZrCl4
Mar_1_B	Operation	100g	20g Fondu	ZrCl4
Mar_2_A	Operation	100g calcined dolomite	20g Fondu	..
Mar_2_B	Operation	100g calcined dolomite	20g Fondu	..
Mar_6_A	Operation	100g calcined dolomite	20g fondu	..
Mar_6_B	Operation	100g calcined dolomite	20g Fondu	..
Mar_8_A	Operation	100g calcined dolomite	20g Fondu	..
Mar_8_B	Operation	100g calcined dolomite	20g Fondu	..

Mar_14_A		100g calcined ADDA	20g fondu	14g ZrN2O7
Mar_14_B		100g calcined ADDA	20g Fondu	14g ZrN2O7
Mar_15_A		100g calcined ADDA	20g Fondu	5g ZrCl4
Mar_15_B		100g calcined ADDA	20g Fondu	5g ZrCl4
Mar_16_A		100g ADDA	20g Fondu	14g ZrN2O7
Mar_17_A		100g Adda	20g Fondu	5g ZrCl4
Apr_23_A		100g Calcined Dolomite	20g Fondu	35.95g Mg(NO3)2.6H2O
Apr_23_B		100g calcined dolomite	20g Fondu	35.95g Mg(NO3)2.6H2O

* Machine: configuration and modification of the setup ; operation: configuration of operation procedure; materia
** yield: the granules at the size range of 250 um to 860 um
** yield: the granules at the size range of 250 um to 1,1mm

Water/solution addition Main parameters in the first, second and final stages
first stage - 60mL, low rpm, roller, spray, 30 min ; second stage- 60mL, low rpm, roller, spray, 20 min ; shaping
first stage -60mL, low rpm, spray with big droplets; second stage- 60mL, low rpm, spray with big droplets; shaping - final product too hard to shape to good sphericals
First stage - 60mL, max rpm, roller, Spray ; Second stage- 30mL, max. Rpm, roller ??,too long and too much water loss; shaping - covered + steam, avoid fast drying of the solid
1) (first stage) 33,49g water added, low rpm 13min, max rpm 2min; 2) 31.16g water added , low rpm, removed roller after 9 minutes. 3) max rpm, 3 min. ;1) 25,7g water added, low rpm 15min, max rpm 5min, stored on closed container
2) 31.16g water, low rpm (5min), removed roller after 5min and 9min, high rpm (7min) 3) NO
1) 25.7g water low rpm (15min), max rpm (min). stored on closed bottle
min
1) 25.54g water added, low rpm, 15 min. 5 min max rpm. tot= 20min
large aggregated), 3) 4 min max rpm.
1) 26,15g water added low rpm (15 min), max rpm (5min). tot time = 20 min
(5min) 3) STORE kuler
1) 24,65g water added (15 min), low rpm., 5 min max rpm
total = 35g water. 2) 10g water, low rpm (10 min). 12 g water max rpm (5min) removed roller, 13g max rpm (5 min),2-4 sprays every min (10). 3) 6 min max rpm no water added

1) 24,9 g water added at low rpm (15 min.) tot water = 41,31 2)10g at low rpm (5min), max rpm (1 min), +10g at max rpm(5min), +7g removed roller after 15min, +4g after (10 min), +5-10 sprays (8min). tot time= 36min 3) 1
1) 25,12 g water added low rpm (15min), max rpm (5min). tot time = 20 min tot water = 51,86g 2) 10g low rpm (5min), max rpm(1min), +10g (5min), +10g removed roller(5 min), +1g (5min), +2g (5min), +5g (5min), +5g (5min),+5 (5min) 3) 3 min, too much
1) 25,9g water low rpm (15min), max rpm (5min)
2) tot water= 65g (56min) 3) 8min
1) 24.8g low rpm (15 min), high rpm (5min) tot water = 57g 2) 10g low rpm (5min), +20g high rpm, removed roller after 15 min (10 min), +17g (5 min) , tot time = 20 min 3) 1 spray to keep humidity (8min)
tot water= 81g tot time = 35. 1) 20g low rpm(5min), +20g low rpm (5min), +10g medium rpm (5 min), +15g max rpm (5min) remove roller, +15g max rpm (5min), +3g max rpm
tot water= 30g 1) 20g (5min), rpm=level2, wait 5min to remove heat(8min), +10g (10min), wait 3min to remove heat(13min), +10g (15min), wait 3 min to remove heat (18), +10g
tot water = 2) 25g (5min) rpm level 2, +15g (10min) +humidifier low level, +20g (15min), +15g (20min) removed roller, +15g (25min) rpm=level8, +20g (30g), +5g (35g) (use roller if
1) T=24 C før start. 5g T=35 (1min) vent 2 min for kjøling level = 2, +5g T=36C (4min) vent 3 min, +5g T=36C (7min) vent 3 min, +5g T=38C (10min) vent 5 min, +5g T=35C (15min) vent 5
2) 25g vann level 2 no heat released T= 24C (5min), +10g vann T= 43C (10min), avkjøling i 5 min + 25g vann (15min) satte på luftfukter low level, +15g level =6 (20min), +15g (25min),
1) T=24,6C, +3g (1min) T=32.8C level =1, +4g T=34,3C (3min), +3 T=33,8C (5min), +5g T = 33.5C (10min) dvs 15g på 10min,+10g (15min) T=26C level 8, rørte 5min level 8 etter
2) low rpm (6min), 20g tilsatt max rpm (10min), removed roller (13min), +4g (15min) a few sprays every minute, +1g (20min) add humidifier, +2g (25min) stoppet vanntilsats. 3) 10min
1) 10g low rpm(6min), almost whole solution (10min), +7g (13min), max rpm(15), stopped (20min)
2) 10g low rpm(4min), +5g high rpm and add humidifyer(6min), +5g (20 min), +1g (10 min), +1g removed roller(12min), +0,5g (14 min), stopped water addition (15). 3) +4 spray to keep humidity (17min), +2spray (20min), tured of humidifyer (23)

0) m_ZrN2O7= 14,45, m_Fondu= 20,84 , rørte cal.dol + fondu for homogen blanding level 1(5min). 1) tilsatt halve løsning (H2O+ZrN2O7) level 1 rpm(5min), har nå tilsatt hele løsning (10min), +7g H2O(15min), level 8 rpm (20min)
2) 10g H2O level = 1 rpm(4min), +2g level=8rpm(6min), +6g (10min), +3g (12min), +3g add humidifyer (14min), removed roller (15min), +5g (20min), +5g (24min), +5g (26min), +0,5g (28min) stoppet vanntilsettse. 3) stoppet(31min)
1) tilsatte hele løsningen av ZrCL4 og vann på 15 min. level = 1(15min), level= 8(20min).
2) 10g level=1(4min), +2g (6min) increased to level=8, +4g (8min), +2 (10min), +3g (12min), +3g (15min) humidifyer added, +0,5g (18min) removed roller (tot water=26) water addition stopped. 3) +2spray (26min), +2spray (30min), +2spray (34min), +2spray (36min), +2spray (38min), STopped (40 min)
1) 15g (8min) level =1, +12g (15min) increased to level =8, stopped (20min)
2) 10g level = 1(5min), øker til level=8 (6min), +10g (10min), +5g (15min) add humidifyer and remove roller (tot water=25g), +5g (took sample 1)(20min), +3g (took sample 2)(25min) stopped water addition. 3) sample 3(30min), +3spray sample 4 (35min), +3spray sample 5 (40min) himidifyer at level 2 for some seconds, sample 6 (45min) turned of humidifyer, sample 7 (50min). stopped. tot water = 33g + few sprays to keep humidity. tot time of stirring after water addition = 25min.
1) 25g vann(15min) level 1, level=8 (20min)
2) 10g (5min) level1, level 8 (6min), +10g (10min), +5g (15min) add humidifier, +5g (20 min), +4g (25min) removed roller, +3g (30min) stoppet vanntilsettelse (tot =37g). 3) +4 spray (35min) , +4spray (40min), +5spray (45min) humidifier set to level 2, +8 spray (50min), +5spray (55min), +5spray (60min), humidifyer level 1 (65min), stopped (70min).
1) 25g vann(15min) level 1, level=6 (20min)
2) 10g level 1 (5min), level 8 (6min), +10g (10min), +5g (15min) add humidifyer level 1, +5g remove roller(20min), +5g (25g). 3) +10spray (30min), +3spray (35min), stopped (45min).

m_zrn2o7= 14.37g, m_H2O= 20,24, m_calADDA= 100g, m_FONDU=20,42. 1) level 1, tilsatte halvparten av væska første 10 min, resten av væska neste 5min (15min), level 6 (20min).
2) 10g level 1(5min), level 8 (6min), +10g (10min), +10g (15min) add humidifyer level1, +5g(20min) remove roller, +5g (25min)stopp water addition. 3)+1g=few sprays (30min). +1g=few sprays (35min), STOPPED (45min). tot water=42g.
m_zrCl4= 5.082g, m_H2O= 25,24, m_calADDA= 100g, m_FONDU=20,48. 1) level 1, tilsatte halvparten av væska første 10 min, resten av væska neste 5min (15min), level 6 (20min).
2) 10g level 1 (5min), level 8 (6min), +10g (10min), +10g (15min) add humidifyer level 1, +5g(20min), +5g (25min) removed roller. 3) +1g (30min), +1g (35min), stopped (45min).
1) blandet ut ca 14g ZrN2O7 med 10g vann. tilsatte halve løsningen første 10 min, level 1 (10 min), hele løsning tilsatt (15min) level=8, +10g vann (25min) add humidifyer and remove roller, +5g (30min) +3spray. water addition stoped. stoppet (35min). 1
1) blandet 5g Zrcl4 med 20g vann. tilsatte hele løsning, level 1 (15min) skrudde opp til level 8(20min), +10g vann (25min) humodifyer level 1 and remove roller, +4g (30min) stopped water addition. 2) +1g (35min), +1g (40min), +1g (45min),
35g 35.95g Mg(NO3)2.6H2O mixed with 20g vann. 1) level 1, approximately half of the solution added (10min), whole soultion added (15min) level 8, stopped (20min).
2) 10g level 1(5min), level 8 (6min), +10g (10min) add humidifyer level 1, +5g (15min) remove roller, +5g (20min)stopp water addition. 3)+4spray (25min) humidifier level 2, STOPPED (30min). tot water=30g.

Objectives	Observations
trial of the new machine, spray with large droplets, the water addition time was long and the shaping stage started too later and difficult to form	able to get small granules; Water droplets and manual scruber need to be moodified for a better production control
trial of the new machine,	water threshhold minimum 60g and maximum 70g. used 70g = Big granules. Bad spray. Next time: need better spray.
test different type sprayers, function of roller, water amount,	the addition of mist as water was too slow ; fast drying process led to production of sand (agglomeration stopped too early)
steam	
I) improve sruber use with stativer; II)rotation speed measurement test; III) improve the use of air moisturizer ; IV) Spray handle	
make hydrated dolomite Ca(OH)2	heat released for the first 20g water added. water addition stopped when small aggregates is observed.
produce granules with spherical shape	removed roller then put it back if large aggregates is formed. remove roller if powder in forming plates. 31.16g is too much water added during 12 min.
make hydrated dolomite Ca(OH)2. max rpm to remove small aggregates	no heat released after the first 20g
produce granules with spherical shape	
make hydrated dolomite Ca(OH)2	
reproduce good results from Jan_29 A&B.	maybe add less water, and stirr longer after water addition next time
reproduce	too much water, need slower water addition
reproduce granules of calcined dolomite	
extended time after water addition	extended time for the final water added. tot time = 36min

extended time after water addition by 5 min by adding one spray of water.	
test wether the properties of calcined ADDA has the same properties as calcined dolomite	heat released for the first 20g water added. water addition stopped when small aggregates is observed. seemed to have the same properties as calcined
-"-	Had to add more water than that of calcined dolomite. Too much were added, got big granules.
repeat good experiment	too dry mixture after 30 min, and alot more water had to be added compared to the best experiments. also; not good shape of granules
investigate wether calcined dolomite follow same granulation procedure as for calcined dolomite	
	good result
simulate upscaling problems related. simulate using uncalcined adda with 2) and 3) stage of calcined ADDA/dolomite.	use low rpm in begining, at high rpm the powder is flying around, also more material is standing behind the scraper. after adding approx. 40g small
simulate scale-up	seemed that 30g water was enough to remove heat and hydrate the calcined adda. maybe some more water could be added just in case... next time add
simulate scale-up. monitor temperature increase while adding water	
	heat released also in 2nd stage of granulation.
temperatur kontroll for 100g dolomitt.	
introduce additives to solution	less heat released than that of only pure dolomite and water. powder seemed sto stick more to the middle of the bowl

introduce additives to solution. Nitrate source for Zr.	
	too much water added. less heat released than that os only pure cal.dol and water.
introduce additives to solution. Now an other source for Zr.	little heat realsed
	low heat release
investigate samples after every 5minute after water addition to compare diameters D1/D2 and make a graph. take picture in SEM and analyse in Fiji	
Reproduce Mar_2, but it did not go as expected.	Mar_2: 33g water added after 25 min, this was to little. added 37g after 30 min, but this is also too little. need to add more next time. 1 spray = 0,1g ca
use level 6 istead of 8 to avoid powder flying around	

compare granules made of cal.dol with cal.ADDA	
Make granules with good size and shape	material seems more humid than that of earlier batches, but it was necessary to add thid amount of water due to the large amount of salt.
	less water than usual added in stgae 2, due to more humid 1)stage

A7.10 Raw data - Mercury Intrusion Porosimetry

SINTEF

REPORT OF POROSITY

Sample ID: 000-500 NO-12
Operator: Lars Erik Parnas
Submitter: Sintef
File: C:\9500\DATA\EKSTERN\000-500.SMP

LP Analysis Time: 16.05.2018 1:06:37
HP Analysis Time: 16.05.2018 2:03:17
Report Time: 16.05.2018 2:03:17

Sample Weight: 0.2054 g
Correction Type: None
Show Neg. Int: No

Summary Report

Penetrometer parameters

Penetrometer:	#s/n - (14) 3 Bulb, 0.412 Stem, Powder				
Pen. Constant:	11.228	µL/pF	Pen. Weight:	62.2190	g
Stem Volume:	0.4120	mL	Max. Head Pressure:	4.6800	psia
Pen. Volume:	3.0519	mL	Assembly Weight:	99.4616	g

Hg Parameters

Adv. Contact Angle:	130.000	degrees	Rec. Contact Angle:	130.000	degrees
Hg Surface Tension:	485.000	dynes/cm	Hg Density:	13.5335	g/mL

User Parameters

Param 1:	0.000	Param 2:	0.000	Param 3:	0.000

Low Pressure:

Evacuation Pressure:	50	µmHg
Evacuation Time:	5	mins
Mercury Filling Pressure:	0.53	psia
Equilibration Time:	10	secs

High Pressure:

Equilibration Time:	10	secs

No Blank Correction

(From Pressure 0.10 to 60000.00 psia)

Intrusion Data Summary

Total Intrusion Volume =	1.1755	mL/g
Total Pore Area =	11.239	m²/g
Median Pore Diameter (Volume) =	11677.5	nm
Median Pore Diameter (Area) =	65.6	nm
Average Pore Diameter (4V/A) =	418.3	nm
Bulk Density at 0.53 psia =	0.6517	g/mL
Apparent (skeletal) Density =	2.7850	g/mL
Porosity =	76.6012	%
Stem Volume Used =	60	%

Pore Structure Summary

Threshold Pressure:	2.78	psia (Calculated)
Characteristic length =	65164.9	nm
Conductivity formation factor =	0.228	
Permeability constant =	0.00442	
Permeability =	4279.5604	mdarcy
BET Surface Area =	230.0000	m²/g
Pore shape exponent =	1.00	
Tortuosity factor =	1.359	
Tortuosity =	3.2804	
Percolation Fractal dimension =	2.962	
Backbone Fractal dimension =	2.830	

Mayer Stowe Summary

Interstitial porosity =	47.6300	%
Breakthrough pressure ratio =	3.3512	

Material Compressibility

Linear Coefficient =	N/A	1/psia
Quadratic Coefficient =	N/A	1/psia²

SINTEF

REPORT OF POROSITY

Sample ID: 000-500 NO-12
Operator: Lars Erik Parnas
Submitter: Sintef
File: C:\9500\DATA\EKSTERN\000-500.SMP

LP Analysis Time: 16.05.2018 1:06:37
HP Analysis Time: 16.05.2018 2:03:17
Report Time: 16.05.2018 2:03:17

Sample Weight: 0.2054 g
Correction Type: None
Show Neg. Int: No

Cumulative Intrusion vs Pressure

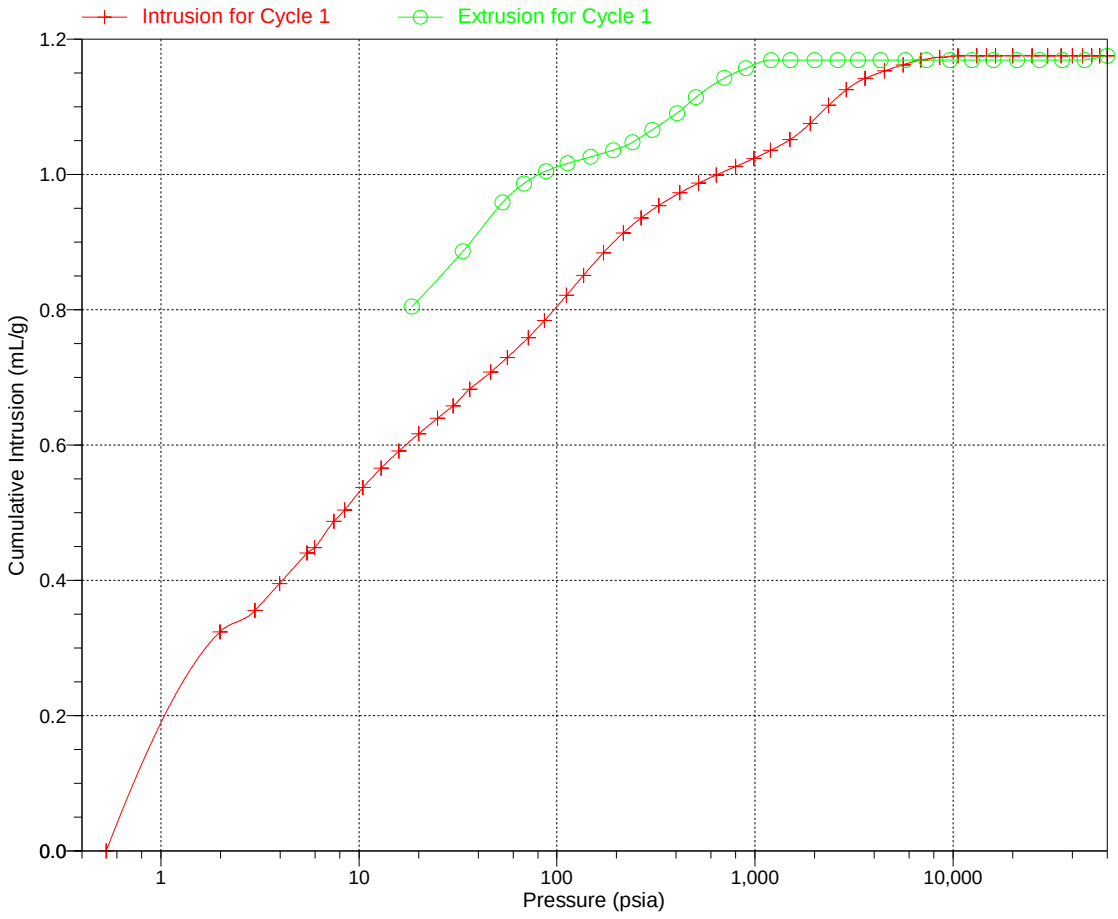

SINTEF

REPORT OF POROSITY

Sample ID: 000-500 NO-12
Operator: Lars Erik Parnas
Submitter: Sintef
File: C:\9500\DATA\EKSTERN\000-500.SMP

LP Analysis Time: 16.05.2018 1:06:37
HP Analysis Time: 16.05.2018 2:03:17
Report Time: 16.05.2018 2:03:17

Sample Weight: 0.2054 g
Correction Type: None
Show Neg. Int: No

Incremental Intrusion vs Pressure

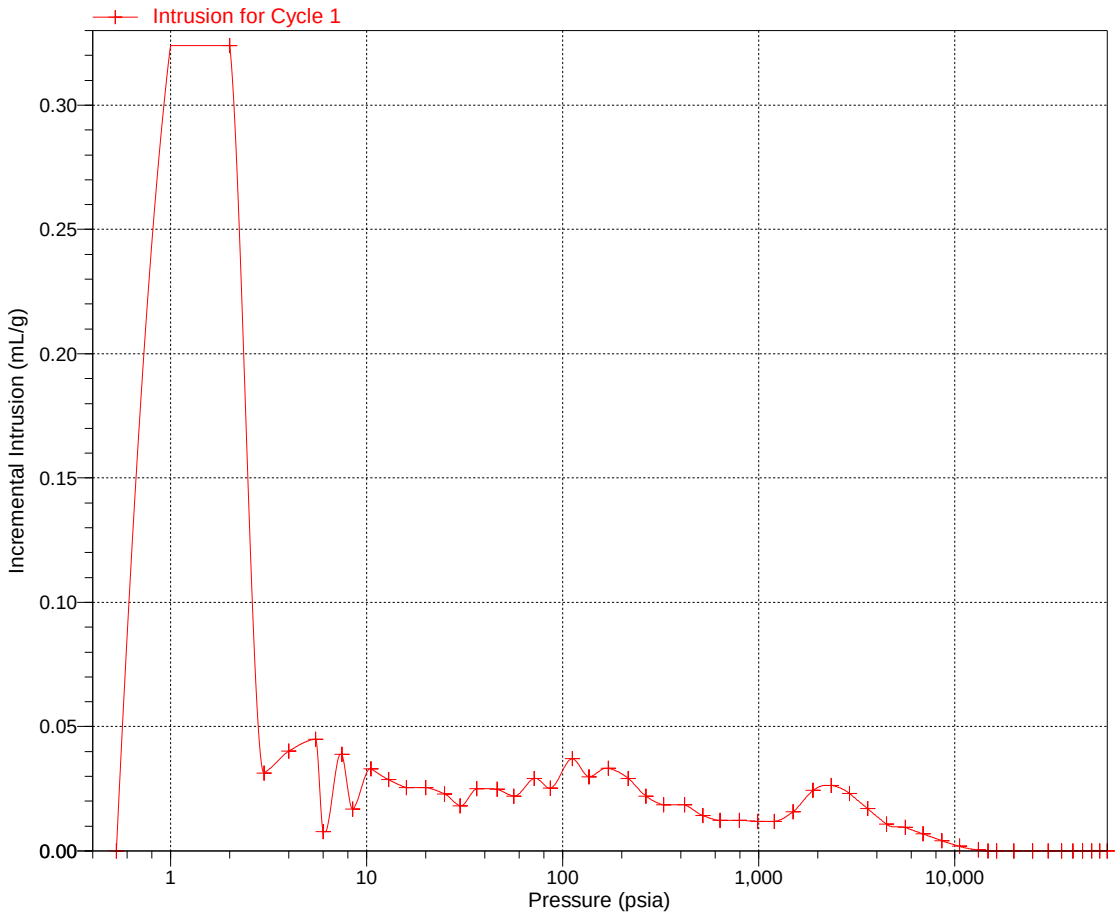

Sample ID: 000-500 NO-12
Operator: Lars Erik Parnas
Submitter: Sintef
File: C:\9500\DATA\EKSTERN\000-500.SMP

LP Analysis Time: 16.05.2018 1:06:37
HP Analysis Time: 16.05.2018 2:03:17
Report Time: 16.05.2018 2:03:17

Sample Weight: 0.2054 g
Correction Type: None
Show Neg. Int: No

Differential Intrusion vs Pore size

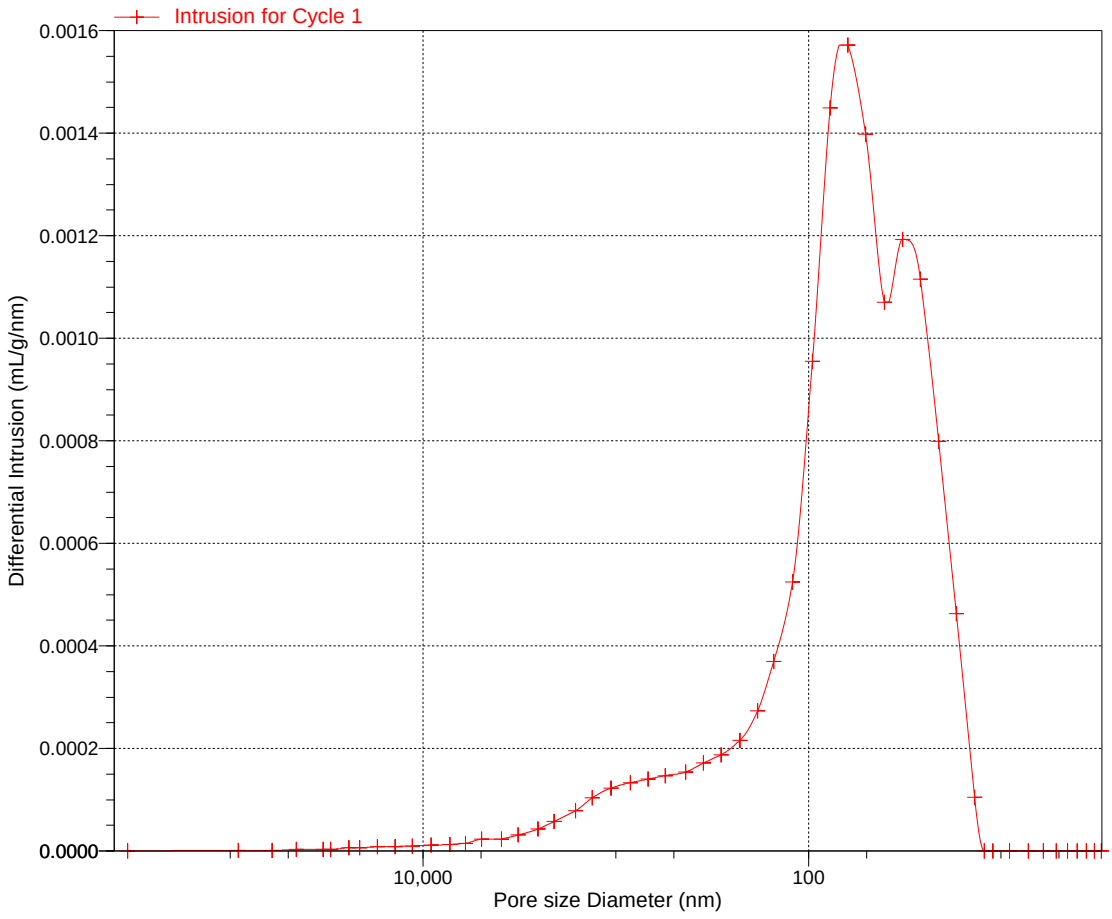

Sample ID: 000-500 NO-12
Operator: Lars Erik Parnas
Submitter: Sintef
File: C:\9500\DATA\EKSTERN\000-500.SMP

LP Analysis Time: 16.05.2018 1:06:37
HP Analysis Time: 16.05.2018 2:03:17
Report Time: 16.05.2018 2:03:17

Sample Weight: 0.2054 g
Correction Type: None
Show Neg. Int: No

Cumulative Pore Area vs Pore size

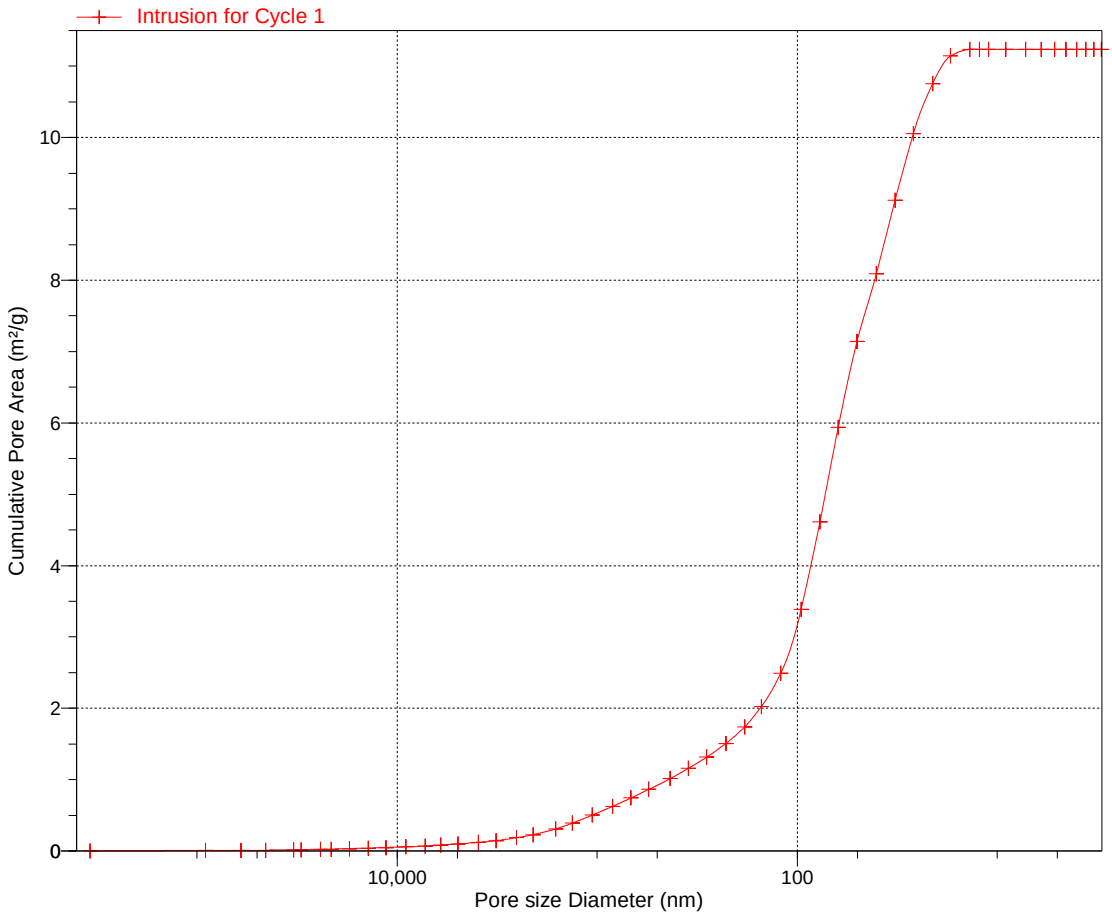

SINTEF

REPORT OF POROSITY

Sample ID: 000-501 Dolomite
Operator: Lars Erik Parnas
Submitter: Sintef
File: C:\9500\DATA\EKSTERN\000-501.SMP

LP Analysis Time: 16.05.2018 1:06:37
HP Analysis Time: 16.05.2018 2:03:17
Report Time: 16.05.2018 2:03:18

Sample Weight: 0.2074 g
Correction Type: None
Show Neg. Int: No

Summary Report

Penetrometer parameters

Penetrometer:	#s/n - (14) 3 Bulb, 0.412 Stem, Powder				
Pen. Constant:	11.117	µL/pF	Pen. Weight:	62.5135	g
Stem Volume:	0.4120	mL	Max. Head Pressure:	4.6800	psia
Pen. Volume:	3.0892	mL	Assembly Weight:	100.2317	g

Hg Parameters

Adv. Contact Angle:	130.000	degrees	Rec. Contact Angle:	130.000	degrees
Hg Surface Tension:	485.000	dynes/cm	Hg Density:	13.5335	g/mL

User Parameters

Param 1:	0.000	Param 2:	0.000	Param 3:	0.000

Low Pressure:

Evacuation Pressure:	50	µmHg
Evacuation Time:	5	mins
Mercury Filling Pressure:	0.53	psia
Equilibration Time:	10	secs

High Pressure:

Equilibration Time:	10	secs

No Blank Correction

(From Pressure 0.10 to 60000.00 psia)

Intrusion Data Summary

Total Intrusion Volume =	1.1206	mL/g
Total Pore Area =	23.064	m²/g
Median Pore Diameter (Volume) =	3177.8	nm
Median Pore Diameter (Area) =	49.1	nm
Average Pore Diameter (4V/A) =	194.3	nm
Bulk Density at 0.53 psia =	0.6532	g/mL
Apparent (skeletal) Density =	2.4375	g/mL
Porosity =	73.2004	%
Stem Volume Used =	57	%

Pore Structure Summary

Threshold Pressure:	2.84	psia (Calculated)
Characteristic length =	63796.3	nm
Conductivity formation factor =	0.116	
Permeability constant =	0.00442	
Permeability =	2093.6320	mdarcy
BET Surface Area =	230.0000	m²/g
Pore shape exponent =	1.00	
Tortuosity factor =	1.400	
Tortuosity =	3.3147	
Percolation Fractal dimension =	2.848	
Backbone Fractal dimension =	2.696	

Mayer Stowe Summary

Interstitial porosity =	47.6300	%
Breakthrough pressure ratio =	3.3512	

Material Compressibility

Linear Coefficient =	N/A	1/psia
Quadratic Coefficient =	N/A	1/psia²

Sample ID: 000-501 Dolomite
Operator: Lars Erik Parnas
Submitter: Sintef
File: C:\9500\DATA\EKSTERN\000-501.SMP

LP Analysis Time: 16.05.2018 1:06:37
HP Analysis Time: 16.05.2018 2:03:17
Report Time: 16.05.2018 2:03:18

Sample Weight: 0.2074 g
Correction Type: None
Show Neg. Int: No

Cumulative Intrusion vs Pressure

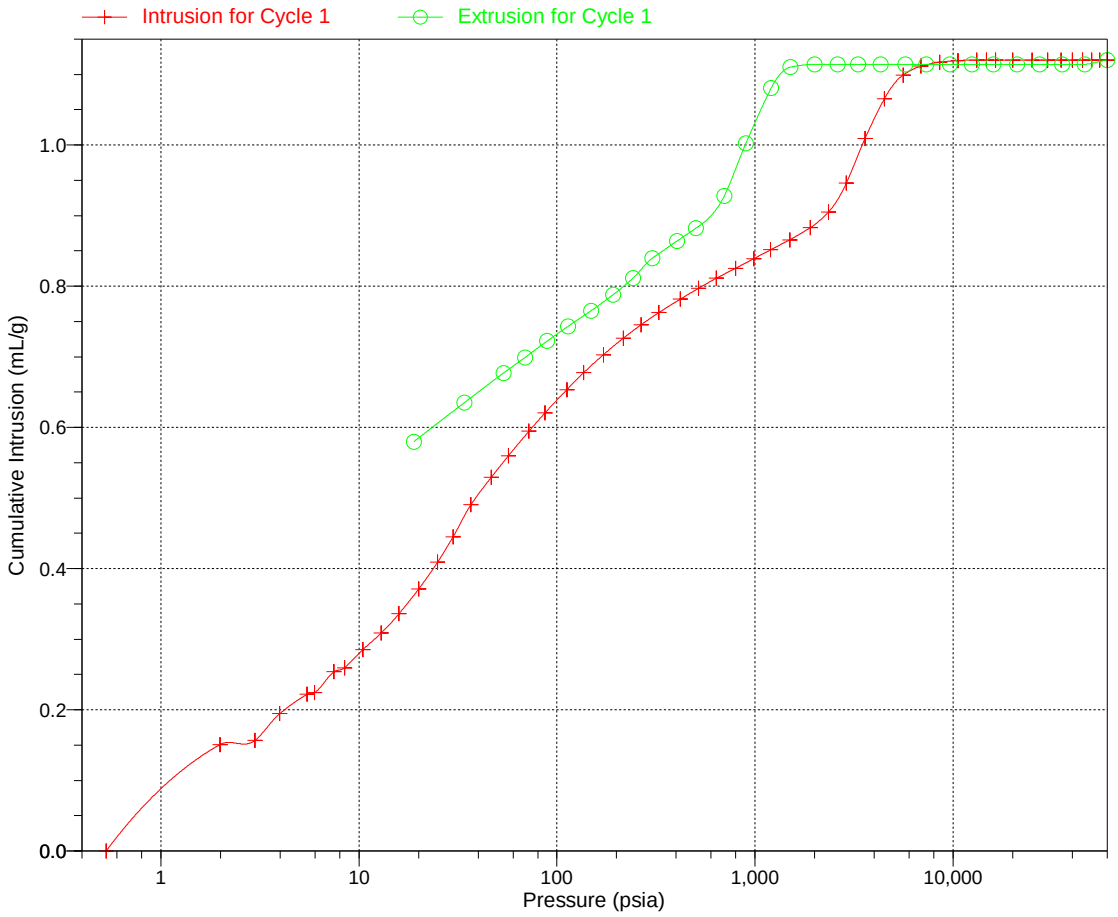

Sample ID: 000-501 Dolomite
Operator: Lars Erik Parnas
Submitter: Sintef
File: C:\9500\DATA\EKSTERN\000-501.SMP

LP Analysis Time: 16.05.2018 1:06:37
HP Analysis Time: 16.05.2018 2:03:17
Report Time: 16.05.2018 2:03:18

Sample Weight: 0.2074 g
Correction Type: None
Show Neg. Int: No

Incremental Intrusion vs Pressure

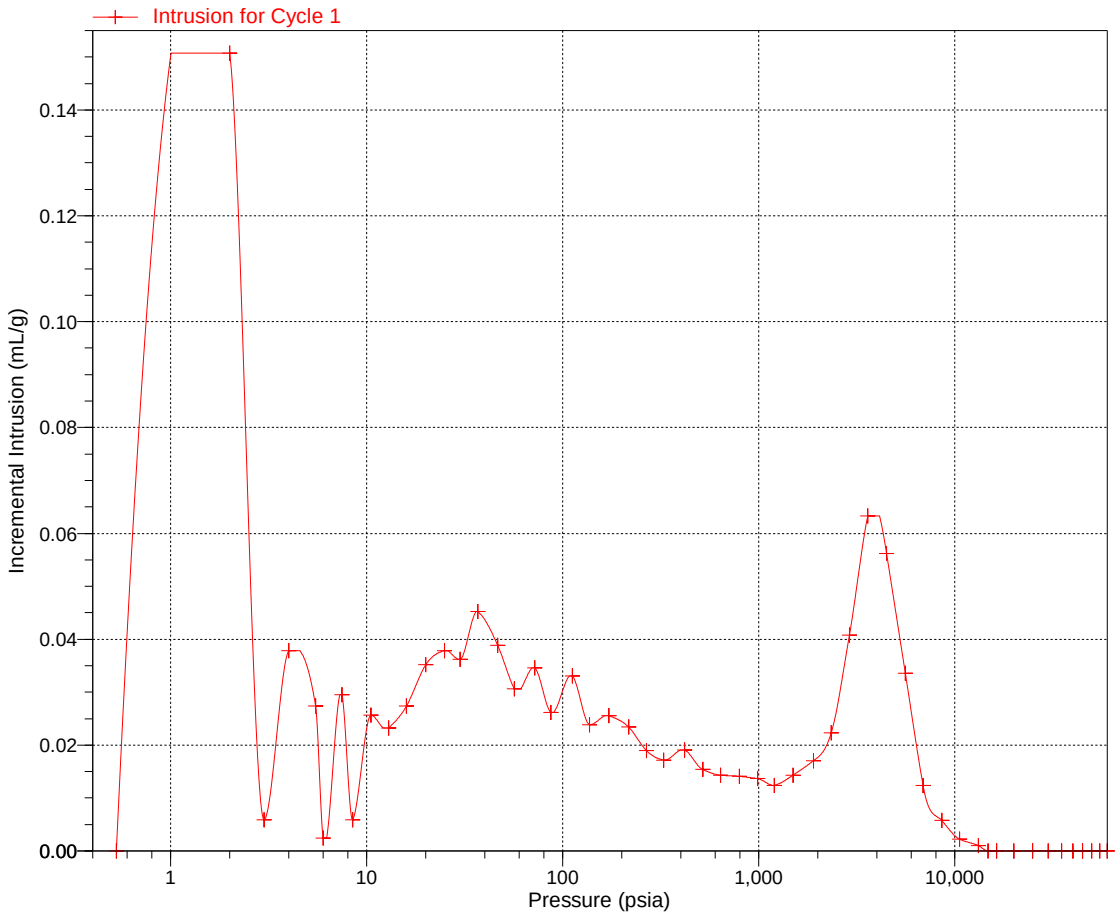

Sample ID: 000-501 Dolomite
Operator: Lars Erik Parnas
Submitter: Sintef
File: C:\9500\DATA\EKSTERN\000-501.SMP

LP Analysis Time: 16.05.2018 1:06:37
HP Analysis Time: 16.05.2018 2:03:17
Report Time: 16.05.2018 2:03:18

Sample Weight: 0.2074 g
Correction Type: None
Show Neg. Int: No

Differential Intrusion vs Pore size

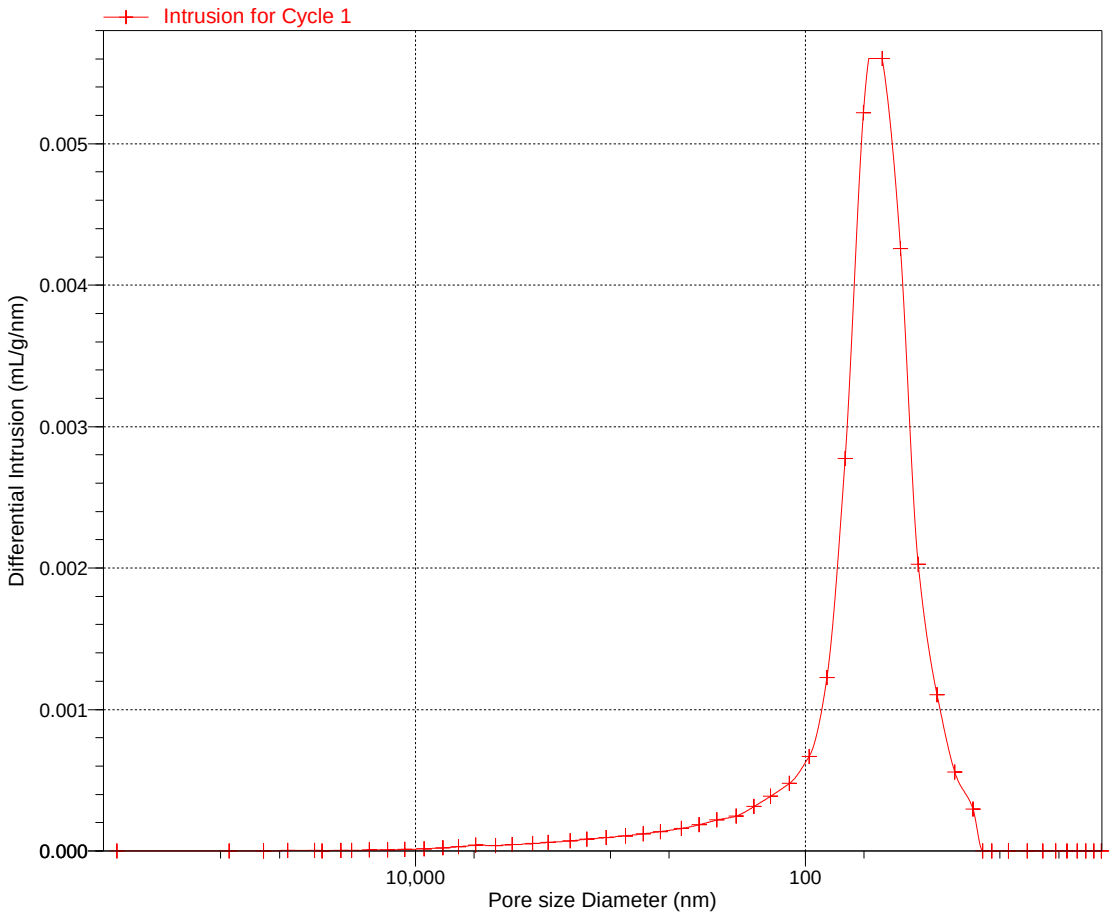

Sample ID: 000-501 Dolomite
Operator: Lars Erik Parnas
Submitter: Sintef
File: C:\9500\DATA\EKSTERN\000-501.SMP

LP Analysis Time: 16.05.2018 1:06:37
HP Analysis Time: 16.05.2018 2:03:17
Report Time: 16.05.2018 2:03:19

Sample Weight: 0.2074 g
Correction Type: None
Show Neg. Int: No

Cumulative Pore Area vs Pore size

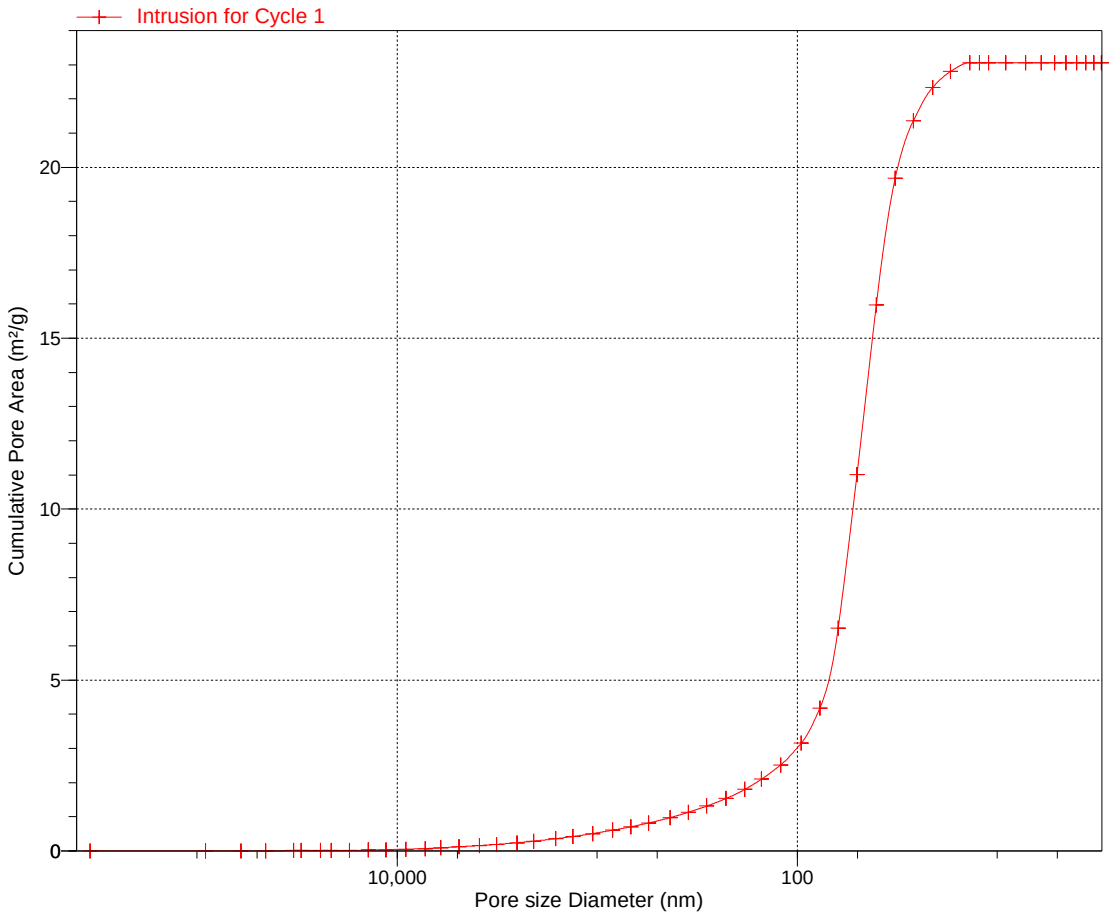

A7.11 Raw data TGA

A7.11.1 Raw data from TGA-dry

Sample: NO-1 500-850um 14.9mmg
Size: -42.0940 mg
Method: 10 cycle kinectic test
Comment: 14.9mg solid Analytical scale; 6%Al 2%Zr;120 g solid scal

TGA

File: C:...\NO-1 10 cycle kinetic baseline.001
Operator: Maria
Run Date: 07-May-2018 08:38
Instrument: TGA Q500 V6.7 Build 203

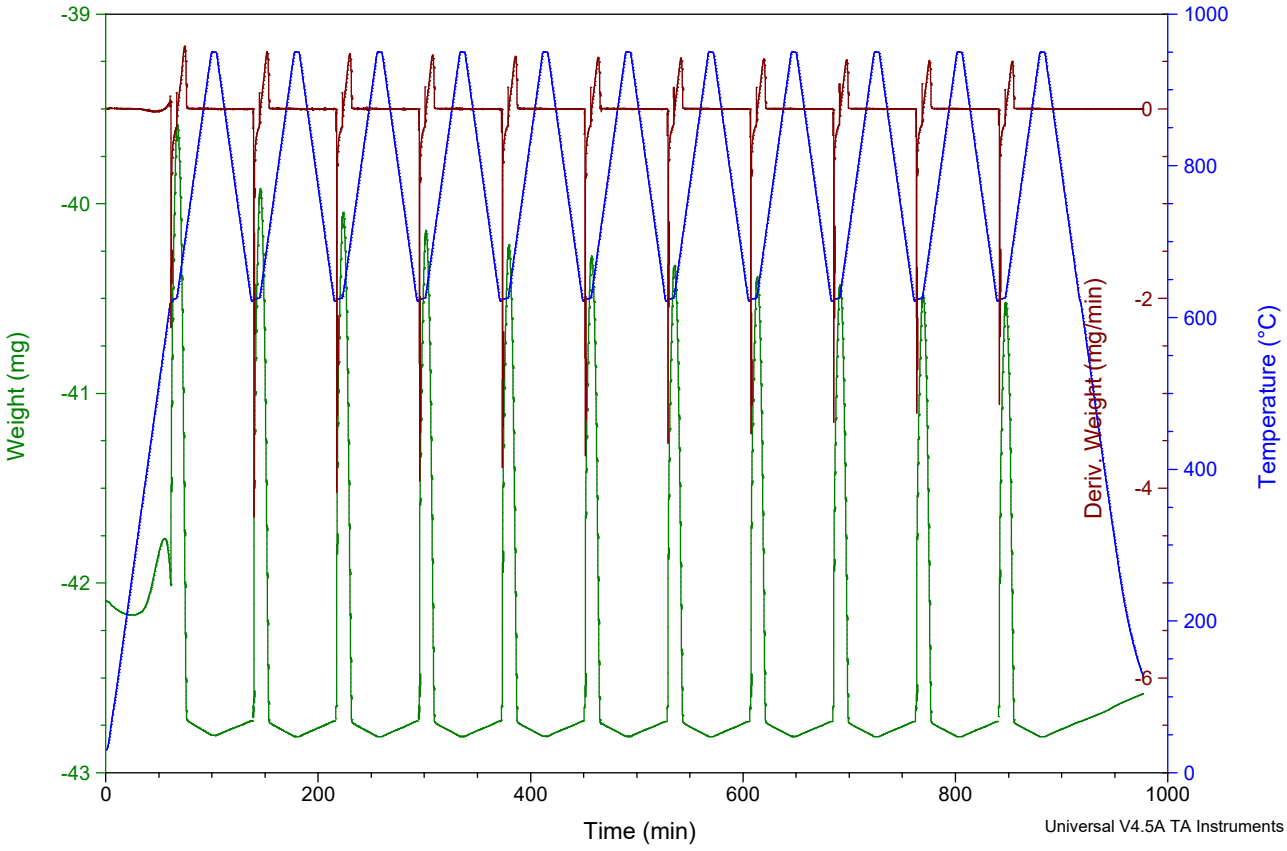

Universal V4.5A TA Instruments

Sample: NO-3 500-850um 15.7mg
Size: -41.1920 mg
Method: 10 cycle kinectic test
Comment: 15.7mg solid Analytical scale; 6%Al 2%Zr;120 g solid scal

TGA

File: C:...\NO-3 10 cycle kinetic baseline.001
Operator: Maria
Run Date: 04-May-2018 11:52
Instrument: TGA Q500 V6.7 Build 203

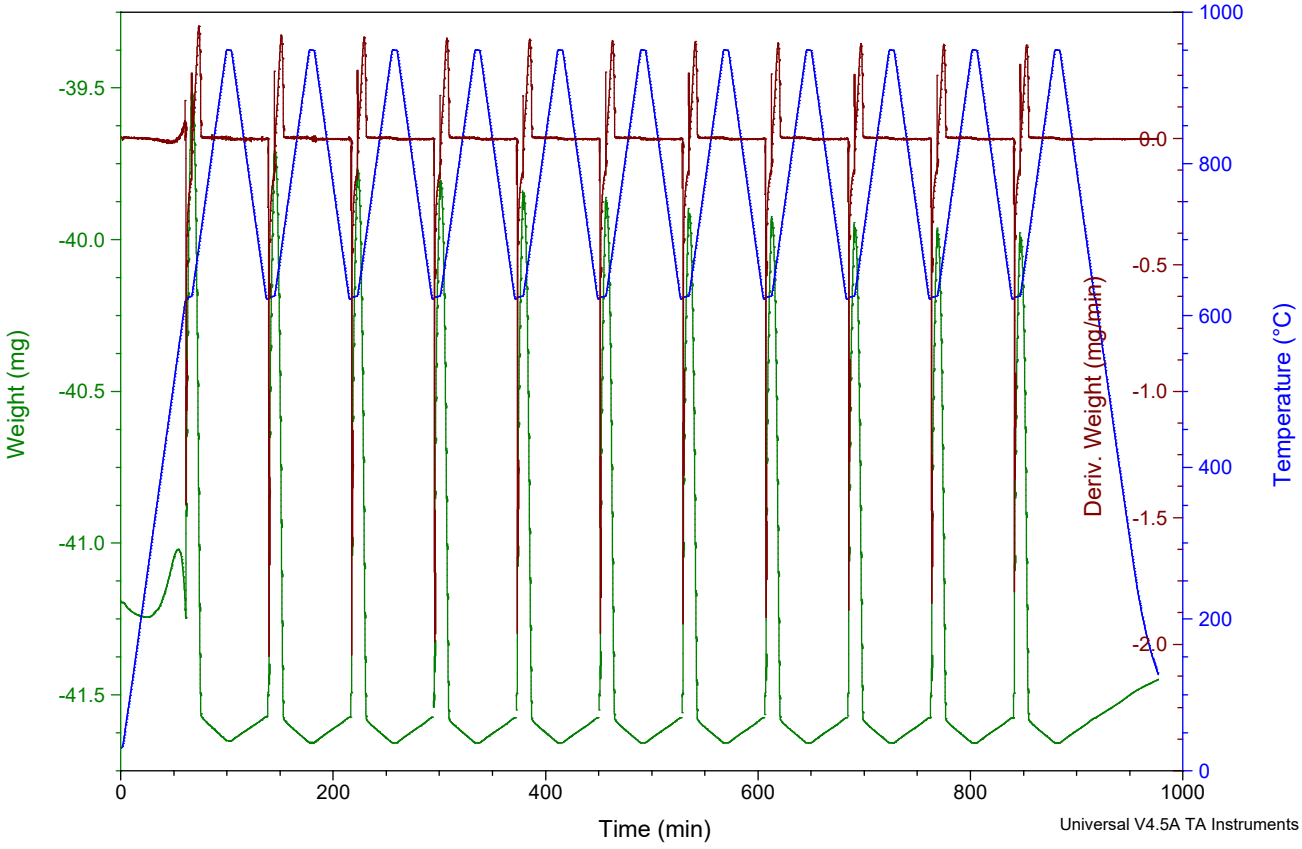

Universal V4.5A TA Instruments

Sample: NO-6 850-500um calcined
Size: 13.3560 mg
Method: 10 cycle kinectic baseline
Comment: 17,4mg at start

TGA

File: C:...\NO-6 10 cycle kinetic baseline.001
Operator: Maria Olsvik
Run Date: 08-Mar-2018 10:58
Instrument: TGA Q500 V6.7 Build 203

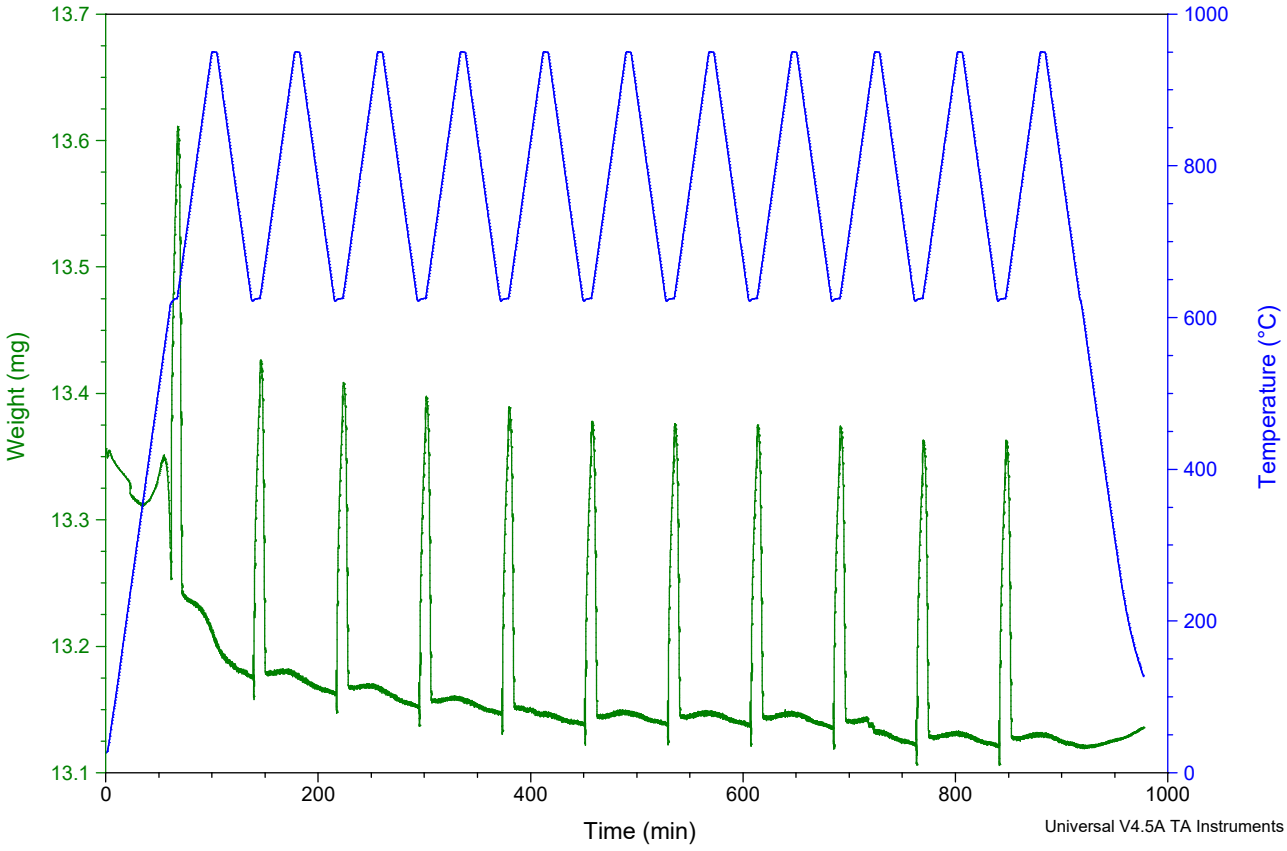

Universal V4.5A TA Instruments

Sample: NO-6 test2 calcined
Size: 46.5820 mg
Method: 10 cycle kinectic baseline
Comment: 18,1 mg before test

TGA

File: NO-6 test2 10 cycle kinetic baseline.001
Operator: Maria Olsvik
Run Date: 20-Mar-2018 11:40
Instrument: TGA Q500 V6.7 Build 203

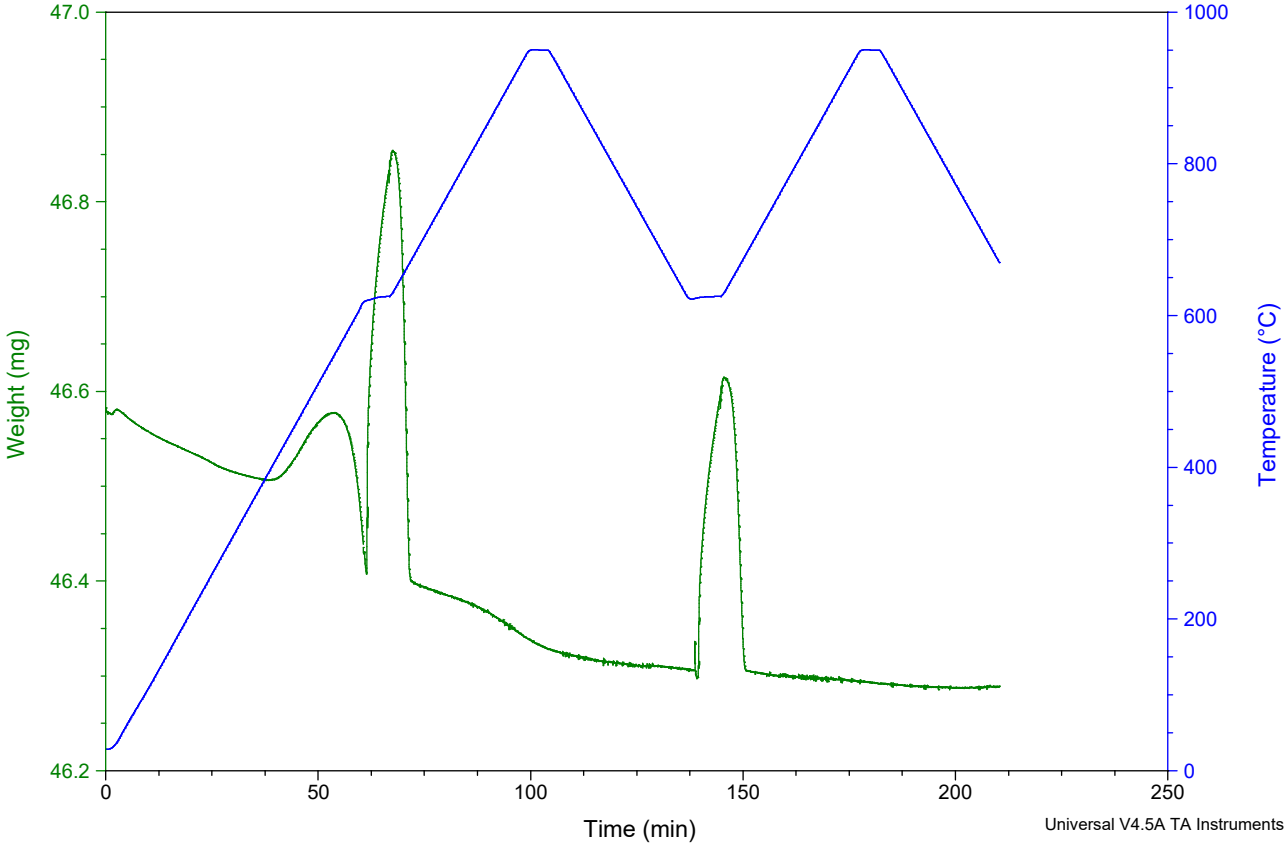

Universal V4.5A TA Instruments

Sample: NO-6m test2 10 cycle kinetic t
Size: -38.5270 mg
Method: 10 cycle kinectic test
Comment: NO-6 milled 5min test 2 m=18.2 mg

TGA

File: NO-6 milled5min test 2 10 cycle kine...
Operator: Maria Olsvik
Run Date: 10-Apr-2018 11:18
Instrument: TGA Q500 V6.7 Build 203

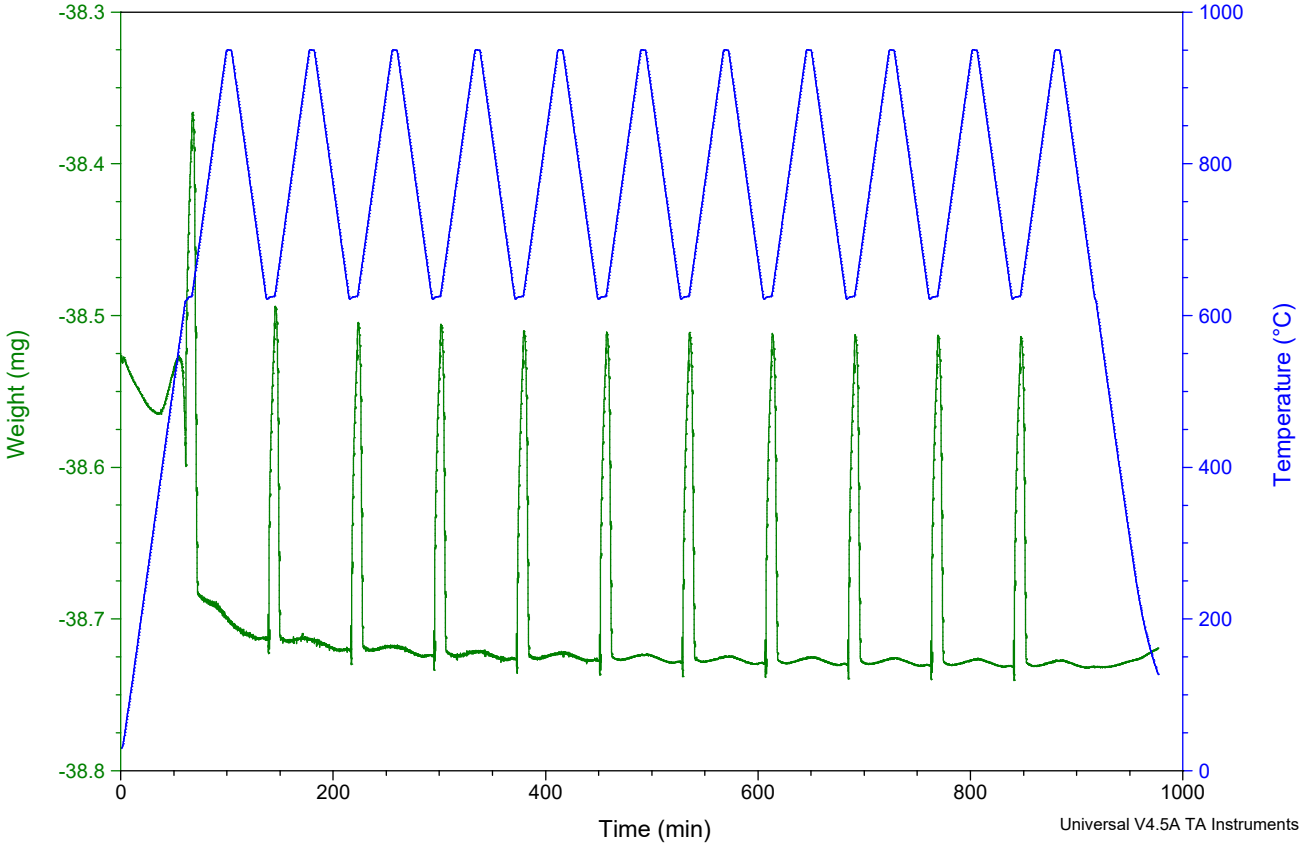

Universal V4.5A TA Instruments

Sample: NO-6m test2 10 cycle kinetic t
Size: -38.5270 mg
Method: 10 cycle kinectic test
Comment: NO-6 milled 5min test 2 m=18.2 mg

TGA

File: NO-6 milled5min test 2 10 cycle kine...
Operator: Maria Olsvik
Run Date: 10-Apr-2018 11:18
Instrument: TGA Q500 V6.7 Build 203

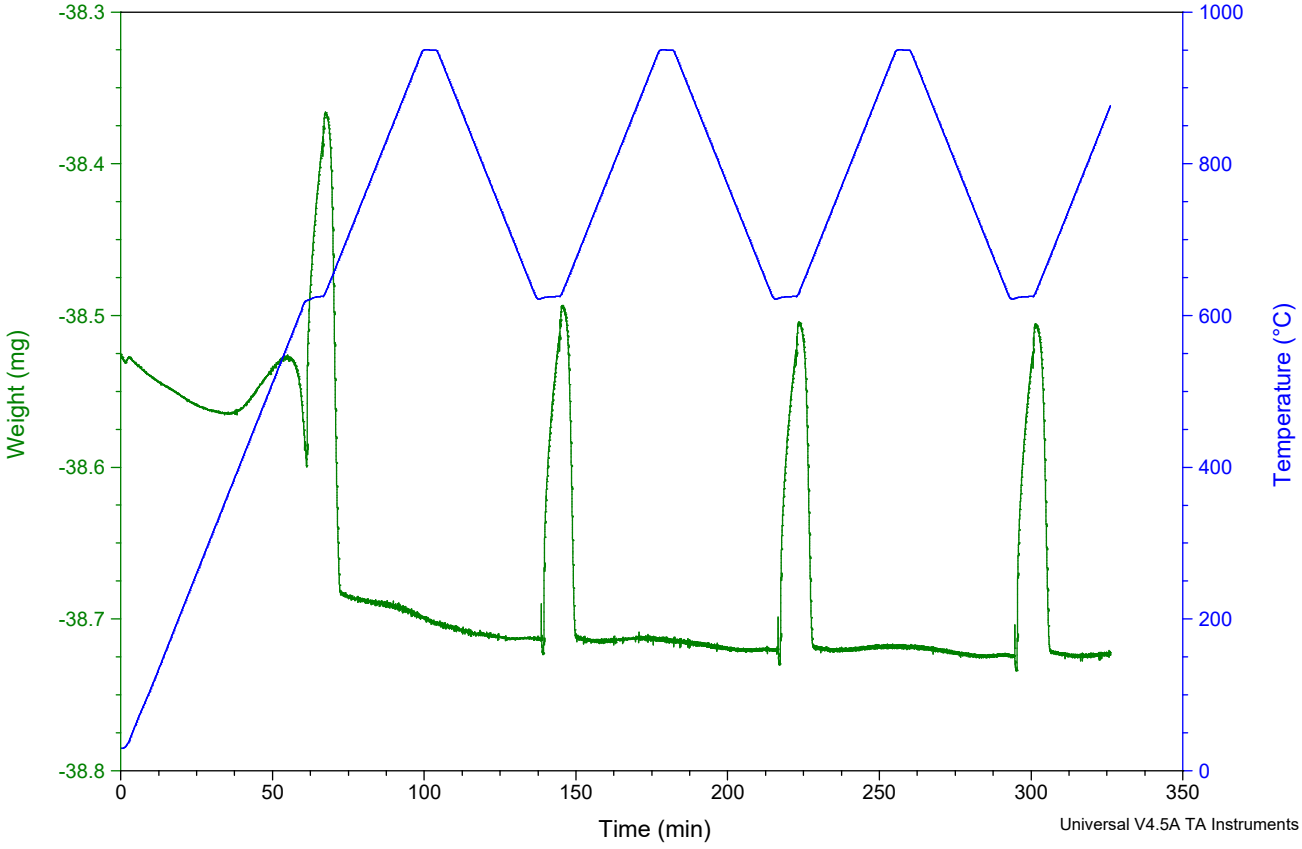

Universal V4.5A TA Instruments

Sample: NO-8 500-850um 15mg
Size: -42.0910 mg
Method: 10 cycle kinectic test
Comment: NO-8 14.9mg

TGA

File: ...\NO-8 10 cycle kinetic baseline.001
Operator: Maria
Run Date: 21-May-2018 15:54
Instrument: TGA Q500 V6.7 Build 203

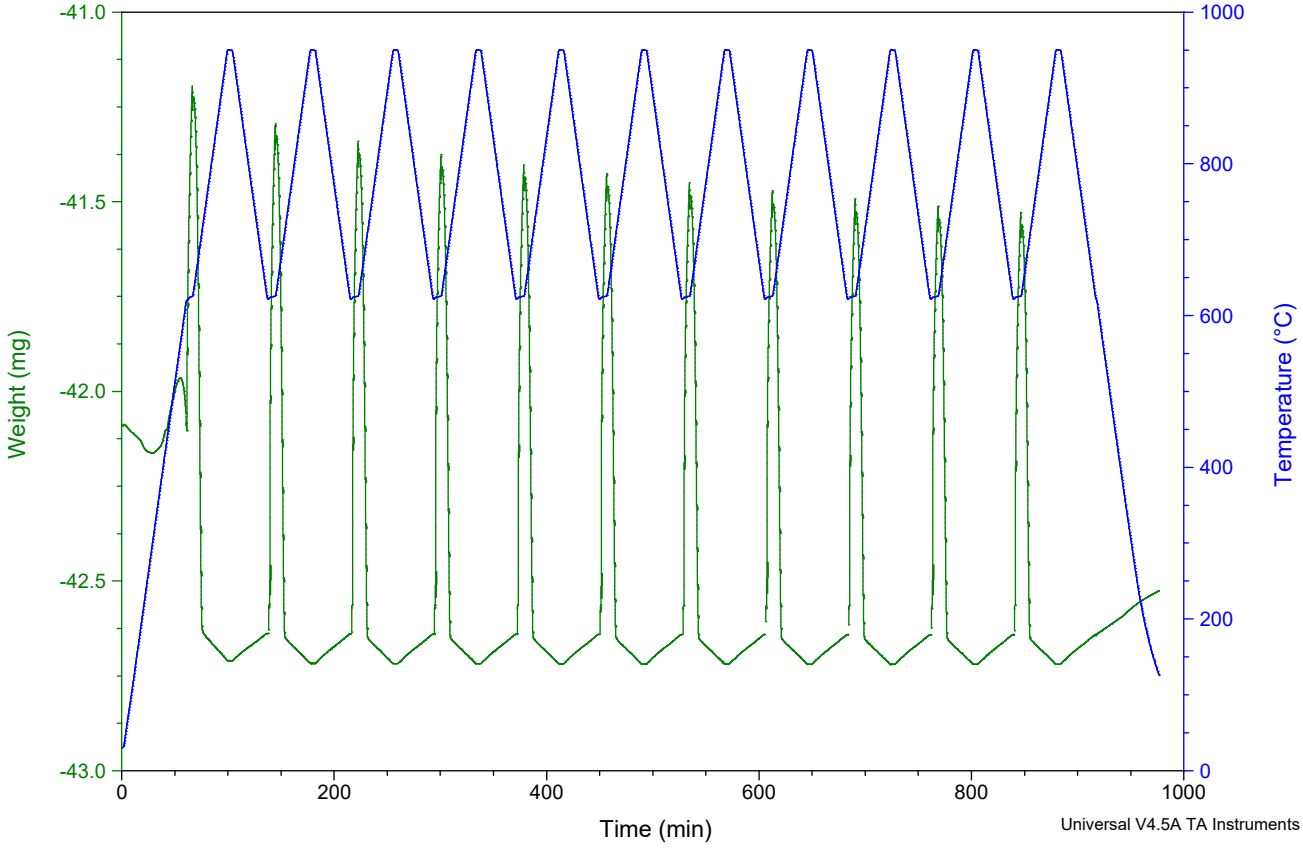

Universal V4.5A TA Instruments

Sample: Mar_2 10 cycle kinetic test
Size: -40.1640 mg
Method: 10 cycle kinectic test
Comment: mar_2 500-850um

TGA

File: Mar_2 test 3 10 cycle kinetic textfil
Operator: Maria Olsvik
Run Date: 05-Apr-2018 09:30
Instrument: TGA Q500 V6.7 Build 203

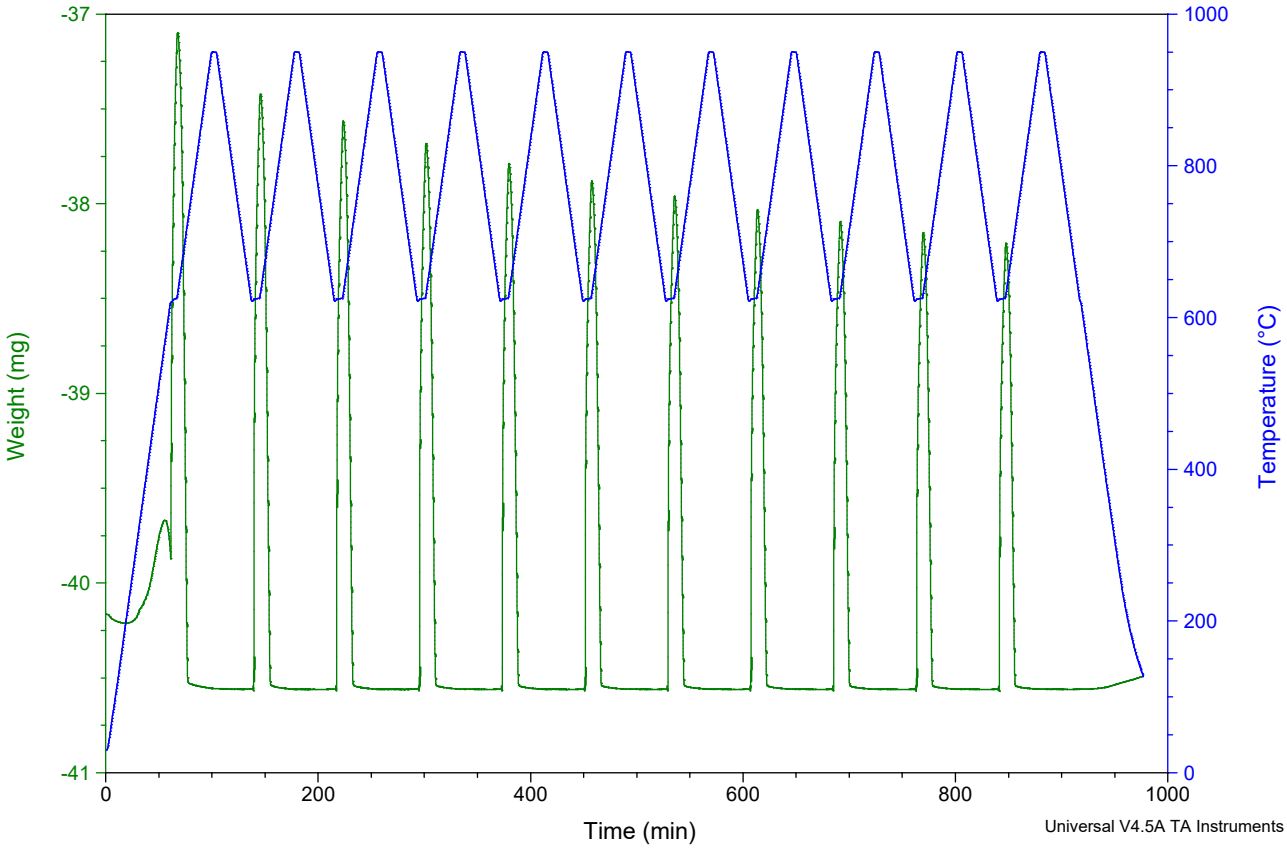

Universal V4.5A TA Instruments

Sample: NO-12 850-500um calcined
Size: 13.3770 mg
Method: 10 cycle kinectic baseline

TGA

File: NO-12 10 cycle kinetic baseline (2).002
Operator: Maria Olsvik
Run Date: 07-Mar-2018 10:28
Instrument: TGA Q500 V6.7 Build 203

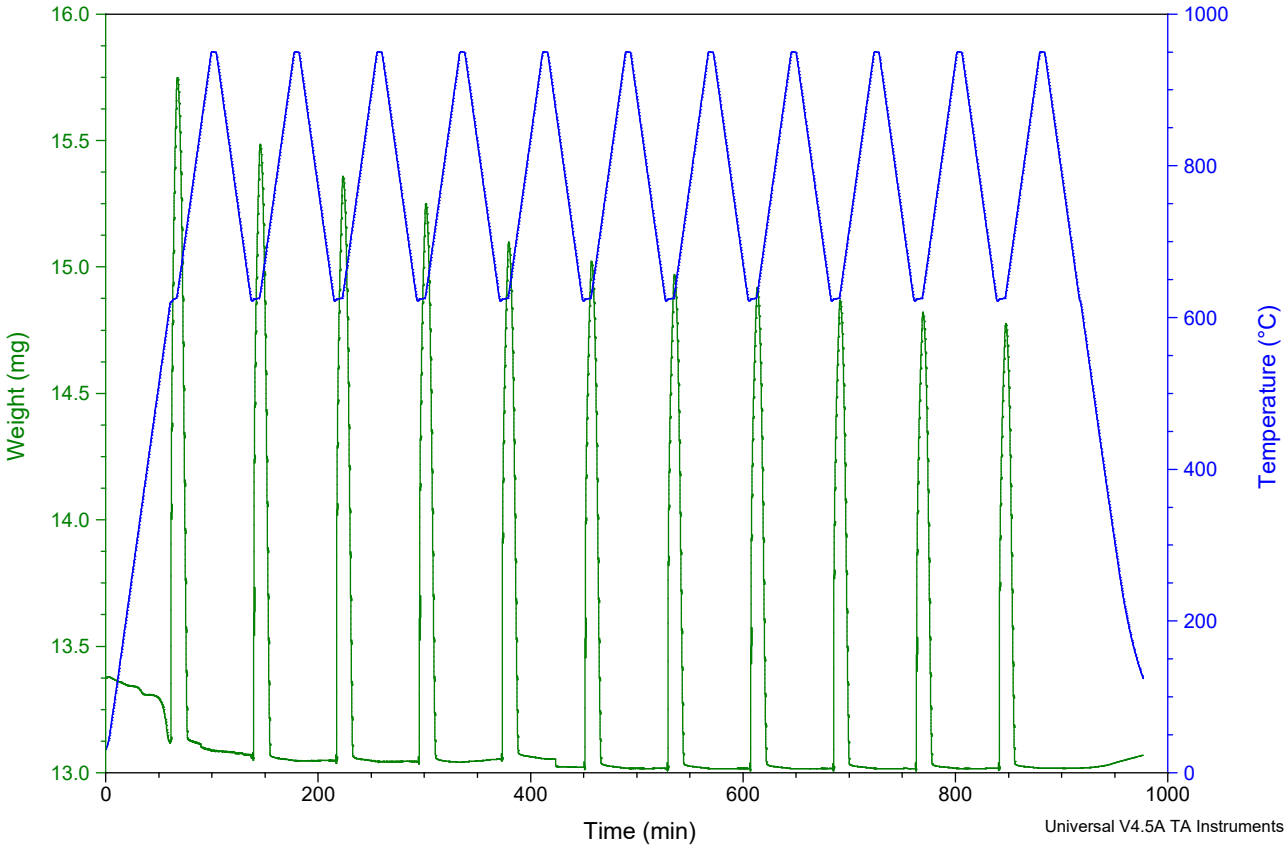

Universal V4.5A TA Instruments

Sample: NO-12 850-500um calcined
Size: 17.3000 mg
Method: 10 cycle kinectic baseline

TGA

File: ...\NO-12 10 cycle kinetic baseline.002
Operator: Maria Olsvik
Run Date: 07-Mar-2018 10:28
Instrument: TGA Q500 V6.7 Build 203

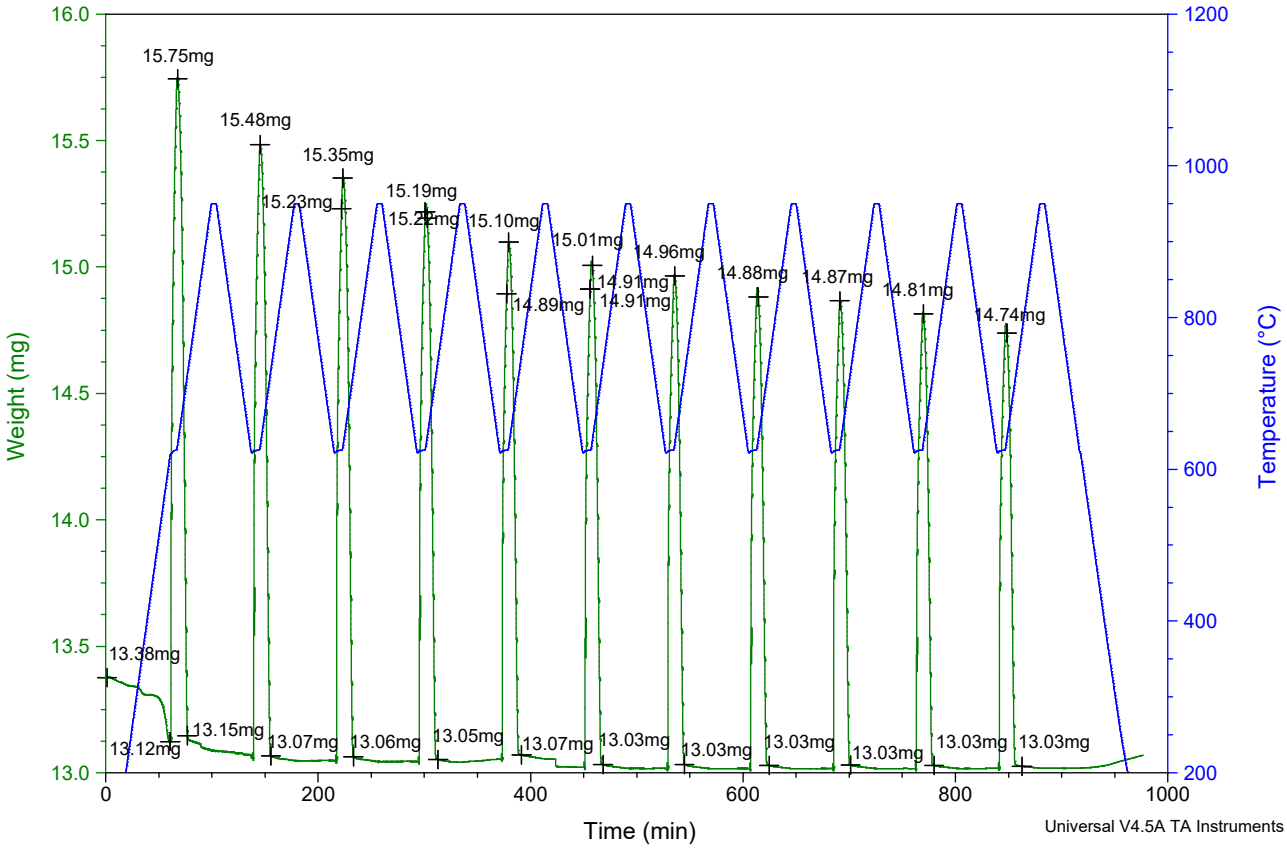

Universal V4.5A TA Instruments

Sample: NO-20 uncalcined 500-850um
Size: -0.0080 mg
Method: cal.+10 cycle kinectic baselin
Comment: 25,7 mg before test

TGA

File: NO-20 10 cycle kinetic baseline+calc...
Operator: Maria Olsvik
Run Date: 21-Mar-2018 10:51
Instrument: TGA Q500 V6.7 Build 203

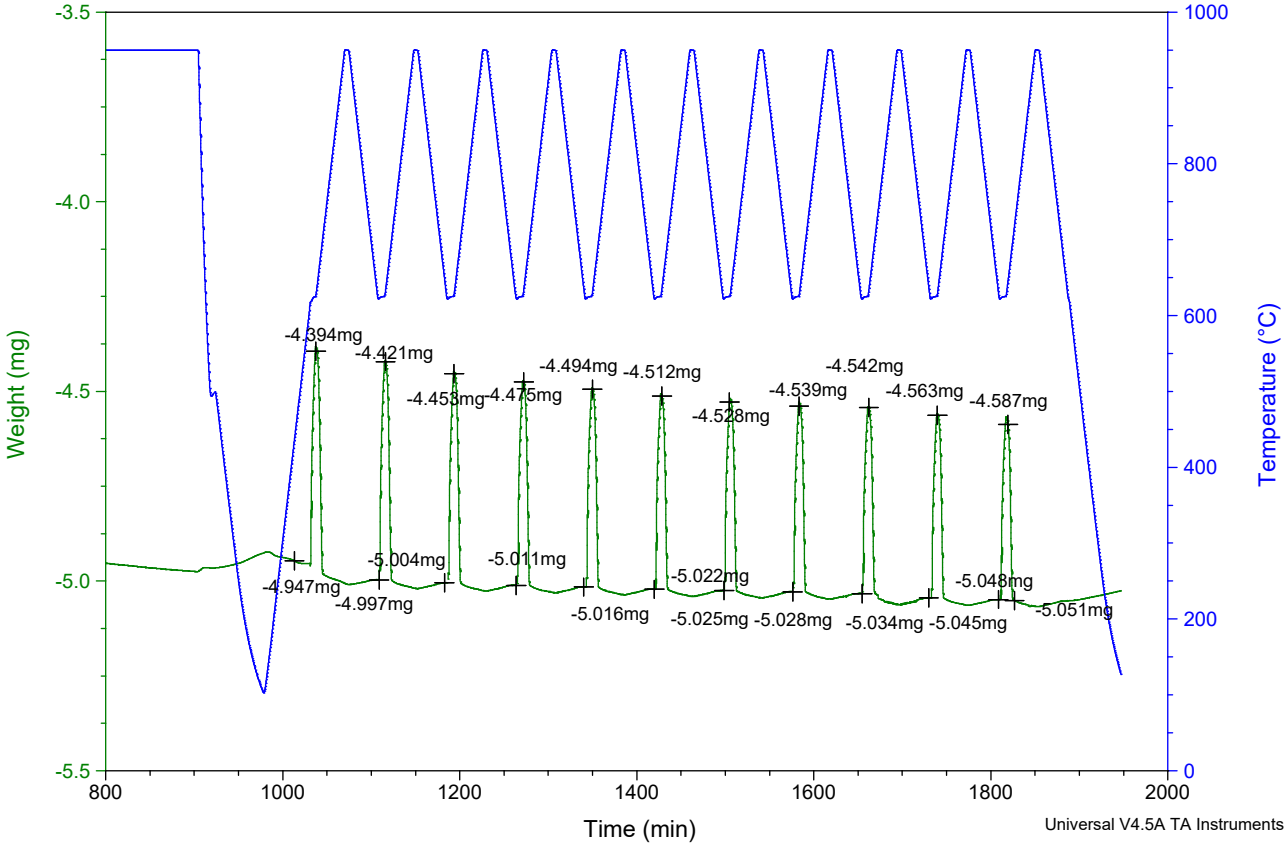

Universal V4.5A TA Instruments

Sample: NO-21 uncalcined 500-850um
Size: 26.3000 mg
Method: cal.+10 cycle kinectic baselin
Comment: 26,3 mg before test

TGA

File: NO-21 10 cycle kinetic baseline+calc...
Operator: Maria Olsvik
Run Date: 23-Mar-2018 10:47
Instrument: TGA Q500 V6.7 Build 203

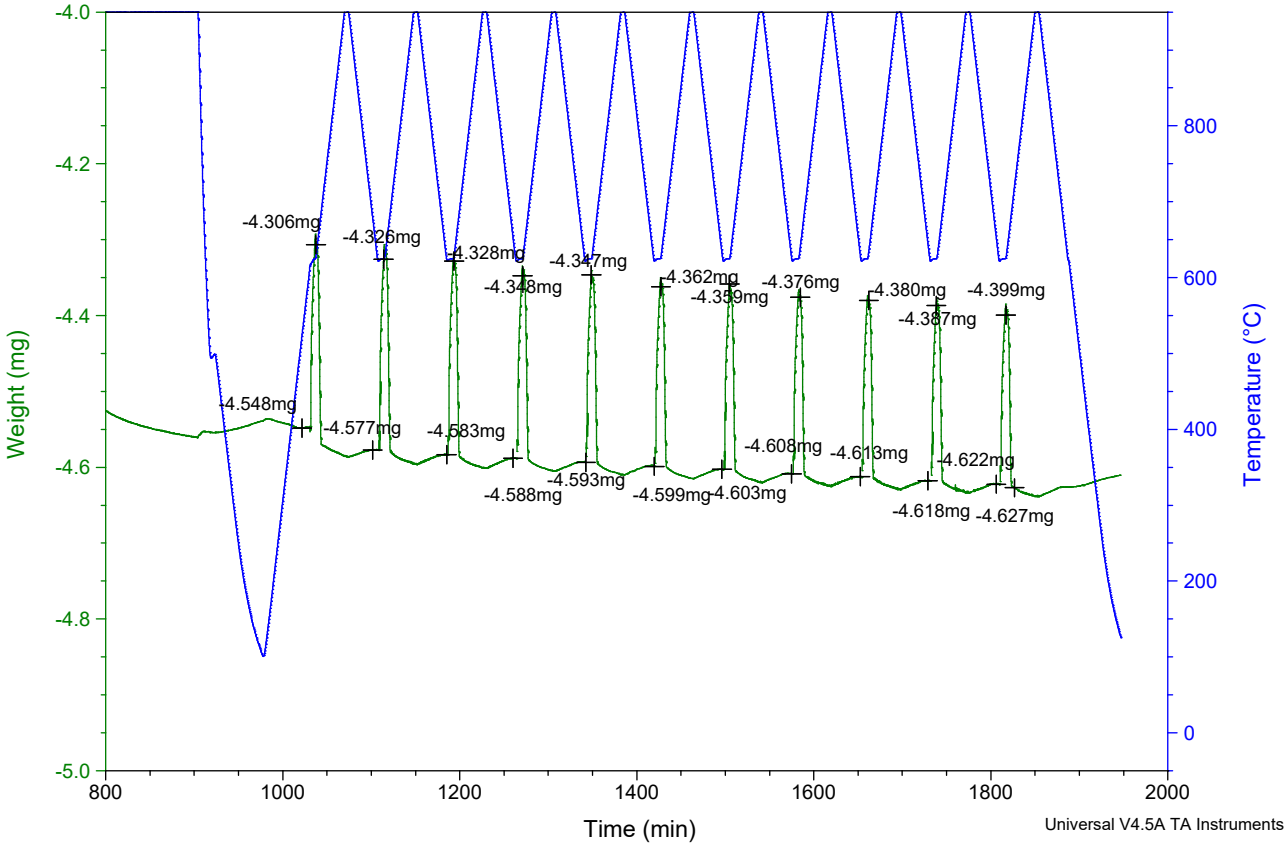

Universal V4.5A TA Instruments

Sample: NO-22 test210 cycle kinetic tes
Size: 15.9000 mg
Method: 10 cycle kinectic test
Comment: NO-22 test 2 m=15.9 mg

TGA

File: C:...\NO-22 test 2 10 cycle kinetic.001
Operator: Maria Olsvik
Run Date: 06-Apr-2018 10:45
Instrument: TGA Q500 V6.7 Build 203

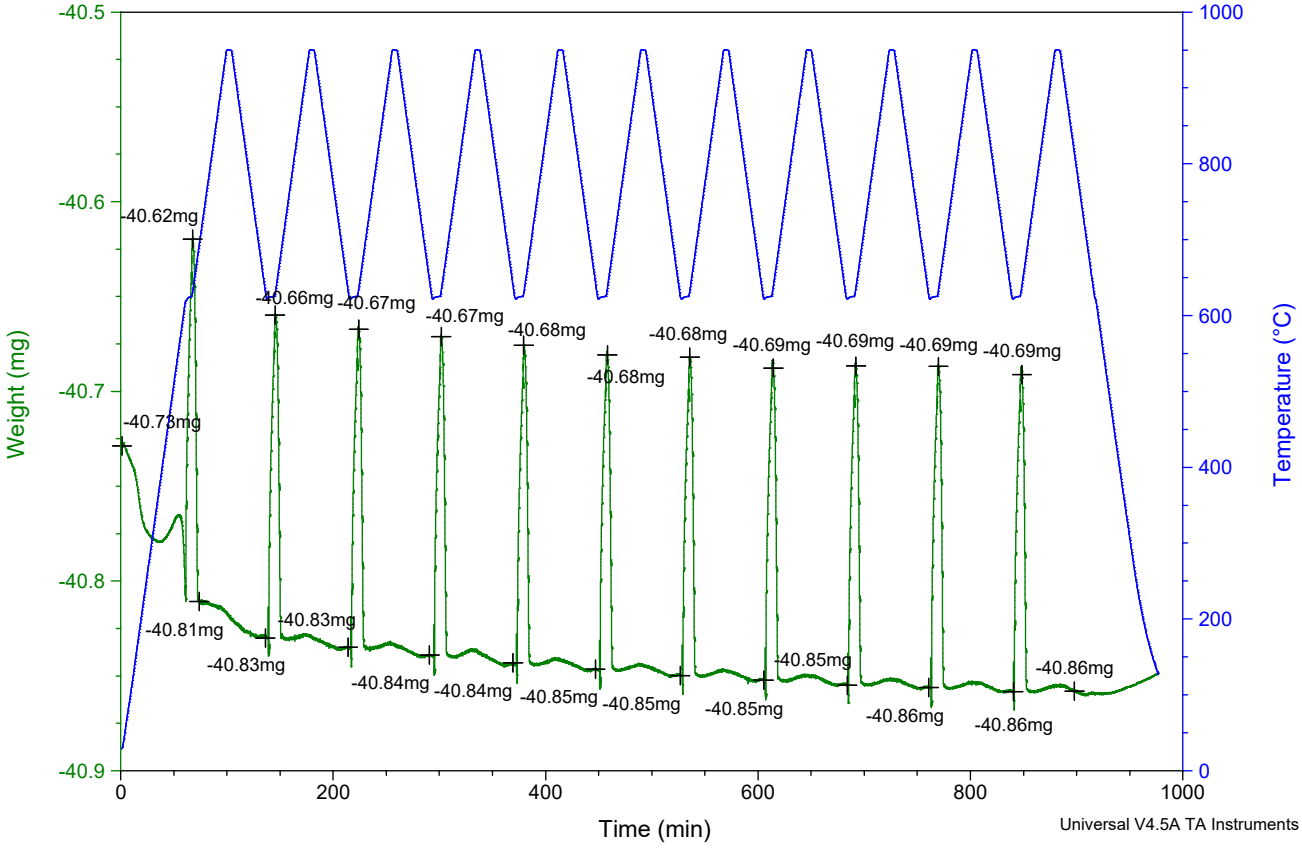

Universal V4.5A TA Instruments

Sample: NO-23 test2 10 cycle kinetic te
Size: -41.6020 mg
Method: 10 cycle kinectic test
Comment: NO-23 test 2 m=15.3 mg

TGA

File: C:...\NO-23 test 2 10 cycle kinetic.001
Operator: Maria Olsvik
Run Date: 09-Apr-2018 08:32
Instrument: TGA Q500 V6.7 Build 203

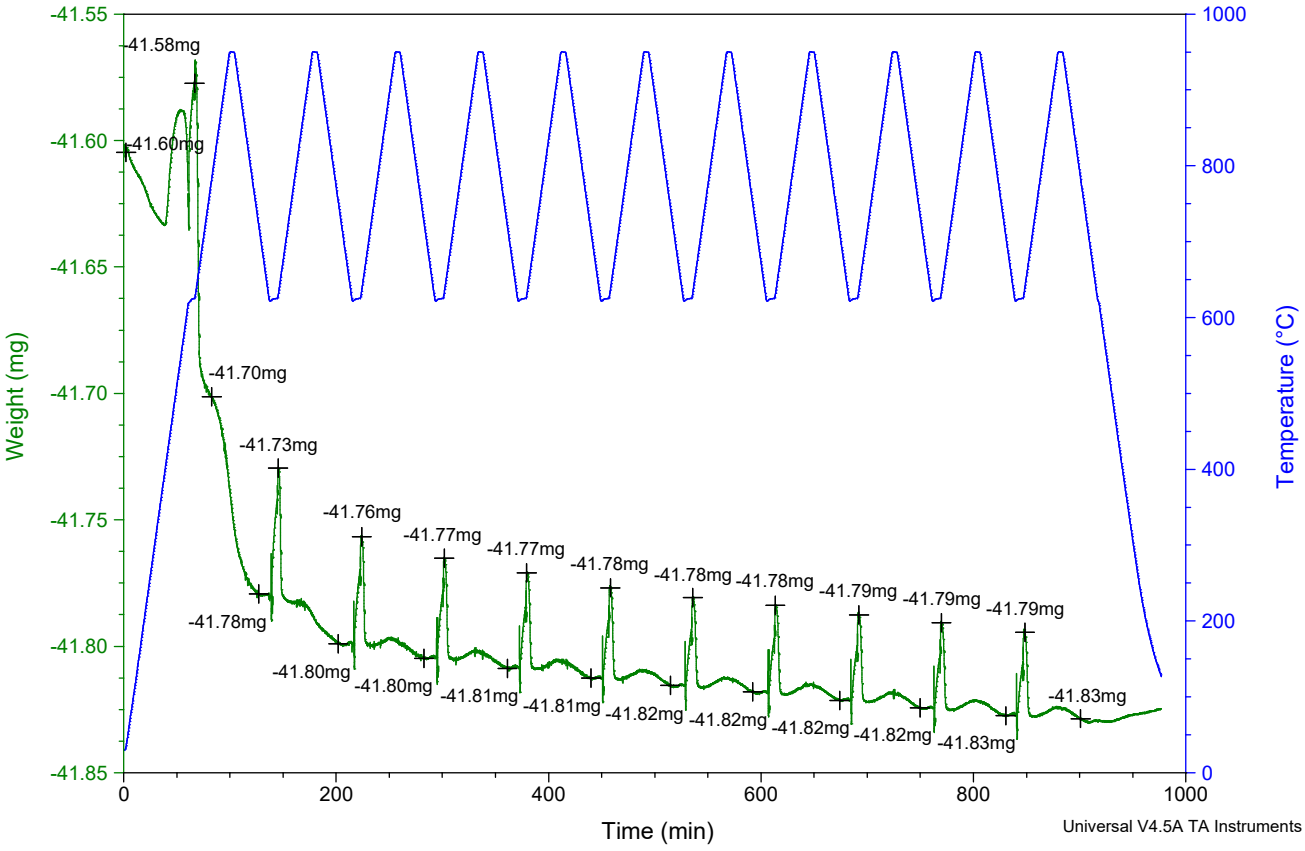

Universal V4.5A TA Instruments

Sample: NO8-12 250-400um 5.1mg test
Size: -51.6960 mg

TGA

File: Granulers 250-400um Fix bed NO8-12 so...
Operator: Maria
Run Date: 25-Apr-2018 14:33
Instrument: TGA Q500 V6.7 Build 203

Comment: 5.1mg solid Analytical scale; 6%Al 2%Zr;120 g solid scal

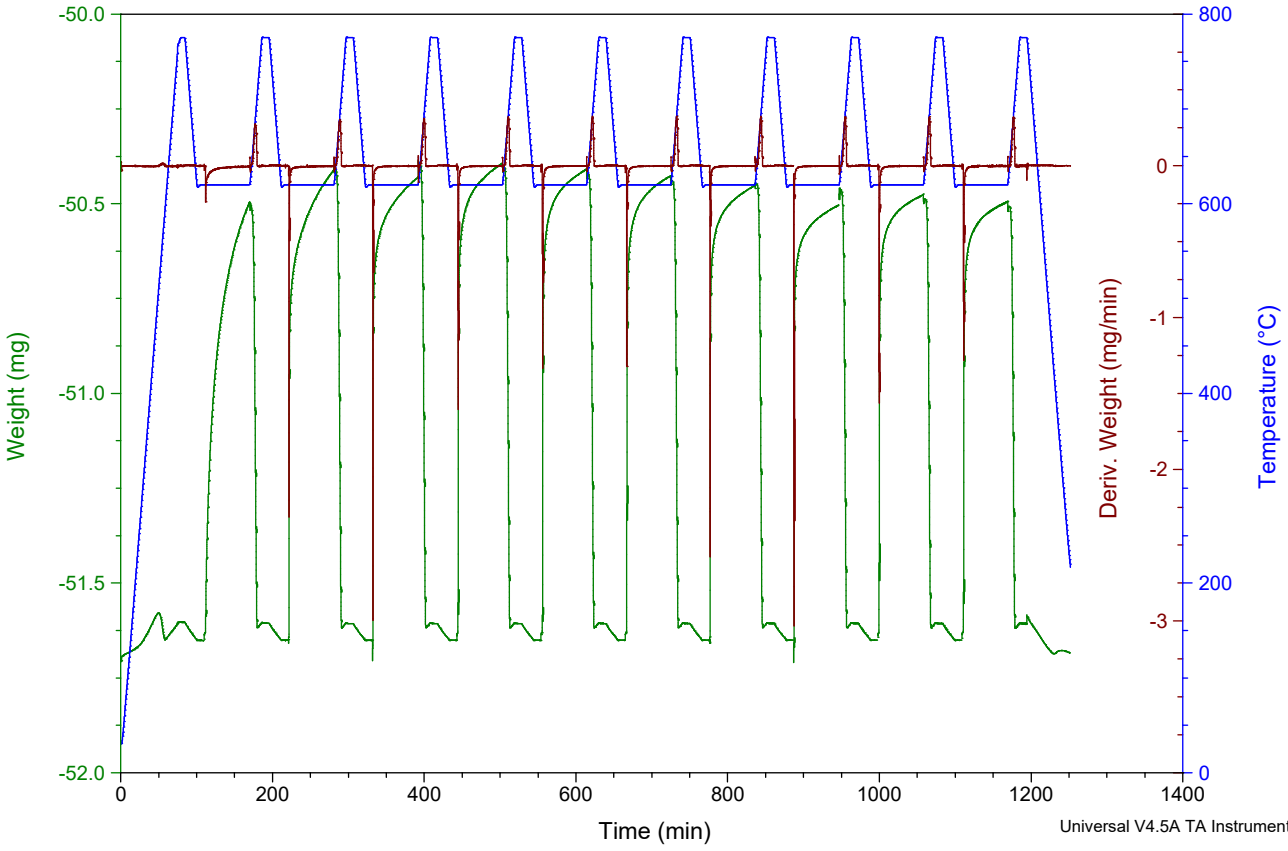

Universal V4.5A TA Instruments

Sample: NO8-12 250-400um 30.1mg test
Size: -26.5340 mg

Comment: 30.1mg solid Analytical scale; 6%Al 2%Zr;120 g solid scal

TGA

File: Granulers 250-400um Fix bed NO8-12 so...
Operator: Maria
Run Date: 26-Apr-2018 12:34
Instrument: TGA Q500 V6.7 Build 203

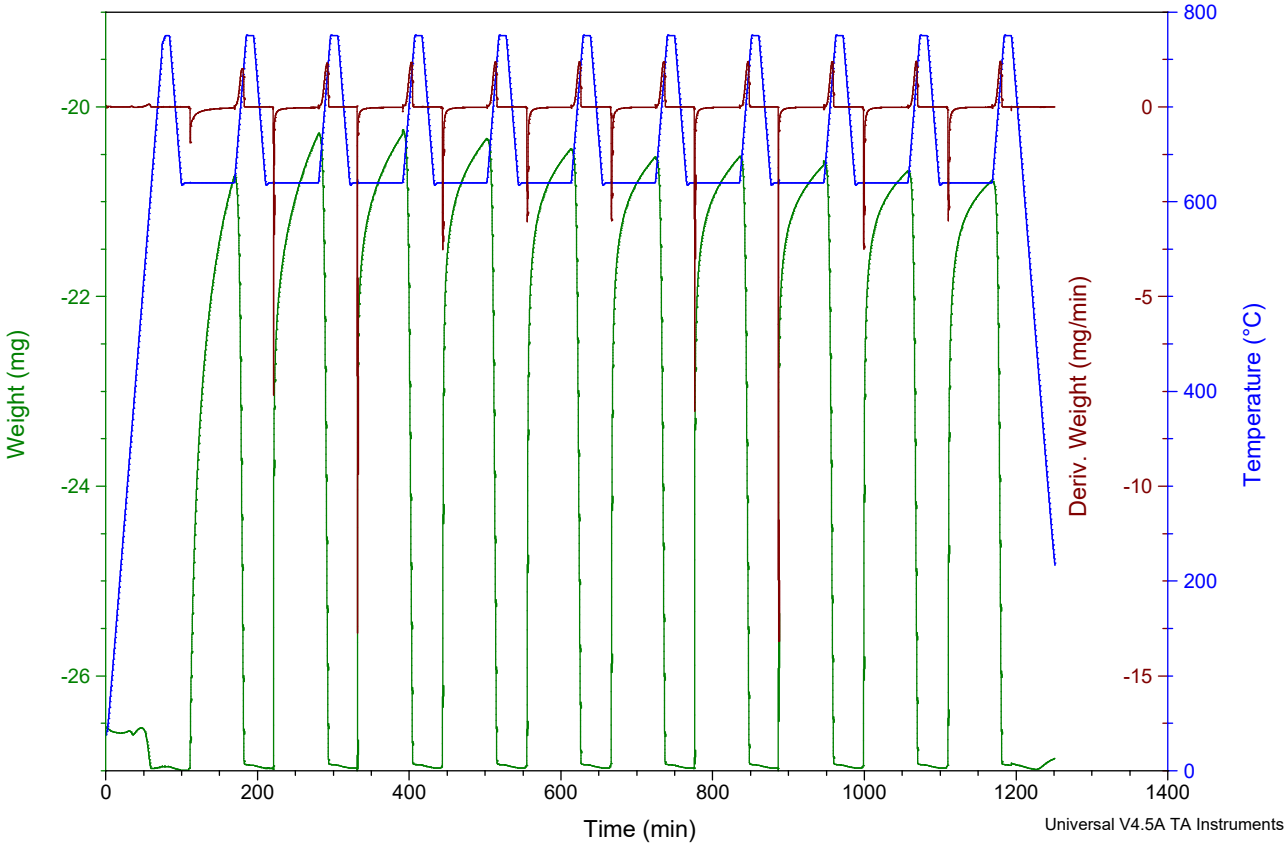

Universal V4.5A TA Instruments

Sample: NO8-12 250-400um 15.7mg 550de
Size: -41.2130 mg

Comment: 15.7mg solid Analytical scale; 6%Al 2%Zr;120 g solid scal

TGA

File: Granulers 250-400um Fix bed NO8-12 so...
Operator: Maria
Run Date: 30-Apr-2018 09:23
Instrument: TGA Q500 V6.7 Build 203

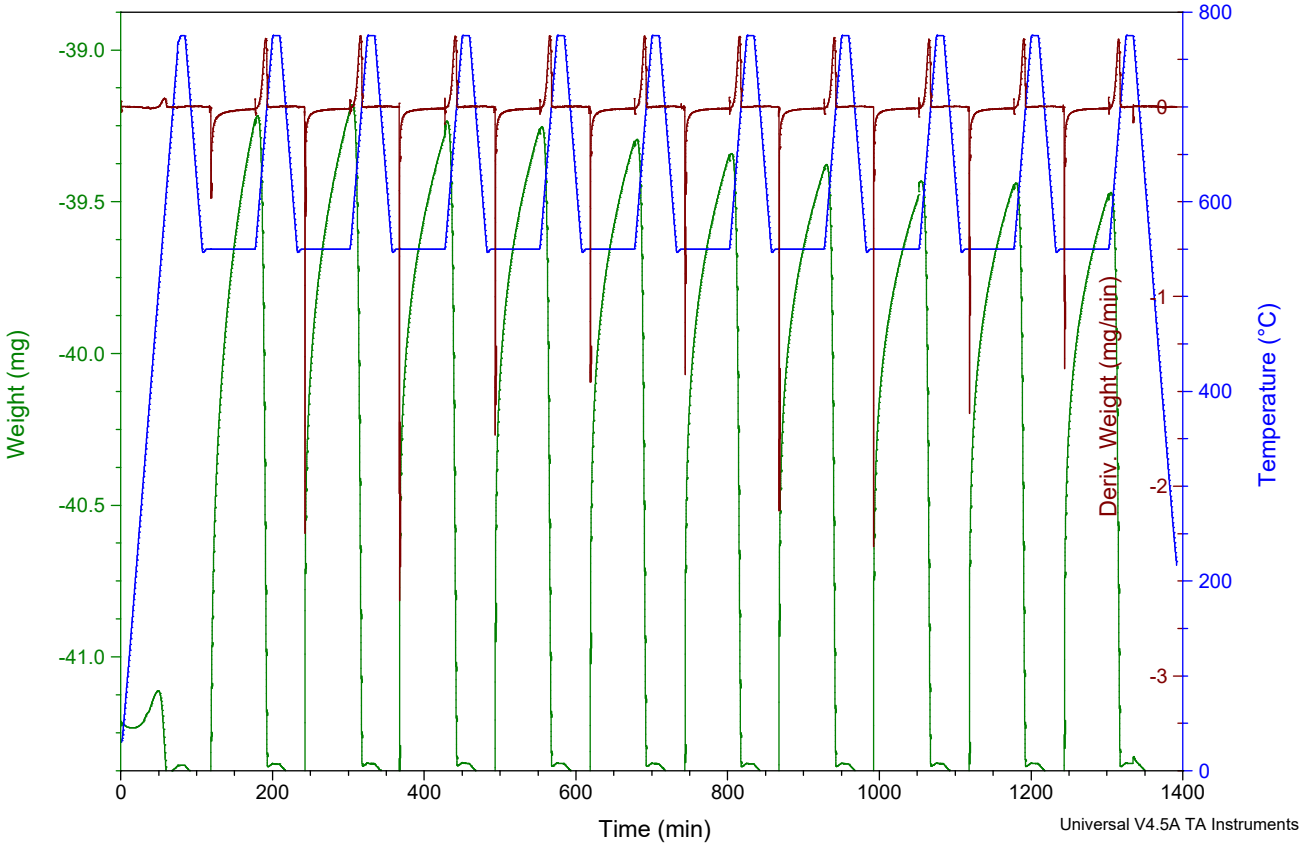

Universal V4.5A TA Instruments

Sample: NO8-12 250-400um 15.1mg 650de
Size: -42.0020 mg

Comment: 15.1mg solid Analytical scale; 6%Al 2%Zr;120 g solid scal

TGA

File: Granulers 250-400um Fix bed NO8-12 so...
Operator: Maria
Run Date: 01-May-2018 11:08
Instrument: TGA Q500 V6.7 Build 203

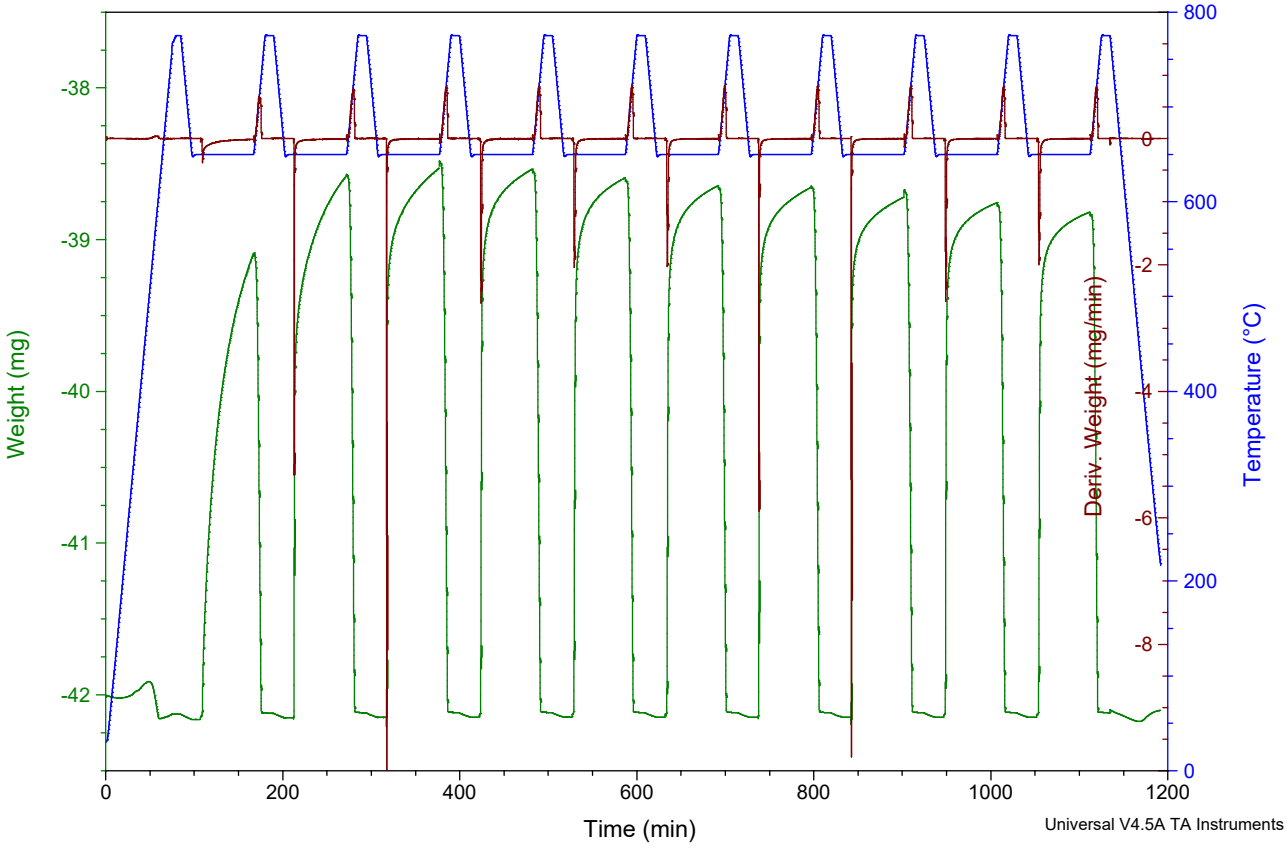

Universal V4.5A TA Instruments

Sample: NO8-12 250-400um 15.2mg 620de
Size: -41.9460 mg

Comment: 15.2mg solid Analytical scale; 6%Al 2%Zr;120 g solid scal

TGA

File: Granulers 250-400um Fix bed NO8-12 so...
Operator: Maria
Run Date: 27-Apr-2018 12:54
Instrument: TGA Q500 V6.7 Build 203

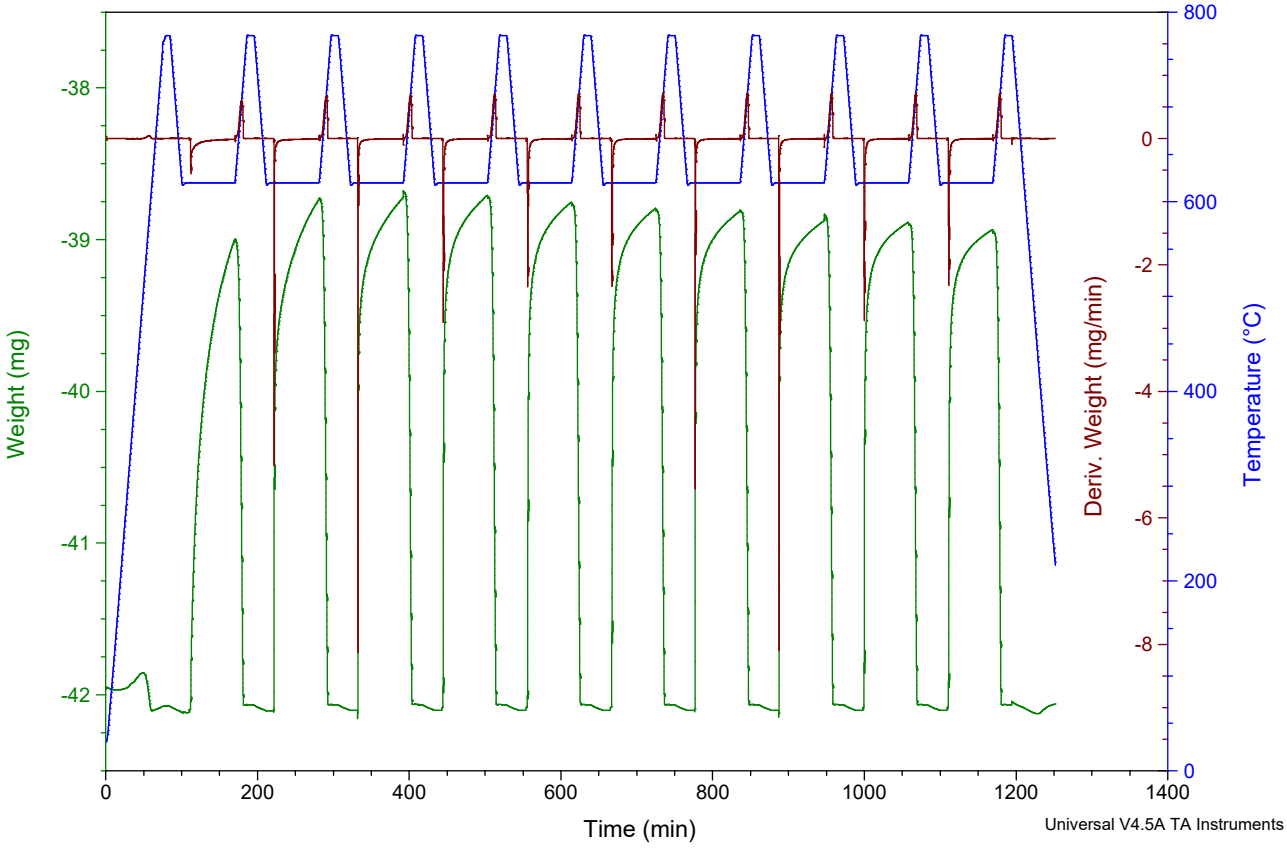

Universal V4.5A TA Instruments

Sample: NO8-12 1.2mm 14.9mg 620de
Size: -42.0290 mg

TGA

File: Granulers 1.2mm Fix bed NO8-12 sorpti...
Operator: Maria
Run Date: 02-May-2018 14:42
Instrument: TGA Q500 V6.7 Build 203

Comment: 14.9mg solid Analytical scale; 6%Al 2%Zr;120 g solid scal

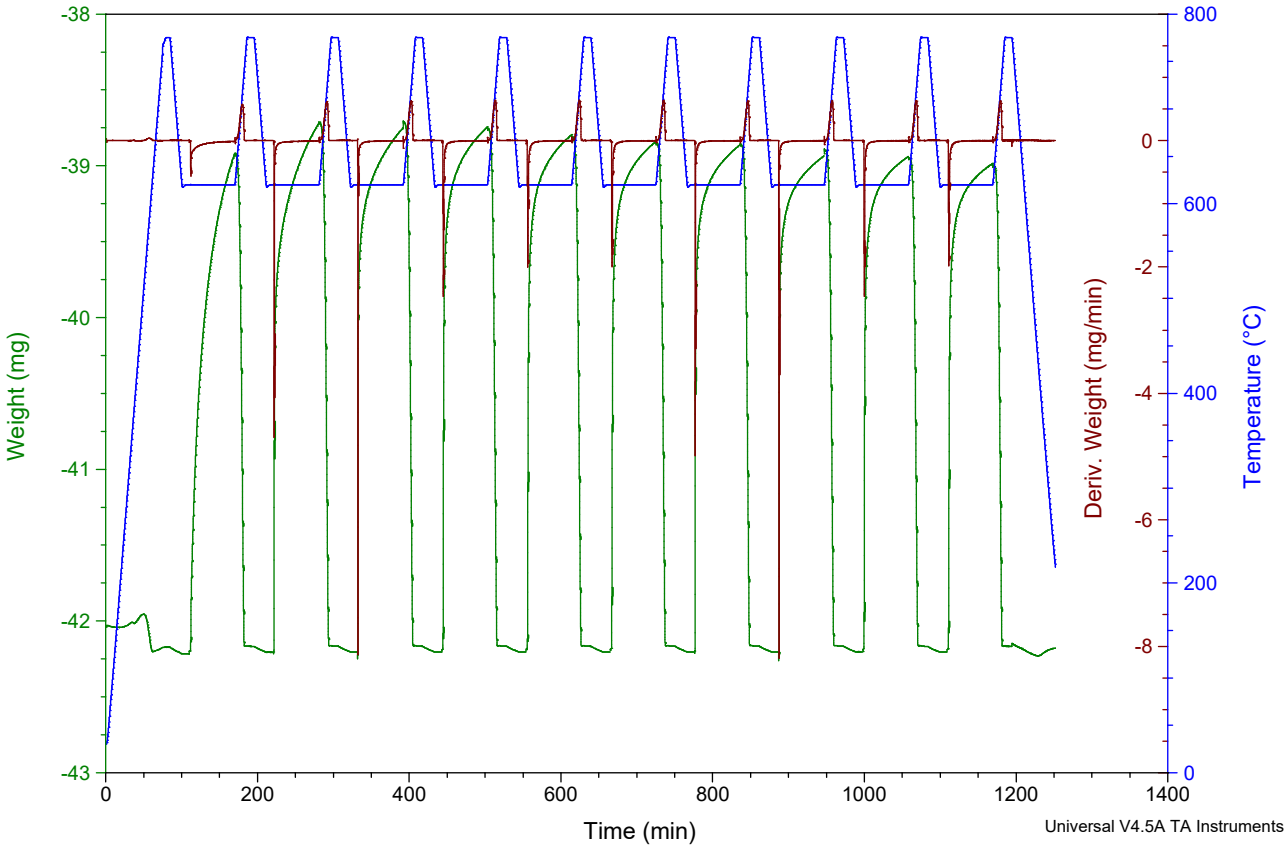

Universal V4.5A TA Instruments

Sample: NO8-12 1.2mm 15.2mg 620de
Size: -41.7910 mg

TGA

File: Granulers 1.2mm Fix bed NO8-12 sorpti...
Operator: Maria
Run Date: 03-May-2018 12:52
Instrument: TGA Q500 V6.7 Build 203

Comment: 15.2mg solid Analytical scale; 6%Al 2%Zr;120 g solid scal

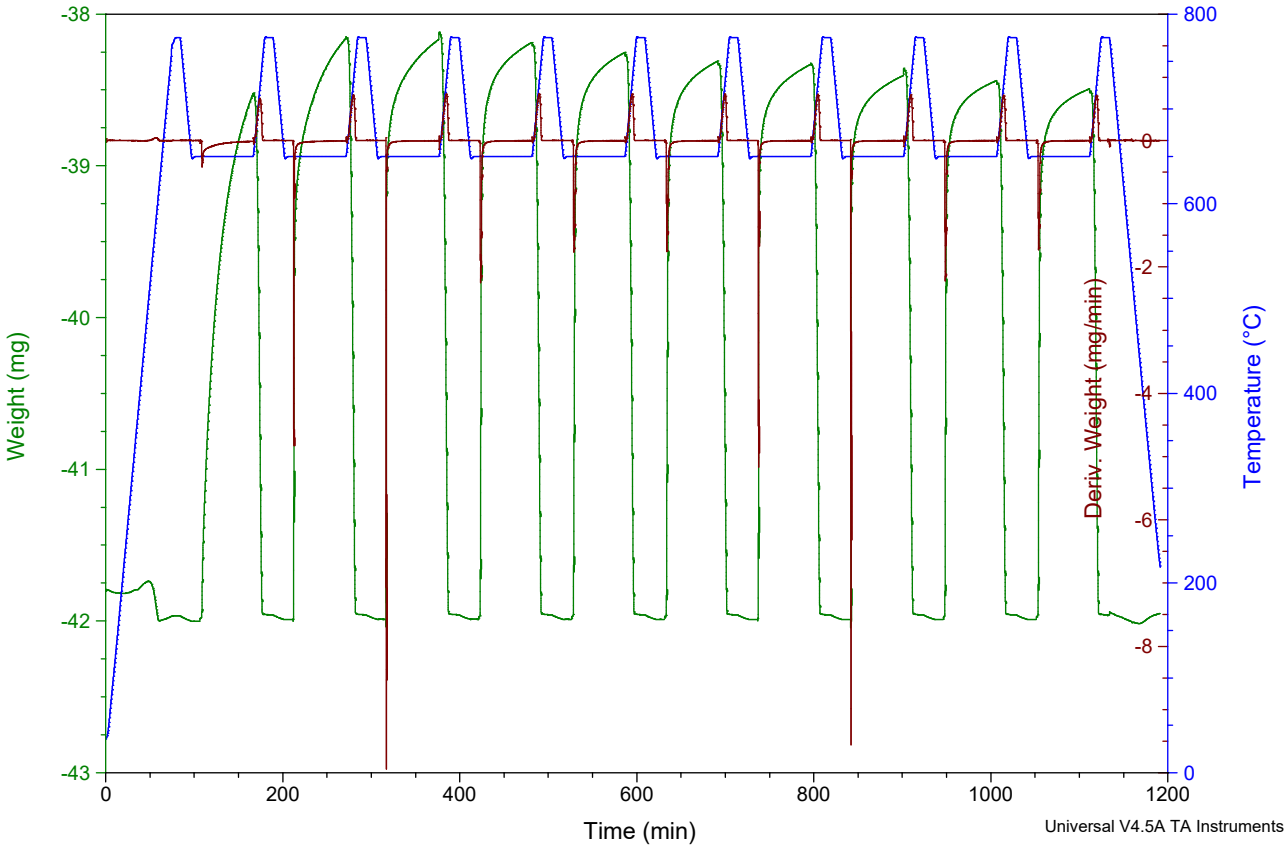

Universal V4.5A TA Instruments

Sample: NO8-12extr 2mm 13,0mg uncalc
Size: -43.6500 mg
Method: calc+10cycles 650degC 150ML N2
Comment: 13 mg solid Analytical scale; 6%Al 2%Zr;240 g solid scal

TGA

File: Granulers 2mm Fix bed NO8-12extrudes ...
Operator: Maria
Run Date: 09-May-2018 15:29
Instrument: TGA Q500 V6.7 Build 203

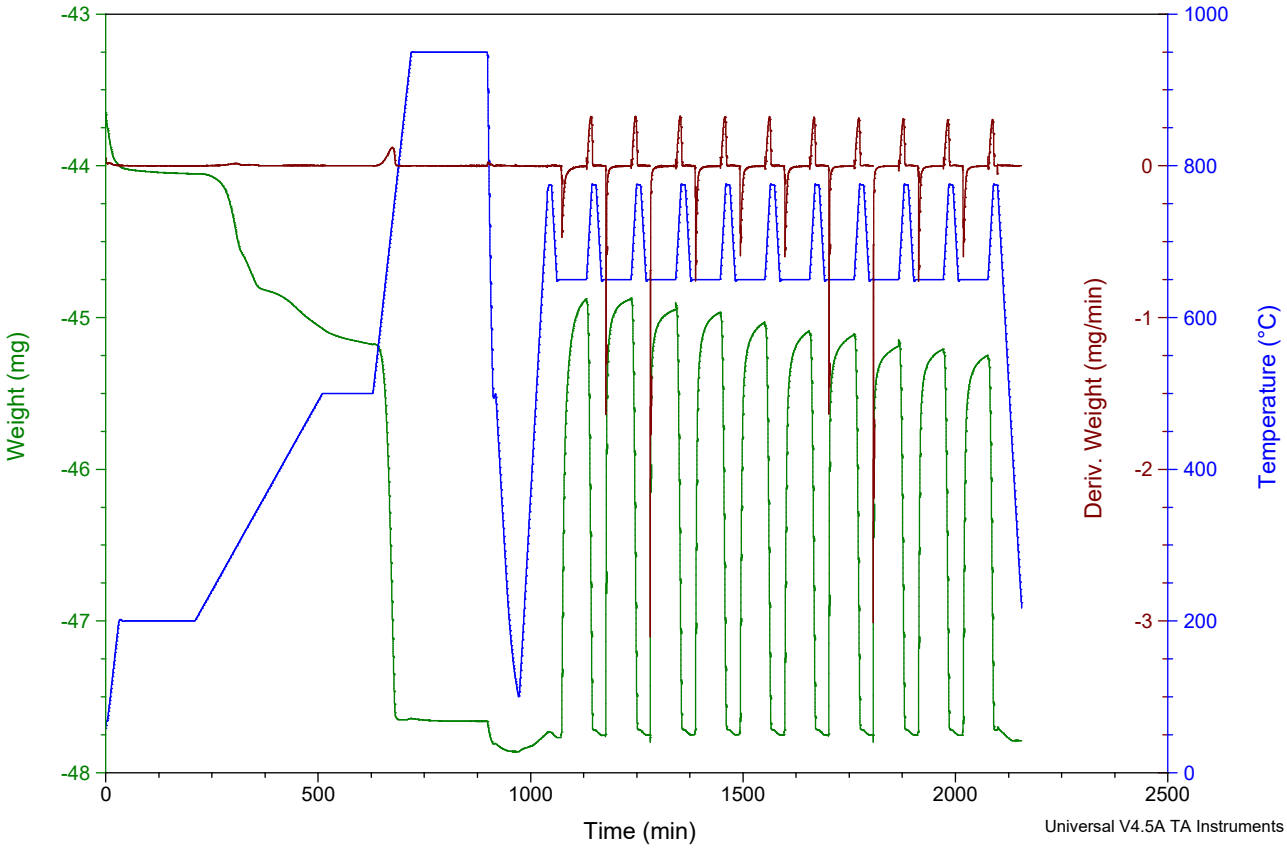

Universal V4.5A TA Instruments

Sample: NO8-12extr 2mm 22.8mg uncalc
Size: -34.2430 mg

TGA

File: Granulers 2mm Fix bed NO8-12extrudes ...
Operator: Maria
Run Date: 16-May-2018 14:28
Instrument: TGA Q500 V6.7 Build 203

Comment: 22.8mg solid Analytical scale; 6%Al 2%Zr;240 g solid scal

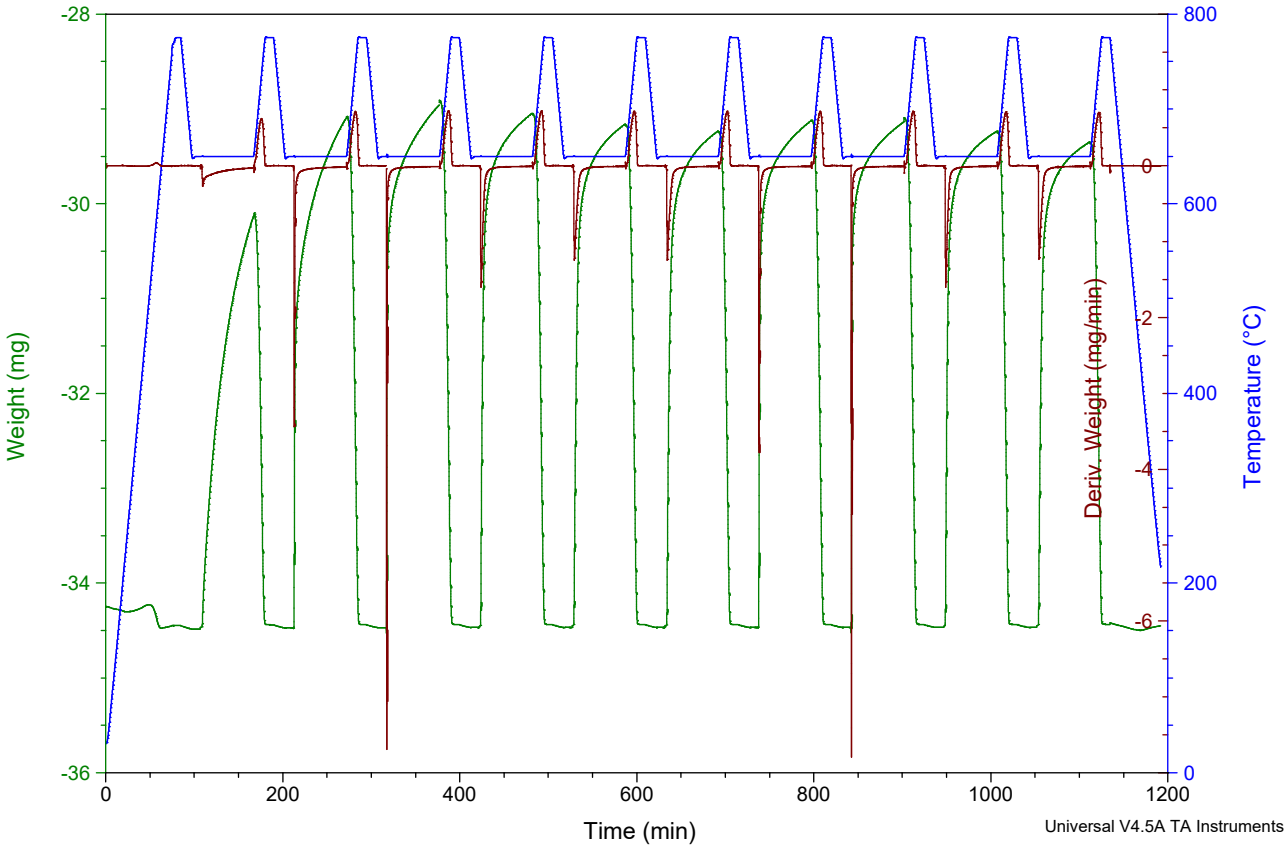

Universal V4.5A TA Instruments

Sample: NO8-12extr 3mm 19.0mg uncalc
Size: -38.0320 mg

TGA

File: Granulers 3mm Fix bed NO8-12extrudes ...
Operator: Maria
Run Date: 14-May-2018 08:47
Instrument: TGA Q500 V6.7 Build 203

Comment: 19.0 mg solid Analytical scale; 6%Al 2%Zr;240 g solid scal

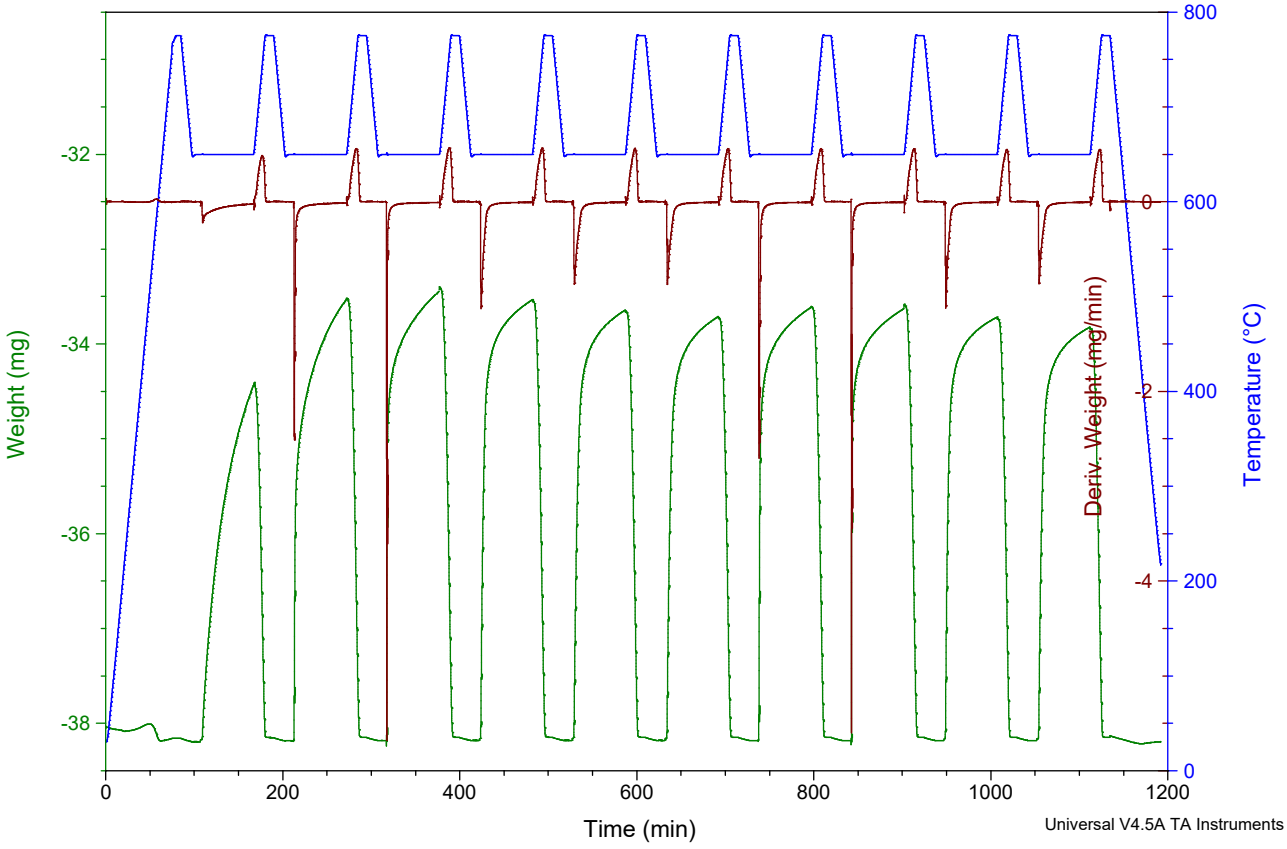

Universal V4.5A TA Instruments

Sample: NO8-12extr 4mm 28,4mg uncalc
Size: -28.5110 mg

TGA

File: Granulers 4mm Fix bed NO8-12extrudes ...
Operator: Maria
Run Date: 11-May-2018 08:39
Instrument: TGA Q500 V6.7 Build 203

Comment: 28,4 mg solid Analytical scale; 6%Al 2%Zr;240 g solid scal

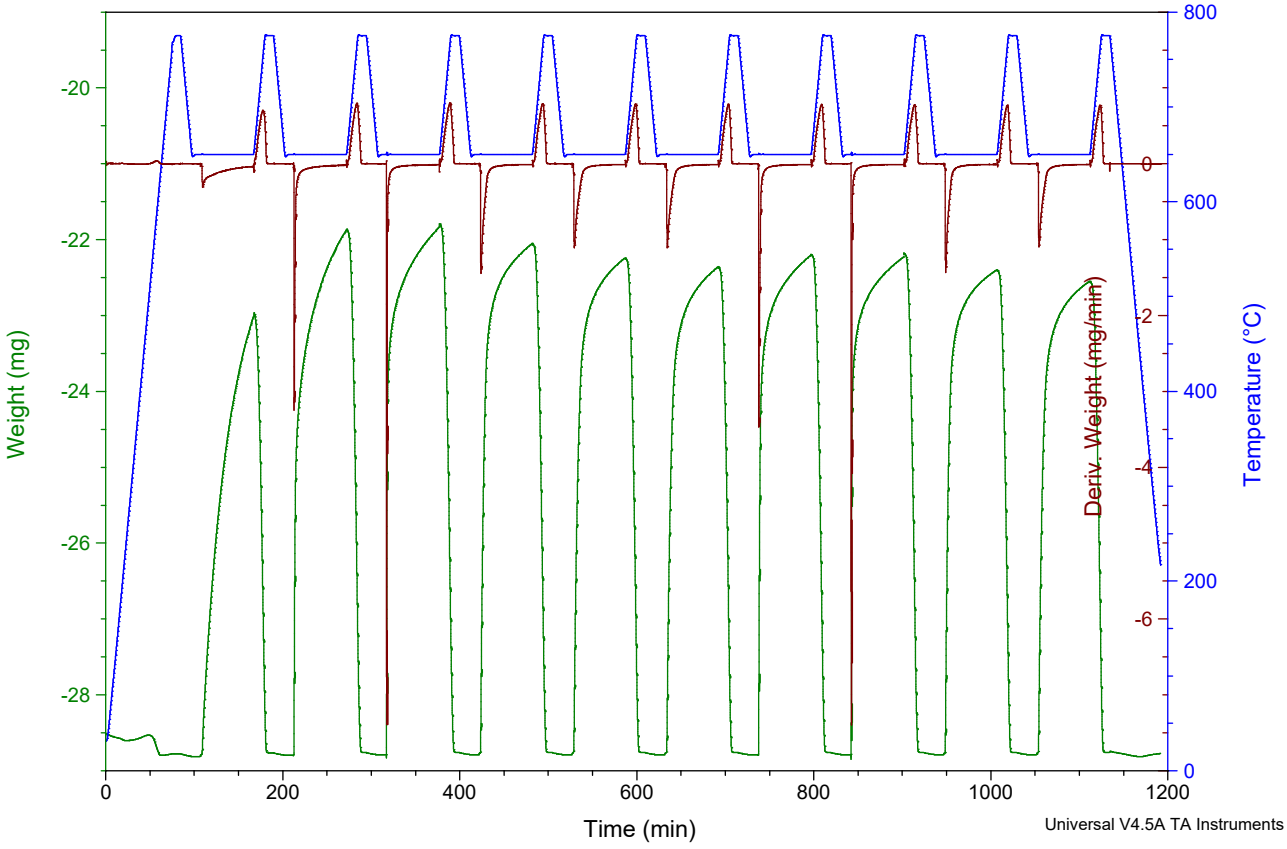

Universal V4.5A TA Instruments

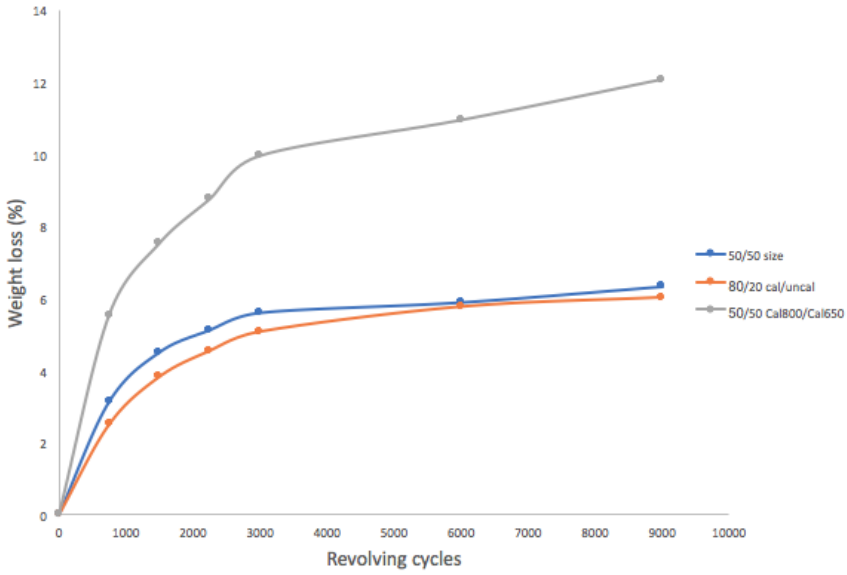

Figure A7.75: Accumulative weight loss (%) as a function of revolving cycles for the 3 calcined pellets (1000°C, 3h).

A7.11.2 Raw data from TGA w/Steam

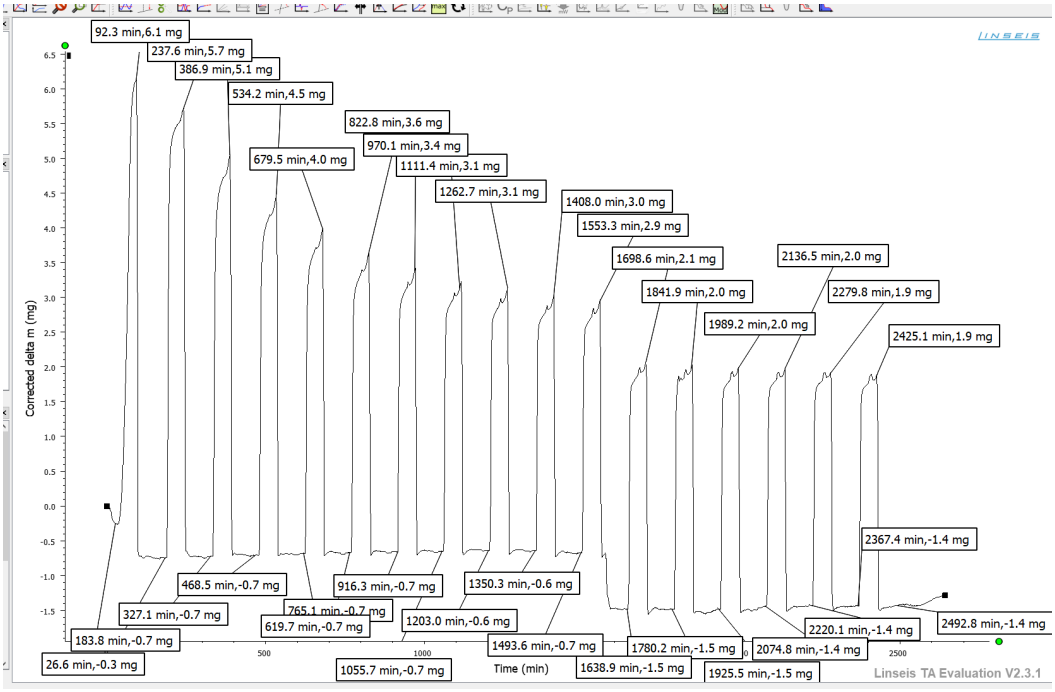

Figure A7.77: TGA - Raw data NO-1 17 cycles

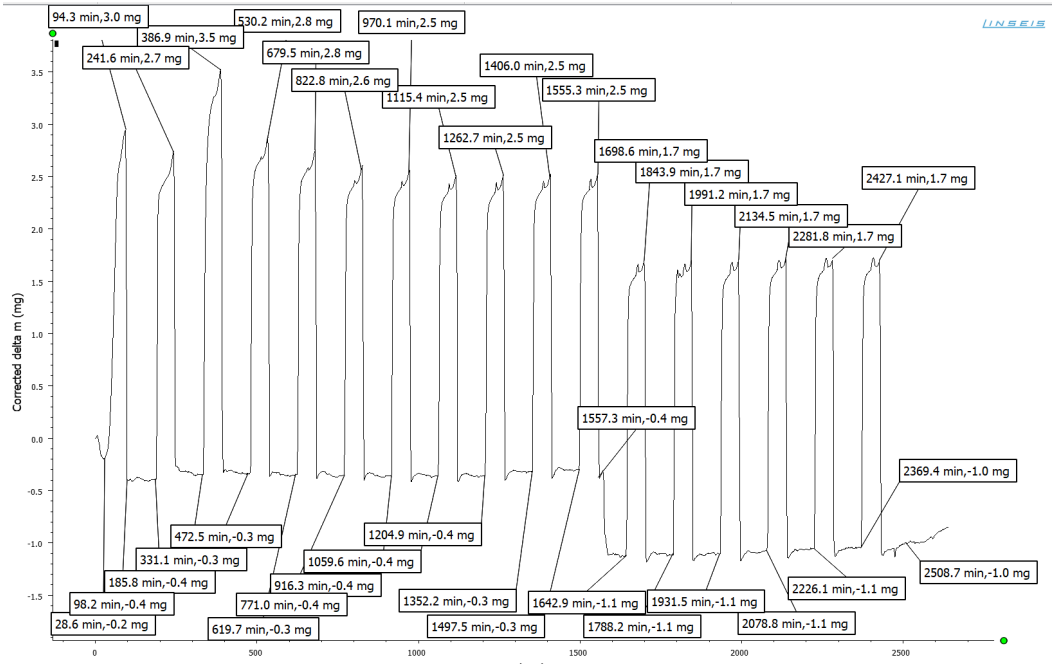

Figure A7.78: TGA -Raw data NO-1 17+17 cycles

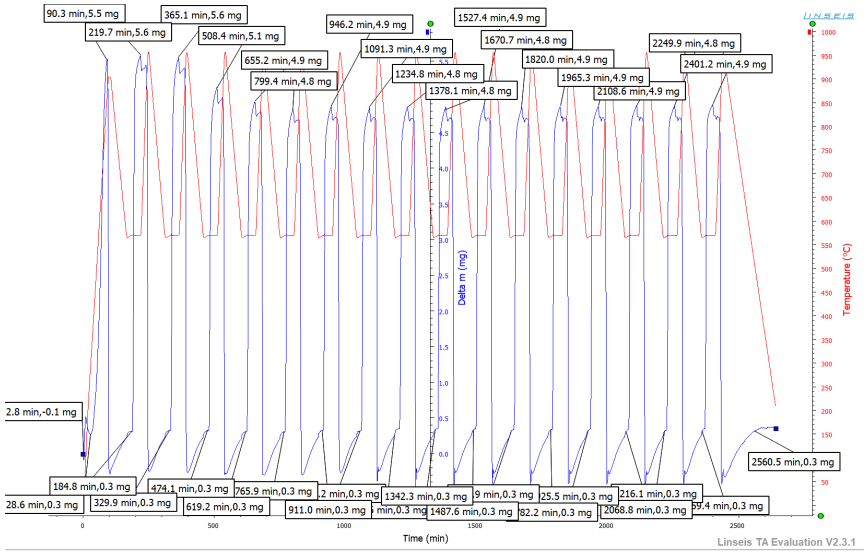

Figure A7.79: TGA -TGA steam, NO-3 17 cycles.

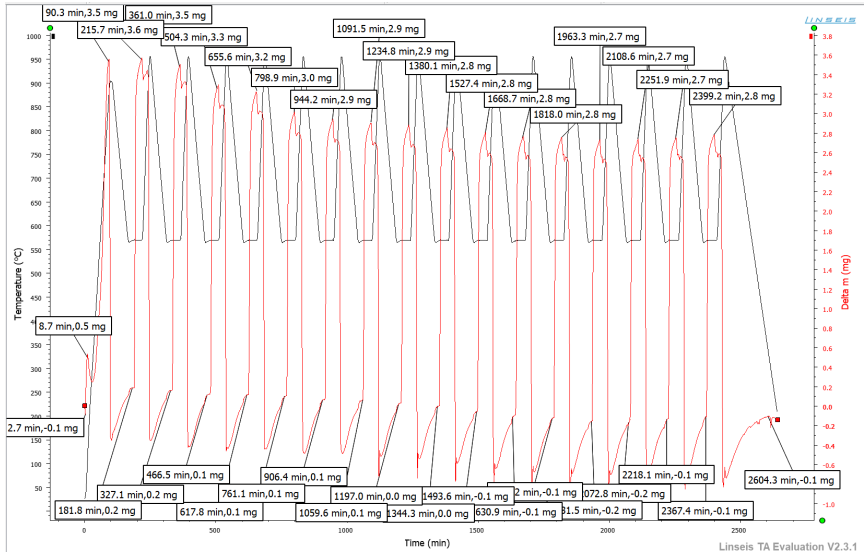

Figure A7.80: TGA steam, NO-8 17 cycles.

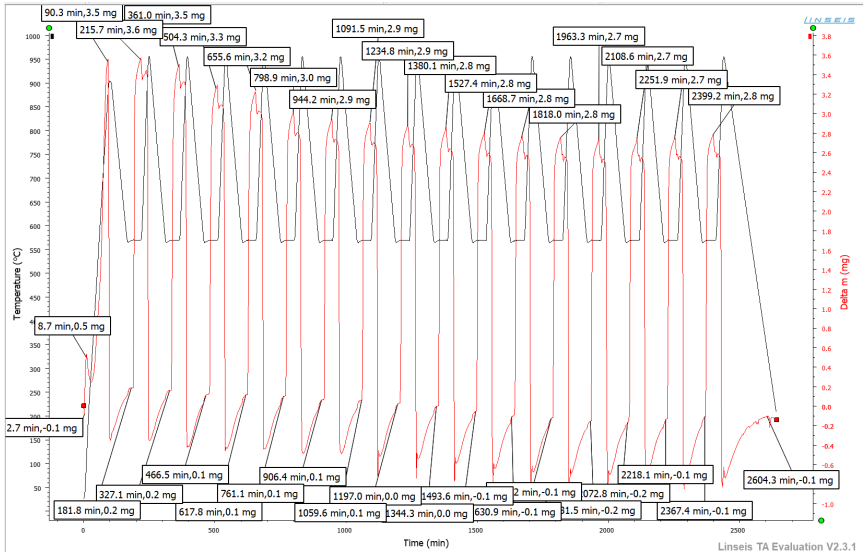

Figure A7.81: TGA steam, NO-8 17+17 cycles.

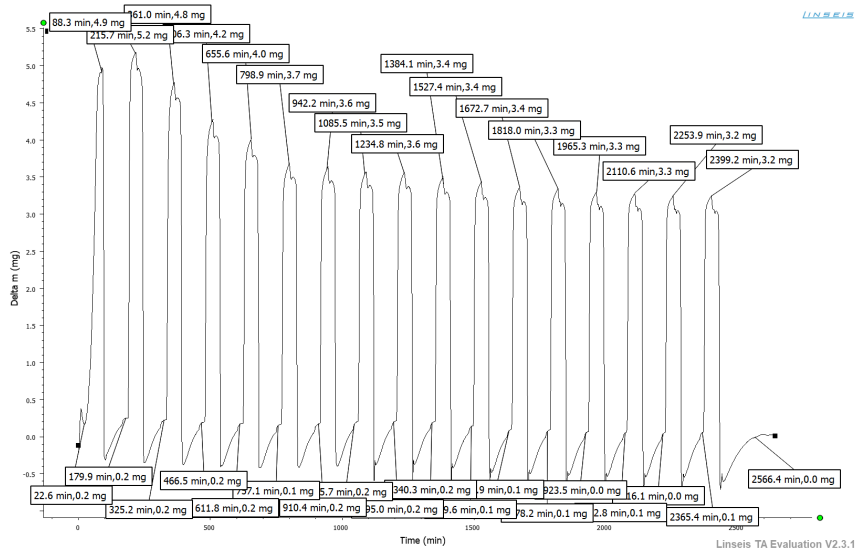

Figure A7.82: TGA steam, NO-10 17 cycles.

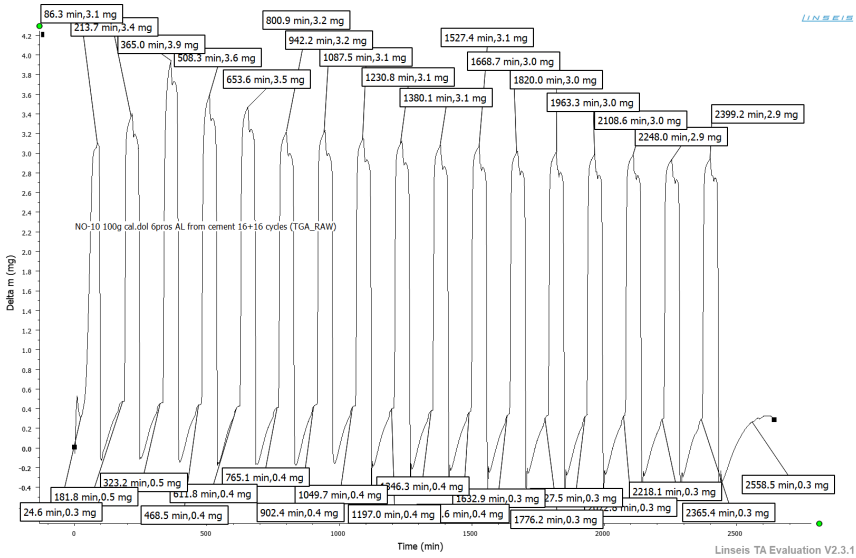

Figure A7.83: TGA steam, NO-10 17+17 cycles.

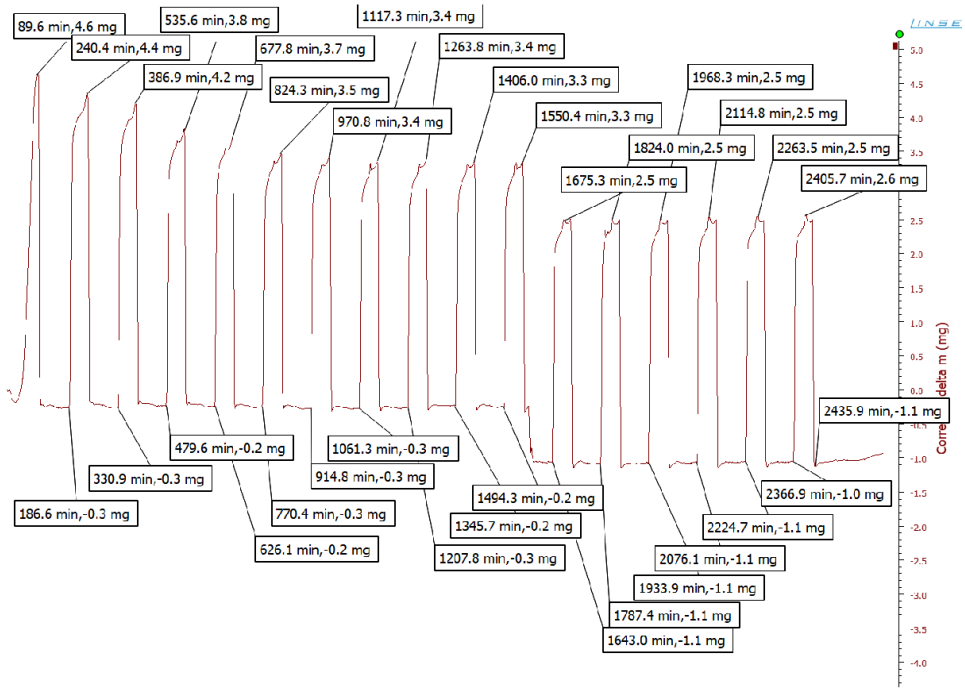

Figure A7.84: TGA steam, NO-12 17 cycles

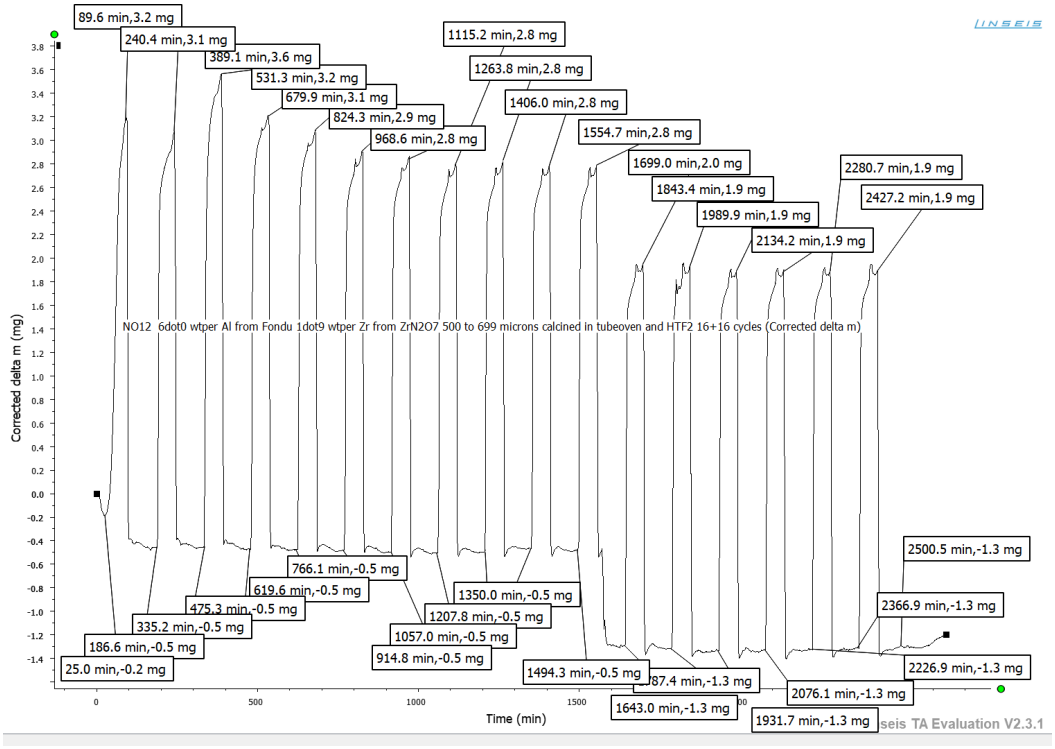

Figure A7.85: TGA steam, NO-12 17+17 cycles

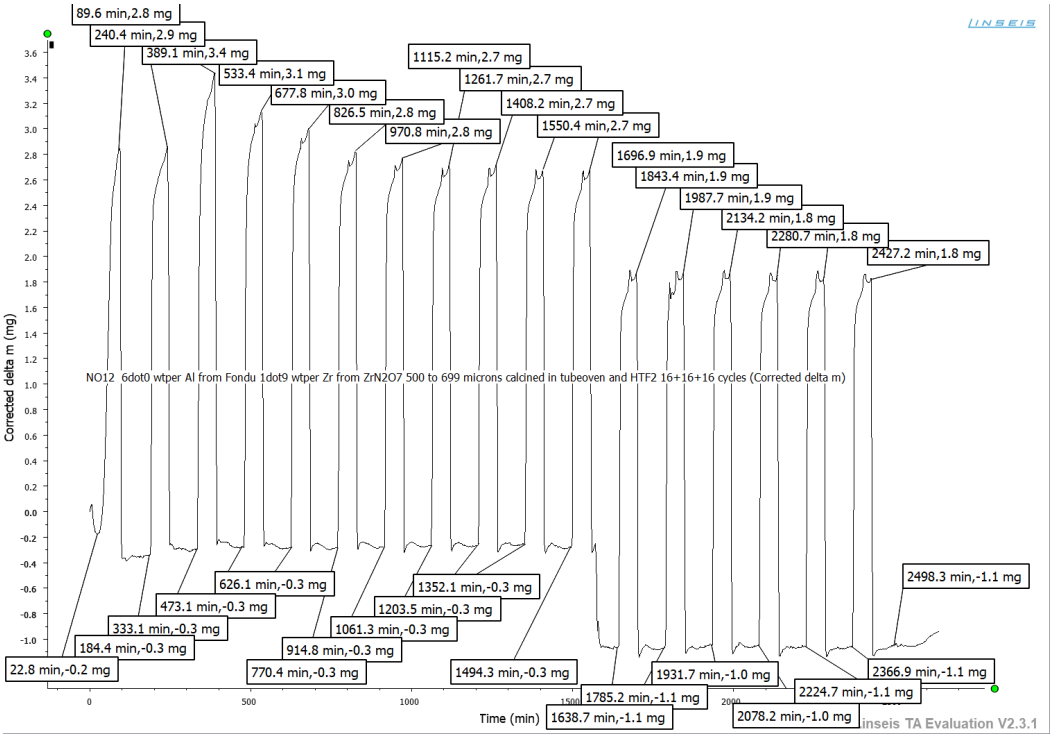

Figure A7.86: TGA steam, NO-12 17+17+17 cycles

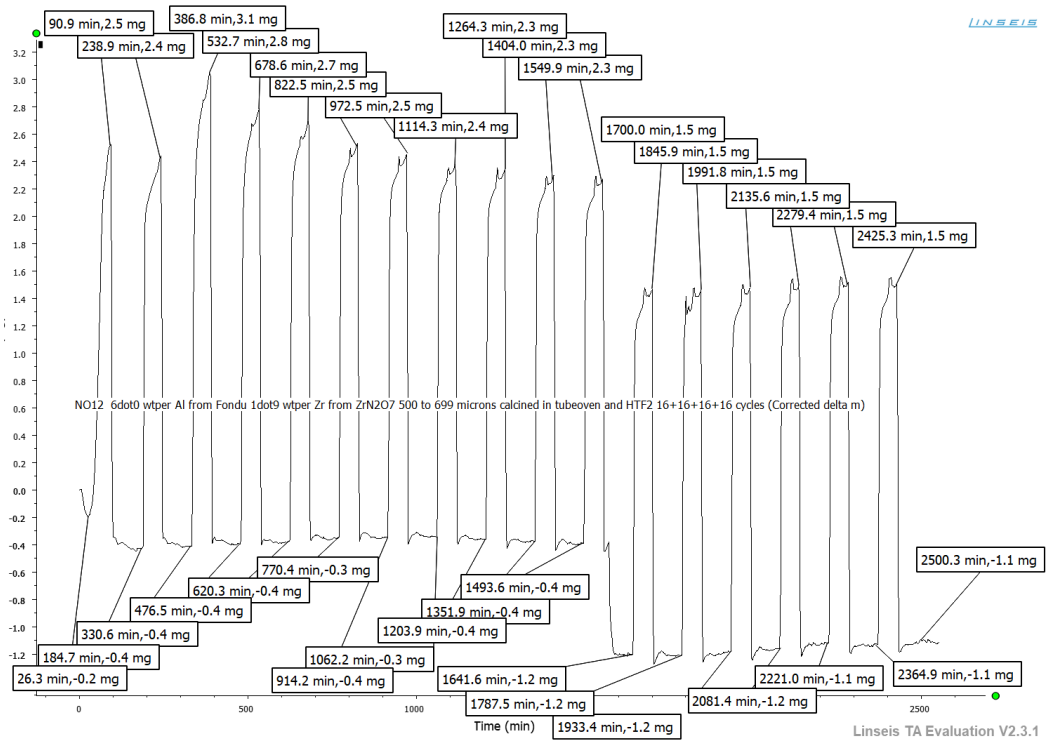

Figure A7.87: TGA steam, NO-12 17+17+17+17 cycles

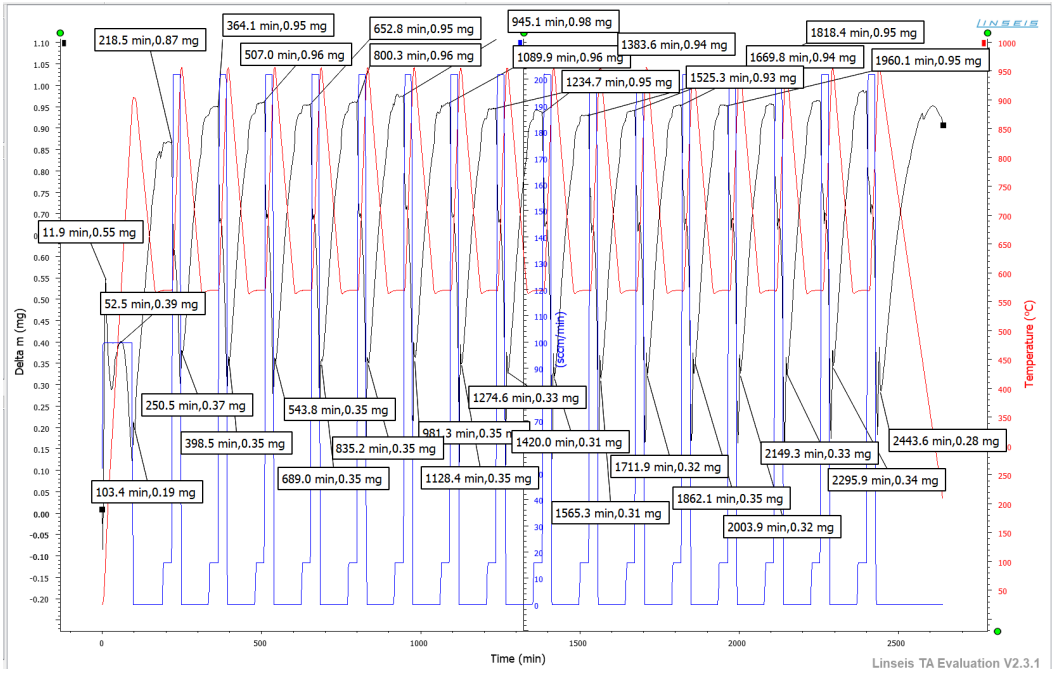

Figure A7.88: Baseline correction

A7.12 Temperature scanning program

Method Log for testing condition for 11 cycles of dry test:

1. Select Gas: 1 (N2)
2. Mass flow 9.0 mL/min
3. Ramp 10.00C/min to 625.00C
4. Isothermal for 1.00 min
5. Select Gas: 2 (CO2)
6. Mass flow 21.0 mL/min
7. Isothermal for 6.00 min
8. Select Gas: 1
9. Mass flow 65.0 mL/min
10. Ramp 10.00C/min to 950.00C
11. Isothermal for 5.00 min
12. Ramp 10.00C/min to 625.00C

13. Isothermal for 1.00 min
14. Repeat segment 1. for 10 times.
15. Ramp 10.00C/min to 30.00C
16. End of method

For the kinetic study, this program were used:

1. Select Gas: 1 (N2)
2. Mass flow 20.0 mL/min
3. Ramp 10.00C/min to 775.00C
4. Isothermal for 10.00 min
5. Ramp 10.00C/min to 620.00C
6. Isothermal for 10.00 min
7. Select Gas: 2
8. Mass flow 10.0 mL/min
9. Isothermal for 60.00 min
10. Select Gas: 1
11. Mass flow 20.0 mL/min
12. Ramp 10.00C/min to 775.00C
13. Isothermal for 10.00 min
14. Ramp 10.00C/min to 620.00C
15. Isothermal for 10.00 min
16. Select Gas: 2
17. Mass flow 25.0 mL/min
18. Isothermal for 60.00 min
19. Select Gas: 1
20. Mass flow 20.0 mL/min
21. Ramp 10.00C/min to 775.00C
22. Isothermal for 10.00 min
23. Ramp 10.00C/min to 620.00C
24. Isothermal for 10.00 min
25. Select Gas: 2

26. Mass flow 56.0 mL/min
27. Isothermal for 60.00 min
28. Select Gas: 1
29. Mass flow 20.0 mL/min
30. Ramp 10.00C/min to 775.00C
31. Isothermal for 10.00 min
32. Ramp 10.00C/min to 620.00C
33. Isothermal for 10.00 min
34. Select Gas: 2
35. Mass flow 12.0 mL/min
36. Isothermal for 60.00 min
37. Select Gas: 1
38. Mass flow 20.0 mL/min
39. Ramp 10.00C/min to 775.00C
40. Isothermal for 10.00 min
41. Ramp 10.00C/min to 620.00C
42. Isothermal for 10.00 min
43. Select Gas: 2
44. Mass flow 10.0 mL/min
45. Isothermal for 60.00 min
46. Select Gas: 1
47. Mass flow 20.0 mL/min
48. Ramp 10.00C/min to 775.00C
49. Isothermal for 10.00 min
50. Repeat segment 3 for 1 time
51. Select Gas: 1
52. Mass flow 10.0 mL/min
53. Ramp 10.00C/min to 200.00C
54. End of method

Here only the soprption temperature at 620 is given, but other temperatures were used as presented in A7.9.

A7.13 Product Spezification for Cement Fondu

CIMENT FONDU®

Refractory applications

Product Data Sheet

Reference FC-CF-RE-GB-KFR-032007

Updated 31/03/2008

1 General characteristics

Ciment Fondu® is a hydraulic binder, with an alumina content of approximately 40%.

The principal components of Ciment Fondu® are calcium aluminates which make it an ideal binder for refractory applications. Its high monocalcium aluminate content yields refractory concrete with excellent mechanical properties. Due to the iron oxide content of Ciment Fondu®, it is unsuitable for refractory concretes where iron oxide may not be tolerated, for example in reducing atmospheres.

The rheological properties of Ciment Fondu® are well adapted for all types of placing methods, particularly for casting and gunning. It is recommended for applications where rapid hardening and excellent performance are required.

Ciment Fondu® does not contain any additives, and is suited to the manufacture of refractory premixes.

Ciment Fondu® is produced and controlled within a quality management system that is certified according to ISO 9001.

2 Specification

The properties of Ciment Fondu® produced in Europe conform to the requirements defined in the norm: EN 14647 : “Calcium Aluminate Cement”

The *specification limits* indicated are determined with an acceptable quality level (AQL) of 2.5% defined in the standard ISO 3951.

The *strict specification limits* define the absolute limits of product conformity applicable for individual values.

The EN specification limits are conformed with the requirement defined in the norm EN 14647.

The *usual range* represents typical values of production.

Chemical composition

Main constituents (%)

	Usual range	Specification limit
Al_2O_3	37.5 - 41.0	> 37.0
CaO	35.5 - 39.0	< 41.0
SiO_2	3.5 - 5.5	< 6.0
Fe_2O_3	13.0 - 17.5	< 18.5
MgO	-	< 1.5
TiO_2	-	< 4.0

Other constituents (%)

	Strict specification limit
S (as sulphide ions)	≤ 0.1
Cl (as chloride ions)	≤ 0.1
$Na_2O + 0,659\ K_2O$	≤ 0.4
SO_3	≤ 0.5

The chemical characteristics of Ciment Fondu® have been determined according to the following:

- EN 196-2: Methods of testing cement - Chemical analysis of cement.

Fineness

	Usual range	Specification limit
Blaine Specific surface (cm2/g)	2850 - 3450	> 2700

- Determined in accordance with EN 196-6: Methods of testing cements - Measurement of fineness.

Neat paste setting time

	Usual range	Specification limit
Initial set (min)	180 - 300	> 120
Final set (min)	210 - 330	< 480

- Determined in accordance with EN 196-3: neat cement paste at standard consistency; mechanical mixing ; Vicat test equipment using 300g weight ; temperature 20°C ; relative humidity >90%.

Kerneos SA
8 rue des Graviers 92521 Neuilly sur Seine France
Tel. : +33 1 46 37 90 00 - Fax : +33 1 46 37 92 00

kerneos™ ALUMINATE TECHNOLOGIES

Mechanical strength

Compressive strength, MPa		
Age	Usual range	Strict specification limit
6 h	35 - 50	> 30
24 h	60 - 80	> 50

- Composition of mortar according to EN 14647: 1350g of sand, 500g of calcium aluminate cement, 200g of water
- Test conditions according to EN 196-1: test prisms 40x40x160mm; temperature 20°C ; prisms cured at >90% relative humidity for 24 hours (NF standard) or 6h (BS standard), followed by immersion in water.

3 Additional data

This information is given for guidance only.

- Principal mineralogical phase*: CA
- Secondary phases*: $C_{12}A_7$, C_2S, C_2AS, C_4AF

* C=CaO, A=Al_2O_3, S= SiO_2, F=Fe_2O_3

- Bulk density: 1100 kg/m^3
- Specific gravity: 3.2 - 3.3 g/cm^3
- Pyrometric cone equivalent (on neat cement paste): 1270 - 1290 °C
- Heat of hydration

6h	340 kJ/kg
24h	445 kJ/kg
5 days	445 kJ/kg

Beyond the minimal requirements of the standard EN 14647, the French production benefits from controls and complementary requirements such as defined in the reference frame NF 002.

Workability - French production

	Specification limit
Spread after 15 min (%)	> 30

The workability of Ciment Fondu® has been determined by measuring the flow properties using the ASTM C230 flow table. The test is carried out using a standard siliceous sand mortar.

- Composition of mortar according to EN 14647: 1350g of sand, 500g of calcium aluminate cement, 200g of water
- Test carried out with 25 shocks after 15 min retained in cone mould, d_1 (diameter of base) = 100mm.
  % of flow = d_2 (mm) - d_1 (mm)

	Usual range	Specification limit
Initial set (min)	130 - 200	> 120
Final set (min)	140 - 220	< 240

Mortar setting time - French production

- Composition of mortar according to EN 14647: 1350g of sand, 500g of calcium aluminate cement, 200g of water
- Preparation according to EN 196-1.
- Measurement according to NF P15-431: Vicat test equipment as EN 196-3 but using a 1000g test weight ; temperature 20°C ; samples immersed in water or cured at > 90% relative humidity.
- Final setting time measured in accordance with NF P15-330: the Vicat needle no longer penetrates the mortar.

Mechanical strength - French production

Mechanical strength in MPa		
Age	Modulus of rupture strict specification limit	Compressive strength strict specification limit
6 h	> 4	> 30
24 h	> 5	> 50
28 d	> 6.5	> 60

- Composition of mortar according to EN 14647: 1350g of sand, 500g of calcium aluminate cement, 200g of water
- Test conditions according to EN 196-1: test prisms 40x40x160mm; temperature 20°C ; prisms cured at >90% relative humidity for 24 hours (NF standard) or 6h (BS standard), followed by immersion in water.

4 Storage and Shelf Life

As with all hydraulic binders, Ciment Fondu® must be stored in dry conditions, off the ground. In this case, it will retain its properties for at least 6 months. In many instances, properties are retained for more than one year.

Kerneos SA
8 rue des Graviers 92521 Neuilly sur Seine France
Tel. : +33 1 46 37 90 00 - Fax : +33 1 46 37 92 00

A7.14 Risk assessment

ID	20322	**Status**	**Dato**
Risikoområde	Risikovurdering: Helse, miljø og sikkerhet (HMS)	Opprettet	15.06.2017
Opprettet av	Maria Olsvik	Vurdering startet	15.06.2017
Ansvarlig	Maria Olsvik	Tiltak besluttet	
		Avsluttet	

Risikovurdering:

CAT, master student, 2017, Maria Olsvik

Gyldig i perioden:

-

Sted:

Kjemibygg 5 i 4 og 2 etg, kjemihall NTNU

Mål / hensikt

Risikovurdering for jobb som skal utføres i sommerjobb/prosjekt/master

Bakgrunn

For å utføre sommerjobb/prosjekt/master trenger man risikovurdering på det som beskrives nærmere under beskrivelse og avgrensninger.

Beskrivelse og avgrensninger

Bæring/bruk av kjemikalier (Mg(NO3)2, ZrCl4, ZrO(NO)3) osv. Dolomitt skal brukes som råvare til å lage sement, ferdig laget sement blir kjøpt fra vanlig bygningsmaterialebutikk med sikkerhetsblad, og laging av vannløsning med disse kjemikalier. Bruke sikkerhetsdatablad
Pulver behandling/håndtering. Sikting og fraksjonering av pulver ved bruk av sikter og siktemaskiner. Bruk av ansiktsmaske.
Bruk av vanlig laboratorieutstyr: vekt, PH-måler, flakser osv.
Tørking (ambient trykk og T, ikke høyere enn 100 grader)
Kalsinering (egen opplæring, tilgjengelig risikovurdering på operasjonsprosedyre)
Granulering (egen opplæring, tilgjengelig risikovurdering på operasjonsprosedyre)
Karakterisering (egen opplæring, tilgjengelig risikovurdering på operasjonsprosedyre) BET, SEM, XRD, TGA, XRF
Materialtest (egen opplæring, tilgjengelig risikovurdering på operasjonsprosedyre): TGA, mikrobalansereaktor

Forutsetninger, antakelser og forenklinger

Antar endelig opplæring før aktivitet utføres og at det finnes tilgjengelig risikovurdering på operasjonsprosedyre av kalsinering, granuering, karakterisering og materialtest. Forutsetter at studenten har riktig håndtering for frakt og bruk av kjemikalier.

Vedlegg

[Ingen registreringer]

Referanser

[Ingen registreringer]

Oppsummering, resultat og endelig vurdering

I oppsummeringen presenteres en oversikt over farer og uønskede hendelser, samt resultat for det enkelte konsekvensområdet.

Farekilde:	**Sement - Adda**
Uønsket hendelse:	**Ved øye og hudkontakt**
Konsekvensområde:	Helse

Risiko før tiltak:  Risiko etter tiltak: 

Farekilde:	**Flytende nitrogen**
Uønsket hendelse:	**Uønsket hudkontakt med flytende nitrogen**
Konsekvensområde:	Helse

Risiko før tiltak:  Risiko etter tiltak: 

Farekilde:	**Kontakt med varme overflater**
Uønsket hendelse:	**Varm overflate ved degassing i BET**
Konsekvensområde:	Helse

Risiko før tiltak:  Risiko etter tiltak: 

Endelig vurdering

Involverte enheter og personer

En risikovurdering kan gjelde for en, eller flere enheter i organisasjonen. Denne oversikten presenterer involverte enheter og personell for gjeldende risikovurdering.

Enhet /-er risikovurderingen omfatter

- Institutt for kjemisk prosessteknologi

Deltakere

Li He

Kumar Ranjan Rout

Lesere

Karin Wiggen Dragsten

De Chen

Edd Anders Blekkan

Andre involverte/interessenter

[Ingen registreringer]

Følgende akseptkriterier er besluttet for risikoområdet Risikovurdering: Helse, miljø og sikkerhet (HMS):

Helse

Materielle verdier

Omdømme

Ytre miljø

Oversikt over eksisterende, relevante tiltak som er hensyntatt i risikovurderingen

I tabellen under presenteres eksisterende tiltak som er hensyntatt ved vurdering av sannsynlighet og konsekvens for aktuelle uønskede hendelser.

Farekilde	Uønsket hendelse	Tiltak hensyntatt ved vurdering
Sement - Adda	Ved øye og hudkontakt	Personlig verneutstyr
Flytende nitrogen	Uønsket hudkontakt med flytende nitrogen	Personlig verneutstyr
	Uønsket hudkontakt med flytende nitrogen	Retningslinjer
	Uønsket hudkontakt med flytende nitrogen	Personlig verneutstyr
Kontakt med varme overflater	Varm overflate ved degassing i BET	Personlig verneutstyr
	Varm overflate ved degassing i BET	Personlig verneutstyr

Eksisterende og relevante tiltak med beskrivelse:

Personlig verneutstyr
Briller, frakk, sko, ansiktsmaske

Avtrekkskap
Riktig bruk av avtrekkskap

Retningslinjer
Følge generelle regler på lab for bruk av utstyr og oppførsel.

Personlig verneutstyr
Bruk av isolerende hansker og frakk

Risikoanalyse med vurdering av sannsynlighet og konsekvens

I denne delen av rapporten presenteres detaljer dokumentasjon av de farer, uønskede hendelser og årsaker som er vurdert. Innledningsvis oppsummeres farer med tilhørende uønskede hendelser som er tatt med i vurderingen.

Følgende farer og uønskede hendelser er vurdert i denne risikovurderingen:

- **Sement - Adda**
  - Ved øye og hudkontakt
- **Flytende nitrogen**
  - Uønsket hudkontakt med flytende nitrogen
- **Kontakt med varme overflater**
  - Varm overflate ved degassing i BET

Detaljert oversikt over farekilder og uønskede hendelser:

Farekilde: Sement - Adda

Sementpulveret kan gi alvorlige øyeskader, irritasjon på hud, irritasjon på luftveier. Kan inneholde kreftfremkallende kjemikalier. Må derfor følge bruksanvisning, slik at man unngår risiko for menneskers helse og miljøet.

Uønsket hendelse: Ved øye og hudkontakt

I kontakt med kroppsvæsker gjor sement en sterk basisk reaksjon. Det vil da virke etsende på hud og øyne. Jevnlig hudkontakt kan gi eksem. Støv og partikler kan rispe og irritere øynene.

Sannsynlighet for hendelsen (felles for alle konsekvensområder): **Lite sannsynlig (2)**

Kommentar:

[Ingen registreringer]

Konsekvensområde: Helse

Risiko:

Vurdert konsekvens: **Liten (1)**

Kommentar: [Ingen registreringer]

Farekilde: Flytende nitrogen

Ved bruk av BET

Uønsket hendelse: Uønsket hudkontakt med flytende nitrogen

Flytende nitrogen kan gi alvorlige forfrysninger

Sannsynlighet for hendelsen (felles for alle konsekvensområder): **Lite sannsynlig (2)**

Kommentar:

[Ingen registreringer]

Konsekvensområde: Helse

Risiko:

Vurdert konsekvens: **Stor (3)**

Kommentar: Dersom man utsetter huden for flytende nitrogen vil man få frostskader

Farekilde: Kontakt med varme overflater

Degassing ved 300 grader for bruk av BET

Uønsket hendelse: Varm overflate ved degassing i BET

Ønsker ikke å komme i kontakt med varmestasjonen som brukes for å forberede prøvene til BET

Sannsynlighet for hendelsen (felles for alle konsekvensområder): **Svært lite sannsynlig (1)**

Kommentar:

[Ingen registreringer]

Konsekvensområde: Helse

Risiko:

Vurdert konsekvens: **Middels (2)**

Kommentar: Dersom man kommer borti varm overflate vil man få en liten brannskade, men utsatt område vil ikke bli stort

Oversikt over besluttede risikoreduserende tiltak:

Under presenteres en oversikt over risikoreduserende tiltak som skal bidra til å reduseres sannsynlighet og/eller konsekvens for uønskede hendelser.

Detaljert oversikt over besluttede risikoreduserende tiltak med beskrivelse:

Detaljert oversikt over vurdert risiko for hver farekilde/uønsket hendelse før og etter besluttede tiltak

A7.15 Theory - Mercury Porosimetry

Mercury Intrusion Porosimetry Theory

Presented by Micromeritics Instrument Corporation

Porosimetry Defined

The term "porosimetry" is often used to include the measurements of pore size, volume, distribution, density, and other porosity-related characteristics of a material. Porosity is especially important in understanding the formation, structure, and potential use of many substances. The porosity of a material affects its physical properties and, subsequently, its behavior in its surrounding environment. The adsorption, permeability, strength, density, and other factors influenced by a substance's porosity determine the manner and fashion in which it can be appropriately used.

Analysis Defined

Since mercury does not wet most substances and will not spontaneously penetrate pores by capillary action, it must be forced into the pores by the application of external pressure. The required equilibrated pressure is inversely proportional to the size of the pores, only slight pressure being required to intrude mercury into large macropores, whereas much greater pressures are required to force mercury into small pores. Mercury porosimetry analysis is the progressive intrusion of mercury into a porous structure under stringently controlled pressures. From the pressure versus intrusion data, the instrument generates volume and size distributions using the Washburn equation.. Clearly, the more accurate the pressure measurements, the more accurate the resulting pore size data.

Theory

It is the non-wetting property of mercury combined with its high surface tension, that almost uniquely qualifies it for use in probing pore space. At each surface interface with a liquid, there is tension that acts tangentially to the interface. This is termed 'surface tension' and acts like an elastic membrane contacting the surface until the surface forces are in equilibrium with the forces tending to increase the surface area of the interface.

Surface tension, then, can be defined as the force per unit length acting along the surface of a liquid at right angles to a line that separates the two phases.

If mercury is placed in contact with a pore opening, the surface tension of the mercury acts along the line of contact with the opening equal in length to the perimeter of the opening and creating a force-resisting entry.

The magnitude of resisting force is proportional to the length of the line of contact, the surface tension (γ) of mercury, and the cosine of the contact angle (θ). For a pore with a circular opening at the surface, the resisting force is expressed as

$$f_R = \pi D\gamma\cos\theta.$$

An externally applied pressure tending to force mercury into the opening acts over the surface of the interface bridging the opening. The externally applied force, therefore, is the product of the pressure (P) and area (A) over which the pressure is applied. For a pore of circular cross-section,

$$f_{Ext} = PA = P\pi D^2/4.$$

At equilibrium, just before the resistive force is overcome, the equation is,

$$-\pi D\gamma\cos\theta = \pi D^2P/4.$$

Therefore, at any pressure, the pores into which mercury has intruded have diameters greater than

$$D = -4\gamma\cos\theta\ /P.$$

By measuring the volume of mercury that intrudes into the sample material with each pressure change, the volume of pores in the corresponding size class is known.

The volume of mercury that enters pores is measured by a mercury penetrometer (an electrical capacitance dilatometer). These devices are very sensitive and can detect a change in mercury volume of under 0.1µL.

The penetrometer is constructed of glass (an insulator) and filled with mercury (a conductor). The stem of the penetrometer is a capillary that acts as a reservoir for the analytical volume of mercury. The stem is plated with metal (a conductor). The two conductors, mercury, and the metal plating, are separated by glass, thus forming a coaxial capacitor. As pressure forces mercury out of the capillary and into the sample, the mercury inside the capillary decreases and so is the capacitance. The decrease in capacitance, therefore, is proportional to the volume of mercury leaving the capillary with each change in pressure.

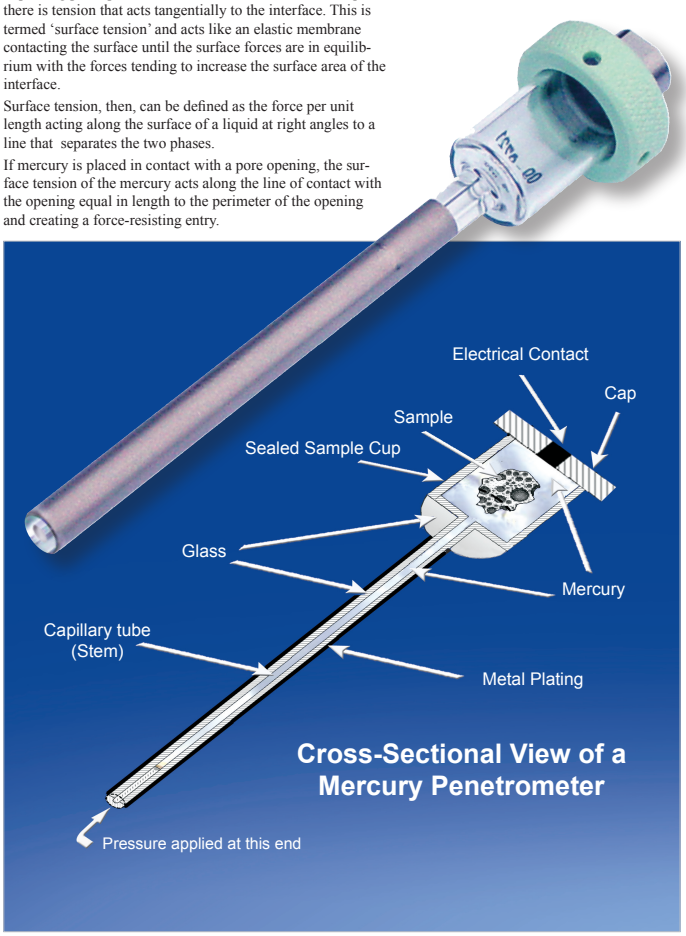

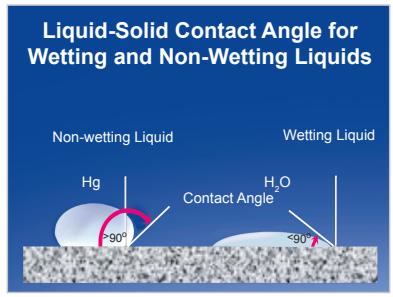

Liquids resting on a solid surface. The different angles of contact are illustrated for wetting and non-wetting liquids.

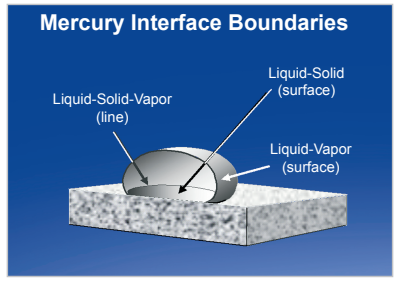

Cross-section of a drop of non-wetting liquid resting on a solid surface. All interfaces are shown.

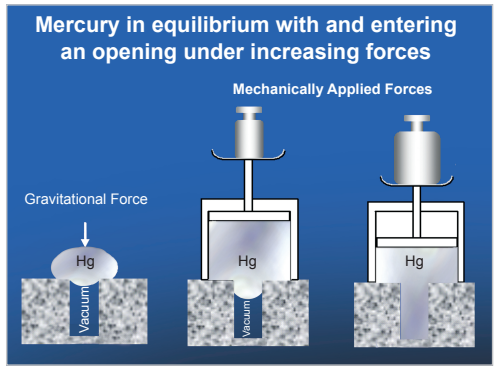

Since mercury does not wet most substances and will not spontaneously penetrate pores by capillary action, it must be forced into the pores by the application of external pressure.

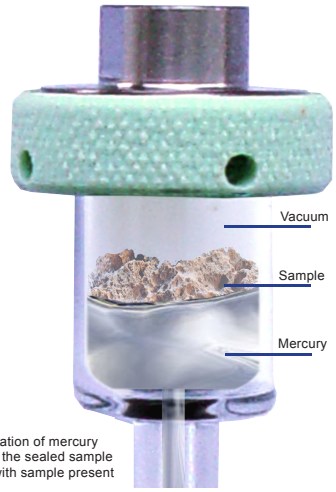

Illustration of mercury filling the sealed sample cup with sample present

micromeritics®

The Science and Technology of Small Particles™

www.micromeritics.com

Micromeritics Instrument Corporation
One Micromeritics Dr., Norcross, GA 30093-1877, USA
US Sales: 770.662.3633, International Sales: 770.662.3660
Customer Orders: 770.662.3636, Fax: 770.662.3696

Part # 950/42901/00 $42.00

Table A7.9: Parameters for the 10 cycles in the kinetic study of sample NO-12.

Cycle number	**Sample gas, CO_2 Set point (mL/min)**	**Balance gas, N_2 Set point (mL/min)**	**CO_2 concentration (%)**
1	10	150	2
2	25	150	11.3
3	56	150	15.6
4	12	150	3.3
5	10	150	2
6	10	150	2
7	25	150	11.3
8	56	150	15.6
9	12	150	3.3
10	10	150	2